UNIVERSITY OF SOUTHAMPTON

FACULTY OF ENVIRONMENTAL AND LIFE SCIENCES

School of Ocean and Earth Science

Anomalous Metal Enrichment of Basin Brines in the Zambian Copperbelt: a comparison of fluid chemistry in contrasting sediment-hosted copper systems

by

James Davey

Thesis for the degree of Doctor of Philosophy

March 2019

University of Southampton

Abstract

Faculty of Environmental and Life Sciences

School of Ocean and Earth Science

Thesis for the degree of Doctor of Philosophy

Anomalous Metal Enrichment of Basin Brines in the Zambian Copperbelt: a comparison of fluid chemistry in contrasting sediment-hosted copper systems

James Davey

The Central African Copperbelt is the largest repository of sediment-hosted copper and cobalt on Earth. Both metals are essential components of developing battery technologies and the 'green energy revolution', and as such, understanding the processes through which they are sourced, transported and precipitated in sedimentary basin environments is fundamental to securing future supply. This thesis presents an investigation of the physicochemical characteristics of palaeofluids from three world-class Cu-Co-(U) deposits in the Zambian Copperbelt, as well as comparisons with considerably smaller systems in the Kalahari Copperbelt (Botswana) and Munster Basin (Ireland).

Pre- to syn-kinematic veins in Zambian deposits host anomalously high temperature-salinity brines with unusually potassic compositions and concomitant enrichments in the principal ore-forming metals. Later fluids are distinctly lower temperature-salinity NaCl-dominant brines with reduced base metal concentrations. Samples hosting dominant populations of fertile ore fluids correspond with those returning halogen ratios typical of highly evaporated bittern brines, whereas barren, later fluids indicate a component of halite dissolution. Stable isotope analyses of kinematically 'early' versus 'late' veins, as well as alteration assemblages associated with temporally distinct vein sets and structures support a model whereby highly evolved, potassic, bittern brines resided in Cu-fertile clastic aquifers for prolonged periods, acquiring high temperatures (>300°C), salinities (>35 wt % NaCl+KCl equiv.) and Cu-Co concentrations (10^2-10^3 ppm) prior to emplacement of mineralised veins. Later, barren fluids dissolved evaporites at the onset of basin inversion and were often emplaced as discordant veins with associated sodic alteration assemblages. Fluids associated with smaller-scale mineralisation in the broadly contemporaneous Kalahari Copperbelt share similar physicochemical characteristics with late NaCl brines from the Zambian Copperbelt, with ultra-potassic, fertile ore fluids apparently absent outboard of the Katangan Basin in the Pan-African belt.

Mineralised and barren vein sets at the Allihies redbed Cu deposit in the Munster Basin display contrasting fluid temperature and salinity characteristics. Primary inclusions in barren, pre-peak orogenic regional vein sets yield moderate homogenisation temperatures (150-190°C) and salinities (~13 wt % NaCl equiv.), with cation compositions indicative of fluid-rock interaction within Devonian Old Red Sandstone aquifers. Later mineralised veins host distinctly higher temperature (~260°C), moderate salinity (~9 wt % NaCl equiv.) fluids with slight Cu enrichments.

Zambian Copperbelt ore fluids are here characterised as anomalously high temperature and salinity brines with correspondingly elevated base metal contents. Few other systems appear to have produced the requisite geologic and physicochemical conditions over sufficient time periods to generate similarly fertile basin brines.

Table of Contents

List of Tables

List of Figures

Research Thesis: Declaration of Authorship

Print name:	James Davey

Title of thesis:	Anomalous Metal Enrichment of Basin Brines in the Zambian Copperbelt: a comparison of fluid chemistry in contrasting sediment-hosted copper systems

I declare that this thesis and the work presented in it are my own and has been generated by me as the result of my own original research.

I confirm that:

1. This work was done wholly or mainly while in candidature for a research degree at this University;
2. Where any part of this thesis has previously been submitted for a degree or any other qualification at this University or any other institution, this has been clearly stated;
3. Where I have consulted the published work of others, this is always clearly attributed;
4. Where I have quoted from the work of others, the source is always given. With the exception of such quotations, this thesis is entirely my own work;
5. I have acknowledged all main sources of help;
6. Where the thesis is based on work done by myself jointly with others, I have made clear exactly what was done by others and what I have contributed myself;
7. None of this work has been published before submission.

Signature:		Date:	

Acknowledgements

First and foremost, I would like to thank Steve Roberts for his guidance and mentorship throughout this project, as well as his support for my numerous geological jaunts over the past four years. I am indebted to Jamie Wilkinson for sharing his exhaustive knowledge of fluid inclusions with me, and in particular, for his guidance during the latter stages of this project. Both Steve and Jamie are also thanked for forming a sizeable proportion of the audience at my first international presentation…

Tom Gernon, Sandy Walker, Ryan Bartlett, Bruce Yardley, Libby Sharman and Cam McCuaig are all thanked for insightful discussions on basin processes, fluid geochemistry and the geology of the Zambian Copperbelt. I am grateful to Cathy Knight, Dave Catterall and the staff of Khoemacau Copper Mining (Ltd) Pty. for their support during fieldwork in Botswana, as well as discussions on the geology of the Kalahari Copperbelt.

I would like to express my gratitude to the Society of Economic Geologists and the Hugh McKinstry Fund for supporting this work, and in particular, Jean Cline, John Muntean and Borden Putnam for a memorable insight into the geology of the Carlin Trend.

I am thankful to Dan Doran and Matt Beverley-Smith for their technical assistance with fluid inclusion wafers, sheds and much more; Yannick Buret and Clara Wilkinson for guidance during laser ablation work at the NHM; Adrian Boyce and Alison McDonald for helping me to obtain and interpret stable isotope data at SUERC; and to Simon Kocher for his assistance on the SEM.

I am particularly grateful to Iain Stobbs for providing distractions where none were necessary, and for setting a benchmark for PhD woes that I could not hope to surpass.

No mention of thanks would be complete without including my parents, who may not understand another word of the succeeding chapters, but who were integral to the writing of every last one of them.

Last but not least, thank you to Abby, my field assistant in life and the most important rock of them all.

Definitions and Abbreviations

FIA	Fluid inclusion assemblage
KCB	Kalahari Copperbelt
LA-ICP-MS	Laser-ablation inductively coupled plasma mass spectrometry
LOD	Limit of detection
NHM	Natural History Museum, London
RSD	Relative standard deviation
SD or σ	Standard deviation
SEM	Scanning electron microscope
SUERC	Scottish Universities Environmental Research Centre
T_{CLATH}	Clathrate melting temperature
T_e	Eutectic temperature
T_{hCO2}	CO_2 homogenisation temperature
T_{hTOT}	Total homogenisation temperature
T_{hVAP}	Vapour homogenisation temperature
T_{HH}	Hydrohalite melting temperature
T_{mCO2}	CO_2 melting temperature
T_{mICE}	Final ice melting temperature
T_{mHAL}	Halite dissolution temperature
T_{mSYL}	Sylvite dissolution temperature
wt %	Weight percent
$\bar{x}$	Mean of population x

Chapter 1 Introduction

Global copper production has increased proportionally with population during the past century, resulting in an exponential increase in absolute copper production since the early 1900s (Fig. 1-1). Copper demand is primarily met through the exploitation of porphyry and sediment-hosted copper deposits which, together, account for over 80% of known copper (Singer, 2017). Although our understanding of porphyry systems and how to efficiently explore for them has advanced significantly in recent years (e.g. Sillitoe, 2010; Wilkinson et al., 2015), research into the fundamental basin-scale processes responsible for mineralisation in sedimentary-hosted copper systems has lagged behind, with only a few, generally deposit-specific, studies published.

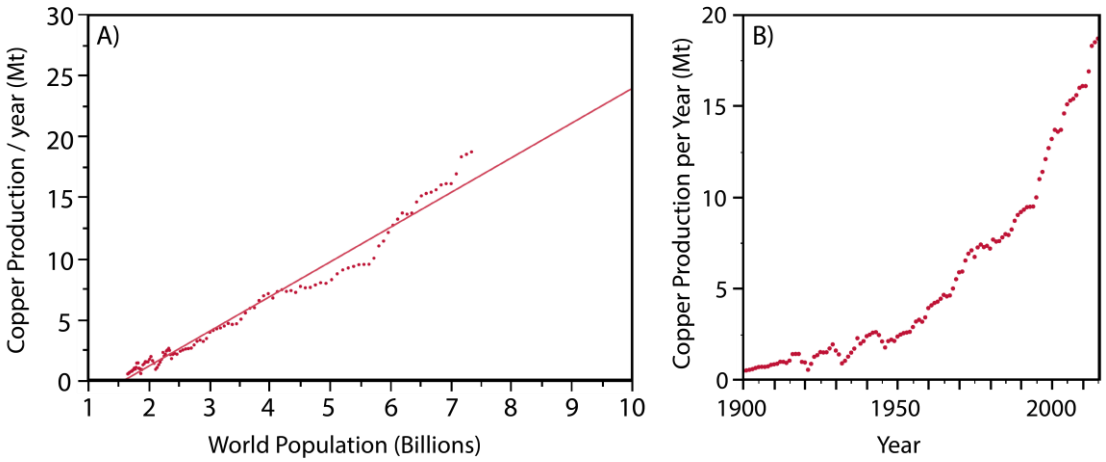

Fig. 1-1 Historic copper production plots A) Linear relationship between global copper production and population. B) Global copper production has increased exponentially since the early 1900s. Modified after Singer (2017).

1.1 Sediment-hosted Stratiform Copper Deposits

Sediment-hosted stratiform copper deposits result from the circulation of moderate temperature saline brines through sedimentary basins and represent the second-largest source of copper (after porphyry-Cu deposits) and the primary global source of Co (Hitzman et al., 2010). Deposits typically occur in fault-controlled sedimentary basins associated with intracontinental rifting, with Cu (± Co, Ag, Pb, Zn, Fe, U) enrichments occurring as broadly stratiform disseminations and within veins. Their high grades (Fig. 1-2) and favourable deposit geometry make them attractive exploration targets.

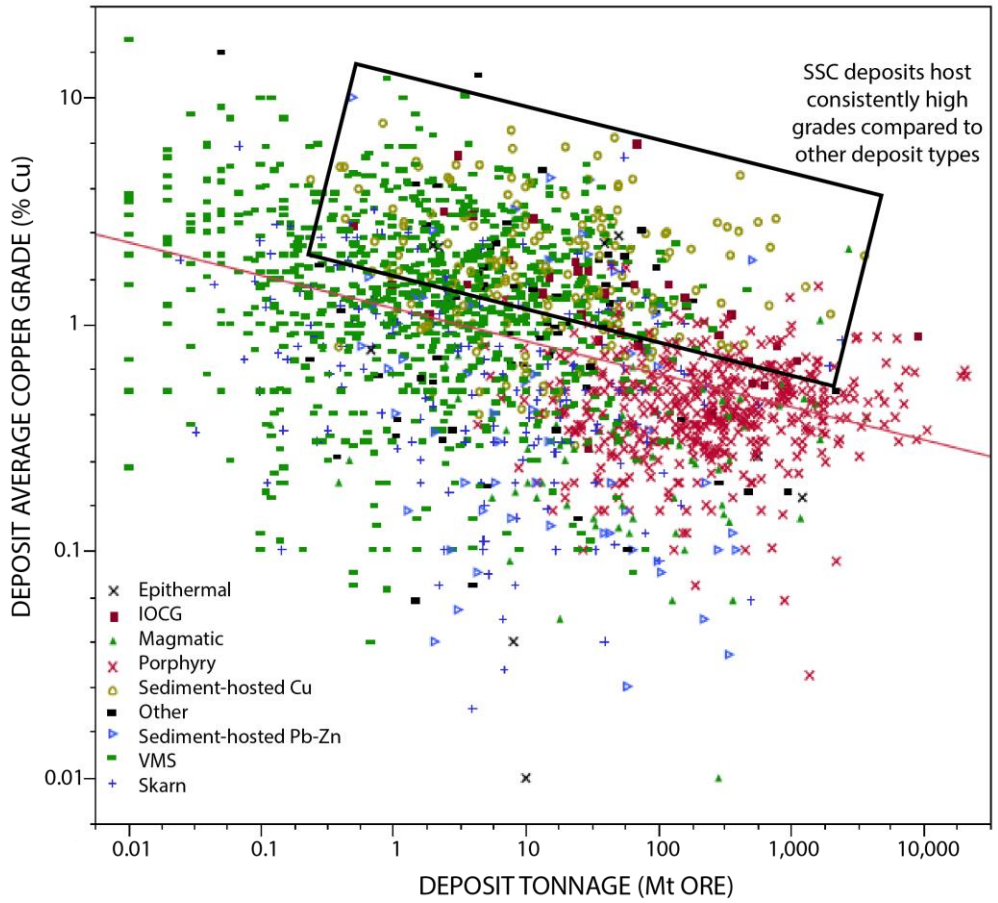

Fig. 1-2 Comparative grade-tonnage plot categorised by deposit type with a linear regression for all deposits, regardless of type. Sediment-hosted stratiform copper deposits consistently host higher Cu grades than most other deposit types, including porphyry systems. Modified after Singer (2017).

Sediment-hosted Cu deposits are characterised by a distinct sequence of rift-related sediments (Fig. 1-3). Thick packages of continental-derived, coarse grained oxidised siliciclastics ('red beds') are deposited during rift initiation and are typically overlain by deeper marine or lacustrine silts and shales. Many systems are capped by thick carbonate sequences and contain variable thicknesses of evaporitic strata. Metals are sourced from iron oxide and oxyhydroxide coatings around sediment grains in red bed sequences (Rose, 1976), with some authors proposing additional basement-derived copper sources (Koziy et al., 2009). Moderate to highly saline oxidised brines transport metals along basin margins or basement highs, primarily as chloride complexes. Metals are precipitated as copper (or copper-iron) sulphides through interactions with an *in situ* reductant (e.g. diagenetic pyrite or bacterially reduced sulphate) via an interaction similar to Equation 1.1, or a mobile reductant such as the mixing of an oxidised sulphate-bearing fluid with trapped hydrocarbons that have accumulated in a structural or stratigraphic trap (e.g. Equation 1.2).

$$2CuCl_3^{2-} + S^{2-} = Cu_2S + 6Cl^- \quad \text{(Equation 1.1)}$$

$$2CuCl_3^{2-} + SO_4^{2-} + CH_4 = Cu_2S + CO_2 + 2H_2O + 6Cl^- \quad \text{(Equation 1.2)}$$

The generation of sediment-hosted stratiform Cu deposits is typically constrained to within 30° of latitude from the palaeoequator due to the requisite presence of evaporites which are increasingly considered as integral in establishing a long-lived, hydrologically closed system in intracontinental rift basins. Evaporites not only provide a source of dense, saline brines for the system, but also act as a regional aquiclude, helping to seal ore fluids within the basin (Fig. 1-3) (Hitzman et al., 2005). Dissolution or rupturing of evaporitic seals during basin inversion has been proposed as a mechanism by which ore fluids may be focussed into areas containing reductants at higher stratigraphic levels (Hitzman et al., 2005; Hitzman et al., 2010).

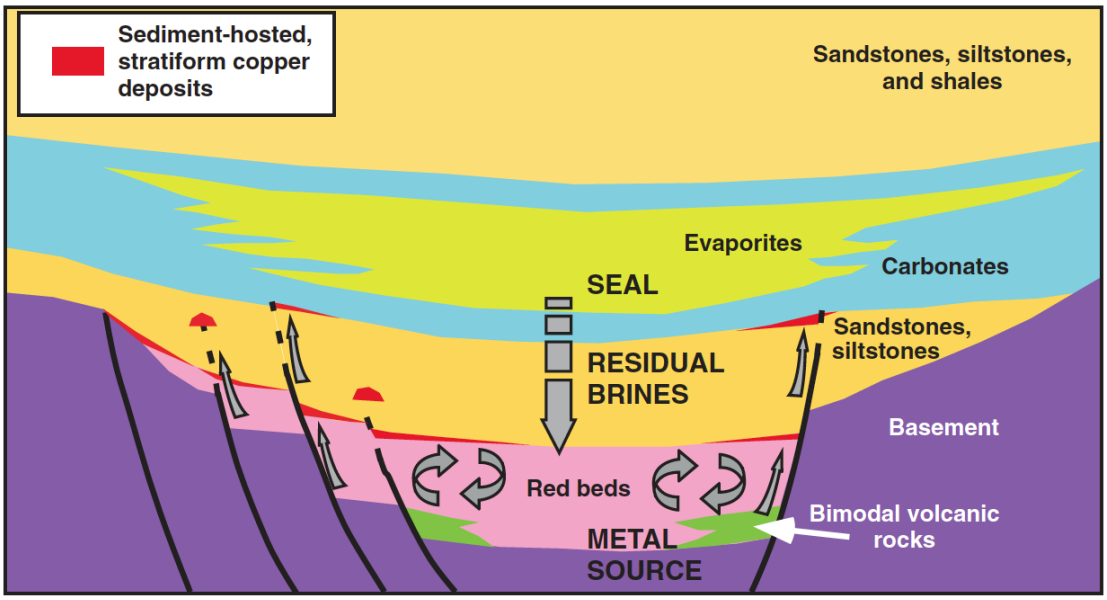

Fig. 1-3 Schematic cross-section through a typical sedimentary sequence in an intracratonic basin capable of generating sedimentary-hosted stratiform copper deposits. Cu is sourced from syn-rift red beds, bimodal volcanics and/or basement lithologies. Reduced, organic-rich siltstones and mudstones provide a redox trap for oxidised metalliferous brines. Heat from burial and/or igneous activity drives brine migration along basin margins, basement highs and deep-seated rift-related fault structures into structural or stratigraphic traps, with evaporites forming an effective seal. After Hitzman et al. (2010).

Establishing all of the necessary conditions to generate sediment-hosted Cu deposits on a large scale has been extremely rare through geological history, with only three known 'supergiant' deposits (>24 Mt contained Cu): the Palaeoproterozoic Kodaro-Udokan basin of Siberia; the Neoproterozoic Katangan Basin (Central African Copperbelt); and the Permian Zechstein Basin of

Central Europe (Kupferschiefer) (Fig. 1-4). Smaller contributions to total global sediment-hosted Cu resources come from the White Pine deposit in Michigan, USA and the Dzhezkazgan deposits of the Chu-Saryu basin, Kazakhstan (Box et al., 2012).

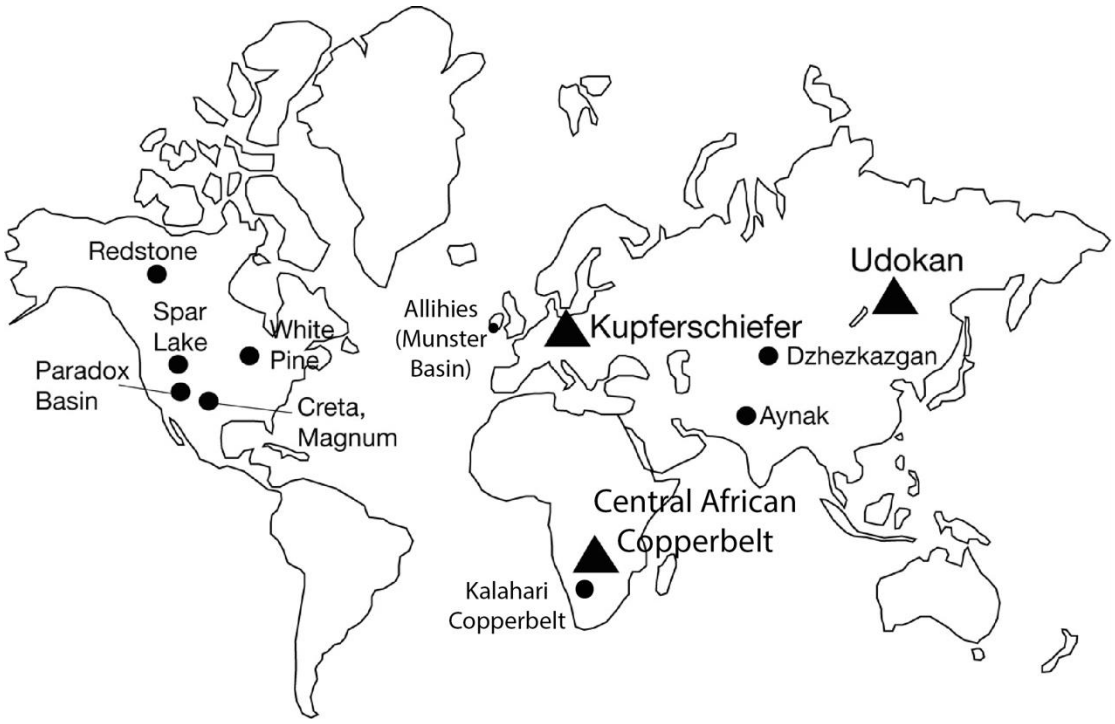

Fig. 1-4 Global distribution of significant sediment-hosted Cu deposits. The three 'supergiant' districts (>24 Mt contained Cu) are represented by triangular symbols. Smaller deposits are denoted by circular symbols. Modified from Hitzman et al. (2010).

The temporal distribution of sediment-hosted stratiform Cu deposits has been controlled by global-scale geologic processes throughout Earth's history, with no deposits forming until after the early Palaeoproterozoic Great Oxidation Event (~2.4 Ga) (Fig. 1-5). Following oxygenation of the atmosphere, oxidised red beds, the primary source of Cu in many basins, became prevalent and basinal brines became oxidised, often rich in sulphate as opposed to H_2S (Hitzman et al., 2010; Large et al., 2017). This transition to oxidising atmospheric conditions has subsequently promoted the diagenetic 'reddening' of basal clastic sequences - a process entailing the breakdown of mafic minerals by oxidised porewaters, forming ferric oxide and oxyhydroxide grain coatings. This process is thought to significantly increase the proportion of the bulk rock Cu content that is 'available' to pore fluids for remobilisation (Brown, 2009).

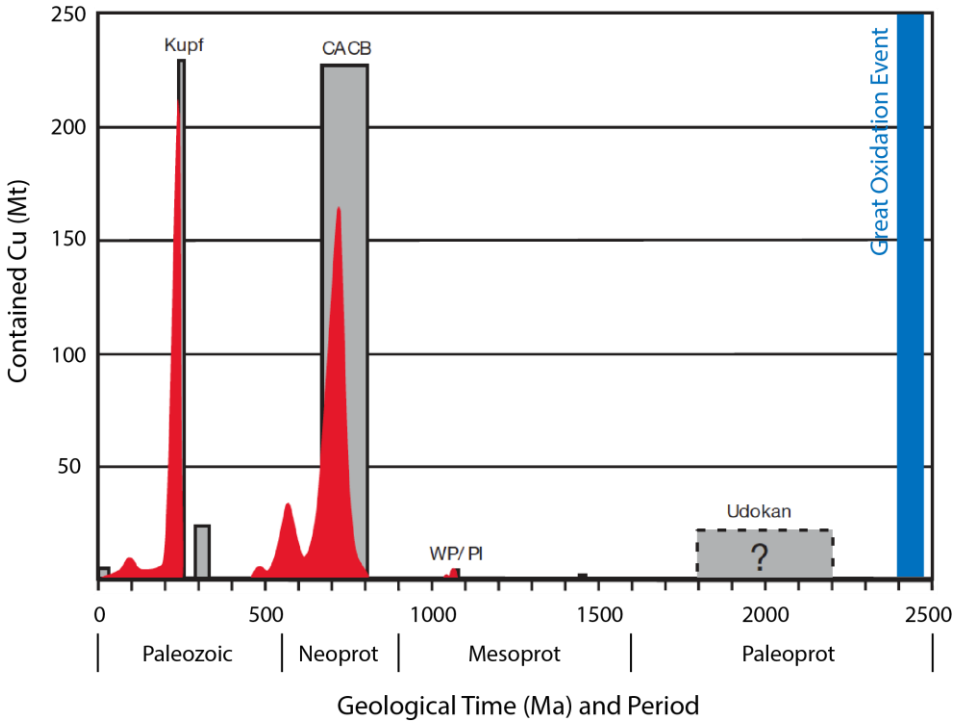

Fig. 1-5 Temporal distribution of major sediment-hosted Cu deposits. Grey bars represent the contained Cu (Mt) and approximate age of each of the major deposits. The red curve schematically illustrates the probable age of mineralisation in each district; the blue bar represents the approximate timing of the early Palaeoproterozoic Great Oxidation Event. Modified after Hitzman et al. (2010).

1.1.1 Brine generation and evaporites

The majority of brines responsible for sediment-hosted stratiform Cu mineralisation are marine-derived. As such, it is important to understand how seawater compositions have changed through time and how these changes might be favourable for the generation of fertile proto-ore fluids. Typically, the cationic composition of seawater-derived brines is susceptible to modification through fluid-rock interaction, particularly in long-lived basins. Anions such as Cl^-, Br^- and I^- behave far more conservatively and remain relatively unmodified through a basin's history.

Evidence for past seawater compositions comes primarily from estimates based on halite-hosted fluid inclusions which show secular variation in chemistry throughout the Phanerozoic (Lowenstein et al., 2003; Lowenstein et al., 2001). Parts of the late Precambrian (544-543 Ma), Permian (258-251 Ma) and Tertiary to present (40-0 Ma) are thought to be periods of relatively elevated Na^+ and Mg^{2+}/Ca^{2+}, with $MgSO_4$ salts prevailing, whereas parts of the Cambrian (540-520 Ma), Silurian (440-418 Ma) and Cretaceous (124-94 Ma) were characterised by relatively low Na^+ and Mg^{2+}/Ca^{2+} (Fig. 1-6) (Lowenstein et al., 2001).

Oscillations between 'calcite seas' (interpreted to generate $CaCl_2$-rich basin brines) and more Mg-rich 'aragonite' seas are thought to be in response to global tectonic cycles, rates of sea floor spreading and volcanism (Hardie, 1996). Prior to the Phanerozoic, secular variation in seawater chemistry is much less well understood, primarily due to the non-preservation of marine evaporite deposits. However primary inclusions in recrystallised halite from the Amadeus and Officer Basins, central Australia, indicate a period of $CaCl_2$-rich (SO_4-poor) seas for up to 200 million years during the middle Neoproterozoic (Kovalevych et al., 2006), broadly coinciding with the breakup of the Rodinian Supercontinent and the formation of several basins which host world-class stratiform Cu deposits.

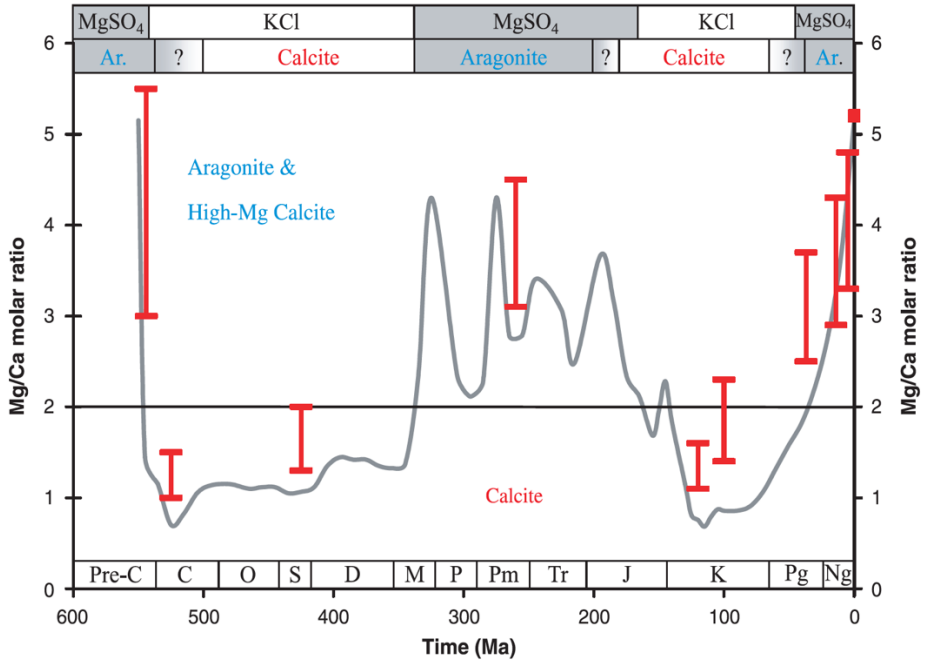

Fig. 1-6 Secular variation of Phanerozoic seawater Mg^{2+}/Ca^{2+} estimated from halite-hosted fluid inclusions. Horizontal line represents approximate threshold between 'calcite seas' and 'aragonite seas'. Red bars represent the primary mineralogies of nonskeletal carbonates precipitated throughout the Phanerozoic. After Lowenstein et al. (2001).

Evaporites form an integral part of most of the largest sediment-hosted Cu systems, acting as a key source of brines as well as channelling and sealing fluid flow. Seawater chemistry is the dominant factor in evaporite mineralogy, with increasing evidence for 'typical' evaporite sequences changing through geologic time (Bąbel and Schreiber, 2014). Evaporation of modern day seawater typically precipitates calcium carbonate $CaCO_3$, followed by gypsum ($CaSO_4$) and halite (NaCl), with magnesium sulphate ($MgSO_4$), sylvite (KCl) and other Mg-K species only precipitated during the advanced stages of evaporation (Fig. 1-7).

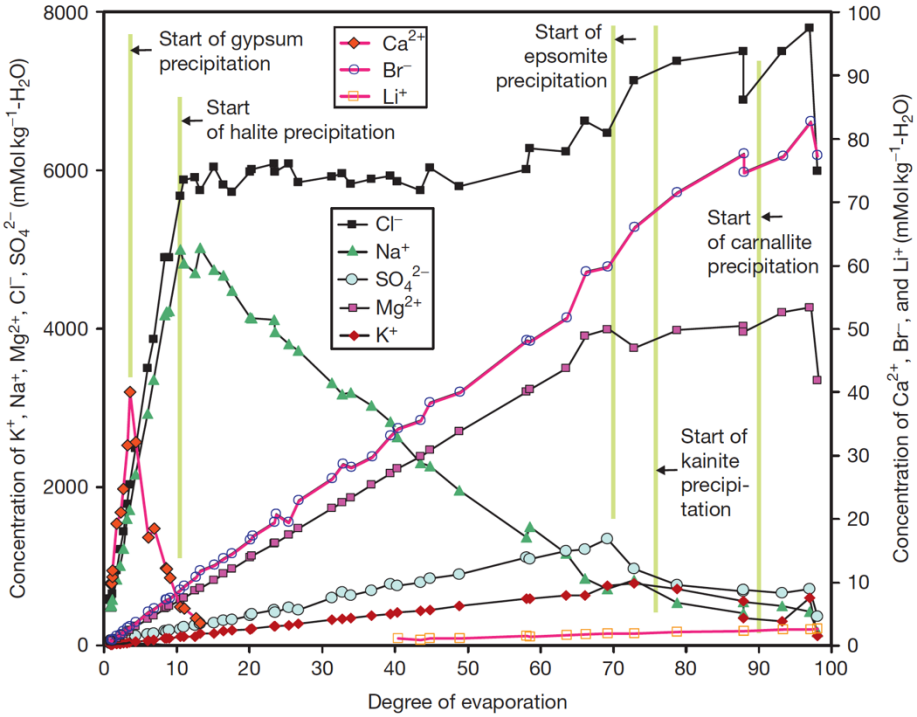

Fig. 1-7 Key ion concentrations in closed system evaporation of modern day Caribbean seawater. Epsomite ($MgSO_4 \bullet 7H_2O$); kainite ($4KCl \bullet 4MgSO_4 \bullet 11H_2O$); carnallite ($KCl \bullet MgCl_2 \bullet 6H_2O$). After Bąbel and Schreiber (2014) using data from McCaffrey et al. (1987) and Warren (2006).

This sequence assumes closed system evaporation of modern-day seawater, when in reality, brine recharge leads to precipitation of modified mineral suites. Evaporation of ancient seawater compositions with relatively low Na^+, Mg^{2+}/Ca^{2+} and SO_4 levels also resulted in contrasting evaporite stratigraphies (e.g. Bonneville Salt Flats, Utah) (Valyashko, 1962). Reconciling paleo-seawater compositions and associated unconventional evaporation sequences with Neoproterozoic evaporitic strata (e.g. Duruchaus Fm., Namibia, Behr et al. (1983)) is, however, invariably challenging due to their non-preservation.

Evaporites continue to expel brines long after evaporitic processes have ceased, with compaction, dewatering and recrystallisation all occurring during burial (Warren, 2016). Further brine expulsion, as well as large-scale porosity, can result from pervasive dissolution of subsurface evaporites later in a basin's history (Jackson et al., 2003; Selley et al., 2018), with rupturing of evaporitic seals during basin inversion advocated as a mechanism by which metalliferous brines may reach higher stratigraphic levels (Hitzman et al., 2005; Hitzman et al., 2010).

1.2 Base Metal Concentrations in Crustal Fluids

Aqueous solutions are the primary transport agent of most precious and base metals through the Earth's crust. Hydrothermal fluids of varying temperature, salinity, pH and redox state facilitate the

dissolution, transport and concentration of economically important minerals from bulk volumes of rock into spatially and chemically concentrated ore deposits. Over the past decades, research has been inconclusive regarding the question of whether hydrothermal fluids require anomalously high levels of a particular metal in order to form an ore deposit (cf. Wilkinson et al., 2009), or whether large volumes of relatively dilute fluids are capable of forming ore deposits, given the correct physicochemical trapping conditions (Barnes, 1979; Fyfe et al., 1978; Yardley, 2005).

1.2.1 Controls on base metal solubility and precipitation

Aqueous crustal fluids possess unique properties enabling them to dissolve, transport and precipitate metals extremely effectively in a range of physicochemical conditions. Water is often termed the 'universal solvent', with polar H_2O molecules ideally suited to stabilising ions and dissociating weaker polar molecules. Fig. 1-8 shows how water is able to dissolve hydrophilic substances such as sodium chloride (NaCl), forming highly saline solutions.

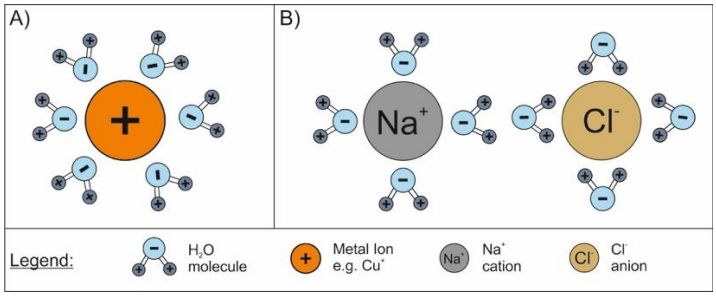

Fig. 1-8 Molecular properties of H_2O as a solvent. A) Stabilisation of a metal ion through the formation of a hydration shell. B) The ionic bonding of polar NaCl molecules is broken apart by the attractive forces of the covalently bonded H_2O molecules. Following dissociation of the NaCl molecule the Na^+ and Cl^- ions are hydrated in a process similar to that shown in (A).

Whilst water molecules are intrinsically suited to the dissolution of many ions, a ligand is required to form a coordination complex capable of being transported in solution. There are a significant number of ligands that can potentially facilitate metal transport, however the availability of ligands as well as the stability of different ligand complexes limits the number of likely complexes in natural systems. Pearson (1963) proposed that in a competitive environment, "hard" acids (small and strongly charged metal ions) will preferentially bond with hard bases, whereas "soft" acids (large, weakly charged metal ions) will preferentially bond with soft bases (Table 1-1). Copper, for example, occurs as either Cu^+ or Cu^{2+} in hydrothermal fluids and is primarily complexed with either Cl^- or HS^-, depending on temperature, pH and ligand availability (Candela and Holland, 1984; Williams-Jones and Migdisov, 2014).

Table 1-1 Common acids and bases classified using the Hard/Soft Acid/Base Principle (Pearson, 1963)

Hard	Borderline	Soft
	Acids	
H^+, Na^+, K^+, Al^{3+}, Fe^{3+}, Co^{3+}, As^{3+}, Si^{4+}, $Zr,^{4+}$, Mo^{4+}, W^{4+}	Fe^{2+}, Mn^{2+}, Co^{2+}, Ni^{2+} Cu^{2+}, Sn^{2+}, Zn^{2+}, Pb^{2+}	Au^+, Ag^+, Cu^+, $Hg^{+,}$ Hg^{2+}, Cd^{2+}, Pt^{2+}, Pd^{2+}
	Bases	
F^-, OH^-, CO_3^{2-}, HCO_3^-, SO_4^{2-}, HSO_4^-, NH_3	Cl^-, SO_3^{2-}	HS^-, H_2S, CN^-, I^-, Br^-

Helgeson (1970) recognised that the chloride anion is the most important complexing ligand for a wide range of base metals, partly due to its ability to bond with a wide range of cations, but also as a result of its abundance in natural fluids relative to other ligands (Yardley, 2005). Most base metals can form multiple different chloride complexes, for example Cu^{2+}:

$$Cu^{2+} + Cl^- = CuCl^+ \quad \text{(Equation 1.3)}$$

$$Cu^{2+} + 2Cl^- = CuCl_2^\circ \quad \text{(Equation 1.4)}$$

$$Cu^{2+} + 3Cl^- = CuCl_3^- \quad \text{(Equation 1.5)}$$

Due to the highly conservative nature of the halogens in hydrothermal solutions, fluid-rock interactions rarely significantly influence their chlorinity, which is instead controlled by the fluid source. A notable exception is interaction with evaporite deposits, where the dissolution of halite can dramatically increase the chlorinity of a fluid. As such, assessing the concentration of Cl^- as well as its role in metal complexation is particularly relevant when studying sedimentary-hosted copper systems, which commonly occur in basins hosting evaporitic strata (Borg et al., 2012; Hitzman et al., 2005). The availability of Cl^- ions is also directly associated with temperature and pressure. With increasing pressure, Na^+ and Cl^- are more stable as simple ions, thereby promoting the abundance of metal-chloride coordination complexes. Perhaps counter intuitively, increasing temperature has the inverse effect, progressively associating the NaCl ion pair, thereby reducing the availability of simple Cl^- ions for complexing (Williams-Jones and Migdisov, 2014). However, metal chloride complexes are typically far more stable at higher temperatures, counteracting decreased chloride ion activity and resulting in a net increase in metal chloride solubility with both temperature and pressure.

Temperature and, to a lesser degree, chlorinity, emerge as first-order controls on the solubility of most base metals in hydrothermal fluids. This conclusion was demonstrated by Yardley (2005) using geochemical analyses of fluids from a broad spectrum of crustal environments. The data showed a strong correlation between temperature ± chlorinity and their base metal concentrations. Here,

the fluid database collated by Yardley (2005) is expanded to include various datasets ranging from low temperature oilfield brines to high temperature-salinity magmatic fluids (Fig. 1-9).

Iron, Mn, Pb and Zn show much stronger correlations with temperature and chlorinity than Cu. This may be, in part, a data bias due to the relative abundance of analyses for Fe, Mn, Pb and Zn, however it also likely reflects the complexing chemistry of each metal, with Fe, Mn, Pb and Zn almost exclusively transported as chloride complexes in naturally occurring hydrothermal fluids, whereas Cu is complexed by both chlorine and sulphur in various different hydrothermal environments. Sulphur typically complexes with copper in the form of hydrosulphide species (HS^- and $H_2S_{(aq)}$). Various simulations and experimental studies in recent years have highlighted the importance of different ligands for copper transport at a range of temperature, pressure, pH and Eh conditions (Brugger et al., 2016; Etschmann et al., 2010; Mei et al., 2013; Seward et al., 2014; Williams-Jones and Migdisov, 2014; Zhong et al., 2015). Typically, copper transport is considered to be dominated by linear chloride complexes of the monovalent ion (Cu[I]) at temperatures <500°C (Etschmann et al., 2010; Zhong et al., 2015), with copper bisulphide complexes predominating in S-bearing high temperature fluids and sulphur-rich or chlorine-poor solutions at lower temperatures (Brugger et al., 2016). A series of molecular dynamics simulations lead Mei et al. (2013) to suggest that Cu(I) shows the following ligand preference: $HS^- > Cl^- > H_2S$. This indicates increased importance for sulphur as a complexing ligand at lower temperatures and is supported by predominance diagrams constructed by Williams-Jones and Migdisov (2014), who show CuHS° as the dominant coordination complex at moderate pH conditions in chlorine- and sulphur-bearing fluids at 200°C. As such, in addition to chlorine, the presence (or absence) of sulphur in a fluid likely imposes a strong control on how copper is complexed and transported over a wide range of temperature, pH and Eh conditions.

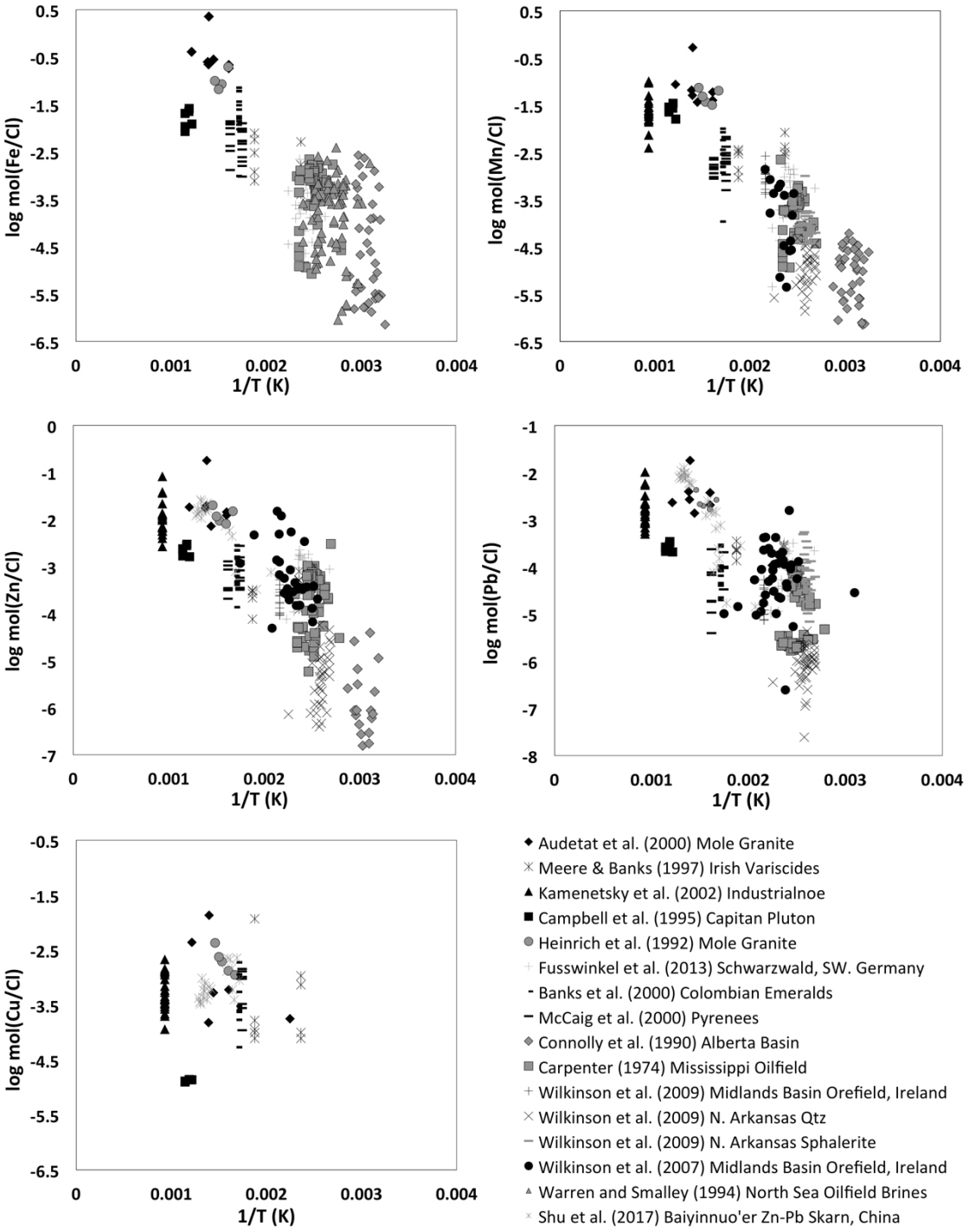

Fig. 1-9 Crustal fluid temperature-chlorinity plots demonstrating their first-order control on hydrothermal fluid base metal concentrations. Temperatures range from approximately ambient temperature to 750°C. Modified after Yardley (2005) with data from (Audetat et al., 2000; Banks et al., 2000; Campbell et al., 1995; Carpenter et al., 1974; Connolly et al., 1990; Fusswinkel et al., 2013; Heinrich et al., 1992; Kamenetsky et al., 2002; McCaig et al., 2000; Meere and Banks, 1997; Shu et al., 2017; Warren and Smalley, 1994; Wilkinson et al., 2007; Wilkinson et al., 2009).

1.2.2 Predicting the base metal content of hydrothermal fluids

Having reviewed the physicochemical factors that control base metal solubility in hydrothermal fluids, a database of crustal fluid compositions, initially compiled by Yardley (2005) and updated in this study, is utilised here to predict the metal content of potential ore-forming fluids based on their temperature and chlorinity alone. The dataset includes examples of shield brines, oilfield brines, metamorphic brines and magmatic and geothermal fluids, none of which have been chosen specifically as 'ore fluids' but simply as fluids locally equilibrated with silicate rocks at given *P/T* conditions (Yardley, 2005). The fluid samples are primarily derived from naturally occurring fluid inclusions, with some deep borehole fluid samples also used to represent relatively low temperature oilfield brines.

In order to test the veracity of metal concentration predictions made using the trends established from magmatic fluids and basinal brines (Fig. 1-9), two data sets with laser ablation ICP-MS major and trace element analysis and corresponding microthermometry of individual fluid inclusions were investigated from different metallogenic systems. Fusswinkel et al. (2013) reported fluid inclusions from a basement-hosted quartz-fluorite-barite-Pb-Zn vein system in the German Schwarzwald. Using these data, Fe, Mn, Zn and Pb concentrations were predicted using the relationship between the log molar ratio of metal/Cl and the reciprocal of the fluid temperature (Fig. 1-10). Predicted metal concentrations are highlighted in red, with measured metal concentrations highlighted in blue. Predicted metal concentrations form a linear trend defined by the dataset presented in Fig. 1-9. The majority of measured Mn, Zn and Pb concentrations from the Fusswinkel et al. (2013) dataset are slightly higher than predicted, implying either a degree of metal enrichment above normal crustal fluid levels or the presence of a more significant role for one of the previously discussed second-order controls on metal solubility such as pH or fO_2. Although measured metal concentrations show a greater degree of scatter, they are in broad agreement (order-of-magnitude) with predicted metal concentrations, supporting the principle that base metal concentrations are predominantly controlled by temperature and chlorinity. Given that the fluids reported by Fusswinkel et al. (2013) are directly associated with Pb-Zn mineralised rocks, Fig. 1-10 also supports the hypothesis that 'ore fluids' need not necessarily be anomalously enriched in the metals of interest and that such fluids are chemically indistinguishable from other crustal fluids (Yardley, 2005).

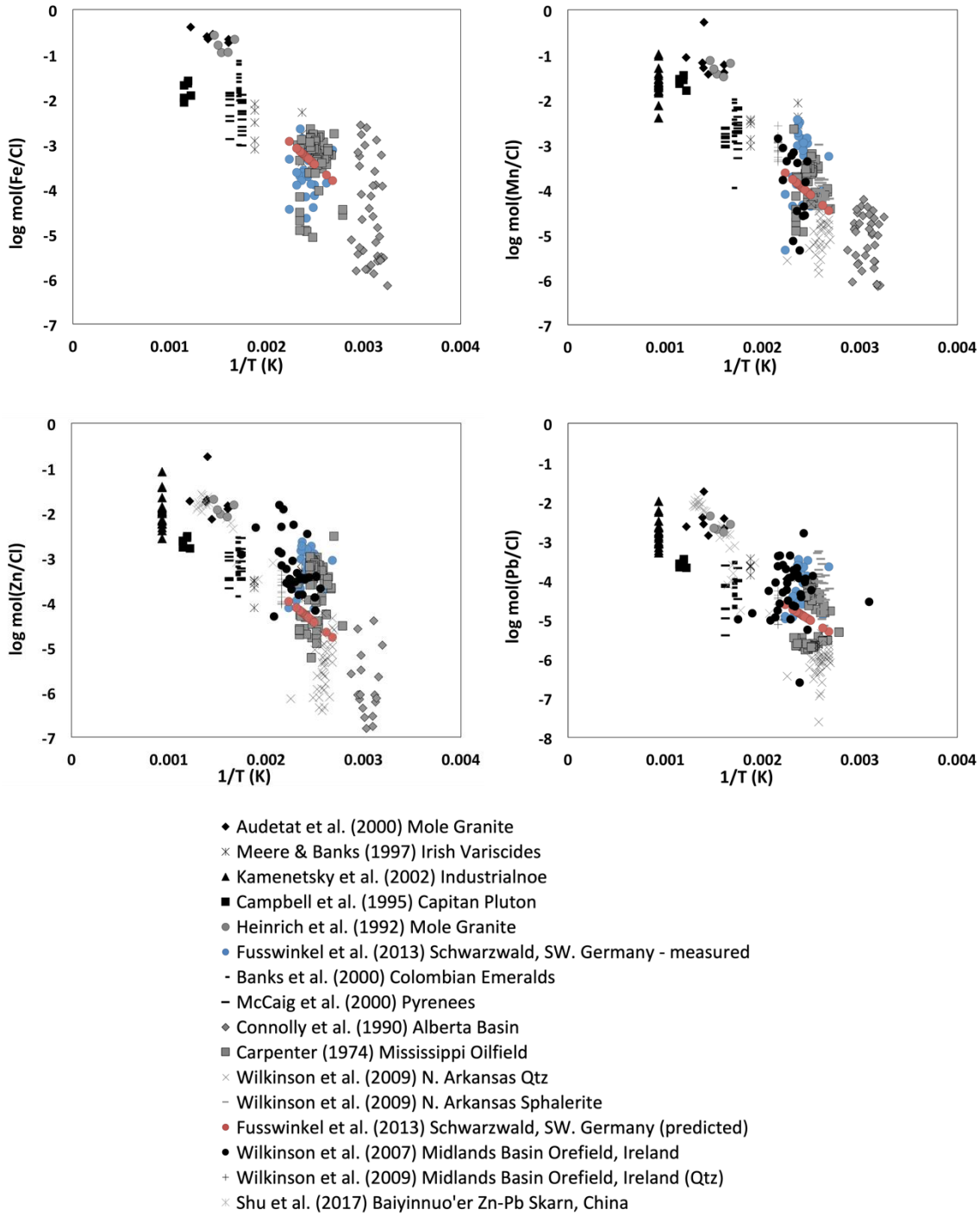

Fig. 1-10 Measured and predicted base metal concentrations in Schwarzwald fluids (Germany). Measured values are highlighted in blue and predicted values in red. Predictions made using the equations for linear trends defining the background datasets (greyscale data points from Fig. 1-9). Schwarzwald data from Fusswinkel et al. (2013). All other data are from the sources cited in Fig. 1-9.

Using the same approach, Pb concentrations in fluid inclusions from co-existing, spatially associated quartz and sphalerite in veins from the Ozark Plateau, Arkansas, were investigated. Fluid inclusion homogenisation temperatures and chlorinity were derived from Wilkinson et al. (2009) and predictions compared to measured Pb concentrations from the same study. These data show a greater degree of spread from predicted values, primarily due to apparent enrichment and depletion of Pb in sphalerite- and quartz-hosted inclusions, respectively. The coincident apparent metal enrichment of sphalerite-hosted inclusions and depletion of quartz-hosted inclusions in Fig. 1-11 could be interpreted as representing an initial phase of Pb-Zn sulphide mineralisation, with 'spent' ore fluids subsequently trapped in co-existing gangue quartz. However this interpretation is not supported by halogen systematics, which suggest that sphalerite and quartz-hosted inclusions were derived from two distinct origins (Stoffell et al., 2008). As such, these data lend credence to the alternative hypothesis that some 'ore fluids' are distinctly enriched in certain metals (by two orders of magnitude or more), resulting in an increased likelihood of the formation of a hydrothermal ore deposit.

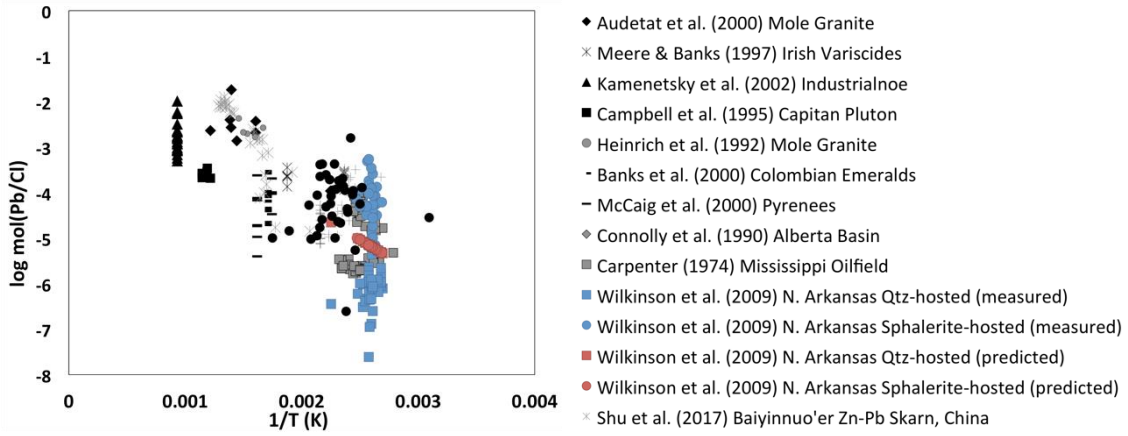

Fig. 1-11 Measured and predicted Pb concentrations in Ozark Plateau fluids. Measured Pb concentrations in co-existing quartz and sphalerite are highlighted in blue, with predicted values in red. Predictions were made using the same method and data as Fig. 1-10 and Arkansas fluid data was sourced from Wilkinson et al. (2009). All other data are from the sources cited in Fig. 1-9.

In order to test the hypothesis that anomalously metal-enriched brines were responsible for the formation of the Central African Copperbelt, approximate concentrations of Fe, Mn, Pb and Zn in ore-forming fluids are predicted and graphically represented in Fig. 1-12. Predictions have been made using the method outlined above, using average primary fluid inclusion homogenisation temperatures, as well as chlorinity estimations derived from leachate analysis of vein-hosted fluids from five Zambian deposits (Lumwana, Nchanga, Kansanshi, Konkola and Konkola North) (Nowecki, 2014). Predicted concentration ranges are intended only as order-of-magnitude estimations and are compared with measured base metal concentrations in Chapter

7. The estimated concentrations will be used to assess whether ore-forming fluids in the Zambian Copperbelt were anomalously fertile or whether they transported predictable base metal concentrations and simply represent thermal ± salinity anomalies relative to other sedimentary basin environments.

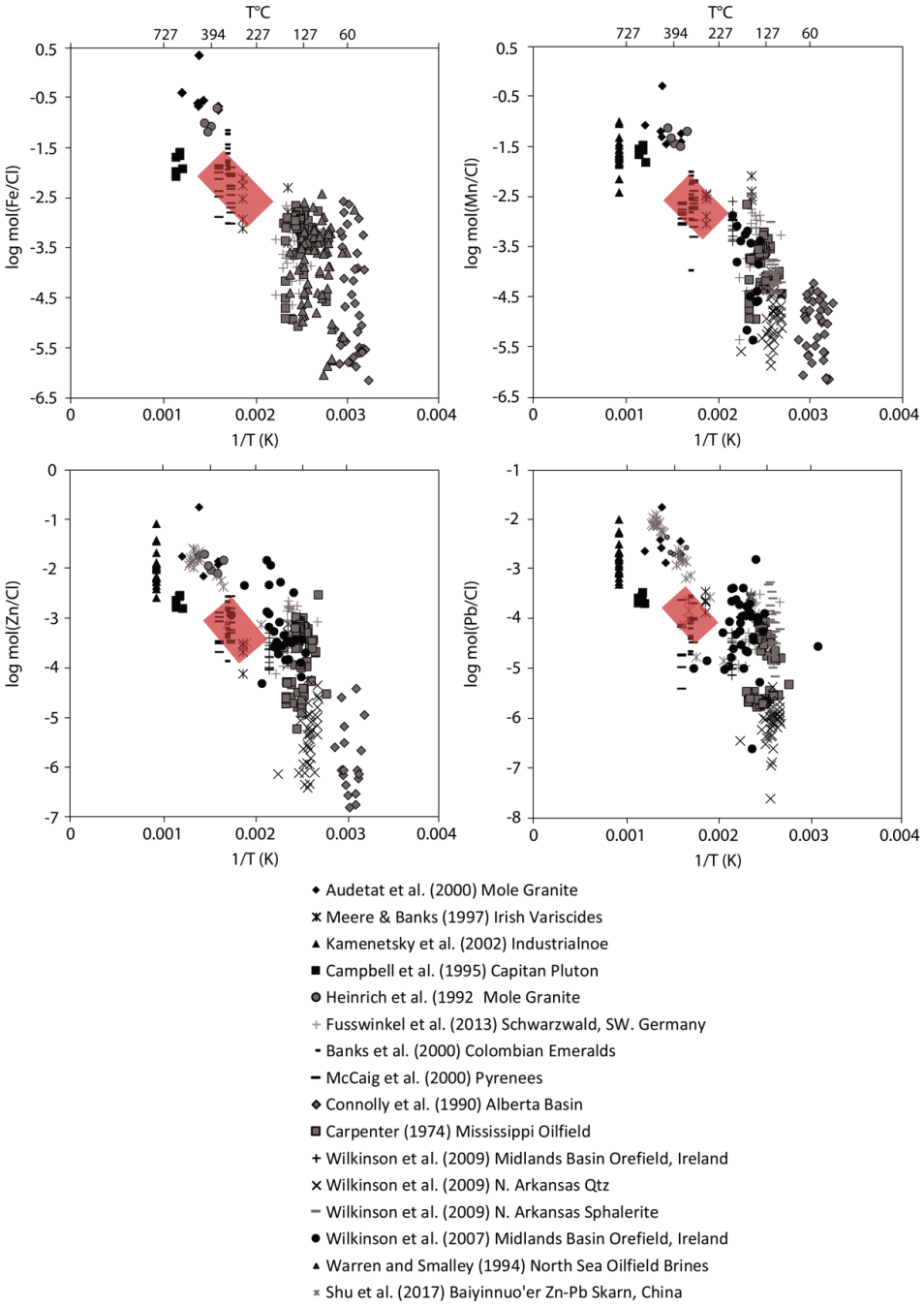

Fig. 1-12 Predicted Fe, Mn, Zn and Pb concentration ranges for Zambian Copperbelt fluids based upon average fluid inclusion homogenisation temperatures and bulk leachate analyses of vein-hosted fluids from five Zambian deposits (Lumwana, Nchanga, Kansanshi, Konkola and Konkola North) using data from Nowecki (2014). Red shaded areas represent order-of-magnitude approximations of base metal concentrations.

1.3 Rationale

As outlined in section 1.1, sediment-hosted copper deposits account for a significant proportion of global Cu supply and represent the primary source of Co. Both of these metals are essential components of developing technologies and the electric vehicle revolution in particular. It is therefore crucial that we understand the primary controls on Cu-Co transport and mineralisation in order to more efficiently explore for these metals in both brownfield and greenfield terrains. This study aims to contribute to our understanding of sediment-hosted copper systems through the characterisation and quantification of fluid chemistries and base metal concentrations in palaeofluids from five deposits across two collisional belts of contrasting ages. Together, Nkana-Mindola, Nchanga and Lumwana in the Lufilian Belt and the Zone 5 prospect in the Ghanzi Ridge region of the Damaran Belt represent four deposits along the Neoproterozoic to earliest Palaeozoic Pan-African collisional belt. The Allihies deposit in the Munster Basin (Ireland) represents smaller-scale, red bed-type mineralisation in the western domain of the Late Palaeozoic Variscan Orogeny. Through a variety of analytical methods, primarily applied to quartz and carbonate vein-hosted fluid inclusions from the five deposits, this study aims to answer the following research questions:

1. Were the fluids responsible for mineralisation in the world's largest repository of sediment-host copper and cobalt, the Central African Copperbelt, anomalously metal enriched or are they chemically indistinguishable from the fluids present in smaller-scale systems?
2. Were fluids in the Zambian Copperbelt equally fertile over the entire duration of basin history or were certain fluid generations and periods of basin history responsible for punctuated mineralisation events?
3. How do metal ratios and the major cation chemistry of palaeofluids differ between deposits, both within and outside of the Zambian Copperbelt, and how does this relate to the metal tenor and ratios of the associated mineralised rocks?

Although studies have quantified metal concentrations in some hydrothermal ore systems (e.g. Irish-type, MVT and porphyry systems) (Audetat et al., 1998; Wilkinson et al., 2009) similar data are largely absent for sediment-hosted Cu deposits and for certain metals, such as Co. It is only through expanding the dataset across a wider range of deposit types and commodities, that the fundamental question of whether 'ore fluids' and 'typical crustal fluids' are physicochemically distinct or identical can be answered.

This thesis is comprised of three original research papers (Chapters 4-6), assessing various aspects of palaeofluid fertility in sediment-hosted Cu systems. Additional chapters provide detail on the methods employed throughout the study, as well as further results and a final discussion

considering the broader implications of all three research papers as a coherent body of work. The subsequent chapters are outlined as follows:

Chapter 2: Methodology

Provides a detailed account of the sampling and analytical procedures used to acquire the data presented in the subsequent chapters.

Chapter 3: Background Geology and Deposit Overviews

This chapter provides an introduction to each of the study areas and presents some introductory field-based data and observations not included in the research papers that follow.

Chapter 4: Copper- and cobalt-rich, ultra-potassic bittern brines responsible for the formation of the Zambian Copperbelt

A short-form research paper presenting some key results from the Nkana-Mindola deposit. The temporal and compositional nature of contrasting brine generations is discussed and a model for the generation of unusually potassic fertile ore fluids is proposed.

Chapter 5: Were Zambian Copperbelt Fluids Anomalously Metal Enriched? A Geochemical Comparison of Basin Brines in the Pan-African Belt

Fluid inclusion petrography, microthermometry, cathodoluminescence, laser ablation ICP-MS, SEM and stable isotope data from all four Pan-African deposits are presented and discussed. Fluid characteristics are broadly consistent between several Zambian Copperbelt deposits and the model proposed in Chapter 4 is expanded. Comparisons are drawn between fluid timings, compositions and origins in the Zambian and Kalahari Copperbelts.

Chapter 6: Sediment-hosted Copper Mineralisation in the Munster Basin: Characterising ore fluid chemistry at the Allihies deposits

A research paper focussed on the composition of palaeofluids in barren and mineralised vein sets at the Allihies sediment-hosted Cu deposit in the Munster Basin. Fluid inclusion petrography, microthermometry, laser ablation ICP-MS and stable isotope data provide insights into the relative timing and mechanisms of mineralisation. Proposed ore fluid compositions are also compared with fertile brines from the world-class deposits of the Zambian Copperbelt and the relative importance of different fluid characteristics is discussed.

Chapter 7: Implications of Fluid Chemistry on the Metal Endowment of the Zambian Copperbelt

A brief discussion addressing the concept of 'anomalous enrichment' of hydrothermal ore fluids with particular reference to the Zambian Copperbelt and an assessment of likely metal sources in such systems using Monte Carlo simulations.

Chapter 8: Conclusions

This chapter draws together the main conclusions from all five deposits, comparing and contrasting fluid histories and assessing the significance of the results within a broader spectrum of sediment-hosted base metal deposits. Recommendations are made for future work to enhance our understanding of sediment-hosted copper systems.

Chapter 2 Methodology

The primary aim of this study is to characterise and quantify the chemistry of palaeofluids associated with sediment-hosted copper (± Co, Ag, Pb, Zn) mineralisation in order to test the hypothesis that world-class deposits are associated with anomalously metal-rich brines. Palaeofluids from a variety of settings and deposits across the Pan-African Belt and the Munster Basin, Ireland, have been characterised, primarily through an extensive fluid inclusion study.

Fluid inclusion petrography and microthermometry provides the basis for this study, with the textural context of approximately 1500 inclusions characterised, along with estimations of salt chemistry, minimum trapping temperature and salinity. This is prerequisite data for more novel analytical techniques such as fluid inclusion laser-ablation inductively coupled plasma mass spectrometry (LA-ICP-MS), whereby individual, texturally constrained, inclusions are ablated and major and trace element concentrations quantified (Gunther et al., 1998; Heinrich et al., 2003). Analysis of stable isotope systematics (oxygen, hydrogen and sulphur) provide insights into fluid sources, mixing and fluid-rock interactions, as well as mineralisation processes and conditions (Taylor, 1997; Thode, 1991).

Fig. 2-1 summarises the typical workflow of analytical methods employed in this study to characterise and quantify the geochemistry of different fluid generations and assess mineralisation processes in contrasting sediment-hosted copper systems.

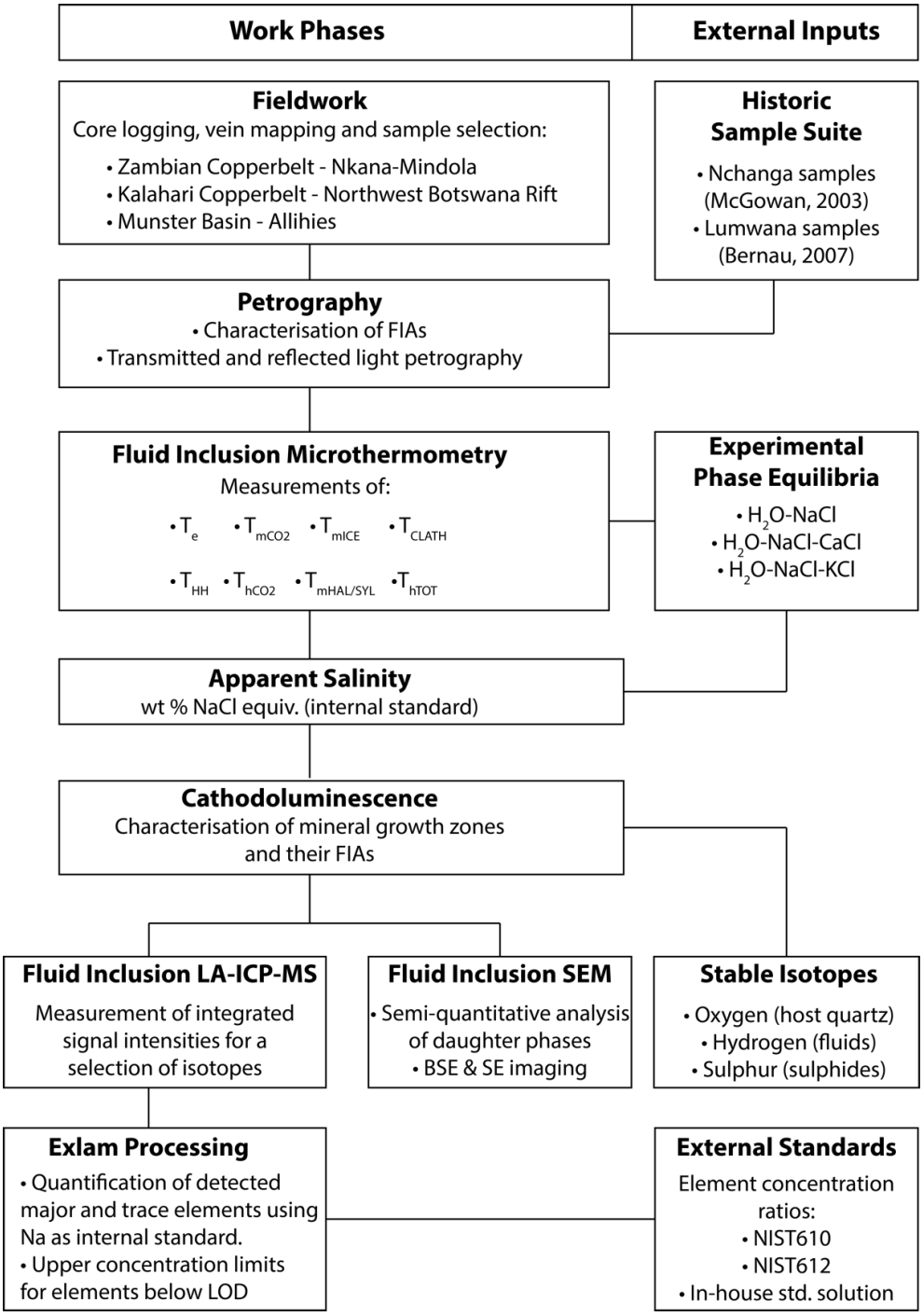

Fig. 2-1 Methodology workflow summarising the principal analytical components of this study. Modified from Heinrich et al. (2003).

2.1 Fieldwork and Sampling

This study primarily focuses on the properties of fluid inclusions trapped in both mineralised and barren quartz and carbonate veins. Vein material, along with representative host rock samples were collected during three separate field campaigns:

Allihies (Munster Basin, Ireland):

Fieldwork took place over a one-week period in March 2016 and involved observation of vein mineralogy, kinematics and relationships with host rocks, as well as measurement of structural features and sampling of 21 veins in the near-mine area and a further 4 veins from Inch, approximately 56 km north of Allihies. Particular note was taken of the structural trends of each vein as well as their timing, relative to Variscan fabrics in the area. A sample list is presented in Appendix A.2.5.

Zambian Copperbelt:

Fieldwork took place over a two-week period in June 2016, with particular focus on the Nkana-Mindola deposits. A total of 26 samples were taken from three different open pits along a strike length of approximately 15 km, with a further 34 samples taken from drillcore in the Mindola North deposit, as well as drillcore from exploration targets elsewhere in the Copperbelt. A total of 1400 m of drillcore was logged, with summary logs and a sample list presented in appendices C.7 and 0, respectively.

Kalahari Copperbelt (Botswana):

Fieldwork took place at the Zone 5 project (Northwest Botswana) in August 2017. A total of eleven drillcores were selected, spanning approximately 4 km strike length, from SW to NE of the Zone 5 prospect. Key intervals of stratigraphy were selected in each of the drillcores for more detailed logging (decimetre scale). A total of 32 samples were taken from the drillcores (quarter core), primarily consisting of quartz-carbonate vein material as well as some host lithologies and examples of disseminated sediment-hosted ore. Digitised summary logs for all 11 drillcores studied are presented in Appendix C.7.

Upon arrival in Southampton, samples were photographed and sub-sampled for the production of doubly-polished fluid inclusion wafers, thin sections, polished thin sections and polished blocks. A portion of each sample was retained for future reference.

In addition to the 60 samples collected from the Zambian Copperbelt during the 2016 field campaign, the author had access to an extensive sample suite from three previous PhD projects at

the University of Southampton (Bernau, 2007; McGowan, 2003; Nowecki, 2014). The samples were from a range of deposits including Nchanga, Lumwana, Kansanshi, Samba, Konkola, Konkola North and Sentinel. Due to the greater degree of understanding of their genesis (Bernau et al., 2013; McGowan et al., 2006), their more substantial sample suites, and their contrasting metal associations, host stratigraphy and temporal characteristics, the Nchanga and Lumwana deposits were selected for further investigation. A subset of approximately 30 samples was chosen for more detailed fluid inclusion analysis and a full sample list is presented in Appendix A.2.2

The aims of this study require that the kinematic context (relative to host rocks, structures and fabrics) of vein samples is well constrained in order to give confidence in the interpretation of geochemical characteristics of temporally distinct fluid generations. Care was taken to record such details during all stages of fieldwork for this study, although the kinematic context of some samples collected for previous studies is less well constrained. As such, any interpretations regarding the relative timing of fluid generations, particularly at Nchanga, are subject to a greater degree of error.

2.2 Fluid Inclusion Analysis

Quartz and carbonate doubly-polished wafers of 150-200 µm thickness were prepared for petrographic characterisation and microthermometry of fluid inclusions at the University of Southampton. Fluid inclusion petrography involved the identification of fluid inclusion assemblages (FIAs), that is, groups of inclusions with similar petrographic features (e.g. phase proportions and textural context) that are interpreted to have been trapped coevally, under the same temperature-pressure conditions (Goldstein and Reynolds, 1994). In addition to their temporal relationship with each other, efforts were made to establish the temporal relationship between FIAs and the host mineral. Wherever possible, FIAs were classified as either ‘primary’, where fluids were trapped during the crystallisation of the host mineral, often as imperfections in the crystal lattice; ‘pseudosecondary’, where inclusions formed along microfractures during crystal growth, typically forming trails or planes which terminate against crystal growth planes; or as ‘secondary’, where inclusions form linear trails or planes, often cross-cutting growth boundaries, after the formation of the crystal (Fig. 2-2) (Roedder, 1972, 1984).

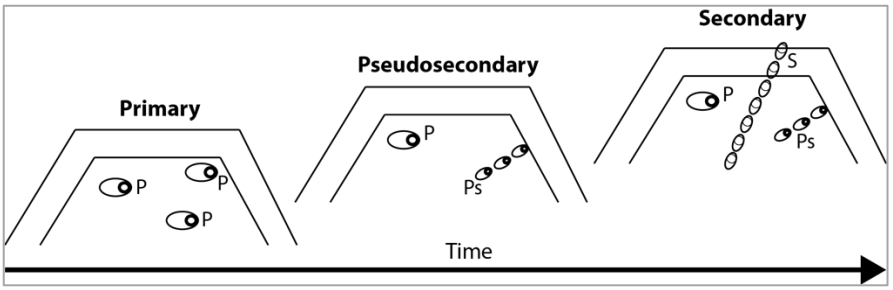

Fig. 2-2 Schematic diagram illustrating the relative timing of fluid inclusions as primary, pseudosecondary or secondary relative to the host mineral. Modified after (Roedder, 1984).

2.2.1 Microthermometry

Following petrographic characterisation of FIAs, fluid inclusion wafers were broken into 1-2 mm chips for microthermometric analysis. Microthermometry was conducted at the University of Southampton using a Linkam THMS 600 heating-freezing stage with a Leitz optical microscope. The stage was calibrated across a temperature range of approximately 360°C, with repeated measurements of CO_2 melting (-56.6°C) at a heating rate of 0.1°C/min, giving a reproducibility of ±0.5°C (2σ). At high temperature, sodium nitrate melting (306.8°C) gave a reproducibility of better than ±2°C (2σ). Pure H_2O melting (0.0°C) and CO_2 homogenisation (31.1°C) were also repeatedly measured in order to plot a 4-point calibration curve (Appendix A.1.1). The equation of this curve was used to calibrate all recorded measurements offline.

Typical cooling-heating profiles involved initially heating each sample to 110°C for 3-5 min in order to drive off water vapour from the chamber. Test runs were completed at cooling/heating rates of approximately 10°C/min in order to determine approximate temperature ranges for key phase changes. Samples were then cooled to -120°C and held for approximately 5 minutes in order to allow all phases to freeze. Where particularly high salinity inclusions failed to freeze, temperatures were dropped to -160°C and then cycled between -80°C and -160°C to promote freezing (Shepherd et al., 1985). Samples were then heated at 10°C/min until the predetermined temperature window of interest was reached, at which point, heating rates were reduced to 0.1°C/min over the CO_2 melting point (T_{mCO2}); 0.5-1°C/min over the expected eutectic point (T_e); 0.5°C/min over the final ice melting (T_{mICE}), clathrate melting (T_{CLATH}), hydrohalite melting (T_{HH}) and CO_2 homogenisation (T_HCO_2) temperatures.

Heating runs were typically at 15-20°C/min until vapour bubbles became agitated or daughter phases evidently commenced dissolving, at which point the heating rate was reduced to 5°C/min in order to record vapour homogenisation (T_{hVAP}), halite melting (T_{mHAL}) and sylvite melting (T_{mSYL}), with homogenisation of the final phase representing the total homogenisation temperature (T_{hTOT}).

Table 2-1 Microthermometry measurements, their abbreviations and inferred fluid properties

Phase Change	**Symbol**	**Inferred Fluid Property**
Carbon dioxide melting	T_{mCO2}	Presence & purity of CO_2
Carbon dioxide homogenisation	T_{hCO2}	CO_2 density
Eutectic temperature	T_e	Dominant salt species
Final ice melting	T_{mICE}	Fluid salinity (depending on bulk composition of the inclusion)
Final hydrohalite melting	T_{HH}	
Final clathrate melting	T_{CLATH}	
Halite/Sylvite melting	T_{mHAL}/ T_{mSYL}	
Total homogenisation temperature	T_{hTOT}	Minimum trapping temperature

Interpretations of fluid properties made using the phase transitions listed in Table 2-1.

are based upon theoretically and experimentally-derived phase equilibria of specific systems such as the H_2O-NaCl (Bodnar et al., 1985), H_2O-NaCl-CO_2 (Bowers and Helgeson, 1983), H_2O-NaCl-KCl (Sterner et al., 1988) and H_2O-NaCl-$CaCl_2$ (Vanko et al., 1988; Williams-Jones and Samson, 1990) systems. Natural fluids, however, are rarely binary or ternary systems and instead consist of complex salt and gaseous components, resulting in uncertainties when using simplified phase equilibria to elucidate their origin.

2.2.2 Cathodoluminescence

In order to accurately ascertain the relationship between FIAs and the host quartz, it is important to visually distinguish between different quartz generations in the form of temporally distinct growth zones. Cathodoluminescence (CL) is a near surface effect that can reveal such growth zones that are otherwise invisible with optical, or other forms of electron microscopy. Cathodoluminescence works according to the solid-state band theory, in which a sample is bombarded by high energy electrons, causing the excitation of electrons from the lower energy valence band to the higher energy conduction band. Upon reduction of the transient energy beam, excited electrons return to ground state energy across the 'band gap', releasing a small amount of radiation in the visible light or ultraviolet regions of the electromagnetic spectrum (Frelinger et al., 2015; Gotze et al., 2001; Marshall, 1988). Electrons may be momentarily retained in the band gap due to imperfections or defects in the quartz and the total luminescence of a given quartz generation is intrinsically linked to the density of defects within this band gap (e.g. inclusions, points of radiation damage or ions that have been substituted into the crystal lattice) (Frelinger et al., 2015; Rusk et al., 2008). Light emissions are captured by a photomultiplier and used to construct a CL-image.

Selected samples were glued to glass slides and subjected to SEM-CL analysis in the Imaging and Analysis Centre at the NHM using a Zeiss EVO 15LS SEM with back-scattered electron (BSE), secondary electron (SE) and CL detectors. Samples were carbon coated (30 nm) and a probe current of 3 nA, with an accelerating voltage of 20 kV was applied at a working distance of 8.5 mm. Corresponding BSE, SE and CL images were taken of whole chips (x250 magnification – each frame is 1.208 mm across), as well as particular sites of interest. In addition to images presented in Chapter 5, further images are included in Appendix C.6.

2.2.3 Laser Raman spectroscopy

In order to qualitatively identify unknown vapour phases in fluid inclusions, selected inclusions were analysed on a confocal Renishaw inVia Raman microscope with a 514 nm Edge Laser at Kingston University (London). Inclusion chips were placed on a Raman-neutral slide and targeted phases within inclusions were analysed using the laser at 100% energy for 30 seconds in order to gain a spectrum. Spectra peaks were compared to published reference values to obtain positive identifications (Burke, 2001; Frezzotti et al., 2012). Qualitative results are summarised in Appendix C.3.

2.2.4 Fluid inclusion SEM analysis

Although many fluid inclusions derived from sedimentary basin brines exist as two phase, undersaturated liquid-vapour inclusions, the Zambian Copperbelt hosts abundant brines that are saturated with respect to various salts (Greyling, 2009; McGowan et al., 2006; Richards et al., 1988). The eutectic temperature of fluid inclusions is controlled by the presence of dissolved species in solution (Roedder, 1972), and as such the chemical composition of saturated salt phases may be inferred. Identification of multiple salt species within a single inclusion, or of other transparent or opaque daughter minerals has historically depended on other physical properties such as colour, solubility, magnetism and crystal habit, however such methods remain speculative. Scanning electron microscope (SEM) analysis of fluid inclusion daughter phases was first attempted in the 1970s and 1980s (Anthony et al., 1984; Kelly and Burgio, 1983; Metzger et al., 1977) but remains a little-used technique. In order to image, and provide semi-quantitative analysis of unknown daughter phases, this method was employed on selected Zambian Copperbelt inclusions in this study.

Suitable FIAs were identified and the corresponding 150-200 µm-thick doubly-polished wafer chips were mounted along their edges in 400-600 µm-wide grooves cut into a standard 25 mm epoxy block. The chips were mounted with superglue under a binocular microscope with an attempt made to align the FIA of interest, with the surface of the epoxy block. In order to expose the daughter

phases, each of the chips was then snapped and the whole block placed into a drying oven at 35°C for 48 hours. Immediately before analysis, the block was coated with carbon.

An FEI Quanta 650 FEG SEM located in the Imaging and Analysis Centre at the NHM was used for analysis. An acceleration voltage of 10 kV was applied for both spot analyses and semi-quantitative element mapping. Element maps were acquired at 2 microseconds per pixel and deconvolved, background-subtracted net intensity maps were produced using the QUANTA X Bruker Esprit software (v2.1). During processing an automatic filter was used to average and smooth colours based on count intensities.

2.2.5 Fluid inclusion laser ablation ICP-MS

Traditional bulk chemical analysis of fluid inclusions is subject to the fundamental limitation of mixing of several, potentially temporally and compositionally distinct fluid generations. As such, emerging technologies such as laser ablation ICP-MS of individual, texturally constrained fluid inclusions *in situ* is increasingly favoured as the most representative way of quantifying fluid chemistry (Audetat et al., 1998, 2000; Gunther et al., 1998; Heinrich et al., 2003; Pettke et al., 2012).

Laser and Mass Spectrometer Setup:

Any fluid inclusion laser ablation ICP-MS setup includes a laser source; a sample chamber; an optical setup to aid the user with sample navigation and the ablation process; an ICP torch and a mass spectrometer (typically quadrupole); and a carrier gas mechanism to transport ablated material from the sample chamber to the inductively coupled plasma without selective element loss (Fig. 2-3).

For this study, fluid inclusion laser ablation ICP-MS analysis was carried out at the Imaging and Analysis Centre at the NHM, using an ESI New-Wave NWR 213 nm laser system equipped with beam homogenisation optics and a two-volume cell. Ablated material was analysed by an Agilent 7700x ICP-MS and transported using gas flows of 1.1 L/min Ar and 450 ml/min He.

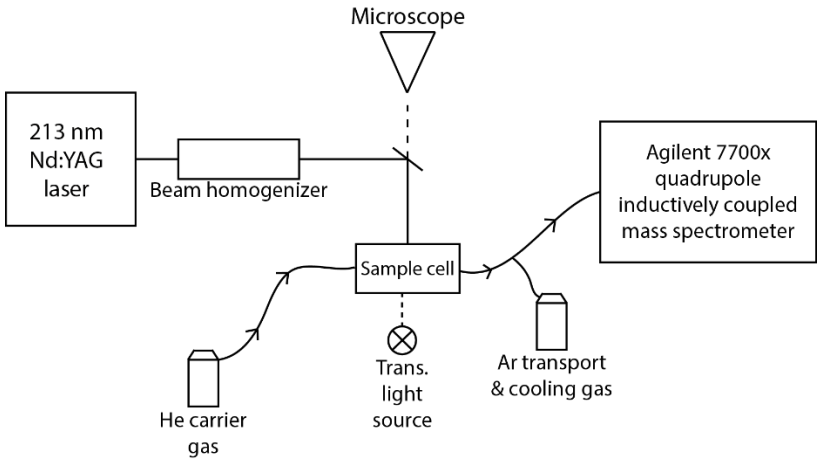

Fig. 2-3 Schematic diagram of the laser ablation ICP-MS setup used for analysis of fluid inclusions at the NHM. Components include a 213 nm yttrium-aluminium-garnet ($Y_3Al_5O_{12}$) (doped with 3 wt % Nd^{3+}) laser source; a transmitted light optical setup; an airtight sample cell and an Agilent 7700x quadrupole ICP-MS. Modified after Heinrich et al. (2003).

Measurement of ions based on their m/Z ratio can result in unwanted interferences when two different ionic species share the same ratio. Polyatomic interferences (where polyatomic ions form in the plasma with the same m/Z ratio as other ions) such as ^{40}Ar + ^{23}Na and ^{63}Cu may be avoided through careful selection of isotopes to be used in an analytical method file (e.g. use of ^{65}Cu instead of ^{63}Cu).

Ablation Process:

Individual 1-2 mm chips of selected fluid inclusion wafers were glued to glass slides. In most cases, only inclusions that had undergone microthermometric work were selected for laser ablation analysis. Analyses were carried out in batches of 15-25 inclusions, with duplicate analyses of NIST 610, 612 (± an in-house solution) at the start and end of each run. NIST glasses were analysed using a 50 µm spot, a frequency of 10 Hz and a fluence of 3.5 Jcm^{-2}. The parafilm covering standard solution ablation wells was initially pierced using a 100 µm spot and low fluence (typically <2 Jcm^{-2}), before fluid ablation proceeded with a 50 µm spot, a frequency of 20 Hz and a fluence of 2-3 Jcm^{-2}. Where fluid inclusions were at a depth >20-25 µm, a stepwise opening procedure was utilised (Gunther et al., 1998), whereby initial coupling of the laser with the matrix is achieved using a small spot size (8-14 µm) in order to minimise 'sharding' at surface, with the spot size (and fluence) then increased sufficiently in order to ablate the entire contents of the targeted inclusion. Due to the lack of variable aperture on the laser used in this study, a stepwise opening was not favoured for shallow inclusions as the inclusion was often breached prior to the spot size being increased to equal or exceed the maximum inclusion diameter. In order to avoid the loss of an unknown proportion of the sample fluid, where inclusions were <20 µm depth in the chip, a spot size ≥

inclusion size was used with low fluence in order to minimise sharding and ablate the entire inclusion. Targeted inclusions ranged in size from 6-50 µm, with the majority of successful inclusions falling in a size range of 10-25 µm.

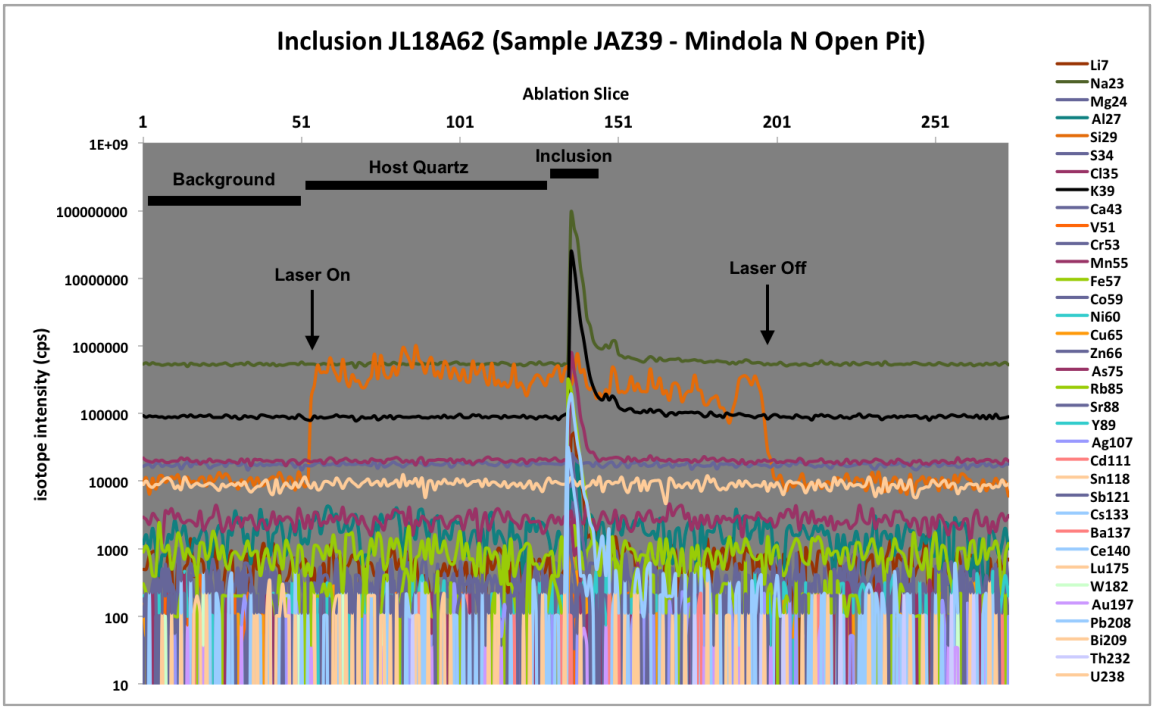

Fig. 2-4 Time-resolved signal for a successful fluid inclusion ablation (inclusion JL18A62 from sample JAZ39). The laser was turned on at approximately ablation slice 51, indicated by an increased Si count. The inclusion was breached at approximately ablation slice 130, with concomitant signals for the inclusion solutes (most notably Na and K).

A single 'method file' was used for the ablation of most inclusions, which included a wide range of elements commonly found in hydrothermal fluids, each with an allocated dwell time Table 2-2).

Increased dwell times allow reduced LODs for elements of particular interest (e.g. Cu, Co), however signal intensities are processed in counts per second (cps) to account for variable dwell times between elements (Pettke et al., 2012).

Table 2-2 Dwell times for elements analysed in fluid inclusions during this study.

Element	Dwell Time (ms)	Element	Dwell Time (ms)	Element	Dwell Time (ms)
^{7}Li	10	^{57}Fe	10	^{118}Sn	10
^{23}Na	10	^{59}Co	30	^{121}Sb	10
^{24}Mg	10	^{60}Ni	10	^{133}Cs	10
^{27}Al	5	^{65}Cu	20	^{137}Ba	10
^{29}Si	5	^{66}Zn	10	^{140}Ce	10
^{34}S	30	^{75}As	10	^{175}Lu	10
^{35}Cl	30	^{85}Rb	10	^{182}W	10
^{39}K	10	^{88}Sr	10	^{197}Au	30
^{43}Ca	10	^{89}Y	10	^{208}Pb	10
^{49}Ti	20	^{95}Mo	10	^{209}Bi	10
^{51}V	10	^{107}Ag	20	^{232}Th	10
^{53}Cr	10	^{111}Cd	10	^{238}U	10
^{55}Mn	10				

Calibration:

In order to accurately quantify the results of ablating any geological material, it is best to ensure that laser conditions, particle sizes and ionisation efficiencies are matched between the external standard reference material and the sample of unknown composition. When an analytical result is dependent on the composition or physical nature of the sample, a process known as 'matrix matching' is required in order to normalise results against a calibration standard with similar properties (Sylvester, 2008).

External standards:

A wide range of external standards for fluid inclusion laser-ablation ICP-MS have been tested across numerous studies, including well characterised, easily available standard glasses (NIST 600 series) (Jochum et al., 2011; Pearce et al., 1997); and less-well characterised in-house standard solutions contained in various forms of capillaries and microwells (Buckroyd, 2008; Gunther et al., 1997); and synthetic fluid inclusions (Bodnar et al., 1985; Buckroyd, 2008; Stoffell, 2007).

The most widely used, and arguably the most reliable and reproducible external standard reference materials are the NIST 600 series glasses. Although they are not matrix matched to fluid inclusions, extensive tests have shown that external calibration using glasses provides reproducible and accurate results with minimal error introduced as matrix effects when compared to other sources of error such as ablation quality, processing techniques and issues with internal standards (Heinrich et al., 2003; Sylvester, 2008; Sylvester and Eggins, 1997). The main limitation of NIST 600 series glasses relevant to this study is the fact that they contain only hundreds ppm Fe, K and Mg – three

elements that are often present in much greater abundances in natural fluid inclusions, ultimately resulting in reduced precision for these elements (Jackson, 2008).

Efforts have been made to produce and analyse matrix-matched external standards in the form of standard solutions and synthetic inclusions with varying degrees of success (Buckroyd, 2008; Gunther et al., 1998; Stoffell, 2007). Stoffell (2007) showed that calibration using synthetic inclusions yielded improved accuracy over NIST glasses, however the time, cost and technical requirements to produce synthetic inclusions, as well as their relatively poor reproducibility between ablations means that they are unlikely to be practical for most laboratories (Vry, 2010).

Ablation of customised in-house solutions provides a relatively cheap and accessible alternative to NIST glasses that also have potential advantages such as improved matrix matching and homogeneity as well as custom compositions that better replicate sample solutions (Buckroyd, 2008; Gunther et al., 1998). Studies using a range of 5-20 wt % (Na-K-Ca-Cl) solutions have indicated that improved accuracy over NIST glasses may be achieved using a 10 wt % solution and Cl as the internal standard (Buckroyd, 2008), however reproducibility is often poor, primarily owing to the highly variable ablation 'styles' which are a function of laser fluence, spot size, beam homogeneity and capillary wall thickness. This study carried out some experimentation with ablation of an in-house standard solution, however reproducibility was a significant issue. In some cases, static effects between the fluid and the parafilm cover resulted in discrete 'bubbles' of solution being ablated, forming a highly heterogeneous time-resolved signal (Fig. 2-5A). Furthermore, a significant degree of evaporation of the fluid was noted throughout a day of analysis, resulting in fractionation of elements and an inevitable increase in the bulk salinity of the solution after 10-12 hours of analysis. This study repeatedly found that an unperforated microwell could entirely evaporate over a 24-hour period (where adjacent wells had been perforated and analysed).

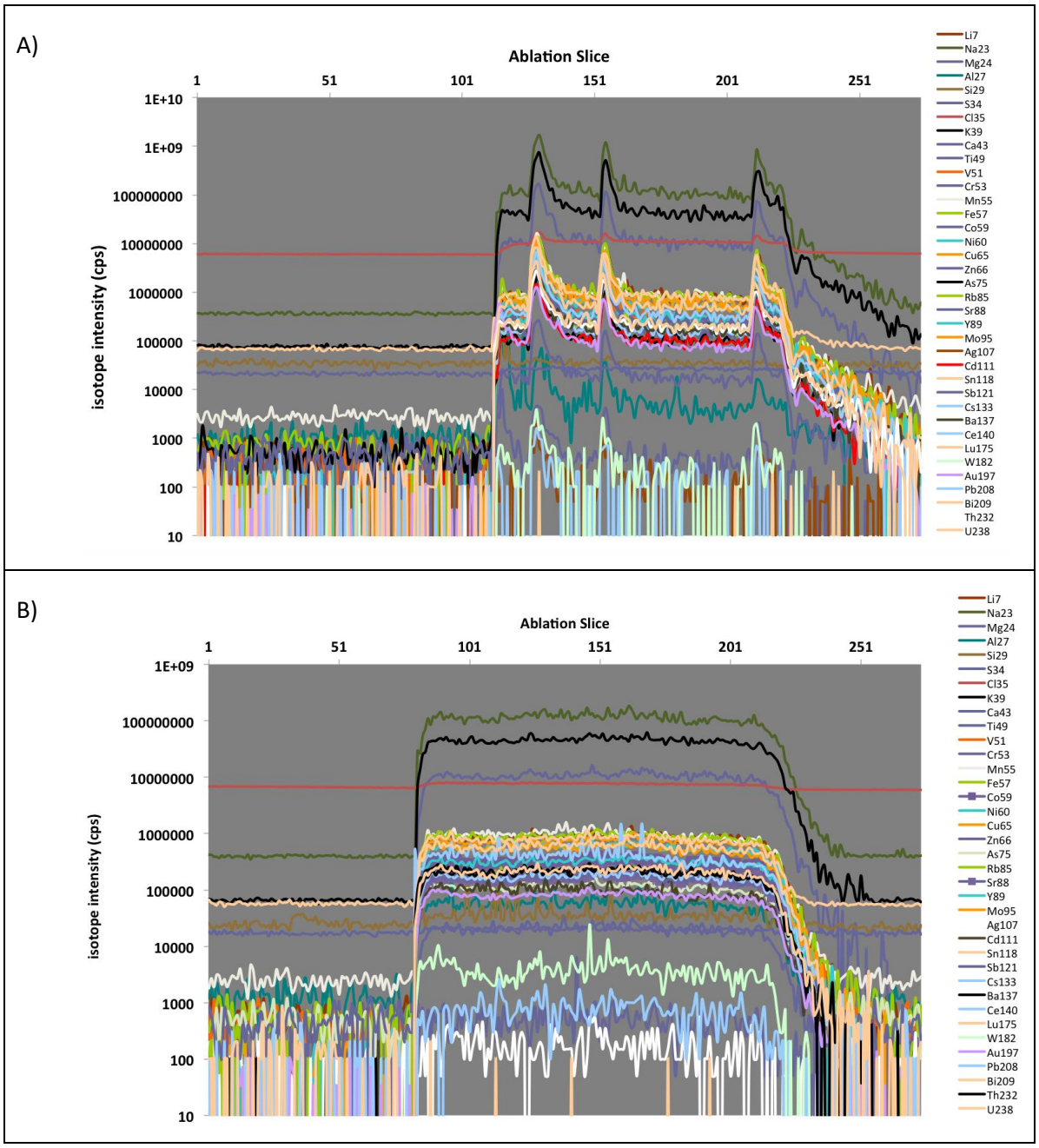

Fig. 2-5 Time-resolved signals showing standard solution ablation. A) Heterogeneous ablation due to static effects between the fluid and parafilm cover. B) A more homogenous ablation of the standard solution. See text for analysis of accuracy and precision of such ablation profiles.

Where multiple broadly homogenous solution ablations (e.g. Fig. 2-5B) were achieved between sample batches over a period of two days, accuracy and precision were highly variable between elements and sometimes between ablations for a given element (Table 2-3).

Table 2-3 Accuracy and precision of 13 standard solution ablations over a two-day period.

Element	Actual Concentration	$\bar{x}$	%RSD*	Relative Error (%)⁺
^{7}Li	234.9	278.2	6.9	18.4
^{24}Mg	1879.5	2088.3	6.8	11.1
^{35}Cl	27023.9	3968.0	130.6	-85.3
^{39}K	4458.3	4597.5	4.4	3.1
^{43}Ca	1268.2	1446.7	52.7	14.1
^{51}V	18.8	25.2	37.6	34.2
^{53}Cr	187.9	235.1	28.3	25.1
^{55}Mn	47.0	58.1	3.0	23.7
^{57}Fe	2584.3	2681.0	20.0	3.7
^{59}Co	18.8	21.4	5.8	14.0
^{60}Ni	94.0	103.5	5.9	10.2
^{65}Cu	187.9	205.9	7.7	9.6
^{66}Zn	94.0	170.1	10.6	81.0
^{75}As	469.9	63.9	34.0	-86.4
^{85}Rb	9.4	11.1	4.4	18.3
^{88}Sr	4.7	8.3	23.3	77.6
^{89}Y	18.8	21.7	8.6	15.3
^{95}Mo	94.0	134.6	24.0	43.2
^{111}Cd	47.0	89.0	11.9	89.4
^{118}Sn	94.0	98.9	24.6	5.2
^{121}Sb	18.8	36.3	96.9	92.9
^{133}Cs	4.7	5.4	5.3	15.1
^{137}Ba	47.0	53.4	9.6	13.7
^{197}Au	94.0	9.2	44.0	-90.2
^{208}Pb	18.8	25.0	10.5	33.0
^{209}Bi	18.8	24.5	21.1	30.3
^{232}Th	4.7	7.5	54.8	60.2
^{238}U	4.7	6.2	9.4	32.2

RSD = 100(StDev/ $\bar{x}$)

⁺Relative error = (mean measured - true value)/true value)*100

Over half of the elements analysed show RSD values >10% for 13 repeat measurements, indicating poor precision, particularly for certain elements of interest such as Ca, Fe and Sr. Accuracy is similarly poor, with only four elements out of 27 returning relative errors of <10%. Due to the poor reproducibility, NIST610 was chosen as the primary external standard for this study, with NIST612 and the in-house standard solution used as secondary and tertiary external standards.

Data Reduction and Internal standards:

All laser-ablation ICP-MS data in this study was processed using the ExLAM2000 software package (Zacharias and Wilkinson, 2007) in order to produce absolute concentrations for the selected suite

of elements. Background and host mineral ablation intervals were subtracted from the inclusion interval, with sensitivity for each element being estimated using the external standard (NIST 610), allowing calculation of element intensity ratios which are converted to absolute concentrations using an element of known concentration in the sample (internal standard) (Heinrich et al., 2003).

The internal standard effectively corrects for differing ablation yields between inclusions and the choice and quantification of an appropriate internal standard is perhaps the single largest source of error in quantifying fluid inclusion compositions. Typically, Na or Cl are chosen as the internal standard due to their abundance in most crustal fluids and their relative ease to estimate through an independent method (microthermometry). Chlorinity is more reliably estimated from microthermometry, with Na values subject to error, particularly in fluids with complex salt chemistry. However, Cl signals during laser ablation analyses are usually much closer to background than Na signals, with ionisation issues often resulting in unrepresentative Cl measurements. Furthermore, Na-based internal standardisation has been shown to produce more accurate results than Cl-based approaches (Pettke et al., 2012). As such, Na was used as the internal standard in the majority of fluids in this study.

In the simplest, low-medium salinity two-phase (L-V) inclusions, wt % NaCl equivalent, estimated from the freezing point depression (Equation 2.1), was used as the internal standard. ExLAM2000 includes a correction function, which modifies NaCl equivalent values by accounting for the contribution of other salts (e.g. $CaCl_2$, KCl) to the freezing point depression which has typically been determined using only a simple binary H_2O-NaCl system (Heinrich et al., 2003).

$$Wt.\%\ NaCl\ equiv. = 1.78\theta - 0.0442\theta^2 + 0.000557\theta^3 \quad \text{(Equation 2.1)}$$

Where θ is the freezing point depression (°C) (Bodnar, 1993).

In higher salinity, 3-phase inclusions, wt % Na, derived from an estimation of wt % NaCl equiv. from halite dissolution temperatures (Equation 2.2) was used for internal standardisation.

$$Wt.\%\ NaCl\ equiv. = 26.242 + 0.4928\gamma + 1.42\gamma^2 - 0.223\gamma^3 + 0.04129\gamma^4 + 0.006295\gamma^5 - 0.001967\gamma^6 + 0.0001112\gamma^7 \quad \text{(Equation 2.2)}$$

Where γ is the dissolution temperature of halite (°C/100) (Sterner et al., 1988).

Perhaps the single largest source of error in the quantification of absolute element concentrations in this study is the internal standardisation of brines with more complex salt chemistries (typically NaCl-KCl and NaCl-KCl-$CaCl_2$). Many fluid inclusions from the Nchanga and Lumwana deposits show Na:K ratios of 1:1 to 1:4. In such instances, the ternary H_2O-NaCl-KCl system was utilised in order to estimate NaCl concentrations. However, many of these inclusions showed evidence of only one daughter phase (assumed to be halite) during petrographic and microthermometry work. As such, wt % NaCl estimates derived only from halite dissolution temperatures in these inclusions were deemed unreliable (primarily due to a known significant, but unquantifiable contribution to this temperature by other chloride species). Instead, an estimate was made directly from the H_2O-NaCl-KCl phase diagram (Sterner et al., 1988) using the Na:K ratios measured for each inclusion during laser ablation work (Fig. 2-6) in addition to the measured halite dissolution temperature.

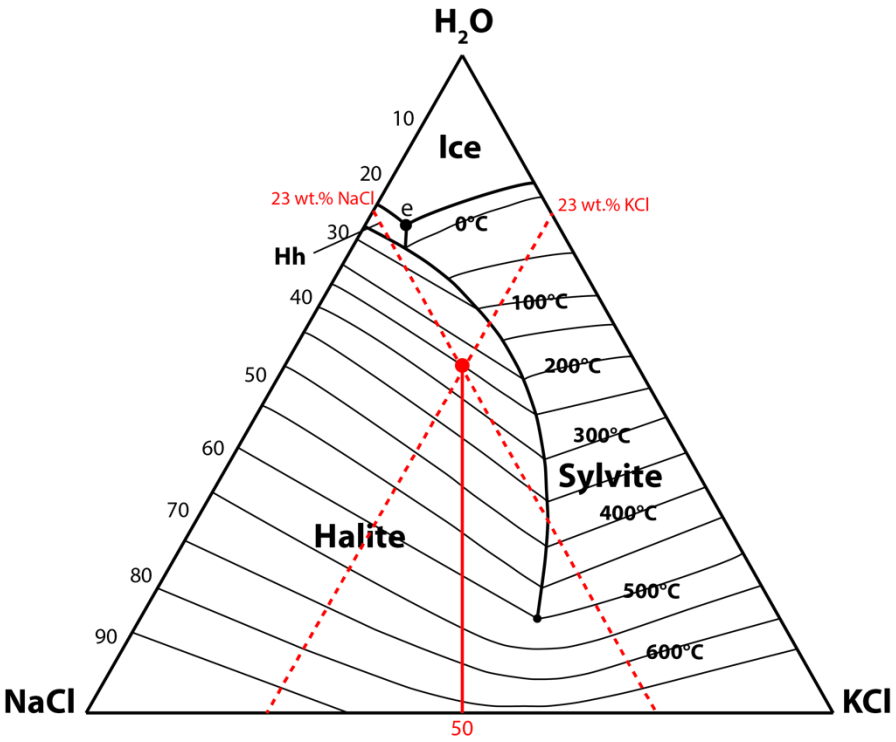

Fig. 2-6 Vapour-saturated solubility surface in the H_2O-NaCl-KCl system. Eutectic point (e) = -22.9°C. Solid red line denotes a NaCl:KCl ratio of 1:1, which for a fluid inclusion where the final solid phase melts at 250°C (halite, in this case), results in a composition of approximately 23 wt % NaCl and 23 wt % KCl. Redrawn and modified after Sterner et al. (1988).

Due to the lack of a published H_2O-NaCl-KCl-$CaCl_2$ quarternary system at elevated temperatures, inclusions with a significant component of Ca, as well as Na and K still had to be interpreted in the H_2O-NaCl-KCl ternary system (assuming the Ca component did not significantly exceed the K component, in which case, the H_2O-NaCl-$CaCl_2$ ternary system was employed), leading to increased

error with these FIAs. In the absence of a reliable method of interpreting a 3-salt system, quantification of absolute elemental concentrations in such inclusions results in an overestimation of Na as an internal standard and a corresponding overestimation of total cations. A potential method to treat such data is detailed in Appendix A.1.4. Difficulties quantifying absolute concentrations of an internal standard element, along with the loss of a significant proportion of Zambian Copperbelt inclusions due to leaking upon heating resulted in significantly reduced numbers of inclusions (~50%) being accurately reported following laser ablation analyses (Chapter 4 to Chapter 6) when compared to the microthermometry dataset presented in Appendix C.1.

Accuracy, precision and limits of detection:

ExLAM2000 calculates a limit of detection (LOD) value for each element in every inclusion, based on the standard deviation of the background signal of the instrument (Longerich et al., 1996). Due to the mass-dependent instrument sensitivity and the variable abundances of each element, LOD values are strongly element-dependent (Heinrich et al., 2003). The LOD values in this study were calculated on the basis that any count intensities below 3 times the standard deviation of the background counts were deemed 'below the limit of detection'. In ExLAM2000, the LOD is calculated by:

$$LOD\ (cps) = 3\sigma_{individual}^{blank}\sqrt{\frac{1}{N^{blank}} + \frac{1}{N^{sample}}} \quad \text{(Equation 2.3)}$$

Where N is the number of ablation slices in each of the selected intervals and $\sigma_{individual}^{blank}$ is the standard deviation of the background counts (Vry, 2010).

Equation 2.3 shows that in addition to the background signal, LODs are also dependent on the signal to background ratio, which is dependent on the size and salinity of the inclusion as well as the specified dwell time per element. As such, a wide range of variables, some within and some outside of the user's control can affect LOD values. In addition to dwell time, one of the main variables that control LODs for a given inclusion is the length of the interval selected for integration across a fluid inclusion signal. In order to assess these effects, fluid inclusion assemblages from Allihies and the Mindola North deposit were chosen for repeat processing with a 'long' integration interval (typically >10 s and until Na and K signals return to background) compared to a 'short' interval (typically <10s and only including the main Na-K peak of the inclusion) (Fig. 2-7). Comparing results shows that selection of an appropriate integration interval has a significant effect on LODs. For inclusions in the ALH-JD-03 Chip A assemblage, LODs were consistently 27% lower (across all elements) for 'short' integration intervals compared with 'long' intervals, with this discrepancy even more significant (37%) for JAZ39 Chip B FIA from Mindola North. The strong internal consistency

(±<1%) across all elements measured for both FIAs indicates that LODs can be systematically lowered through manual selection of the shortest possible integration interval that remains representative of all ablated phases.

A)

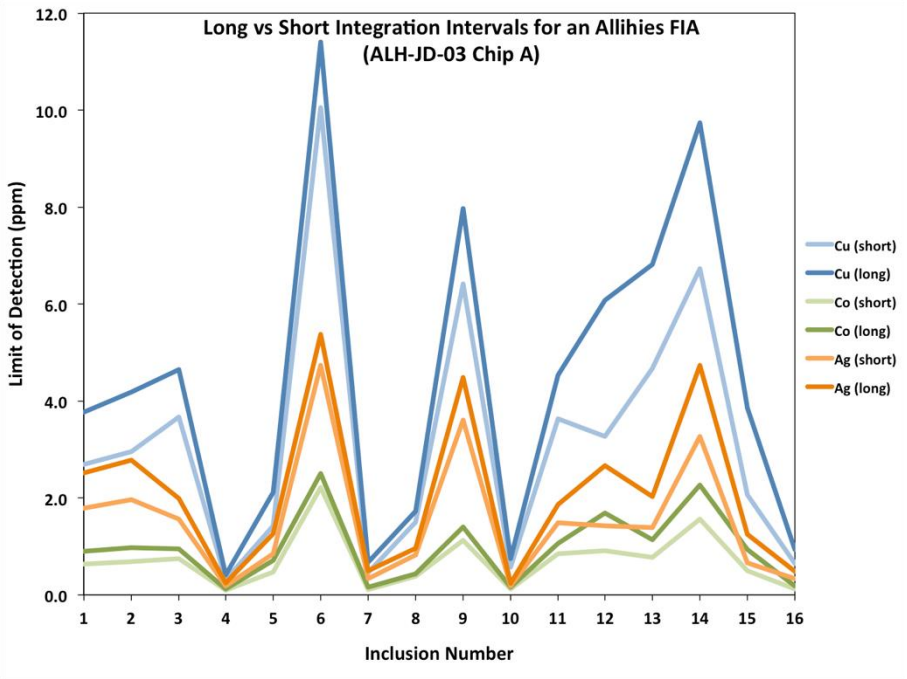

B)

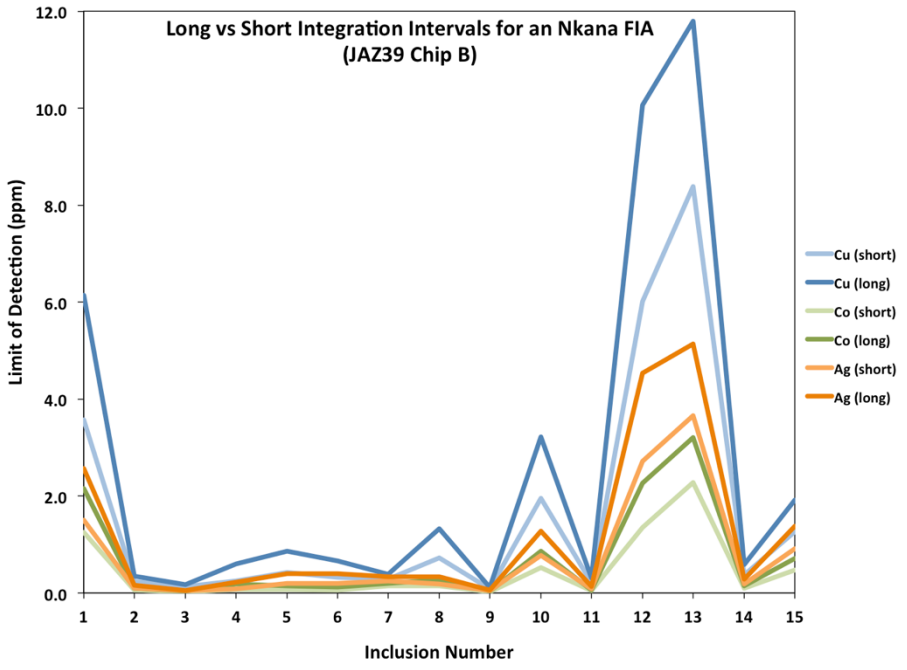

Fig. 2-7 Limit of detection values as a function of integration interval. In all fluid inclusions from both the ALH-JD-03 Chip A and the JAZ39 Chip B assemblages, 'short' integration intervals result in lower LODs than 'long' integration intervals.

Instrumental precision and accuracy have been assessed using the primary external standard for this study, NIST 610, as well as NIST 612 as a secondary standard. Precision is represented by %RSD (and a more stringent assessment of 2σ as a percentage of the mean), with most elements having 2σ values of <10%. Only As shows poor precision (2σ = 36.8%) and is excluded from further discussion in this study. When NIST 612 is used to assess instrumental precision, %RSD values are slightly higher (Table 2-4) but remain within acceptable limits (<10%) for the majority of elements (excepting Fe, with a %RSD value of 23.3%). Accuracy was determined by calculating relative error, which is excellent (<5%) for all elements in NIST 610. Relative error of ten elements (Mg, S, Ti, Fe, As, Mo, Sb, Lu, Au and Th) exceeded 10% using NIST 612. Iron is the only one of these elements present in any of the analysed inclusions in appreciable concentrations and will be treated with caution in this study. Full tables and graphs of instrumental precision and accuracy are presented in Appendix A.1.3.

Table 2-4 Summary of instrumental precision and accuracy statistics for 35 elements in NIST 610 and NIST 612 (excluding S and Cl). Full results in Appendix A.1.3

	NIST 610*			**NIST 612+**		
	Min	*Max*	*Average*	*Min*	*Max*	*Average*
%RSD	0.9	19.4	2.4	2.3	35.2	5.5
2σ (%)	1.9	36.8	4.8	4.5	46.6	11.0
Relative Error (%)	-1.3	2.0	0.2	-24.8	54.7	-3.3

* 122 measurements

+ 96 measurements

Instrumental precision may also be calculated from %RSD of homogenous fluid inclusion assemblages (Heinrich et al., 2003; Pettke et al., 2005), however such assemblages of two-phase inclusions in this study typically had a large proportion of elements below the LOD, whilst results from multi-solid inclusion assemblages were more heterogeneous, likely due to partial ablation of daughter minerals.

2.3 Stable Isotopes

Stable isotope analyses were carried out at the Scottish Universities Environmental Research Centre (SUERC) in East Kilbride.

2.3.1 Sulphur

Sulphur isotope analyses were carried out on handpicked sulphide separates using minor modification of the method of Robinson and Kusakabe (1975). Approximately 6 mg of sample was ground in an agate mortar and pestle with 200 mg of cuprous oxide (Cu_2O) and reacted in vacuo

with silica wool at 1025°C for 20 minutes to obtain SO_2 gas. Sulphur dioxide was analysed using a Thermo Fisher MAT 253 dual inlet mass spectrometer, and $\delta^{66}SO_2$ converted to $\delta^{34}S$ by calibration with three standards (NBS 123, at 17.1‰; IAEA-S-3, at -32.3‰; CP1, at -4.6‰). Repeat analyses of samples gave a reproducibility of better than ±0.4‰ (2σ) and data is reported in standard notation ($\delta^{34}S$), as per mil deviations from the Vienna Canyon Diablo Troilite (V-CDT) standard.

2.3.2 Oxygen

Oxygen isotopic signatures of vein quartz material from the Zambian Copperbelt, Kalahari Copperbelt and Allihies were obtained via laser fluorination following the process of Sharp (1990). Quartz material was handpicked from fluid inclusion wafers in order to correlate fluid inclusion results with isotopic signatures of their host vein quartz. Where samples comprised of intergrown quartz and carbonate, quartz was first checked optically, and then underwent an acid digest using 4 M HCl to remove excess carbonate. Approximately 2 mg of pure quartz material was loaded into stainless steel sample holders and fluorinated (ClF_3) in an evacuated chamber overnight. Samples were combusted using a CO_2 laser as a heat source (>1500°C), releasing 100% of O_2 from the crystal lattice, before reaction with excess ClF_3. O_2 was reacted with a heated platinised graphite rod to produce CO_2, which was analysed using a VG SIRA 10 mass spectrometer. Accuracy of the technique was established by systematic analysis of YP2 (16.4‰), GP147 (7.3‰), UWG2 (5.8‰) and JJB8 (30.3‰) standards, with reproducibility better than ±0.2‰ (2σ). Results are reported in standard notation ($\delta^{18}O$) as per mil (‰) deviation from Vienna Standard Mean Ocean Water (V-SMOW).

2.3.3 Hydrogen

Using transmitted light microscopy, samples were inspected and only deemed appropriate for hydrogen isotope analysis where a single fluid inclusion population was volumetrically dominant. Approximately 1 g of quartz or carbonate mineral separates were handpicked, with quartz samples undergoing an acid digest in Aqua Regia prior to analysis. Samples were loaded into degassed platinum crucibles and heated at 140°C in a vacuum overnight in order to drive off any further volatiles. Samples were heated in a furnace (quartz samples at 700°C and carbonate at 400°C) for 60 minutes to release fluid inclusions, with hydrogen gas obtained from H_2O by reduction in a chromium furnace (Donnelly et al., 2001). Hydrogen was analysed using a VG-Micromass 602D mass spectrometer. Repeat analyses of the SUERC internal lab standard Lt. showed a reproducibility of ± 4‰ (2σ), however reproducibility for individual vein samples is likely higher due to heterogeneity within fluid inclusion populations. Results are reported in standard notation (δD) as per mil deviation from V-SMOW.

Table 2-5 Accuracy and precision of stable isotope results

Element	Mineral	Standard	True Value	$\bar{x}$ (n)	σ_x	2σ	%RSD	Relative Error (%)
Oxygen	Quartz	YP2	16.4	16.4 (6)	0.1	0.1	0.4	0.0
Oxygen	Quartz	GP147	7.3	7.3 (3)	0.1	0.1	0.8	0.2
Oxygen	Quartz	UWG2	5.8	5.8 (4)	0.1	0.2	1.4	0.0
Oxygen	Quartz	JJB8	30.3	30.3 (1)	-	-	-	-
Sulphur	Chalcopyrite	CP1	-4.6	-4.7 (1)	-	-	-	-
Sulphur	Ag2S	IAEA-S-3	-32.3	-32.2 (1)	-	-	-	-
Sulphur	Sphalerite	NBS 123	17.1	17.2 (1)	-	-	-	-
Hydrogen	H_2O	LT	-94	-90 (2)	2	4	-2.4	-4.8

Chapter 3 Background Geology and Deposit Overviews

3.1 Zambian Copperbelt

3.1.1 Pan-African regional tectonics

The Zambian Copperbelt forms the southern half of the world's premier sediment-hosted Cu-Co province, the Central African Copperbelt. The Central African Copperbelt is located in the south-eastern section of the 900 km-long Neoproterozoic Lufilian Arc, one of several Pan-African fold belts which stretch from the Damaran Belt in southwest Africa to the Mozambique Belt along the east coast of southern Africa (Fig. 3-1). The succession of Pan-African belts mark the suture along which the Angola-Kalahari and Congo-Tanzania plates rifted apart during the breakup of Rodinia, before Neoproterozoic convergence during the assembly of Gondwana (John et al., 2004; Johnson et al., 2005; Kampunzu and Cailteux, 1999).

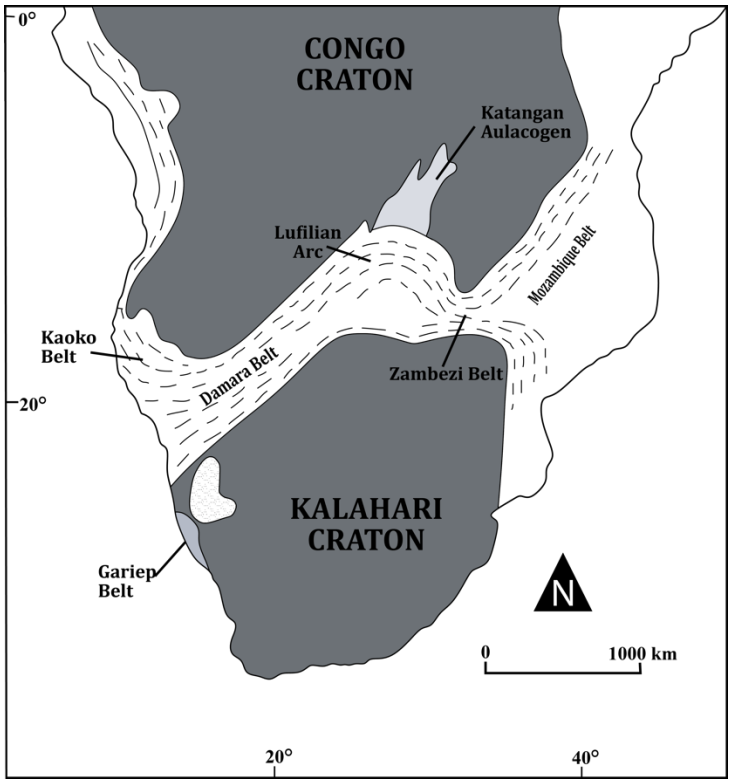

Fig. 3-1 Sketch map of the Pan-African mobile belt, including the Lufilian and Damaran belts which host the Zambian and Kalahari Copperbelts, respectively. Modified after Kampunzu and Cailteux (1999).

The Lufilian Arc straddles the border between north-western Zambia and the Democratic Republic of the Congo (DRC) and is surrounded by a series of Palaeoproterozoic-Neoproterozoic orogens and stable cratonic blocks (Daly et al., 1984; Porada, 1989). The arc broadly comprises Archaean to Mesoproterozoic basement metavolcanics and metasediments, overlain by a thick succession of Katangan Supergroup metasediments deposited during the development of an intracontinental rift basin in the Neoproterozoic. The belt has traditionally been split into four distinct structural domains (De Swardt and Drysdall, 1964; Porada, 1989), however the regional tectonics and basin evolution of the Central African Copperbelt are relatively poorly understood. As such, this study provides only a brief summary of the empirical observations pertinent to a summary of the evolution of the Katangan Basin (Section 3.1.3).

3.1.2 Stratigraphy

Basement:

Central African Copperbelt basement rocks range in age from Archaean to Mesoproterozoic and predominantly comprise metavolcanics, metasediments, migmatites and intrusive granitoids (Mendelsohn, 1961). Basement lithologies have undergone polyphase deformation and metamorphism resulting from the Ubendian, Kibaran and Lufilian orogenies. Basement inliers of the Domes Region have undergone amphibolite facies metamorphism whilst the Kafue Anticline displays lower grade greenschist facies metamorphic grades (John et al., 2004; Rainaud et al., 2005).

The oldest basement lithologies are those belonging to the Lufubu Metamorphic Complex, which comprises the Lufubu Schists along with various gneisses and granitoids returning U-Pb SHRIMP zircon ages of 1980 ± 7 Ma to 1874 ± 8 Ma (Rainaud et al., 2005). The Lufubu Metamorphic Complex was interpreted by Rainaud et al. (2005) to represent a metamorphosed calc-alkaline volcanic arc sequence that formed episodically over a 200 million year time period between 2050 – 1850 Ma, stretching from northern Namibia to northern Zambia and the Marungu Plateau of the DRC. The Lufubu Metamorphic Complex is unconformably overlain by Palaeoproterozoic quartzites and metapelites of the Muva Supergroup, dated at 1882 ± 30 Ma to 1824 ± 19 Ma (De Waele and Fitzsimons, 2004,). Amongst the youngest basement lithologies are the Mesoproterozoic cupriferous Mtuga aplites which crosscut Palaeoproterozoic granitic gneisses and have been dated at 1059 ± 26 Ma, intruding during the Irumide Orogeny (Rainaud et al., 2005).

In addition to relatively minor and low grade basement-hosted copper occurrences such as the Mtuga aplites, basement lithologies host significant concentrations of copper in some areas of the Copperbelt, including the Samba and Lumwana deposits. The Samba deposit is hosted in the pre-Katangan basement of the Kafue Anticline and hosts sulphides as disseminations, stringers and

veinlets in quartz-sericite schists (Wakefield, 1978). The sequence was metamorphosed prior to te deposition of the Katangan Supergroup and underwent pervasive potassic metasomatism following Lufilian Orogenesis (490 Ma) (Hitzman, 2010). Disseminated mineralisation is hosted within a sericitic alteration zone which has been constrained in age to between 462 and 464 Ma, based on ^{39}Ar-^{40}Ar dating (Hitzman, 2010). The Lumwana deposits (Malundwe and Chimiwungu) are located in the Domes Region of north-western Zambia and are discussed in more detail in section 3.1.7.

Katangan Supergroup:

The majority of copper and cobalt across the Central African Copperbelt is hosted within the sediments of the Lower Roan Subgroup of the Katangan Supergroup. The Katangan Supergroup forms a 1-4 km thick succession of metasedimentary basinal rocks, with a pre-erosional thickness of up to 11 km (Fig. 3-2) (Selley et al., 2018). The sediments unconformably overlie the basement, with the Nchanga Red Granite (883 ± 10 Ma, Armstrong et al. (2005)) and the Grand Conglomerate (approximately 740 Ma, Key et al. (2001)) imposing maximum and minimum age constraints, respectively. The sediments fill a series of north-northwest trending synclines or basins along the margins of basement domes, with the largest example being the Kafue Anticline (Selley et al., 2005).

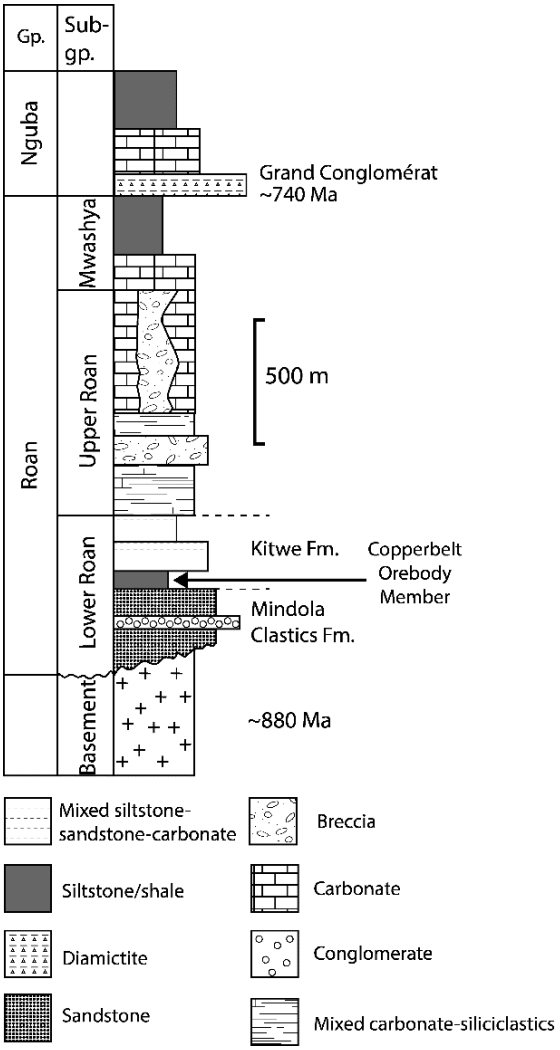

Fig. 3-2 Simplified stratigraphy of the Katangan Supergroup in the Zambian Copperbelt. Modified after Selley et al. (2005).

The Lower Roan stratigraphy hosts the majority of Cu-Co mineralised rocks in the Central African Copperbelt and comprises the Mindola Clastics Formation and overlying Kitwe Formation. The Mindola Clastics Formation is characterised by texturally immature conglomerates and upward-fining subarkosic sandstones deposited in fluvial, alluvial fan and fan delta environments (Selley et al., 2005; Woodhead, 2013). The sediments were deposited in spatially and structurally distinct sub-basins controlled by half grabens, resulting in highly variable lateral and vertical facies variations. These sub-basins mark the onset of basin rifting and resulted in highly variable sediment thicknesses, reaching up to 2 km north of the Domes inliers and pinching out completely elsewhere (Selley et al., 2018). Estimating the total thickness of initial rift phase sediments is challenging due to a lack of exposure of the basin depocentres, however regional gravity modelling indicates up to 5 km of Lower Roan syn-rift strata (Duffett et al., 2010). The lowest reaches of the rift stratigraphy are regionally decoupled along an evaporitic interval which may represent structural

reconfiguration of the basin and the first instance of significant marine waters becoming isolated (Bull et al., 2011; Jackson et al., 2003).

The coarse-grained, continental, oxidised nature of the Mindola Clastics is typical of a 'red bed' sequence, where Cu is concentrated in Fe-oxide, oxyhydroxide and clay coatings around siliciclastic grains following diagenetic alteration or destruction of mafic minerals (Rose, 1976).

The Kitwe Formation lies above the Mindola Clastics, with the lowermost Copperbelt Orebody Member forming the main Cu-Co-bearing reduced horizon. The Ore Shale comprises 20-30 m of shales and laminated dolomitic siltstones, thought to have been deposited during the 'rift climax' phase of basin development (Selley et al., 2005). Deposition of the Copperbelt Orebody Member was widespread across a larger, interconnected depocenter resulting in more laterally continuous subaqueous, reduced (pyritic) rocks (Woodhead, 2013). Abundant desiccation cracks locally replaced by anhydrite nodules are thought to represent episodic subaerial exposure in evaporitic conditions during this generally transgressive phase of basin evolution (Muchez et al., 2008).

Stratigraphically above the Copperbelt Orebody Member lies a 200 m-thick package of cyclical terrestrial conglomerates and subarkoses as well as marginal marine-evaporitic argillaceous siliciclastics of the Kitwe Formation (Selley et al., 2005).

Upper Roan Subgroup sediments are distinguished from the Lower Roan Subgroup by the predominance of carbonate strata over siliciclastic sediments (Mendelsohn, 1961), with the Upper Roan typically displaying laterally extensive metre-scale upward-fining cycles of sandstone, siltstone, dolomite and localised algal (Selley et al., 2005). Significantly, dolomitic strata of the Upper Roan Subgroup commonly displays nodules and 'chicken-wire' structures often interpreted as indicative of evaporitic processes in a sabkha environment (Selley et al., 2005). Similarly, unsorted, ungraded, massive polylithic breccia bodies, each up to tens of metres thick which commonly occur throughout the Upper Roan sediments are thought to be the result of widespread evaporite dissolution (Broughton et al., 2004; Selley et al., 2005). Analogous breccia units are present on a much larger scale in the Congolese Copperbelt, with individual, carbonate-dominated 'mega fragments' up to kilometres in scale hosting many of the Cu-Co ore bodies in the DRC (Jackson et al., 2003; Selley et al., 2018).

The Mwashya Subgroup and Nguba Group

Although the majority of historical Cu-Co discoveries have been made in sediments of the Lower Roan Subgroup, the upper Katangan Supergroup stratigraphy is gaining increasing attention from exploration companies. Mineralised rocks at Kansanshi, the largest copper mine in Africa (First Quantum Minerals F., 2019), have been correlated with strata of the Mwashya Subgroup and the

lowermost Nguba Group (Broughton et al., 2002), demonstrating the potential prospectivity of significant thicknesses of stratigraphy above the Copperbelt Orebody Member.

The Mwashya Subgroup sediments lie unconformably above Upper Roan Subgroup strata and are typically marked by a brecciated base, both in the DRC and in northern Zambia. Although the Mwashya Subroup is traditionally defined as a shale-dominant package, it is manifested as a sequence of dolomite and mixed dolomite-clastic intervals across the DRC as well as at the Konkola and Mufulira deposits in northern Zambia (Selley et al., 2005). In western and north-western Zambia, mafic volcanic units form part of the Mwashya Subgroup, yielding ages of between 760 ± 5 Ma and 745 ± 7.8 Ma, indicating a period of extensional mafic magmatism at this time (Armstrong, 2000; Key et al., 2001; Master et al., 2005).

Nguba Group sediments lie conformably above the Mwashya strata, marked by the base of the Grand Conglomérat, a sequence of debris flows and diamictites ranging from 10 to 100 m in thickness in Zambia, and up to 1300 m thick in the DRC (Selley et al., 2005). The Grand Conglomérat has been correlated globally with Sturtian diamictites (namely the Gubrah member in Oman), often associated with a global glaciation or 'Snowball Earth' event between approximately 750 and 700 Ma (Hoffmann et al., 2004; Hoffmann and Li, 2009; Key et al., 2001; Master et al., 2005). The Grand Conglomérat clast assemblage includes rare rounded clasts of basement material however it is dominated by sub-angular clasts of Upper Roan and Mwashya Subgroup sediments, indicating significant erosion of the middle part of the Katangan Supergroup (Selley et al., 2005).

The stratigraphy of the upper part of the Nguba Group comprises 400-500 m of carbonates and fine siliciclastic sediments, overlain by a rarely preserved second diamictite, the 'Petit Conglomérat' (Master et al., 2005; Selley et al., 2005).

3.1.3 Tectonic Evolution of the Katangan Basin

Although the fundamental stratigraphic components of the Katangan Basin have been described extensively in the literature, the processes by which the basin formed remain uncertain, with contrasting evidence for active syn-sedimentary rifting and more passive subsidence-dominated models (Kampunzu et al., 2000b; Mendelsohn, 1961; Selley et al., 2005). A lack of deep marine facies, syn-sedimentary faulting and magmatism in the Lower Roan stratigraphy all indicate the absence of active rifting during early basin formation, with Binda (1994) instead proposing a more significant role for eustasy. More recent studies have suggested that the basin underwent two main phases of active rifting (Selley et al., 2018). The onset of phase one rifting is marked by the oxidised clastics of the Mindola Clastics Fm., with the Copperbelt Orebody Member marking rift climax and marine inundation of the basin, followed by a period of basin starvation, evaporite precipitation

and carbonate deposition marked by Upper Roan rocks. The second stage of rifting is marked by the more reduced, shale-dominant lithologies of the Mwashya Subgroup, along with its broadly coeval mafic intrusives and perhaps involved a greater degree of crustal thinning (Armstrong, 2000; Key et al., 2001).

A series of metamorphosed basalts, dolerites and gabbros from the Katangan Aulacogen, External Fold and Thrust Belt and the Domes Region may indicate progressive rifting of the Congo-Kalahari margin. Continental tholeiites represent the earliest stages of intraplate breakup, followed by a series of alkaline and tholeiitic basalts formed during continental rifting, with late-stage tholeiitic basalts with E-MORB signatures indicating the formation of proto-oceanic crust. Kampunzu et al. (2000b) suggest this geochemical evolution represents distinct phases during active rifting of the margin, from pre-rift continental break-up, through an East African Rift-style continental rift, to a Red Sea-style incipient oceanic rift basin.

Basin inversion along the Congo-Kalahari suture produced broad folding and relatively minor reverse faulting throughout the Zambian and Congolese copperbelts, with tighter, more extensive folding in the Domes region (Selley et al., 2018). Inversion was accompanied by a thermal event in the Domes region, with peak P-T conditions of 600°C and 700 MPa evidenced in the Kabompo Dome (Meighan, 2015). Peak metamorphic conditions typically produced amphibolite grade rocks in the Domes Region, with greenschist facies assemblages more common in the Zambian Copperbelt (Selley et al., 2005). Where present in the Domes Region, phlogopite, kyanite and Mg-chlorite-bearing metamorphic rocks have recently been reinterpreted as hydrothermal in origin, with the traditional interpretation of high-grade 'whiteschist' assemblages, formed through near-isothermal (750°C) decompression during retrograde metamorphism (Cosi et al., 1992; John et al., 2004), challenged (Meighan, 2015). In the Zambian Copperbelt, Lufilian folding typically nucleated on earlier normal fault structures which were commonly reactivated, producing net reverse movement (Selley et al., 2018).

3.1.4 Zambian basin brines – a review

Microthermometric studies of fluid inclusions from several Zambian Copperbelt deposits have helped to outline palaeofluid conditions across a range of stratigraphic and geographic domains, from relatively early in basin history to post-orogenic times (McGowan et al., 2006; Muchez et al., 2010; Richards et al., 1988; Speiser et al., 1995). Table 3-1 provides a summary of palaeofluid properties from Zambian and Congolese Copperbelt deposits as well as deposits from the Kundelungu Plateau, north of the copperbelt.

Early basinal brines

Primary fluid inclusions from a mineralised vein at Chambishi, interpreted by Greyling et al. (2005) to immediately postdate stratiform mineralisation, are low homogenisation temperature (T_{hTOT} = 86-129°C) and moderate salinity (11.9-23.1 wt % NaCl equiv.) aqueo-carbonic solutions. Secondary inclusions, including aqueous and aqueo-carbonic solutions (± methane) form two populations, namely a high-salinity, lower-homogenisation temperature brine (18-23 wt % NaCl equiv.; 130-160°C) and a low-salinity, medium-homogenisation temperature fluid (6 wt % NaCl equiv.; 140-210°C). Greyling et al. (2005) interpreted these populations to represent an increasingly saline late diagenetic basinal brine and an early metamorphic fluid, respectively. Primary inclusions from nodules within the ore shale at Chambishi show similar temperature-salinity properties (T_{hTOT} = 110-180°C; 9-22 wt % NaCl equiv.) (Annels, 1989).

Early basinal brines have also been recorded at Kamoto and Luiswishi in the Congolese Copperbelt where El Desouky et al. (2009) described an early diagenetic two-phase (L+V) "type-I" fluid associated with finely disseminated stratiform sulphides with a T_{hTOT} range of 115-220°C and salinities of 11.3-20.9 wt % NaCl equiv. A similar temperature-salinity range (T_{hTOT} = 80-195°C and 8.4-18.4 wt % NaCl equiv.) has been recorded for primary inclusions from authigenic quartz associated with hypogene stratiform Cu sulphides at Kamoto and Musonoi (Dewaele et al., 2006).

Orogenic and post-orogenic fluids

Studies assessing the relationship between mineralised rocks and inversion structures at Nchanga (McGowan et al., 2006; McGowan et al., 2003), as well as an assessment of the relationship between vein-hosted and disseminated stratiform mineralisation across the Central African Copperbelt (Sillitoe et al., 2010), have highlighted the potential importance of fluids associated with basin inversion and orogenesis in the mineralisation of the copperbelt. McGowan et al. (2006) reported the presence of H_2O-NaCl ± $CaCl_2$ ± $MgCl_2$ with rare CO_2 at Nchanga, with salinities of 31-38 wt % NaCl equiv. and modal T_{hTOT} of 185°C and 155°C for the Lower and Upper Ore Bodies, respectively.

Orogenic fluids have also been recorded at Nkana where Muchez et al. (2010) and Greyling (2009) measured H_2O-NaCl/KCl-$MgCl_2$ brines, often with a gaseous component. Primary fluid inclusions in layer-parallel veins indicate temperatures of approximately 450°C during peak metamorphism. Cooler, secondary fluid assemblages from layer-parallel, irregular and massive veins have T_{hTOT} of 100-250°C and salinities of 18.1 - >23.2 wt % NaCl equiv., potentially representing late-stage retrograde metamorphic fluids (Muchez et al., 2010).

Fluid inclusions from mineralised quartz veins cutting the ore shale at Musoshi are halite-saturated high temperature fluids (T_{hTOT} = 397 ± 5°C) with approximately 39 wt % NaCl and 15 wt % KCl ± minor CO_2 (Richards et al., 1988). Similarly high temperature-salinity brines are reported from Kamoto and Luiswishi in the Congolese Copperbelt. El Desouky et al. (2009) described a three-phase (S+L+V) brine with a T_{hTOT} range of 270-385°C and salinities of 35-45.5 wt % NaCl equiv. These 'type-II' fluids are associated with syn-orogenic coarse-grained Cu sulphides and were interpreted to represent near-peak orogenic fluids, similar to those at Musoshi and Nchanga.

Fluid inclusions from the Kansanshi deposit in the Domes Region of the Zambian Copperbelt have complex salt compositions with NaCl, KCl, $CaCl_2$ and $MgCl_2$ in three-phase (S+L+V) inclusions with salinities of 30-43 wt % NaCl equiv. and T_{hTOT} ranging from 230°C to 310°C (Speiser et al., 1995). These fluids are hosted by quartz-carbonate veins which cross-cut metamorphosed sedimentary rocks of the Katangan Supergroup. Re-Os and U-Pb dating of molybdenite and monazite from these veins indicates that these are amongst the latest mineralising fluids identified in the copperbelt to-date, yielding post-orogenic ages of 502.4 ± 1.2 Ma to 512.4 ± 1.2 Ma (Torrealday et al., 2000).

Inferred primary fluid inclusions hosted within mineralised veins at the Enterprise hydrothermal Ni deposit in the Domes Region of north-western Zambia represent high temperature (>300°C) and salinity (40-70 wt % NaCl equiv.) brines with complex Na-K-Ca-Mg salt chemistries (Zimba, 2012). Laser ablation ICP-MS analysis of a small number of inclusions from a single mineralised vein sample returned average base metal concentrations of approximately 16,000 ppm Fe, 2,400 ppm Ni, 1,500 ppm Zn, 800 ppm Cu and 100 ppm Pb (Zimba, 2010).

These data suggest that relatively high temperature, saline brines were present throughout the Katangan Basin from late diagenetic to post-orogenic times, with a potential trend towards higher temperature-salinity brines during the onset of basin inversion.

Table 3-1 Summary of palaeofluid properties from a range of deposits across the Lufilian Arc

	Zambian Copperbelt Deposits					*Congolese Copperbelt Deposits*		*Kundelungu Plateau*	
	Chambishi	Nkana	Nchanga	Musoshi	Kansanshi	Kamoto & Luiswishi	Kipushi	Lufukwe & Mwitapile	Dikilushi
Fluids	Lateral secretion vein: (1) Primary (2) Secondary (3) Secondary	(1) Primary FIA in layer parallel veins (2) Secondary FIA in layer parallel, irregular & massive veins	(1) Upper Ore Body (2) Lower Ore Body	Primary FIA in mineralised veins cutting ore shale	Mineralised veins cross-cutting Katangan sediments	Authigenic quartz associated with mineralisation	Dolomite & quartz associated with Zn-Cu sulphides	(1) Primary FIAs in authigenic quartz (2) Secondary FIAs associated with mineralised rocks	(1) Primary Cu-Pb-Zn-Fe fluids (2) Secondary Cu-Ag fluids
Composition	H_2O-NaCl ± KCl ± $CaCl_2$ ± $MgCl_2$ ± CO_2 ± CH_4 ± N_2	H_2O-NaCl/KCl ± $MgCl_2$ ± gas?	H_2O-NaCl ± $CaCl_2$ ± $MgCl_2$	H_2O-NaCl-KCl ± $CaCl_2$ ± $FeCl_3$ ± CO_2	H_2O-NaCl ± KCl ± $CaCl_2$ ± $MgCl_2$ ± CO_2 ± CH_4	H_2O-NaCl ± unknown salts	H_2O-NaCl ± CO_2 ± CH_4 ± unknown salts	H_2O-NaCl- $CaCl_2$	(1) H_2O-NaCl- $CaCl_2$ (2) H_2O-NaCl-KCl
Temp (°C)	(1) 86-129 (2) 130-160 (3) 140-210	(1) 450 (2) 100-250	(1) 155 (2) 185	397	230-310	(1) 115-220 (2) 270-385 (3) 80-195	(1) 149-360 (2) 80-170	(1) 80-182 (2) 120-280	(1) 90-140 (2) 65
Salinity (wt % NaCl equiv.)	(1) 11.9-23.1 (2) 18-23 (3) 6	(1) – (2) 18.1->23.2	31-38	39 wt% NaCl 15 wt% KCl	30-43	(1) 11.3-20.9 (2) 35-45.5 (3) 8.4-18.4	(1) 30-43 (2) 23-31	(1) 18.8-25.5 wt.% $CaCl_2$ (2) 1.9-19.8 wt.% $CaCl_2$	(1) 20-25 wt.% $CaCl_2$ (2) ≥19
Stratigraphic Level	Lower Roan	Lower Roan	Lower Roan	Lower Roan	Nguba Group	Mines Subgroup (Lower Roan)	Mwashya-Lower Kundelungu	Nguba & Kundelungu	Kundelungu
Approx. Timing in Basin Evolution	(1) Post-mineralisation (2) Late diagenetic (3) Metamorphic/ orogenic fluid	(1) Peak metamorphism (2) Retrograde metamorphism	Basin inversion	Peak orogenic (?)	Post-peak orogenic	(1) Early diagenetic (2) Peak orogenic (?) (3) Diagenetic?	(1) Orogenic? (2) Post-orogenic	(1) Post-orogenic (2) Post-orogenic	(1) Post-orogenic (2) Post-orogenic
Reference	Greyling et al. (2005)	Muchez et al. (2010)	McGowan et al. (2006)	Richards et al. (1988)	Speiser et al. (1995)	(1) & (2) El Desouky et al. (2009) (3) Dewaele et al. (2006)	Heijlen et al. (2008)	El Desouky et al. (2008a & b)	Haest et al. (2009)

Homogenisation temperatures reported as T_{hTOT} and salinities as wt % NaCl equiv. unless otherwise stated.

Bulk crush-leach analysis of Zambian Copperbelt brines has provided an insight into fluid origins through the study of halogen systematics (Heijlen et al., 2008; Nowecki, 2014; Selley et al., 2018). Halogen systematics generally remain unmodified by fluid-rock interactions throughout a fluid's history and are therefore a reliable tool for determining fluid origins. The co-variance of Cl and Br during the evaporation of seawater until the halite saturation point implies that similar processes control both elements during evaporation. The molar Cl/Br ratio of seawater throughout this process remains approximately 656. Beyond the halite saturation point Cl is preferentially removed from the liquid, leaving the residual fluid enriched in Br (Cl/Br <656). Dissolution of evaporite deposits is the most common process by which halogen systematics are altered, with the dissolution of sylvite (commonly enriched in Br) reducing Cl/Br and the dissolution of halite increasing the Cl/Br ratio, often into the tens-of-thousands.

Two recent overviews of palaeofluids across the Zambian Copperbelt have taken vein chronologies into account and defined two temporally and geochemically distinct fluid generations (Nowecki, 2014; Selley et al., 2018). Two distinct phases of veining were recognised, pre-syn- and post-kinematic. The pre- to syn-kinematic veins host fluid inclusions with low Cl/Br ratios, indicating that they were derived from bittern brines, with Br-enrichment resulting from the evaporation of seawater beyond the point of halite saturation and/or a component of sylvite dissolution (Fig. 3-3). The second, post-kinematic vein generation hosts fluid inclusions characterised by higher Cl/Br ratios, mainly above that of seawater, indicating Cl-enrichment through the dissolution of *in situ* halite deposits. The evaporite deposits in the Central African Copperbelt are thought to have dissolved during a protracted history of basinal fluid flow, tectonic brecciation and basin inversion and rocks with abundant evaporitic textures including breccia sequences are present in the Upper Roan subgroup of the Katangan Basin (Selley et al., 2005).

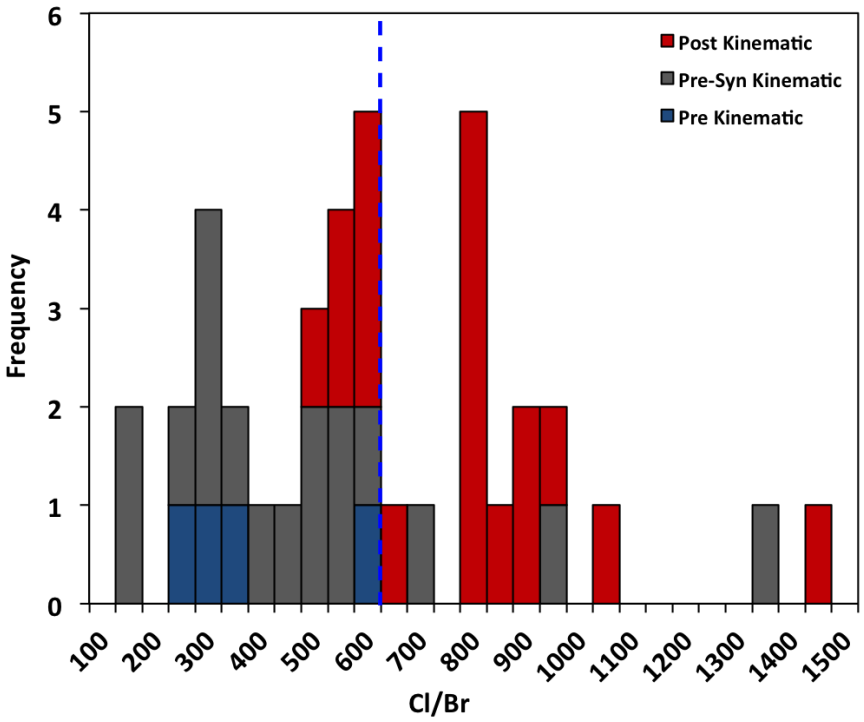

Fig. 3-3 Cl/Br ratios for Zambian Copperbelt palaeofluid leachates from vein material (categorised by relative age) from various deposits (Nchanga, Lumwana, Kansanshi, Konkola, Konkola North, Samba, Enterprise, Sentinel). Dashed blue line represents the molar Cl/Br of modern day seawater. Modified after Nowecki (2014).

In addition to a comparison of the fluid characteristics of different sediment-hosted copper provinces globally, this study will focus on, and compare, 3 deposits within the Zambian Copperbelt (Nkana-Mindola, Nchanga and Lumwana). Nkana-Mindola and Nchanga are both located on the south-western margin of the Kafue Anticline and represent more 'typical' Zambian Copperbelt deposits, whereas Lumwana is located approximately 350 km to the northwest, in the Domes Region, with mineralisation hosted in basement lithologies stratigraphically below the Katangan Supergroup sediments. These deposits were selected to give an overview of the P-T-*X* evolution of brines in the Zambian Basin from pre- to post-Lufilian times. All three deposits contain disseminated and vein-hosted sulphides, often strongly structurally controlled and arguably all show evidence for multiple phases of mineralisation over a prolonged time period. Nchanga and Lumwana have been the subject of previous detailed studies within the research group at the University of Southampton (Bernau et al., 2013; McGowan et al., 2006), and samples have been taken from these suites for further fluid inclusion analysis in this study. Additionally, the author visited several open pits and logged drillcore from the Nkana-Mindola deposit in order to provide a similarly detailed fluid study of a third major mineralised system. The following sections review the geological setting of each deposit.

3.1.5 Nkana-Mindola

The Nkana-Mindola Cu-Co deposit is located in the Kitwe area of the Zambian Copperbelt on the western limb of the Kafue Anticline. Mining is primarily focussed at the Nkana South, Nkana Central and Mindola North ore bodies on the north-eastern limb of the northwest-plunging Nkana Syncline (Chambishi Basin) (Fig. 3-4). The Nkana ore bodies are separated from the Mindola deposit by the Kitwe barren gap (1.2 km along-strike). To date, no economic ore has been found along the south-western limb of the Syncline (Brems et al., 2009; Muchez et al., 2010). As of 2013, the mineral resource estimated at Nkana-Mindola was 702 million tons grading 2.17% Cu and 0.06% Co, totalling 15.2 Mt of contained Cu and 428,602 tons of contained Co (Taylor et al., 2013).

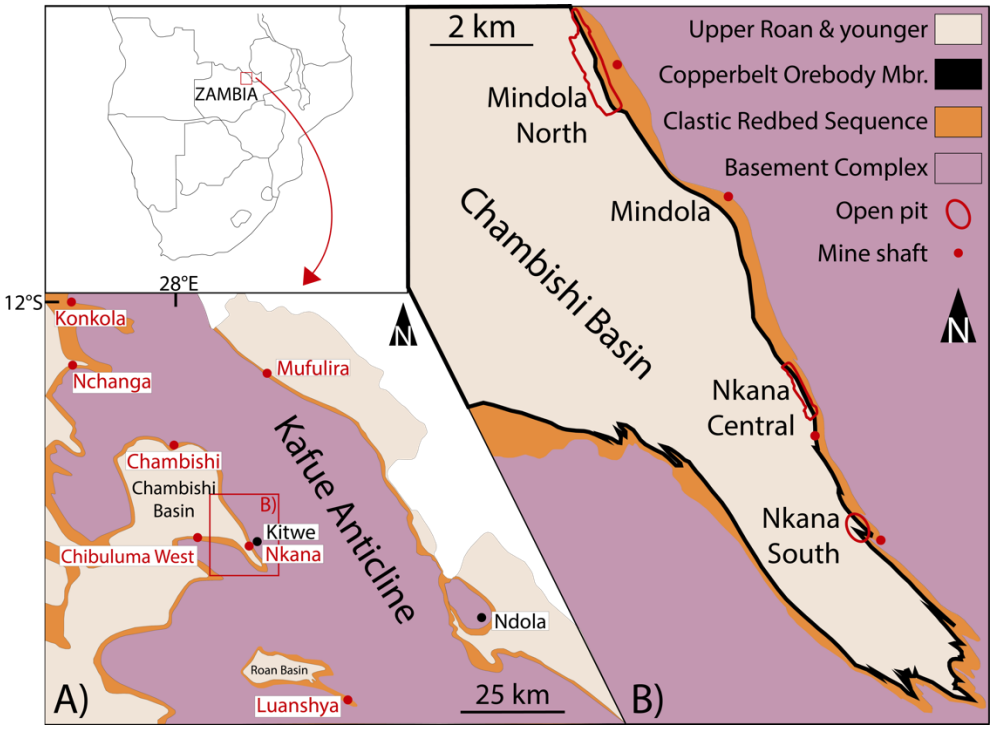

Fig. 3-4 Schematic geological map of the Chambishi Basin (A) and its wider geological context on the western limb of the Kafue Anticline (B). The main Nkana-Mindola open pits and mine shafts are highlighted along the Copperbelt Orebody Member. Modified after Torremans et al. (2014) and McGowan et al. (2006).

Sediments of the Lower Roan Subgroup unconformably overlie the Basement Complex at Nkana, with the 0-25 m-thick Basal Conglomerate (terrestrial talus screes and fluvial sediments) infilling palaeo-valleys in the basement topography (Fig. 3-5) (Brems et al., 2009; Clemmey, 1974). Immediately above the Basal Conglomerate lies the more substantial Basal Quartzite, a 5-160 m-thick argillaceous-to-feldspathic quartzite with intermittent pebble beds and giant cross-beds, indicating an aeolian environment (Jordaan, 1961). The Basal Quartzite is overlain by the 20-35 m-thick Footwall Sandstone unit that consists of arkosic to argillaceous and carbonate-rich

sandstones, sandwiched between lower and upper conglomerates. Above the Footwall Sandstone, the Ore Formation, consists of a series of variably altered and mineralised argillites, typically 10-35 m thick and containing abundant anhydrite veins and lenses (Jordaan, 1961). Above the Ore Formation, the Hangingwall Quartzite forms the, a 1-5 m-thick feldspathic quartzite deposited in a shallow marine or tidal flats environment (Clemmey, 1974).

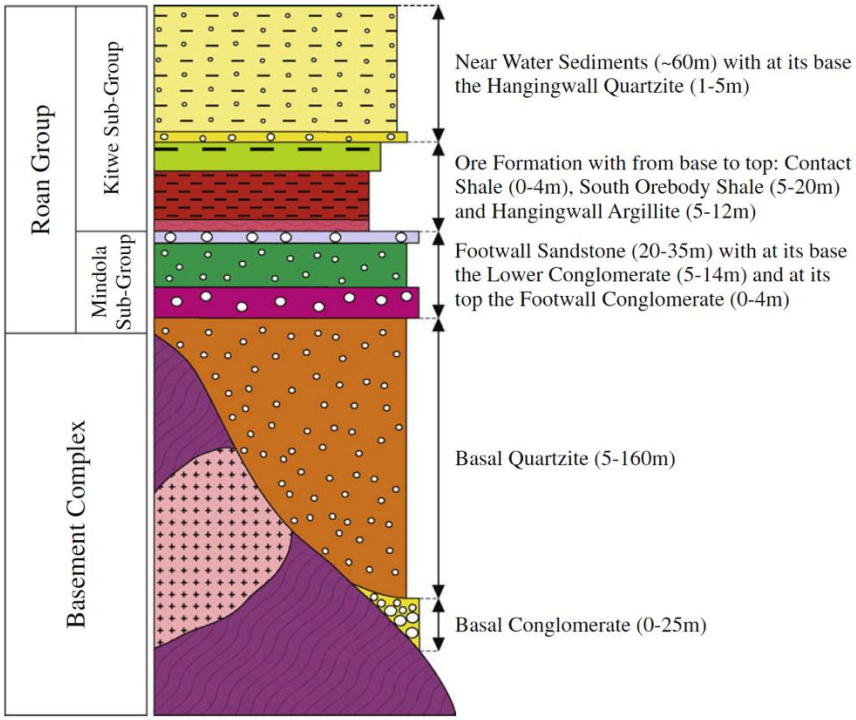

Fig. 3-5 Simplified lithostratigraphy of the Lower Roan strata at Nkana South. After Brems et al. (2009).

Metamorphic mineral assemblages within the argillites of the Ore Formation comprise of biotite, chlorite, tremolite, talc, sericite and albite, indicating greenschist facies metamorphic grades were reached during basin inversion (Muchez et al., 2010). The resultant folding is polyharmonic, ranging from 1st order basin-scale folds to decimetre and sub-metre-scale 2nd and 3rd order isoclinal folds (Croaker, 2011; Torremans et al., 2014). A strong bedding-parallel S_1 cleavage is developed within the argillites of the Ore Formation along the entire 14 km strike length of the Nkana-Mindola deposits, whereas an axial planar S_2 cleavage is less pervasive and more strongly developed in the Nkana South Orebody (Torremans et al., 2014).

Mineralisation:

Copper ± Co sulphides occur as both fine disseminations and in coarser aggregates within veins in all three of the major ore bodies at Nkana-Mindola, however their styles tend to vary along strike. The Nkana South Orebody comprises an altered Contact Shale, the graphitic South Orebody Shale and the pyritic Hangingwall Argillite (Jordaan, 1961). The majority of sulphides occur as coarse, vein-

hosted aggregates, however some disseminated chalcopyrite is present, primarily in the fissile, black South Orebody Shale unit.

The Nkana Central Orebody can be subdivided into two units – a lower Tremolite Schist, an altered, interbedded package of darker argillaceous sediments and lighter coloured micaceous dolomites with disseminated bornite, chalcopyrite and carrollite, and an upper Micaceous Shale containing chalcopyrite and carrollite (Jordaan, 1961). Much of the mineralised rocks here are present as fine-coarse disseminations along laminations.

The Mindola Orebody comprises a series of lithologies, notably more arenaceous than at the Nkana orebodies, such as banded sandstones and cherts with a relatively minor argillaceous component. The sulphide assemblage primarily consists of bornite, chalcopyrite and carrollite, with minor chalcocite and pyrite within the Porous Sandstone package (Brems et al., 2009; Jordaan, 1961).

At the Nkana South and Central Orebodies sulphides are zoned, from predominantly bornite-chalcopyrite-carrollite in the argillaceous units, to chalcopyrite-carrollite in the more carbonaceous shales, with sulphide zones trending sub-parallel to the plunge of the syncline. At Mindola, sulphide zoning is not associated with facies changes, with bornite, bornite-chalcopyrite-carrollite and chalcopyrite-carrollite zones overprinting relatively homogenous lithologies across large vertical and lateral extents (Jordaan, 1961). Copper grades also show a degree of structural control, with more intensely deformed zones (Nkana South), typically showing higher grades than less deformed regions such as Mindola North.

Vein-hosted Cu sulphides are also present at Nkana-Mindola, with more ubiquitous veining further south along the orebody. Several vein generations have previously been recognised and typically split into three categories based on their relative timing (Table 3-2) (Brems et al., 2009; Muchez et al., 2010; Van Wilderode et al., 2015).

Table 3-2 Summary of published vein generations at the Nkana South mine (Muchez et al., 2010; Torremans et al., 2014).

	Layer-parallel	Irregular	Massive
Mineralogy	Qtz-musc-cal-dol-py-cpy-cc-po	qtz-cal-musc-bio-py-dol-kspar-cpy-bn-cc-po	Qtz-cal-dol-kspar-musc-py-po-cpy-bn-cc-carr-pen
Kinematics	Sub-parallel to stratification	Cross-cut folded layer-parallel veins. Often parallel to axial planar cleavage	Cross-cut S_0, S_1 and previous vein generations
Proposed Timing	Before and during the onset of orogenesis	Peak orogenesis	Post-peak orogenesis

This study primarily focuses on two end-member vein generations - bedding-parallel veins and massive, cross-cutting veins:

Bedding-parallel veins:

Typically, quartz-carbonate-sulphide veins, most abundant in the carbonaceous/graphitic shales of the Nkana South and Nkana Central orebodies, but also present in more dolomitic lithologies in the Mindola North open pit. These veins range from <1 cm wide at Mindola, to a maximum of approximately 25 cm wide in the Nkana South open pit. Veins range from planar to folded and boudinaged and typically host abundant bn-cpy with lesser py-cc-po. These veins were likely emplaced prior to, or at the onset of, Lufilian folding, prior to the development of the axial planar S_2 cleavage visible in the argillaceous lithologies at Nkana South. As such, bedding-parallel veins are also referred to as 'pre- to syn-kinematic' veins hereafter.

Massive, cross-cutting veins:

Massive quartz veins with lesser carbonate and minor sulphides (often just cpy) often cross-cut bedding, as well as the sub-parallel S_1 and axial planar S_2 (Fig. 3-6). These veins are typically 40-60 cm wide and occur in both the argillites of the Ore Formation as well as the hanging wall siliciclastics. Although most veins are broadly planar and continuous, examples of tension gash arrays were observed in the Nkana South open pit (Fig. 3-6). These are likely the result of late/post-orogenic dilational tectonics. Cross-cutting relations and vein kinematics indicate that these veins were emplaced post-peak orogenesis and as such, are also referred to as 'post-kinematic' hereafter.

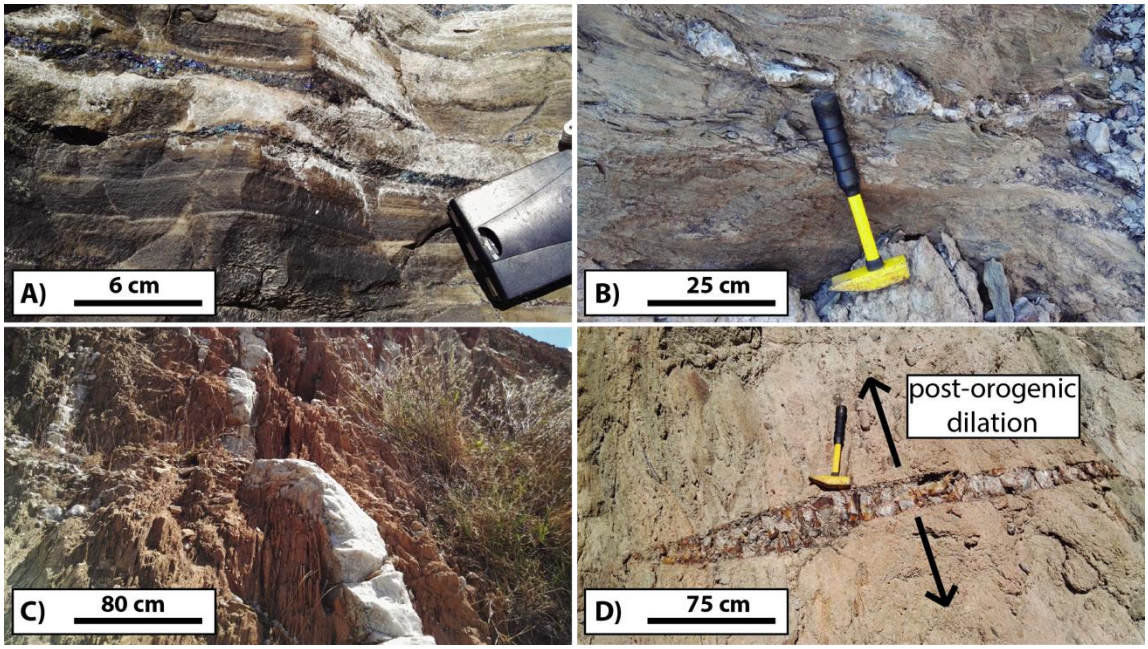

Fig. 3-6 Nkana-Mindola vein images. A) Quartz-bornite-chalcopyrite layer-parallel veinlets within calcareous arenite in the Mindola North open pit. B) Layer-parallel boudinaged quartz-bornite-chalcopyrite-carrollite vein within the ore shale unit at the Nkana South Orebody. C) Massive (60 cm-wide) discordant quartz vein cross-cutting the S_1 fabric within the hanging wall sediments and Ore Formation at the Nkana Central Orebody. The vein is largely barren, with minor fine chalcopyrite. D) Lowermost barren quartz vein within a tension gash array spanning approximately 20 m of vertical extent in the hanging wall stratigraphy above the Nkana Central Orebody.

Using Sr and Nd isotope ratios from gangue carbonates at Nkana, Van Wilderode et al. (2015) proposed source regions for three phases of mineralisation. Pre- to syn-kinematic mineralisation may have been sourced from felsic basement rocks of the Domes Region; a second, syn-kinematic mineralisation phase resulting from remobilisation of earlier sulphides; and then a final, late-kinematic mineralisation event, with some form of Co-rich mafic component. However, there remains a lack of credible mafic material in the lower Katangan stratigraphy, and the relationship between the basement rocks of the Kafue Anticline and the mineralised rocks at Nkana-Mindola is unclear.

Re-Os dating of chalcopyrite, carrollite and bornite at Nkana suggests a pre-kinematic mineralisation event at 583 ± 24 Ma (based on a five point isochron from vein-hosted sulphides at Nkana, Chibulumba and Nchanga), followed by a late-kinematic age of 525.7 ± 3.4 Ma for late, chalcopyrite-bearing veins (Barra et al., 2004). However Re-Os dating of relatively early sulphides in the Zambian Copperbelt remains contentious (Sillitoe et al., 2017).

Sampling:

Samples of quartz-carbonate vein material were taken from veins representing a variety of contrasting kinematics from the three main orebodies along 14 km of strike at Nkana-Mindola, as well as from Mopani Mines borehole MX0236. The borehole was drilled obliquely up-section 290 m through the footwall from underground at the Mindola North mine (level 440 m).

Bedding-parallel veins were taken from both the argillaceous sediments at Nkana Central and Nkana South, as well as the more siliceous dolomite lithologies representing the majority of the orebody at Mindola North. Massive, cross-cutting veins were only observed and sampled from the open pits at Nkana Central and Nkana South. Samples selected for fluid inclusion study were typically milky quartz veins with associated sulphide mineralisation.

3.1.6 Nchanga

Nchanga is one of the largest mineralised systems in the Zambian Copperbelt and lies on the southwestern limb of the Kafue Anticline, approximately 75 km northwest of Kitwe and the Nkana-Mindola deposits (Fig. 3-4). The deposit consists of a lower and upper orebody which host Cu-only and Cu-Co mineralisation, respectively, totalling approximately 13.8 Mt contained Cu and 131,000 tons of Co (Taylor et al., 2013).

Copper enrichments are hosted in arenites and shales of the Lower Roan Subgroup stratigraphy, which unconformably overlies the basement, including the Lufubu Schists and Gneisses, the Muva Quartzites and the Nchanga Red Granite, which has been dated at 883 ± 10 Ma (Armstrong et al., 2005). Above the basement lie basal conglomerates and the Lower Arkose, which were deposited directly onto the pre-Katangan topography, resulting in highly variable thicknesses between 50 and 300 m (Fig. 3-7) (McGowan et al., 2006). The Lower Orebody straddles the uppermost strata of the Lower Arkose (70%) and the lowermost section of the Lower Shale above (30%). Stratigraphically above the Lower Shale, the Mixed Arenite and Shale unit comprises up to 50 m of heavily deformed intercalated arenites, dolomitic sandstones and shales, which are typically barren (McGowan et al., 2006). The Mixed Shale and Arenite Unit is overlain by the Feldspathic Quartzite unit (TFQ), which hosts 90% of Cu and Co in the Upper Orebody, with the overlying Upper Shale hosting the remainder. The Upper Shale marks the transition from Lower Roan Subgroup to Upper Roan Subgroup stratigraphy, with carbonate lithologies dominating the stratigraphy above the Upper Orebody at Nchanga (McGowan et al., 2006). This sequence represents a transition from an intracratonic basin environment, to a shallow marine evaporitic and then platform carbonate environment into the Upper Roan (Fleischer et al., 1976).

The basement lithologies at Nchanga display irregular fault-block geometries, with high angle (~80°) normal faults propagating into the footwall clastic sequences, indicating deposition of footwall sediments during active extension of the basin (McGowan et al., 2006). Subsequent basin inversion during the Lufilian Orogeny subjected the Nchanga stratigraphy to greenschist facies metamorphic conditions. Compressional tectonics resulted in the formation of fault-propagation folds that detach at the base of the Lower Arkose and verge towards the northeast (McGowan et al., 2003). Much of the thrusting at Nchanga is associated with a strong planar fabric, typically sub-parallel to bedding, which is controlled by the west-northwest-plunging Nchanga Syncline – a 12 km-long asymmetric structure formed from north-south compression (Daly et al., 1984).

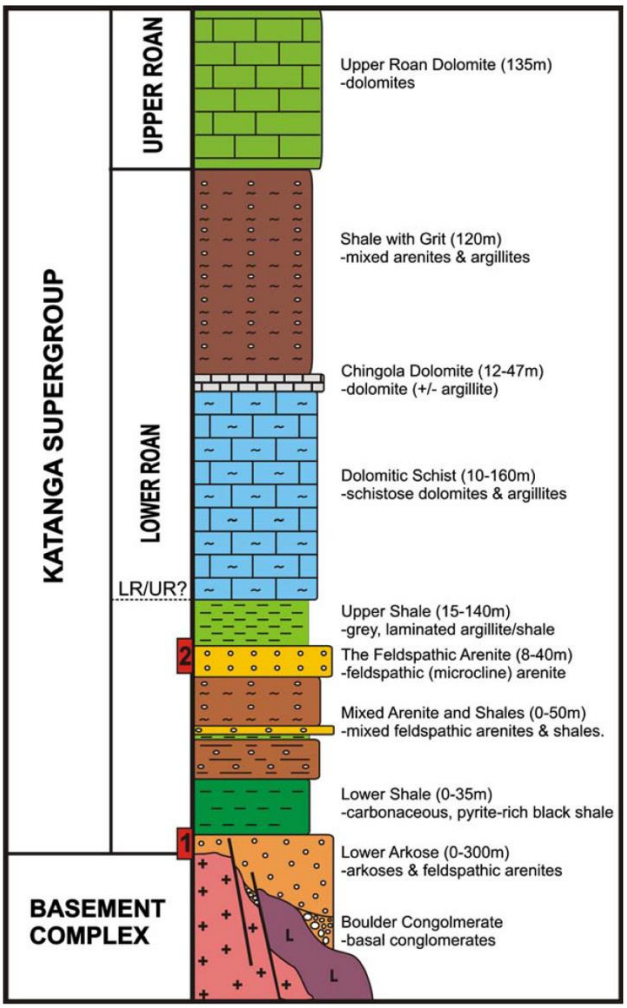

Fig. 3-7 Stratigraphy of the Lower Roan and basement complex at Nchanga, including the position of the Lower Orebody (1) and Upper Orebody (2). After McGowan et al. (2006).

The Lower Orebody:

The Lower Orebody (copper only) is hosted in the Lower Arkose and the overlying Lower Shale and is continuous for approximately 5 km along-strike. It ranges in thickness from 0.5 m to 20 m, with the resource typically grading 2-3% Cu over 6-10 m. The majority of mineralisation within the Lower

Orebody is hosted by the coarser grained Lower Arkose unit, indicating porosity and permeability may have been a key control on ore distribution (McGowan et al., 2006). Mineralisation occurs as both fine disseminations and in quartz veins and is dominated by replacement chalcocite and malachite, with some evidence for a replacement mineral paragenesis of diagenetic anhydrite replaced by pyrite > chalcopyrite ± bornite > chalcocite > malachite (McGowan et al., 2003). The highest ore grades are strongly associated with the tectonised contact between the Lower Arkose and Lower Shale, as well as basin inversion structures.

The Upper Orebody:

The Upper Orebody (copper and cobalt) is primarily hosted in the Feldspathic Arenite unit, with lesser metal enrichment of the overlying Upper Shale. Grades average 2.5-3% Cu and up to 1% Co, with Co restricted to the Nchanga Open Pit (McGowan et al., 2006). Mineralisation occurs as bornite, chalcopyrite and carrollite which replace pyrite, with chalcocite typically rimming and replacing primary copper sulphides (McGowan et al., 2003). Cobalt (and to a lesser degree, copper) shows a strong relationship with compressional structures such as fault-propagation folds, with mineralised rocks absent at the Upper Orebody level in relatively undeformed sections of the Katangan stratigraphy.

Ore Genesis:

In a detailed structural, mineralogical, isotopic and fluid inclusion study of the Nchanga deposit, McGowan et al. (2006) proposed an epigenetic mineralisation model for Nchanga based on the following criteria:

- A strong relationship between mineralised rocks and inversion structures indicates syn-tectonic ore formation.
- With the majority of mineralised rocks being hosted in the Lower Arkose and the Feldspathic Arenite units, porosity and permeability appear to have played a key role in controlling fluid migration at Nchanga, with the overlying shales acting as seals.
- Hydrothermal alteration around the ore bodies, consisting of phlogopite ± sericite, followed by later dolomite indicate *in situ* thermochemical reduction of slightly acidic, sulphate-rich metalliferous brines.
- Contrasting $\delta^{34}S$ values between diagenetic pyrites of the Lower Shale, and sulphides of the Upper and Lower Orebodies precludes a relatively early, diagenetic, bacteriogenic sulphide contribution. Instead, the positive $\delta^{34}S$ values from Nchanga may indicate thermochemical sulphate reduction.

- With carbonates commonly produced during thermochemical reduction of sulphate, anomalously light $\delta^{13}C$ and $\delta^{18}O$ values from Nchanga carbonates also indicate *in situ* reduction of an oxidised Cu-Co-bearing fluid with an additional organic carbon contribution, perhaps in the form of structurally trapped methane within the clastic reservoirs of The Feldspathic Arenite and Lower Arkose units (Fig. 3-8).

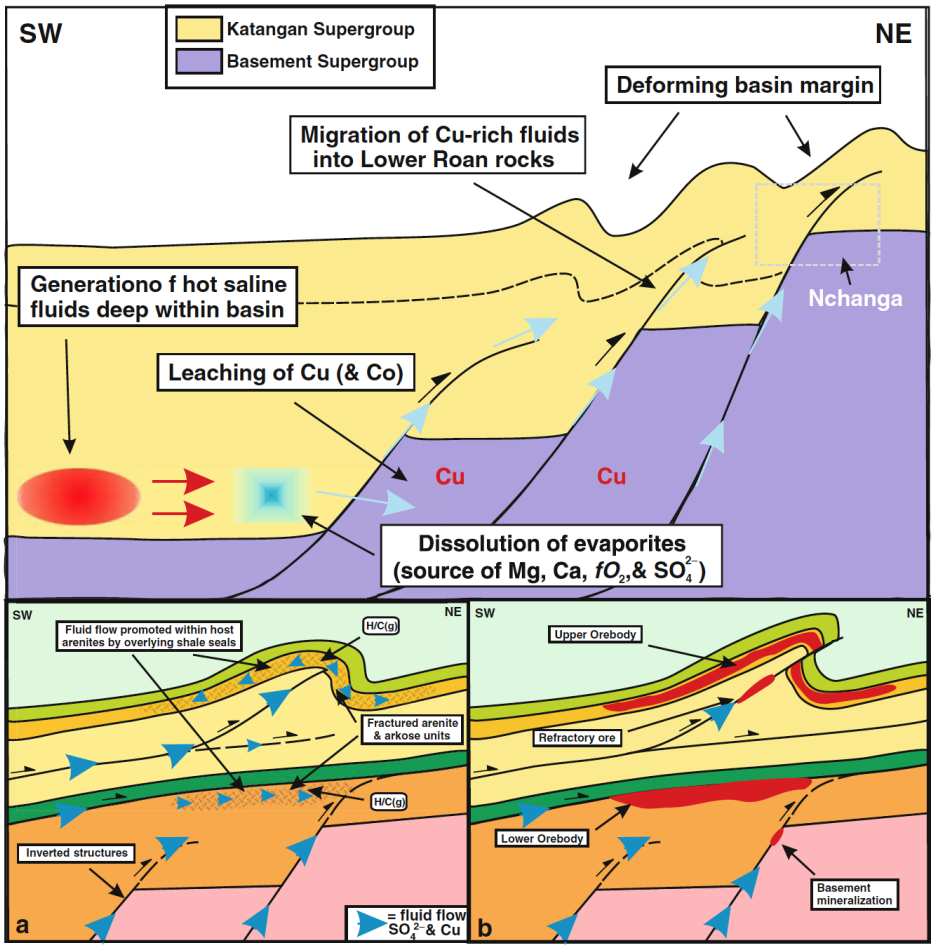

Fig. 3-8 Genetic model illustrating epigenetic mineralisation at Nchanga as a result of *in situ* thermochemical reduction of high temperature sulphate- and Cu-Co-bearing brines. a) Fluid migration was aided by high angle inverted rift structures in the basement and Lower Arkose, as well as low angle thrust structures within the Katangan sediments. b) Fluids were sealed by overlying shale units, and rapidly reduced by methane-rich reservoirs in structural traps, causing sulphide precipitation. After McGowan et al. (2006).

Sampling:

Veins from Nchanga were taken from the sample set of R. McGowan, a previous PhD student within the research group at the University of Southampton. The majority of samples for this project were selected from the most economically productive units of the Nchanga stratigraphy – the Lower Arkose (Lower Orebody) and the Feldspathic Arenite (Upper Orebody). Several vein samples were

also selected from granites within the basement, stratigraphically below the Lower Orebody in order to gain a representative suite of fluids from the basement to the Upper Orebody.

3.1.7 Lumwana

The Lumwana Cu (± Co-U) deposits are located approximately 350 km northwest of Kitwe, in the Domes Region of the Central African Copperbelt. The Domes Region is characterised by a sequence of Early- to Mid-Proterozoic basement inliers or 'domes', each surrounded by onlapping metasediments of the Katangan Supergroup. The Domes are typically comprised of a series of granites, gneisses, migmatites and schists displaying strong metamorphic fabrics and pervasive shear zones (Bernau et al., 2013). The Lumwana deposits, comprised of the Chimiwungo, Malundwe and Lubwe orebodies, are hosted within the Mwombezhi Dome, located between the Solwezi Dome to the east and the Kabompo Dome to the west, and host a total of approximately 6.9 Mt contained Cu (Taylor et al., 2013).

The core of the Mwombezhi Dome is primarily composed of migmatitic granitic gneisses with boudins of garnet-bearing amphibolites. These lithologies typically preserve a sub-horizontal S_1 fabric; overprinted by a later, parallel S_2 fabric defined by muscovite, and have been interpreted as pre-Katangan basement (Bernau et al., 2013; Eglinger et al., 2016; Turlin et al., 2016). The basement units are surrounded by a series of Katangan Supergroup metasediments, separated by a major shear zone (Fig. 3-9) (Bernau et al., 2013; Eglinger et al., 2016; John et al., 2004).

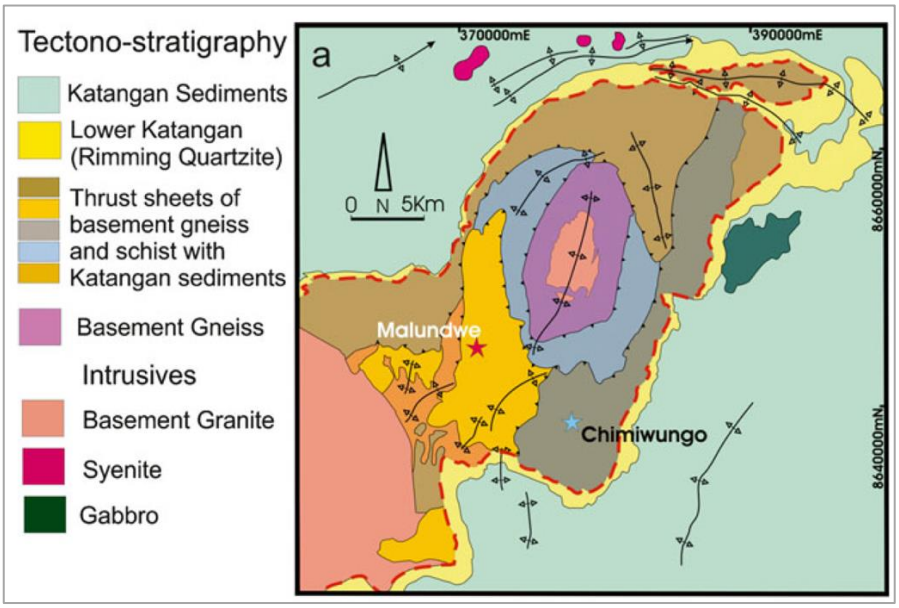

Fig. 3-9 Simplified geology map of the Mwombezhi Dome with the Chimiwungo and Malundwe deposits marked. The red dashed line represents a major shear zone separating basement lithologies from Katangan Supergroup sediments. After Bernau et al. (2013).

The basement and lower Katangan metasediments exposed at Lumwana have undergone at least three phases of deformation, as outlined by Turlin et al. (2016):

> *D_1:* Deep burial during subduction of the Congo margin during collision of the Congo and Kalahari Cratons.
>
> *D_2:* Syn-orogenic exhumation (a decompressing, approximately isothermal system).
>
> *D_3:* Post-orogenic exhumation during gravitational collapse of the orogeny.

In a complimentary study of the tectono-metamorphic evolution of the western Zambian Copperbelt, Eglinger et al. (2016) reconstructed the *P-T-t-d* path of basement and lower Katangan metasediments using thermobarometry and geochronology. The study attributed peak *P-T* conditions of 900-1100 MPa and 640-660°C to the D_1 event, dated at *ca.* 530 Ma using garnet whole-rock Lu-Hf isochron dating. This implies a maximum burial depth of 40-50 km with geothermal gradients of 15-20°C/km during peak Pan African orogenesis. Later syn-orogenic exhumation (D_2) is characterised by broadly isothermal decompression, to *P-T* conditions of 600-800 MPa between *ca.* 530-500 Ma, with an increased geothermal gradient of 25-30°C/km. Post-orogenic gravitational collapse resulted in decompression and temperatures of approximately 580-620 ± 50°C, according to Zr-in-rutile geothermometry (Turlin et al., 2016).

Chimiwungo Orebody:

Chimiwungo is a large, tabular body with a strike length of approximately 4 km and an average grade of 0.64% Cu and 0.01% Co (Taylor et al., 2013). It comprises three distinct ore schist horizons with intermittent barren strata. The footwall typically consists of a quartz-biotite-feldspar banded gneiss, while the hanging wall comprises a granitic gneiss and a banded to augen gneiss (Bernau et al., 2013). The Upper, Middle and Lower Ore Schist units average 10, 60 and 12 m in thickness, respectively, with slightly differing sulphide assemblages in each, from chalcopyrite and pyrite ± pyrrhotite, through chalcopyrite-bornite, to a lowermost zone of bornite ± chalcopyrite ± cobaltiferous phases (Bernau et al., 2013). Sulphides are typically aligned with the S_1 fabric or occur as inclusions in kyanite porphyroblasts and associated pressure shadows (Bernau et al., 2013; Turlin et al., 2016). Vein-hosted sulphides are common, with the most highlyenriched veins typically being boudinaged and sheared, indicating pre- to syn-orogenic emplacement. Discordant veins which cross-cut the metamorphic fabric in the hanging wall and footwall are typically barren or host very minor chalcopyrite, indicating remobilisation of earlier sulphides.

Malundwe Orebody:

The Malundwe orebody hosts significantly less mineralisation than Chimiwungo, with only one ore schist horizon, averaging 15 m in thickness and grading 0.89% Cu, with negligible Co (Taylor et al., 2013). The ore schist is a biotite-muscovite-quartz-bornite-chalcopyrite-kyanite schist, with fewer internal gneiss units than at Chimiwungo, and grades upwards into a more melanocratic, biotite-rich gneiss in the hanging wall (Bernau et al., 2013). The footwall is comprised of barren kyanite schists, overlying a marble, amphibolite and metapelite sequence, which has been interpreted as a remobilised fault-bound, deformed sliver of Katangan Supergroup lithologies (Bernau et al., 2013; Cosi et al., 1992).

Comparisons of the relative enrichment/depletion of different elements between the ore schist and the hanging wall gneiss indicate pervasive replacement of feldspars by biotite at Lumwana – a characteristic of progressive deformation and alteration of high-silica gneisses into schists (Bernau et al., 2013). Along with the fabrics and zones of intense shearing, this serves as strong evidence for a phase of pre- to syn-kinematic mineralisation, as is also evident at Nkana and Nchanga.

Inclusions of chalcopyrite, bornite and pyrrhotite in the earliest generation of kyanite at Lumwana have lead several authors to propose a Cu-rich or pre-mineralised protolith for the ore schist (Benham et al., 1976; Bernau, 2007; Turlin et al., 2016). A second generation of sulphides has been proposed as coeval with the development of the S_2 schistosity during exhumation of subducted basement lithologies during the D_2 phase of Turlin et al. (2016). A final phase of sulphides, comprising chalcopyrite with lesser bornite, form in pressure shadows around kyanite grains and are interpreted to represent a syn- to late-kinematic phase of mineralisation (Turlin et al., 2016). This phase of mineralisation is broadly contemporaneous with dates obtained from syn-metamorphic uraninite and molybdenite at Lumwana:

- 531 ± 5 Ma - U-Pb dating (Eglinger et al., 2016)
- 534.4 ± 2.2 Ma and 524.8 ± 2.2 Ma - Re-Os dating (Nowecki, 2014)

Sulphur isotope data from syn-metamorphic sulphides at Lumwana are consistent with thermochemical reduction of sulphate as opposed to diagenetic-related biogenic sulphate reduction, with the highest $\delta^{34}S$ values associated with cobalt mineralised rocks, as is the case at Nchanga (Bernau et al., 2013; McGowan et al., 2003).

Sampling:

Although the Lumwana deposit does not represent a classical Zambian Copperbelt deposit *sensu stricto*, assessing the nature of mineralising fluids in a deposit within the Domes Region allows a useful comparison with more 'typical' Zambian Copperbelt deposits such as Nkana-Mindola and Nchanga which are hosted within a different stratigraphic interval and display contrasting metamorphic grades and metasomatic assemblages.

Veins from Lumwana were taken from the sample set of R. Bernau. An array of different vein types were sub-sampled from both drillcore and open pit for fluid inclusion studies. These include barren, or very weakly mineralised discordant and bifurcating veins from the hanging wall and footwall lithologies, as well as mineralised (typically cpy-bn), deformed and boudinaged veins from the ore schist horizons.

3.2 Kalahari Copperbelt

The Kalahari Copperbelt (KCB) is an 800 km-long terrane trending southwest-northeast from central Namibia to the Northwest province of Botswana. The Ghanzi-Chobe ridge in northwestern Botswana defines the eastern sector of the copperbelt and hosts Cu-Ag mineralised rocks within the lowermost sediments of the Ghanzi Group. The Ghanzi Group is a 5-10 km-thick package of rift-related sediments deposited during early Neoproterozoic rifting between the Congo and Kalahari cratons. Rocks of the KCB form the southern margin of the Damaran belt, part of the regional Pan-African Damaran-Lufilian orogenic belt which formed following the closure of a series of Neoproterozoic sedimentary basins between approximately 580 and 500 Ma (Fig. 3-10).

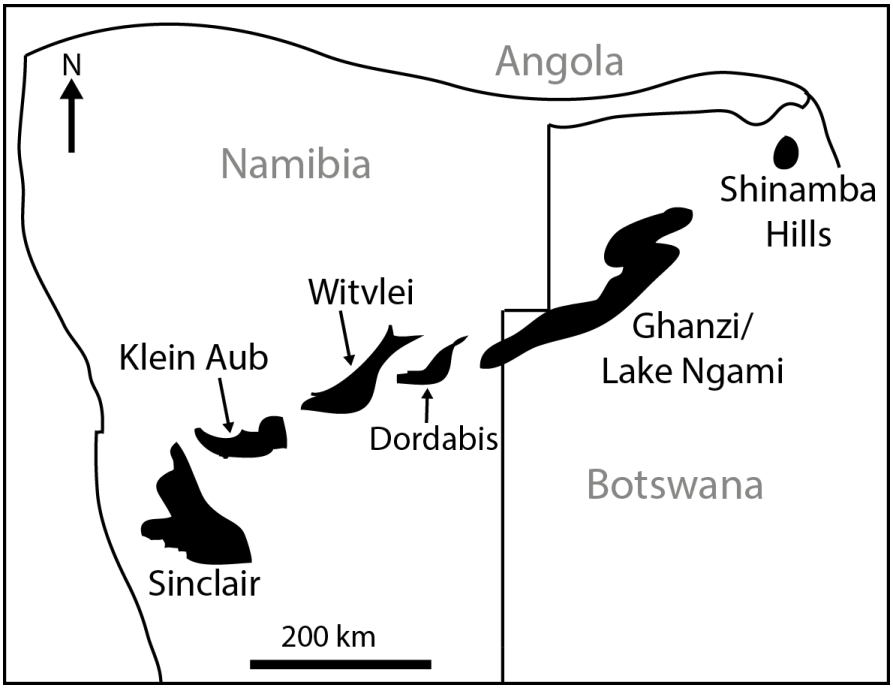

Fig. 3-10 Meso- to Neoproterozoic volcano-sedimentary basins of the Kalahari Copperbelt. Modified after Borg (1995).

Operation of the Klein Aub Cu mine, located in central Namibia, between 1964 and 1987 (Modie, 2000), as well as regional geophysical studies linking the stratigraphy of central Namibia with northwestern Botswana (Lehmann et al., 2015), have prompted renewed exploration interest in the Kalahari Copperbelt in recent years. In Botswana, the Boseto Cu-Ag mine, located 80 km southwest of Maun and 20 km southwest of Lake Ngami, commenced operations in 2012, before entering care and maintenance status in mid-2015 due to high operating costs and declining copper prices. Nonetheless, historic discoveries and broad comparisons with the world class Central African Copperbelt in the age-equivalent Lufilian Arc have promoted continued interest in this largely unexplored domain.

In addition to being underexplored, the KCB remains relatively poorly understood, with a significantly sparser history of research than the Central African Copperbelt. Relatively recent studies in northwest Botswana have focussed on establishing a stratigraphic framework and characterising mineralisation styles, as well as geochronology in the Northwest Botswana Rift (Hall, 2013; Hall et al., 2018). Almost no work has focussed on the geochemical characteristics of the hydrothermal fluids responsible for mineralisation, or the timing and source of such fluid activity.

3.2.1 Tectonics and stratigraphy of the Ghanzi-Chobe belt

The Ghanzi-Chobe Belt in north-western Botswana forms a chain of late Mesoproterozoic to Neoproterozoic volcano-sedimentary rocks deformed during the Neoproterozoic to early Palaeozoic Damaran Orogeny. The northeast-trending belt is approximately 500 km long and 100 km wide, stretching from Mamuno, near the Namibian border, to the Goha and Shinamba Hills in northern Botswana (Fig. 3-10) (Modie, 2000; Modie, 1996). The belt comprises the basal Kgwebe Volcanic Complex and the unconformably overlying Ghanzi-Chobe Supergroup sedimentary succession (Fig. 3-11), host to the majority of Cu-Ag mineralised rocks in the Kalahari Copperbelt.

Belt	Group	Subgroup	Formation	Lithology	Deposit. Setting
Pan African System (Ghanzi-Chobe Supergroup)	Okwa	Boitsevango	Bere	Lst., sst & cong.	Lacustrine changing to fluviatile
			Chobukwane	Sst., shale & dol.	
		Kacgae	Tswaane	Sst., silt, mudst. & cong.	Distal lacustrine changing to high energy fluviatile
			Takatswaane	Silt., shale-cong., & dol.	
	Ghanzi		Mamuno	Shale, silt, ark, lst.	Alluvial system changing to shallow marine and progradational shoreline
			D'Kar	Shale, silt, lst., ark.	
			Ngwako Pan	Shale, silt, ark, cong.	
Kibaran	Kgwebe Volcanic Complex			Metarhyolite, tuff, metabasite, sst.	Bimodal volcanism
Eburnian	Okwa Basement Complex			Metarhyolite, gneiss & granites	

Fig. 3-11 Lithostratigraphy of the Ghanzi-Chobe belt. Modified from Ramokate et al. (2000).

The Kgwebe Volcanic Complex forms the base of the Ghanzi-Chobe Belt and primarily comprises of a suite of bimodal volcanics which were extruded into a late Mesoproterozoic basin (Modie, 2000). The volcanics form a series of inliers or 'domes' within younger Kalahari cover sediments, and attain a maximum thickness of 2500 m near the Kgwebe Hills, thinning towards the southwest (Schwartz et al., 1995). In a geochemical study of the bimodal suite of intrusives, Kampunzu et al. (1998) suggested that Kgwebe mafic rocks were ponded during Namaqua-Natal subduction at the start of the Kibaran orogenic cycle (*ca.* 1.4-1.2 Ga), while the rhyolitic flows resulted from remelting of lower crustal calcalkaline rocks. The Kgwebe Volcanics, therefore, represent extrusive magmatism associated with rifting and extensional collapse at the end of the Mesoproterozoic Kibaran collision.

U-Pb dating of zircons in the Kgwebe rhyolites has returned dates of 1106 ± 2 Ma and 1085.5 ± 4.5 Ma, imposing a maximum constraint on the age of the deposition of overlying Ghanzi Group sediments (Hall et al., 2018; Schwartz et al., 1996).

Initial proposals of laterally younging volcanics from Klein Aub in Namibia towards the Ghanzi-Chobe Belt, and a resultant 'plume hypothesis' were dismissed by Modie (2000) due to a series of unreliable whole rock ages. Instead, a series of relatively consistent ages for sub-volcanic plutons in the north (*ca.* 1107 Ma); porphyritic rhyolites further southwest into Namibia (1094 ± 20 Ma); and meta-rhyolites from the Rehoboth inlier in Namibia (1107 ± 2 Ma) all indicate approximately contemporaneous volcanism along the length of the Ghanzi-Chobe Belt (Hegenberger and Burger, 1985; Pfurr et al., 1991; Singletary et al., 2003). Singletary et al. (2003) inferred that simultaneous magmatism along the belt resulted from widespread rifting as opposed to anorogenic plume-related activity, supporting the Kibaran orogenic collapse theory posited by Kampunzu et al. (1998). Key and Mapeo (1999) named the series of basins along the northeast trend the 'Northwest Botswana Rift', with Kgwebe bimodal volcanism subsequently being included in the Umkondo large igneous province which can be traced over large parts of southern Africa (Hanson et al., 1998).

Unconformably overlying the Kgwebe Volcanic Complex is the Ghanzi-Chobe Supergroup – a basin-fill package with a maximum thickness of approximately 13,500 m near the Namibian border, thinning to 5000 m near the study area in north-western Botswana (Litherland, 1982). The lower Ghanzi Group hosts Cu-Ag mineralised rocks in northwestern Botswana and comprises the Kuke, Ngwako Pan, D'Kar and Mamuno Formations, deposited between approximately 1.1 Ga and 0.63 Ga (Kampunzu et al., 2000a). The majority of Ghanzi Group sediments are thought to be derived from the volcanic and sandstone units of the Mesoproterozoic Kgwebe Volcanic Complex along rift basin axial fluvial systems (Kampunzu et al., 2000a). Unconformably overlying the Ghanzi Group is the Okwa Group, deposited between approximately 580 Ma and 540 Ma, immediately prior to peak Damaran orogenesis (Ramokate et al., 2000).

Following active rifting along the northwestern margin of the Kalahari Craton in late Mesoproterozoic times, the cratonic margin collided with the Congo Craton during the main phase of Pan-African orogenesis between approximately 580 and 500 Ma (Gray et al., 2006). Rocks of the Ghanzi Group underwent fold-and-thrust style deformation along the southern foreland of the Damaran Orogen during the closure of the basin and construction of Gondwana (Modie, 1996). Deformation along the southern foreland occurred between approximately 580 and 500 Ma, peaking at approximately 530 Ma (reaching lower greenschist facies metamorphic grades), according to K-Ar dating of white micas from the lateral equivalent to the Okwa Group in Namibia (Gray et al., 2006; Horstmann et al., 1990). The major isoclinal fold axes in the Ghanzi-Chobe Belt strike northeast-southwest, with fold asymmetry defining a northwest to southeast direction of shortening for the majority of folds. Folds are typically 2-8 km apart and plunge 0-15° to the northeast or southwest (Hall, 2013; Schwartz et al., 1995). Shear zones and thrusts along fold limbs evidently played a significant role in channelling hydrothermal fluids to favourable trapping sites

during syn-kinematic mineralisation events. The pre-Karoo erosive base level at approximately 350 Ma indicates that the Damaran mountain chain was almost entirely eroded within 180 Ma of peak orogenesis in the region (Miller, 1983).

The Damaran Orogeny, along with its broad time equivalent, the Lufilian Arc in Zambia and the DRC, represent a single, intercratonic Pan-African collisional event between the Kalahari and Congo cratons which appear to have had profound implications for the present day metallogeny of south-central Africa.

3.2.2 Mineralisation

Regional exploration programmes in the 1960s and 1970s identified anomalous copper occurrences throughout central Namibia in a series of basins stretching from the Sinclair Basin near the Namib Desert in the southwest, to the Ghanzi/Lake Ngami Basin in North-western Botswana (Fig. 3-10). Klein Aub, the first operational mine in the Kalahari Copperbelt, is located approximately 140 km southwest of Windhoek, and operated between 1966 and 1987, producing 5.5 million tonnes of ore, grading 2% Cu and 50 g/t Ag (Schneider and Seeger, 1992). Chalcocite-dominated Cu enrichments occur in up to seven dark siltstone/shale beds adjacent to the Klein Aub fault – a regional-scale reverse fault which is thought to have channelled ore fluids up-section, forming sulphide zonation (Maiden and Borg, 2011). Sulphides occur in cleavage-parallel lenticles, veins and breccias, with little evidence for remobilisation of earlier diagenetic sulphides, leading Maiden and Borg (2011) to conclude that all of the copper at Klein Aub was emplaced during basin inversion.

Mining in the Sinclair Basin, approximately 60 km southwest of Helmeringhausen, occurred on a small scale between 1913-1914 and again from 1927 to 1932, producing several hundred tons of high grade (16-40% Cu) hand-picked ore (Borg, 1995). Sulphides comprise of quartz vein-hosted chalcocite-bornite along orogenic structures, likely derived from nearby cupriferous mafic volcanics during Damaran orogenesis (Borg, 1995).

Mineralised rocks were also identified in the Dordabis/Witvlei Basin further northeast, across several prospects including Malachite Pan, Copper Causeway and Witvlei Pos (Lehmann et al., 2015). Copper enrichments have been recognised in a range of lithologies including mafic and felsic volcanics, sandstones and minor pyritic siltstones. However occurrences are very erratic and often focussed in vugs and amygdales in altered basalts – the proposed Cu source in much of the region (Borg, 1995). The timing of these deposits remains unclear.

Mineralisation in the Ghanzi/Lake Ngami Basin in north-western Botswana was first recognised during exploration programmes in the mid-twentieth century, with Johannesburg Consolidated Investments conducting work around Boseto in the 1960s and Anglovaal South West Africa pursuing

soil anomalies around the present day Zeta deposit between 1967-1970 (van der Heever et al., 2009). Drilling by U.S. Steel, Anglo American, Delta Gold, Kalahari Gold & Copper, BHP Billiton and Discovery Metals in subsequent years resulted in the delineation of the Zeta, Plutus and Banana prospects. The Zeta deposit was briefly mined by open-pit methods by Discovery Metals Ltd in 2012, with ore processed at the nearby Boseto concentrator. Cupric Canyon Capital and its subsidiary, Khoemacau Copper Mining (Pty.) Ltd presently hold the license areas covering all of the Boseto deposits, including Zeta, Plutus, Zone 5, Zone 5 North, Zone 6, Selene and Banana Zone (Cupric Canyon Capital, 2019).

Copper sulphides in the Lake Ngami area are not strictly stratiform and are more closely controlled by Damaran age structures and fabrics, with the highest grades restricted to areas of abundant veining. Early studies of the Boseto deposits concluded that mineralisation was a two-stage process, involving early-late diagenetic primary mineralisation which was later remobilised by hydrothermal fluids during the Damaran Orogeny (Borg, 1995; Schwartz et al., 1995). However more recent studies have emphasised the importance of orogenic-related structures in sulphide distributions, with Maiden and Borg (2011) concluding that most copper was "emplaced both during and after the main cleavage-forming event", and Hall (2017) providing syn-orogenic Re-Os dates for mineralisation.

Across the Kalahari Copperbelt, evidence is mounting that copper was sourced from the underlying Kgwebe Volcanic Complex (or equivalents in Namibia) as opposed to solely from haematitic red beds, with Schwartz et al. (1995) noting a correlation between the presence of Kgwebe metabasites and overlying copper grades in the Lake Ngami area, and Borg (1995) highlighting copper-filled vugs and amygdales in metabasites proximal to sedimentary-hosted copper deposits in the Dordabis area, Namibia. This observation, along with discoveries such as Zeta and Zone 5, and a resultant emphasis on the structural, as opposed to stratigraphic, controls on mineralisation have sparked renewed interest in the Kalahari Copperbelt and in particular the Ghanzi Ridge area.

3.2.3 The Zone 5 and Zone 5 North prospects

The Zone 5 and Zone 5 North prospects lie in the north of the Khoemacau Copper Mining license area in the Northwestern region of Botswana. Over 200,000 m of drilling has been completed in the Zone 5 region, delineating a measured, indicated and inferred resource of 100.3 Mt at 1.95% Cu and 20 g/t Ag, with a 1.0% Cu cut-off grade (Cupric Canyon Capital, 2019). Mineralisation is continuous along 4.2 km of strike, dipping at 60°, averaging 9-10 m in true thickness and to depths of approximately 1200 m (Cupric Canyon Capital, 2019). Zone 5 lies on the southeast-dipping limb of a Damaran-age anticline which trends southwest to northeast (approx. 045°), with Zone 5 North representing the same stratigraphic interval on the opposing limb (Fig. 3-12). The Zone 5 anticline

represents Ghanzi Group sediments folded around a central rigid structure highlighted by airborne magnetic surveys (Fig. 3-12). The age of this structure relative to the anticline remains unclear and similar circular structures are highlighted by magnetic anomalies along fold axes southwest of Zone 5 (Fig. 3-12) (Catterall, 2017). The Kgwebe Hills are located approximately 5 km northwest of Zone 5 and represent the nearest significant outcrop of the Kgwebe Volcanic Complex.

During a two-week visit to Khoemacau's Zone 5 camp in August 2017, a total of 12 drillcores were logged (eight from Zone 5 and four from Zone 5 North – see Appendix C.7) and 32 samples were taken. Drillcores that were logged and sampled (black circles) and those that were just sampled (red circles) are marked on Fig. 3-12. The green and pink circles on Fig. 3-12 represent mafic and felsic volcanic samples taken from outcrops in the Kgwebe Hills (Kgwebe Volcanic Complex). Boreholes were selected based on mineralised intercepts and quantity of veining, as well as gaining a good coverage along-strike. Samples were selected to be representative of different vein generations, host lithologies and sulphide zones, as well as from different levels in the stratigraphy, including deep in the footwall and high in the hanging wall in order to assess how fluids developed during migration through the stratigraphy. Table 3-3 shows the drillcores logged and number of samples taken from each core.

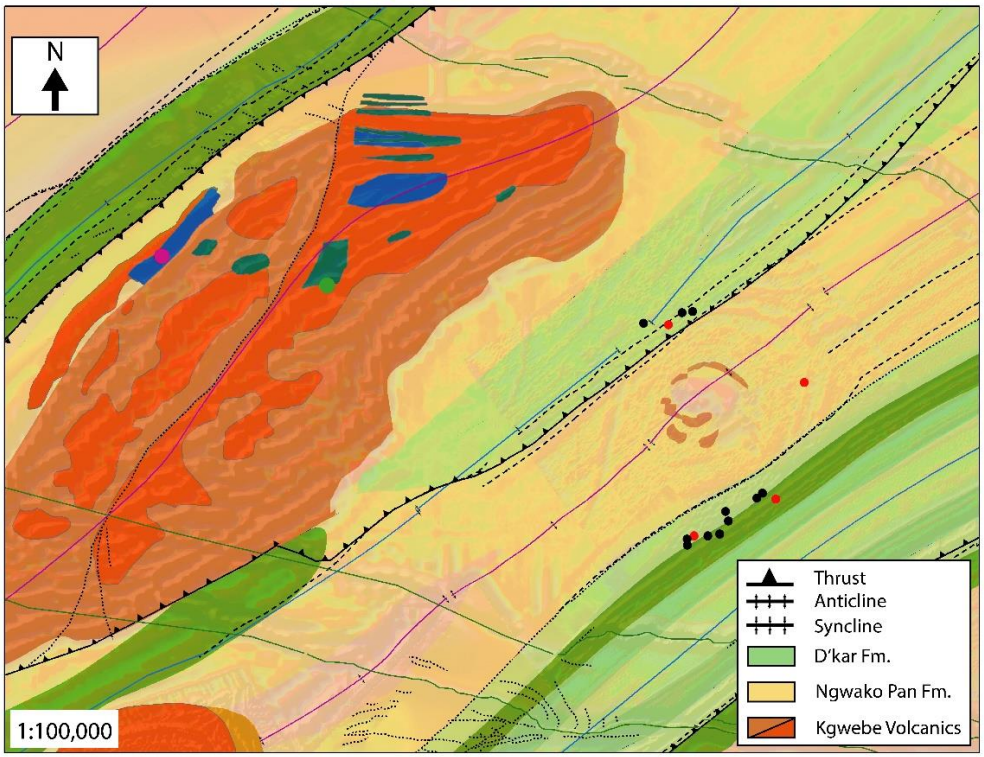

Fig. 3-12 1:100,000 scale geology map underlain by aeromagnetic survey. The Zone 5 anticline trends northeast across the map, with drillcores logged and sampled denoted by black circles, drillcores just sampled, by red circles, and Kgwebe Hills outcrop samples denoted by green

and pink circles. Note the circular feature highlighted by the magnetic survey in the core of the Zone 5 anticline. Map courtesy of Khoemacau Copper Mining and D. Catterall.

Table 3-3 Zone 5 and Zone 5 North drillcores logged and sampled

Hole	From (m)	To (m)	No. Samples
Zone 5			
HA-989-D	740.00	806.70	4
HA-929-D	610.00	663.90	3
HA-1049-D	1065.00	1137.30	6
HA-1020-D	1155.00	1239.00	1
HA-947b-D	702.00	767.00	0
HA-981-D	470.00	539.70	1
HA-957-D	615.00	672.05	4
Zone 5 North			
HA-1099b-D	1060.00	1101.00	1
HA-1087-D	395.00	425.32	1
HA-1085-D	380.00	419.95	1
HA-1077-D	225.00	269.95	2

Stratigraphy

With the exception of the Kgwebe Hills, much of the Boseto and Zone 5 region is covered by up to 60 m of Tertiary-age Kalahari Group sands, meaning that geological mapping has largely been completed using geophysical surveys (primarily airborne magnetics) and a stratigraphy has been delineated through drillcore intercepts of Ghanzi Group sediments. A section of interest was selected for logging in each drillcore that represented the mineralised interval between two correlative marker beds – the Ngwako Pan red sandstone (footwall), and the 'Massive Marker Sandstone' (hangingwall). The following section summarises each of the lithologies within this stratigraphic package of interest, from lowermost to uppermost.

Ngwako Pan Formation:

Typically only the uppermost 10-20 m of the Ngwako Pan Fm. has been studied, due to drill holes terminating soon after intersecting the barren footwall, however one sterilisation hole (HA-1112-D) penetrated to the base of the Ngwako Pan Fm., offering a unique insight into the lower stratigraphy of this approximately 4500 m-thick formation (Ramokate et al., 2000). The formation is characterised by red-brown fine-medium grained meta-arkoses with occasional lithic-rich grit beds, planar-parallel laminations and planar cross-bedding. The meta-arkoses are typically massive and composed of quartz with subordinate plagioclase, potassium feldspar and lithic fragments ±

mica ± chlorite, cemented with quartz ± calcite cements. These sandstones are typically referred to as 'red beds' within the wider stratigraphy due to their characteristic red colour (Fig. 3-13A).

Petrographic study of the Ngwako Pan red sandstone revealed coarse detrital quartzite grains (Fig. 3-13C), as well as abundant recrystallised muscovite, often wrapping around quartz and plagioclase grains in zones with a weakly developed fabric (Fig. 3-13D). Notably, haematitic grain coatings were largely absent (Fig. 3-13B-D), indicating that the red beds may not represent as significant a source of copper as previously assumed.

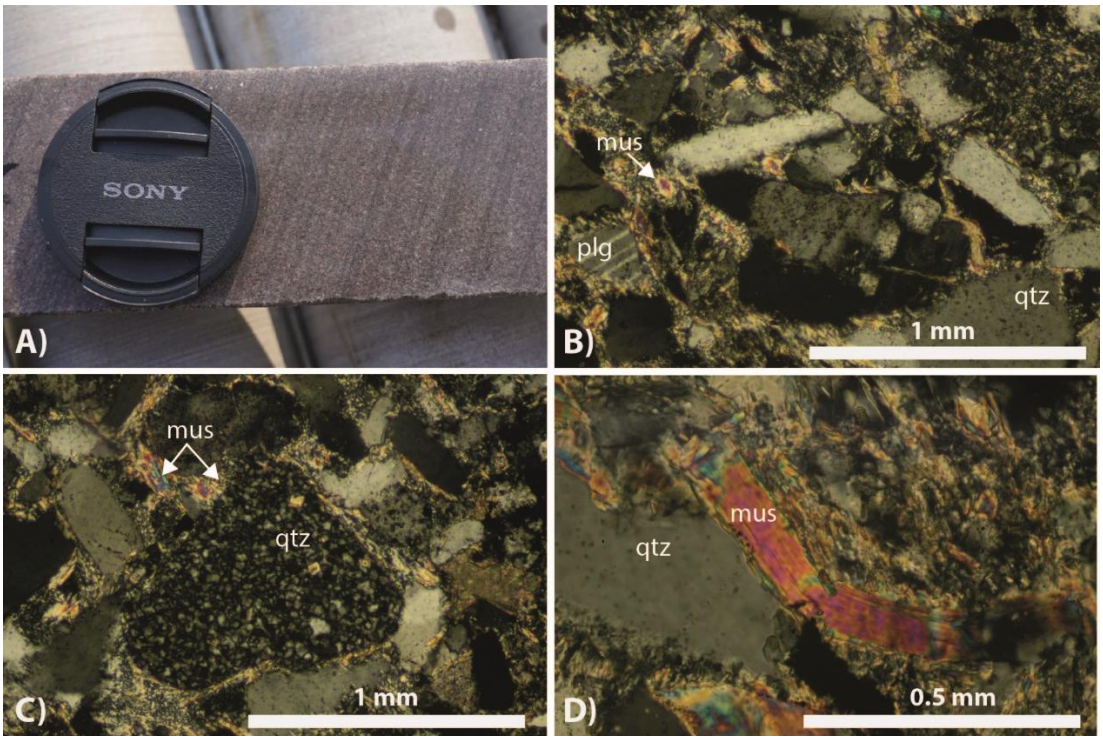

Fig. 3-13 Ngwako Pan red sandstone. A) Typical Ngwako Pan sandstone with lithic-rich banding. B) Cross-polarised photomicrograph showing typical mineralogy of the grain-supported Ngwako Pan red sandstone. In order of abundance: quartz, plagioclase, muscovite and microcline. C) Cross-polarised photomicrograph of a coarse quartzite clast surrounded by detrital quartz and recrystallised muscovite. D) Cross-polarised photomicrograph showing coarsely recrystallised muscovite wrapping around a detrital quartz grain in a zone with a weak fabric.

Anglo American trenching between 1990 and 1993 indicated that the Ngwako Pan Fm. unconformably overlies the Kgwebe Volcanic Complex (Schwartz et al., 1995), whereas the contact with the D'Kar Fm. above is more well defined (Modie et al., 1998). The change from poorly sorted, high mudstone matrix lithologies in the lower Ngwako Pan Fm. to well sorted red sandstones at the top, with intermittent pebble beds indicates an initial distal alluvial fan environment grading into channelised flow deposits before a marine transgression at the end of this depositional period (Modie, 1996).

D'Kar Formation:

The D'Kar Fm. comprises a 3000 m-thick package of more reduced grey-green marls, siltstones, arkoses and limestones deposited during a marine transgression as the basin underwent thermal subsidence (Modie, 1996; Ramokate et al., 2000). Only the lowermost 50-90 m of the D'Kar stratigraphy was systematically logged during this study, comprising the informally named 'ore zone package' above the Ngwako Pan red sandstones, up to the Massive Marker Sandstone in the lower D'Kar Fm. This package is typically thicker (50-90 m) in Zone 5 and more condensed (35-55 m) in Zone 5 North. A representative log of the ore zone package is illustrated in Fig. 3-14.

Immediately above the Ngwako Pan-D'Kar contact is a thin (sometimes absent) limestone interval, termed the 'lower limestone' in this study. This is typically a 0.1-5 m-thick barren fine-grained grey-pink partially recrystallised limestone with minor marl and silty intervals (Fig. 3-15A).

Where present, the lower limestone grades up into the ever-present 'lower marl' unit. The lower marl averages 3-5 m thick and is characteristically banded, with light grey-pink 'cleaner' limestone laminations and darker, siliciclastic-rich marly laminations (Fig. 3-15B). The lower marl often shows a pervasive cleavage sub-parallel to bedding which occasionally hosts disseminated bn-cc within very fine quartz-calcite stringers. This is the lowest stratigraphic level where mineralisation is sometimes well developed.

The lower marl transitions into the 'alternating sequence' above. The alternating sequence is typically 20-40 m thick and primarily comprises alternating marls and limestones with subordinate siltstones. Marls are typically banded, mid-grey, very fine-grained calcareous silts, interbedded with cleaner calcareous laminations/beds. Limestones are typically grey-pink and fine grained with interbedded silty and marly intervals. More siliciclastic-rich intervals typically show a stronger cleavage, usually sub-parallel to bedding and sometimes host sulphides. The alternating sequence is often heavily veined (Fig. 3-15C), with abundant quartz-carbonate ± sulphides veins, primarily parallel with cleavage. The alternating sequence often hosts the stratigraphically lowest well-developed sulphides, typically comprising bn-cc ± cpy, increasing in grade up-section. In some boreholes (notably HA-1020-D), the base of the alternating sequence is marked by an altered limestone breccia (Fig. 3-15D). The breccia is monolithic, with sub-angular to sub-rounded limestone clasts with chlorotic rims and occasional ghost structures due to partial recrystallisation. It is thought that these breccias may represent limestone talus from the collapse of a fringing reef on the slope margin (Catterall, 2017).

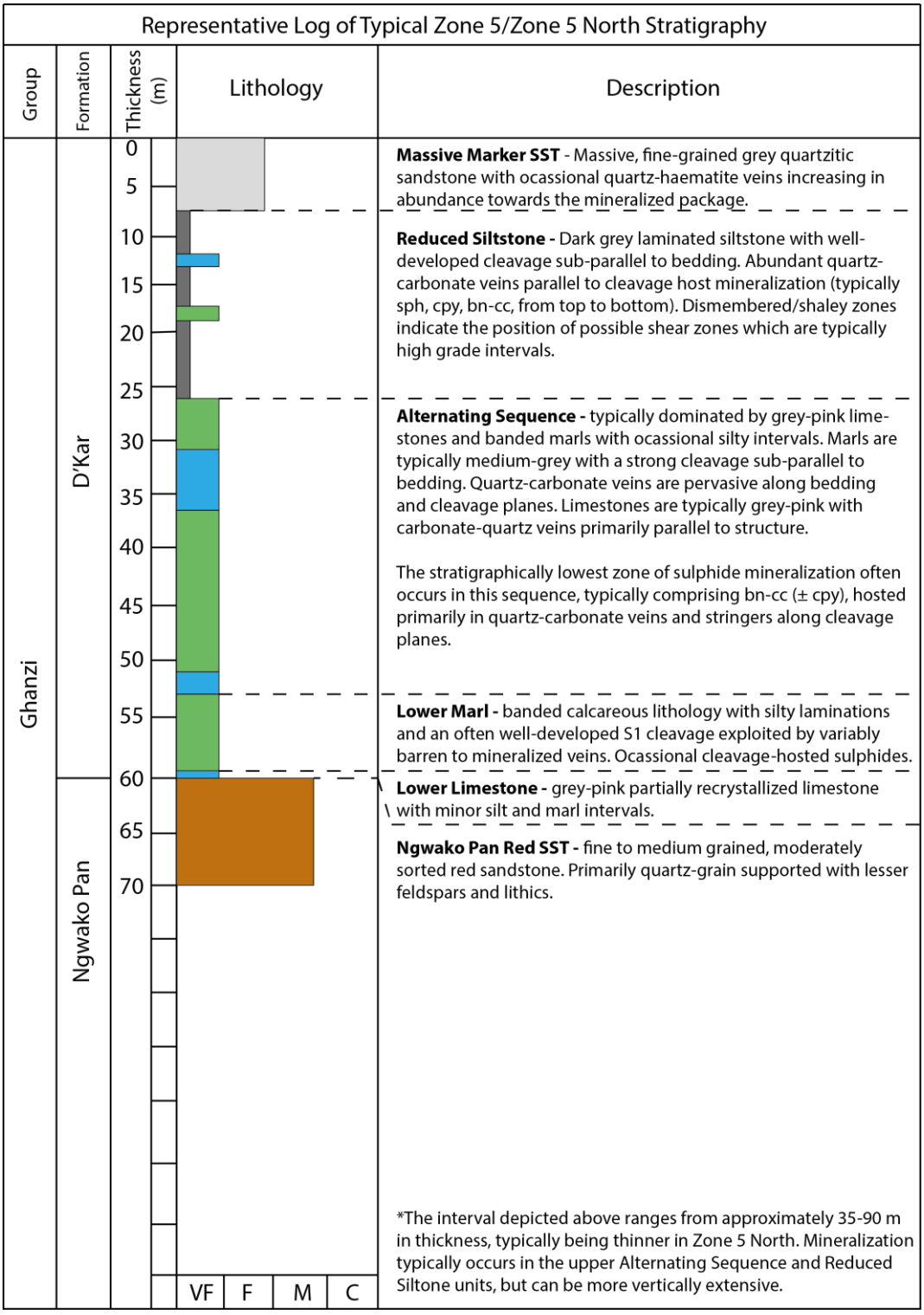

Fig. 3-14 Representative log of typical Zone 5 and Zone 5 North stratigraphy between the ore zone package footwall (Ngwako Pan red sandstone) and hanging wall (Massive Marker sandstone).

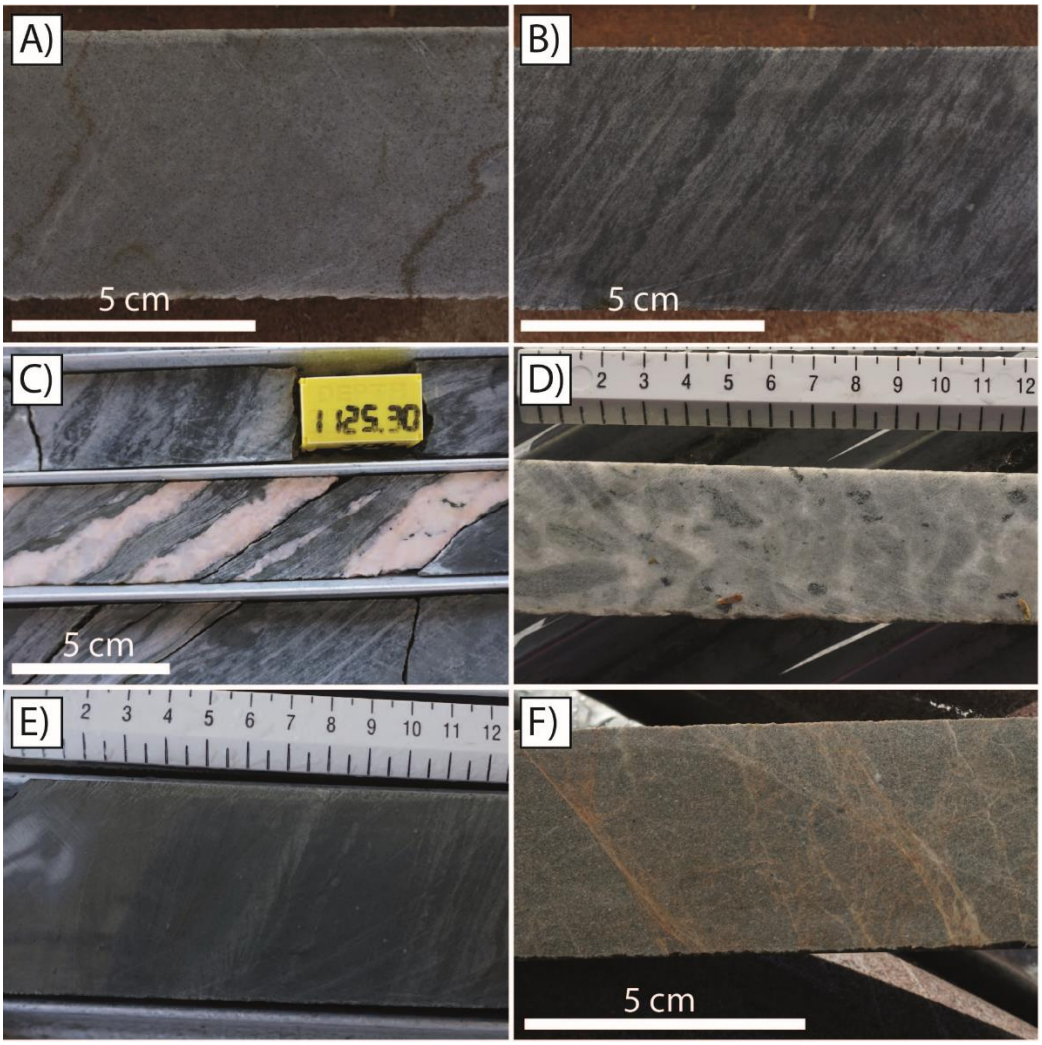

Fig. 3-15 D'Kar Formation lithologies. A) Fine-grained grey lower limestone. B) Banded lower marl unit with lighter coloured, more 'clean' limestone laminations and darker, more siliciclastic-rich layers. C) Cleavage-parallel pink carbonate-quartz veins in calcareous-rich marl unit with interbedded grey limestones. D) Limestone breccia/talus with chlorite alteration and recrystallisation 'ghost textures'. E) Laminated calcareous dark grey siltstone. F) Fine-grained grey Massive Marker Sandstone with web-textured quartz-haematite veins.

Siliciclastic-rich marls of the alternating sequence typically grade up into darker grey calcareous reduced siltstones (Fig. 3-15E). Siltstones are often laminated with variable calcite and chlorite content in contrasting lamina. Very fine disseminated pyrite is common, along with abundant quartz-carbonate-sulphide veins, which commonly follow a well-developed foliation sub-parallel to bedding. The laminated nature of this very fine-grained lithology indicates suspension sedimentation below storm wave base in a relatively low energy marine setting. These deposits have previously been referred to as rhythmites (Schwartz et al., 1995).

The dark grey veined siltstones always grade up into a characteristic fine- to medium-grained grey sandstone known informally as the 'Massive Marker Sandstone', the uppermost lithology logged in this study (Fig. 3-15F). The Massive Marker Sandstone is moderately sorted and dominated by sub-angular detrital quartz grains with subordinate potassium feldspar, plagioclase and micas, with a quartz/calcite cement (Hall, 2013). The Massive Marker Sandstone appears almost structureless and contains far fewer veins, with just occasional quartz ± sph veins, often forming conjugate sets in the ore zone package hanging wall. This unit shows significantly more alteration in Zone 5 North, where web-like structures of quartz-haematite veinlets are pervasive throughout the lowermost 5-20 m.

Palaeoenvironment

The medium-grained arkosic red beds of the Ngwako Pan Fm. have traditionally been interpreted as distal alluvial fan material, grading upwards into axial-trough fluvial sediments within an active rift basin (Modie, 1996). However recent reinterpretations have suggested that the uppermost Ngwako Pan sediments were deposited along a shoreface setting, with pebble-rich plane-parallel beds representing tidal or wave reworking of fluvially-derived material (Catterall, 2017; Hall, 2013). The D'Kar Fm. reflects a significant marine transgression resulting from sea level rise or thermal/tectonic subsidence. Interbedded limestones and laminated marls represent alternating periods of contrasting siliciclastic input into the basin and quieter periods of shallow marine carbonate deposition. The overlying calcareous siltstones represent siliciclastic suspension sedimentation in a low energy marine setting. Logging of the upper D'Kar section by Hall (2013) indicates coarsening upwards successions, characteristic of a silty to sandy pro-delta environment. There is no evidence in the Ghanzi-Chobe Supergroup for active sea floor spreading, indicating that the Ghanzi-Chobe Belt simply represents a failed intracratonic rift system, later inverted during the Damaran Orogeny (Modie, 1996).

Mineralisation

The majority of Cu-Ag mineralised rocks at Zone 5 and Zone 5 North reside in the lowermost 35-80 m of the D'Kar Fm. which represents a relatively reduced package of shallow marine sediments compared with the alluvial and shoreface red beds of the underlying Ngwako Pan Fm. The major sulphide minerals, in order of decreasing abundance, are chalcocite, bornite, chalcopyrite, pyrite, sphalerite and minor galena. Sulphides show a strong zonation from proximal cc-bn (± wittichenite) > cpy > sph-py > gl in the central and southwestern section of Zone 5, whereas sulphides appear mixed and Pb-Zn are absent from other areas of Zone 5 North and north-eastern Zone 5. No systematic lateral sulphide zonation was observed whilst logging boreholes along the strike of the Zone 5 deposit. Minor marcasite (within py), pyrrhotite (within py and cpy) and

arsenopyrite have also been noted by other workers (Hall, 2013; Schwartz et al., 1995). Minor enrichments (tens-of-ppb) of gold and platinum group elements have been reported from some bornite-rich ore zones, however analyses for these metals has been rare and sporadic.

Copper-Ag mineralisation is typically hosted in the uppermost marls and limestones of the alternating sequence, as well as the overlying dark grey siltstones where the highest grades are often developed, and occurs in two main forms:

1. Elongate cleavage-hosted sulphides (Fig. 3-16A), often associated with microscopic quartz-carbonate stringers.
2. Quartz-carbonate veins, typically, but not exclusively exploiting sub-parallel bedding or cleavage planes (Fig. 3-15C).

In Zone 5 the ratio of vein-hosted to disseminated sulphides has previously been reported as ~9:1 (Gorman, 2013). Although this study found this ratio to be ~7:3, there is undoubtedly a significant bias towards vein-hosted sulphides, particularly within ore zones of economic significance.

Cleavage-hosted mineralisation is strongly controlled by the effective permeability of different lithologies and is visibly more abundant where a better-developed cleavage is present (Fig. 3-16B). Mineralised and barren veins show a variety of styles, textures and kinematics and typically show greatest enrichment either along their margins (where cooling was quickest) or within a central siliceous core (Fig. 3-16D), perhaps suggesting that the ore fluid was a predominantly siliceous fluid, and that carbonate occurring along vein margins has been remobilised from carbonate wall rocks during vein emplacement. Laminated veins and crack-seal textures (Fig. 3-16E) likely represent multiple fluid injections during progressive shear along the existing fabric, with each band representing a distinct shearing and injection event as well as a plane of weakness for future reactivation. Periods of intense, voluminous fluid flow through relatively focused stratigraphic packages are evidenced most strongly in Zone 5 North, where contacts between zones of mineralised massive veining and wall rocks are often vuggy and heavily altered (Fig. 3-16F).

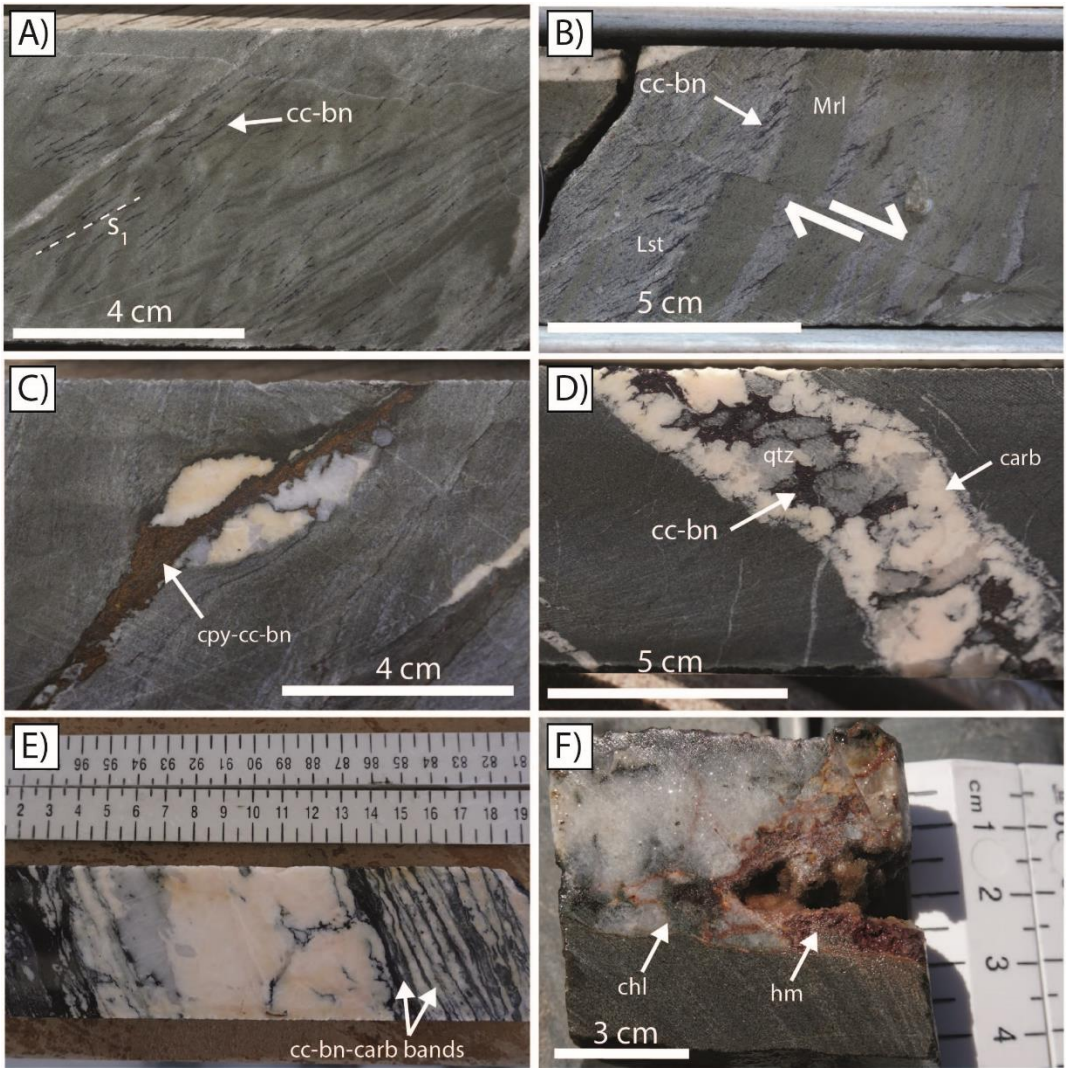

Fig. 3-16 Zone 5 and Zone 5 North mineralisation. A) Cleavage-hosted cc-bn with cleavage-parallel quartz-carbonate veinlets in banded marl of the alternating sequence. B) Laminated marls and carbonates highlight permeability differences between lithologies, with more abundant cleavage-hosted cc-bn in carbonate laminations. Laminations and Cu sulphides offset by late displacement at a high angle to bedding. C) Cleavage-parallel quartz-carbonate vein-hosted cpy-cc-bn (syn-kinematic?). D) Vein with a quartz-cc-bn core and (remobilised?) carbonate margins. E) Central carbonate-quartz-cc-bn vein with banded mineralised margins, each representing a distinct phase of progressive shear and fluid injection during orogenesis. F) Vuggy quartz vein margin with abundant haematite alteration and minor chlorite.

Both mineralised and barren veins occur predominantly along bedding or cleavage structures, showing evidence of both compression (folding) and extension (boudinage). Exploitation of a pervasive cleavage indicates syn-kinematic vein emplacement, with parasitic folds (Fig. 3-17A) indicating ongoing compression during Damaran orogenesis. Where pre-orogenic veins are present, they are usually barren and form at high angles to bedding, often cross-cut by mineralised syn- to

post-kinematic veins (Fig. 3-17B-C). Such pre-kinematic veins also record evidence for progressive shear along bedding planes, marking clear displacement sub-parallel with cleavage on a cm-scale.

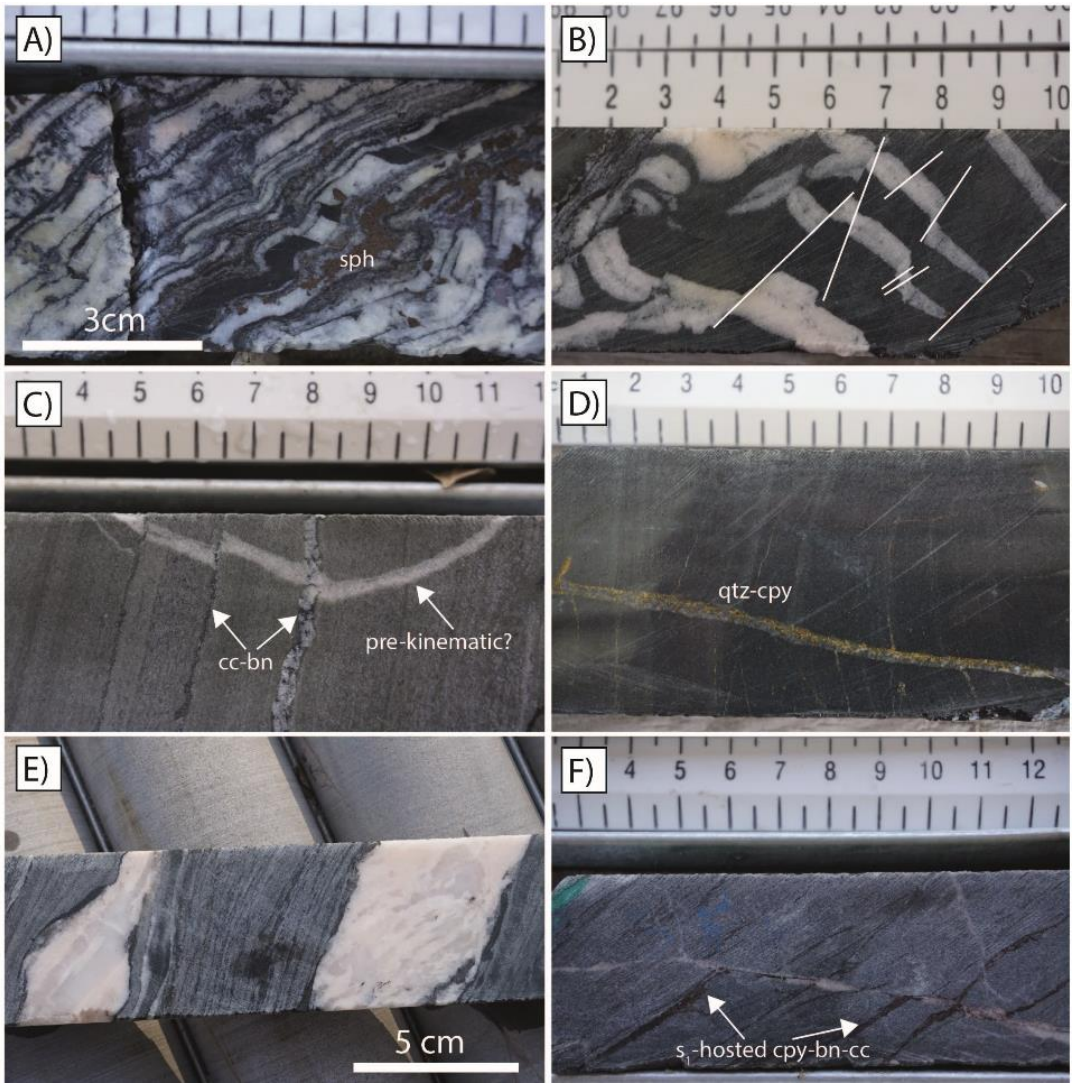

Fig. 3-17 Vein kinematics at Zone 5. A) Cleavage-parallel laminated carbonate-quartz-sph vein with parasitic folding. A lamination of siltstone host rock has been sandwiched through repeated shearing and fluid injection along fabric. B) Barren pre-kinematic high-angle quartz-carbonate veins displaced by slip along bedding/cleavage-parallel structures (white). A syn- to post-kinematic quartz-carbonate-sph vein also cross-cuts and displaces pre-kinematic structures. C) Cleavage-parallel cc-bn veinlets cross-cut a barren, high angle, pre-kinematic quartz vein. D) Late- to post-kinematic high angle quartz-cpy vein crosscuts fabric in reduced siltstone. Fluid appears to have pervaded along the S1 fabric from the parent vein. E) Massive, bedding-parallel, barren quartz-carbonate veins showing pinch and swell features (possible post-orogenic extension?). F) Cleavage-hosted cpy-bn-cc displaced by a later high angle quartz-carbonate veinlet. Cross-cutting veinlet has remobilised some sulphide up-section.

Although the majority of mineralised veins appear to be syn-kinematic in nature, some do show evidence of relatively late mineralisation events, with mineralised veins occasionally cross-cutting bedding and cleavage at a high angle. In the example shown in Fig. 3-17D, mineralisation likely occurred relatively soon after the formation of the regional S_1 fabric which maintained relatively permeable cleavage planes for fluid flow. There is also evidence that fluids continued to circulate beyond post-peak orogenic times, with veins that both penetrate the regional fabric and then underwent extension (evidenced by boudinage), potentially during orogenic collapse (Fig. 3-17E), and veins that cross-cut cleavage-hosted mineralised veins, remobilising sulphides up-section (Fig. 3-17F).

All styles of mineralisation occur tens of metres above the 'first reductant', which is often represented by a relatively reduced lower marl at the base of the D'Kar Fm. This, in addition to the strong preference for mineralisation along Damaran structures, suggests that macro and micro-scale structures played the most important role in mineralisation. By creating effective permeability throughout the D'Kar stratigraphy, shearing and fracturing due to flexural slip and parasitic folding, respectively, may have promoted a simple temperature-controlled sulphide zonation up-section.

Alteration

Much of the relatively fine-grained silty and calcareous sediments of the D'Kar Fm. have undergone significant recrystallisation during Damaran Orogenesis and regional metamorphism (lower greenschist facies), making primary diagenetic alteration assemblages, if present, difficult to distinguish from hydrothermal alteration assemblages related to Damaran orogenesis. The most heavily altered lithologies observed in this study are a suite of metabasites belonging to the Kgwebe Volcanic Complex. The vesicular metabasites host an alteration assemblage consisting of epidote-actinolite-quartz with subordinate chlorite and haematite (Fig. 3-18). Examples of more heavily altered, porous basalts were collected from the Kgwebe Hills (Fig. 3-18A-B), whilst slightly less altered, amygdaloidal metabasites were recovered from the base of a borehole which penetrated deep into the footwall, below the Ngwako Pan sandstones at Zone 5 (Fig. 3-18C-D).

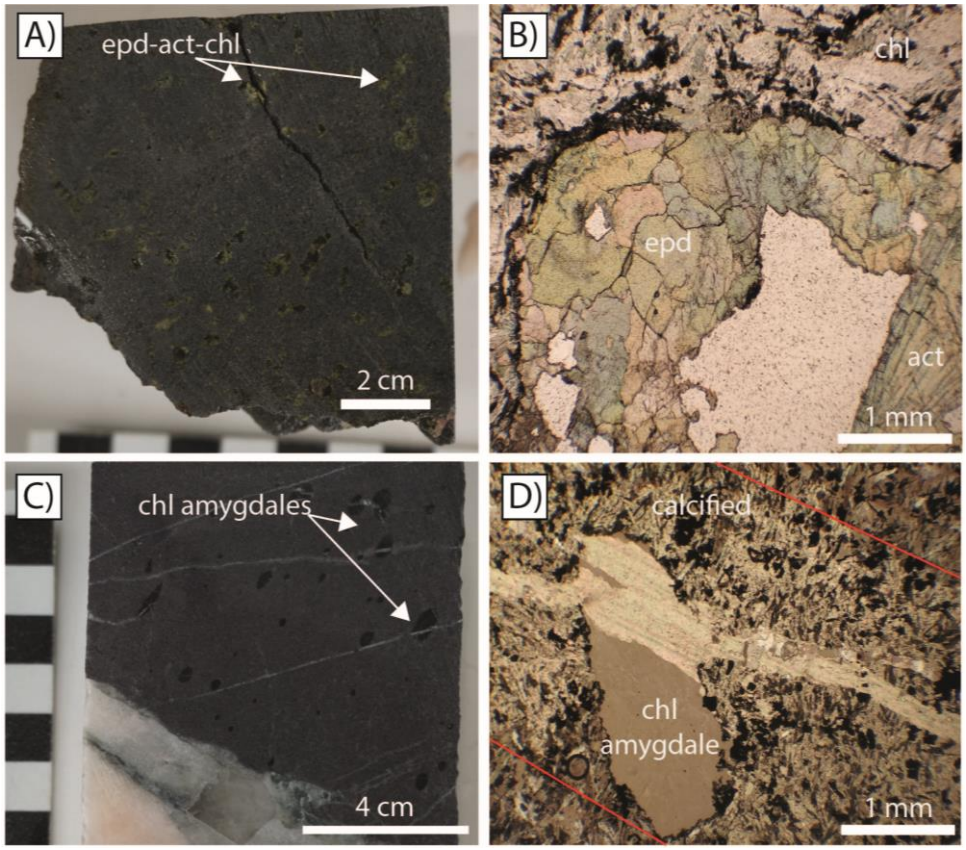

Fig. 3-18 Altered Kgwebe metabasite mineralogy. A) Heavily altered greenschist facies vesicular metabasite with epidote, actinolite and chlorite associated with vesicles. B) Coarse epidote and actinolite rimming a vesicle (plane polarised light). C) Metabasite recovered from drilling beneath the Ngwako Pan sandstones shows chlorite amygdales and barren quartz-calcite veining. D) Fine grained chlorite amygdale with cross-cutting calcite vein and associated zone of calcification in sample shown in (C) (plane polarised light).

Borg and Maiden (1987) suggested that these rocks represent the primary source of metals in the Kalahari Copperbelt, with Cu, Zn and Co being liberated during Damaran-age hydrothermal fluid flow before migrating up-section, through the Ngwako Pan sandstones and precipitating in the relatively reduced D'Kar Fm. shallow marine sediments.

Within the ore zone package of the lower D'Kar Fm. alteration is less pervasive, with only certain areas such as Zone 5 North and the northeastern section of Zone 5 displaying evidence of intense hydrothermal fluid alteration associated with mineralised rocks (Fig. 3-19). Haematite is the most abundant alteration mineral and can be pervasive, from the footwall, throughout the mineralised zone and into the hanging wall, forming web-like veinlet structures in host sediments (Fig. 3-19A), laminations along cleavage and bedding planes (Fig. 3-19B) and accompanying sulphides directly (Fig. 3-19C). All of these textures are interpreted as replacement textures, resulting from relatively late fluid flow. This interpretation is supported by abundant haematite accompanying malachite in

regions of particularly vuggy/porous mineralised siltstones – a texture and oxidised mineral assemblage that clearly postdates primary sulphide precipitation (Fig. 3-19D).

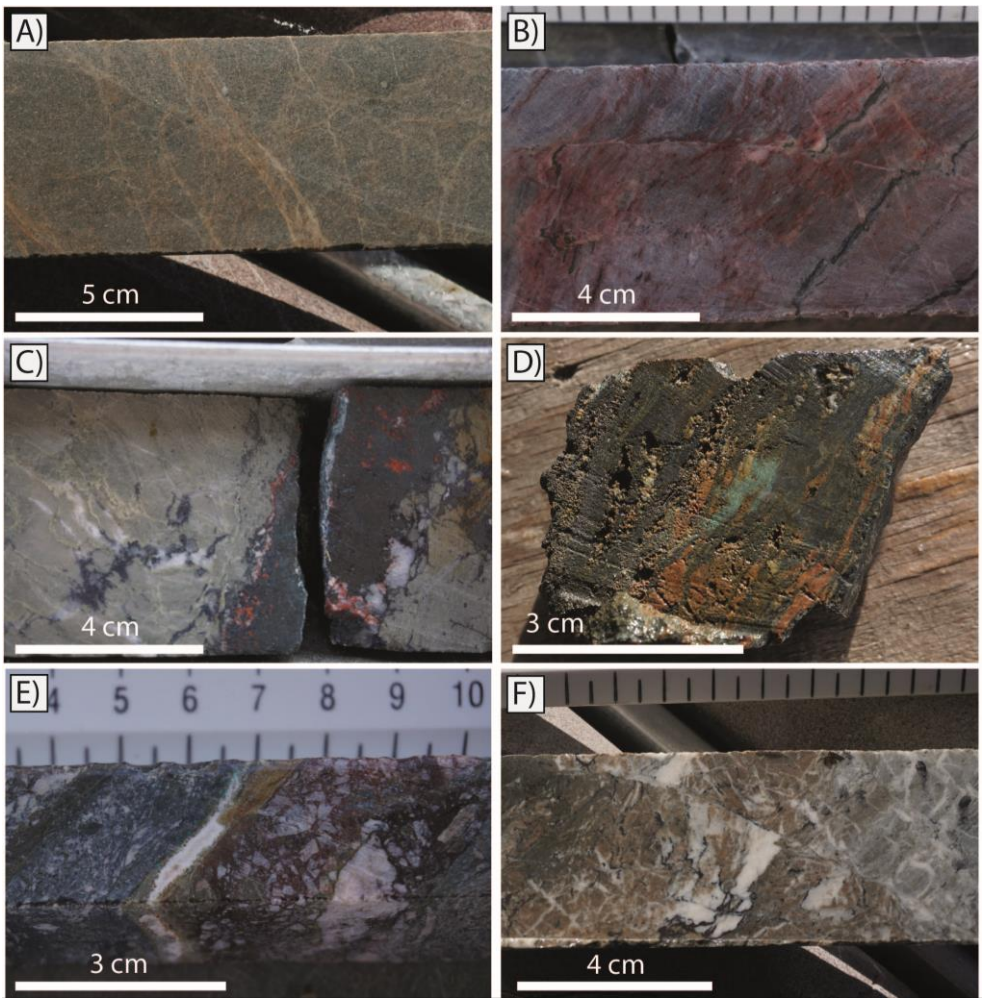

Fig. 3-19 Alteration of D'Kar Fm. lithologies. A) Web-like haematite veinlet alteration in Massive Marker Sandstone above the ore zone package in the northeast of Zone 5. B) Pervasive haematite alteration along structural fabric within laminated marl and carbonate unit of the alternating sequence (within ore zone package) in Zone 5 North. C) Haematite-albite ± chlorite alteration associated with chalcocite within a zone of massive veining in carbonates of the alternating sequence. D) Vuggy/porous mineralised siltstone with late, oxidised, haematite and malachite alteration in Zone 5 North. E) Possible hydrothermal breccia showing evidence of silica flooding and late haematite (+ minor malachite) alteration in laminated marls and carbonates from the alternating sequence in Zone 5 North. F) Albite-quartz-carbonate-K-feldspar-haematite alteration of a mineralised limestone interval towards the top of the ore zone package in the northeast section of Zone 5.

The origin of several, potentially hydrothermal breccias remain unclear (Fig. 3-19E). The breccias are typically associated with Cu enrichments in Zone 5 North and often show evidence of silica flooding, with angular, silicified clasts. This may represent a syn-mineralisation hydrothermal

brecciation process, which, due to increased porosity and permeability, has subsequently been overprinted by late haematite and malachite.

The timing of other alteration assemblages, including albite, quartz, potassium feldspar and chlorite, is less clear, with quartz, potassium feldspar and chlorite often being intimately associated with sulphides and perhaps representing fluids in thermal equilibrium with lower greenschist facies host rocks during Damaran orogenesis (Fig. 3-19F).

3.3 Allihies, Munster Basin

Chapter 6 presents results from a fluid inclusion study of temporally distinct barren and mineralised vein sets from Allihies, in the west of the Beara peninsula, as well as Inch, from the northern margin of the Devonian Munster Basin. Given the self-contained nature of the long-form research paper, a comprehensive review of the pertinent literature as well as the field geology completed during this study are reported towards the beginning of Chapter 6 and are not repeated here.

Chapter 4 Copper and cobalt-rich, ultra-potassic bittern brines responsible for the formation of the Zambian Copperbelt

ABSTRACT

The Central African Copperbelt (CACB) represents Earth's largest repository of sediment-hosted copper and cobalt. The criticality of these elements in battery technology and electricity transmission establishes them as fundamental components of the carbon-free energy revolution. Understanding the formation of extractable concentrations of these elements is key to developing predictive models for future resource discovery. In the CACB, the relative timing of mineralisation, and the nature and origins of fluids involved, are controversial. As essential components of the mineral system, constraining these characteristics is central to developing an understanding of the unique metal endowment of the CACB. We present microthermometry, scanning electron microscopy and laser ablation ICP-MS analysis of fluid inclusions from barren and mineralised samples from the Nkana-Mindola deposits in Zambia. Results show that base metal concentrations vary by one to two orders-of-magnitude between 'barren' and 'ore' fluids, with concomitant distinctions in major salt chemistry. Mineralised pre- to syn-kinematic veins are associated with anomalously high temperature-salinity brines, characterised by K/Na ≥1, with elevated metal concentrations (10^2 to 10^3 ppm Cu and Co). Conversely, typically barren, post-kinematic veins contain lower temperature-salinity primary inclusions, characterised by K/Na <1 and low metal contents (<10^2 ppm Cu and Co). These fluids also occur as secondary inclusions in all vein types. A model invoking high-temperature, sulphate-deficient, metalliferous and ultra-potassic bittern brines residing at sub-salt levels correlates with palaeofluid halogen ratios which imply ore fluids underwent advanced evaporation during early basin development. During basin closure, lower temperature, halite-undersaturated fluids interacted with evaporites, forming structurally-controlled sodic metasomatism.

4.1 Introduction

Hydrothermal fluids are the primary transport agent for precious and base metals in the Earth's crust. Although studies have quantified metal concentrations in some magmatic-hydrothermal Cu-Au and sediment-hosted Pb-Zn systems (e.g. Audetat et al., 1998; Wilkinson et al., 2009), similar data are largely absent for sediment-hosted copper deposits, which comprise approximately 12% of the global copper budget (Singer, 2017). The CACB is the largest source of sediment-hosted copper and cobalt in the world (Hitzman et al., 2005), yet the origins, composition and relative

timing of ore fluid migration remain unclear. Here, we report evidence for the passage of two temporally- and chemically-distinct brines in the Nkana-Mindola deposits in Zambia. Pre- to syn-orogenic, potassic ore fluids typically display 1-2 orders-of-magnitude higher Cu-Co-(Pb-Zn) concentrations than later sodic brines. We reconcile fluid chemistries and base metal concentrations with reported alteration assemblages from across the CACB and conclude that highly evolved, ultra-potassic bittern brines were critical to the formation of this unique, world-class metallogenic province.

4.2 Geologic Setting

Copper and Co mineralised rocks of the Zambian Copperbelt are primarily hosted within Lower Roan clastic units of the late Precambrian Katangan Supergroup. Ore bodies are typically hosted within condensed sequences, fringing a series of Archaean to Mesoproterozoic granitic, metavolcanic and metasedimentary basement inliers. The youngest granitic basement suite constrains the maximum age of the unconformably overlying Katangan Supergroup sediments to 877 ± 11 Ma (Armstrong et al., 1999). Katangan sediments were deposited during two main rift phases, with the Lower Roan Subgroup rocks largely reflecting the earliest stage of rifting, during periods of predominantly terrigenous and shallow marine clastic deposition. The basin was inverted and metamorphosed, typically to greenschist facies, during the Lufilian Orogeny which peaked at 545 to 530 Ma (John et al., 2004; Turlin et al., 2016).

The Nkana-Mindola deposits are located on the western flank of the Kafue Anticline (Fig. 4-1). Major ore bodies include Nkana South, Nkana Central and Mindola, which are all located on the north-eastern limb of the northwest-plunging Nkana Syncline (Chambishi Basin). The Nkana ore bodies are separated from the Mindola deposits by the so-called Kitwe barren gap (1.2 km along strike). The Nkana South and Central ore bodies are hosted by a series of shales, pyritic argillites and schists, whereas the Mindola ore body is hosted by arenaceous lithologies including banded sandstones and cherts. Copper ± cobalt enrichments occur as disseminated sulphides and as coarser aggregates within veins in all the major Nkana-Mindola ore bodies. The principal ore minerals are bornite, chalcopyrite and carrollite, with minor chalcocite and pyrite (Brems et al., 2009).

The abundance of veins spanning the pre-orogenic and Lufilian stages at Nkana-Mindola provides an excellent opportunity to assess the compositional and temporal evolution of fluids involved in at least some of the mineralising events in the CACB. Based on their kinematics relative to peak orogenesis, we can divide the veins into two end-member generations. Approximately bedding-parallel, quartz-carbonate-sulphide veins are most abundant in the carbonaceous shales of the Nkana South and Central orebodies, but are also present in more dolomitic lithologies in the

Mindola North open pit. Such veins range from <1 cm to ~25 cm thick and occur in planar, or folded and boudinaged arrays (Fig. 4-1C), implying formation prior to peak orogenic conditions.

In contrast, massive quartz veins with lesser carbonate and rare sulphides typically cross-cut bedding and the Lufilian cleavage fabrics (Fig. 4-1D), indicating that these veins are post-orogenic. Such veins are typically 40-60 cm thick and often transgress both mineralised argillites and hanging-wall siliciclastics.

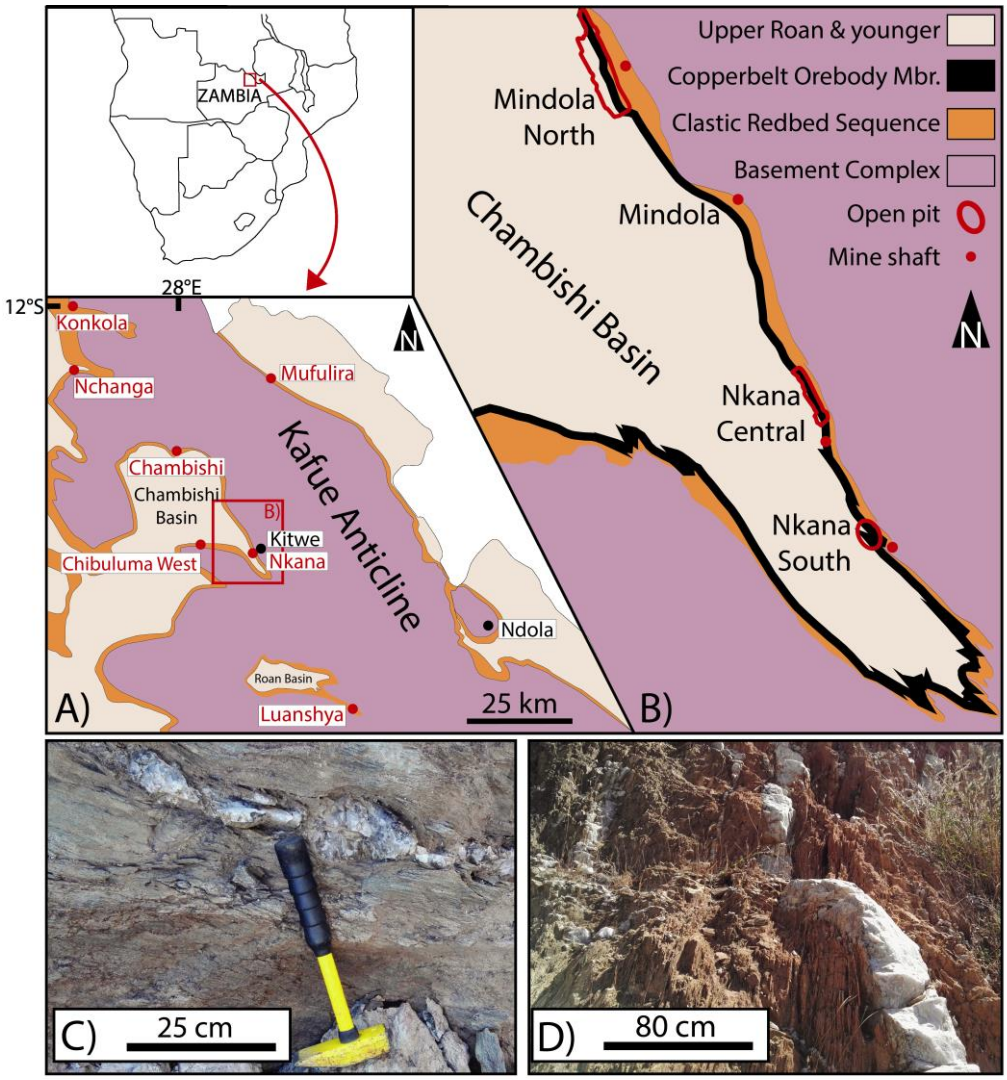

Fig. 4-1 Geology of the Nkana-Mindola deposit. A) Geological map of the Zambian Copperbelt showing Archaean-Mesoproterozoic basement complexes with younger metasedimentary rocks of the Katangan Supergroup flanking the Kafue Anticline. The inset shows the position of this map in southern Africa. B) Enlarged area showing the geology, Nkana-Mindola open pit outlines and mine shafts on the eastern flank of the Chambishi-Nkana Basin. Adapted from Torremans et al. (2014) and McGowan et al. (2006). C) An example of a shale-hosted pre- to syn-kinematic boudinaged quartz-bornite-(chalcopyrite) vein in the Nkana South open pit. D) Example of an

arkose and shale-hosted discordant quartz vein (barren) cross cutting the Lufilian foliation in the Nkana Central open pit. Primary fluid inclusions in such veins (red) are interpreted as post-orogenic.

4.3 Results

Fluid inclusions in 14 vein samples from Nkana-Mindola were categorised as either primary or secondary based on conventional criteria (Roedder, 1984), SEM-cathodoluminescence imaging, and by the relative age of their host vein. Microthermometric analyses of ~165 fluid inclusions and 138 laser ablation analyses were completed (Fig. 4-2, Fig.4.3). High resolution, background-subtracted, net intensity element maps of solid daughter phases within fluid inclusion cavities were also acquired using SEM backscattered electron imaging. Sample locations and details of analytical methods are provided in the Data Repository.

Primary fluid inclusions hosted by barren post-kinematic veins, as well as secondary inclusions hosted in all vein types, contain NaCl-dominant solutions (eutectic melting close to -21°C) with low to moderate homogenisation temperature-salinity characteristics (~100-250°C and 6-21 wt.% NaCl equiv.).

Primary inclusions spatially associated with copper- and cobalt-sulphides in pre- to syn-kinematic veins contain KCl-enriched solutions with higher homogenisation temperatures and salinities (~200-300°C and >40 wt.% NaCl + KCl equiv.). Fluid inclusions with multiple, discrete daughter phases are rare within this population, with SEM element intensity maps indicating the presence of unusual intergrowths of halite and sylvite within single, anhedral, salt masses (Fig. 4-2).

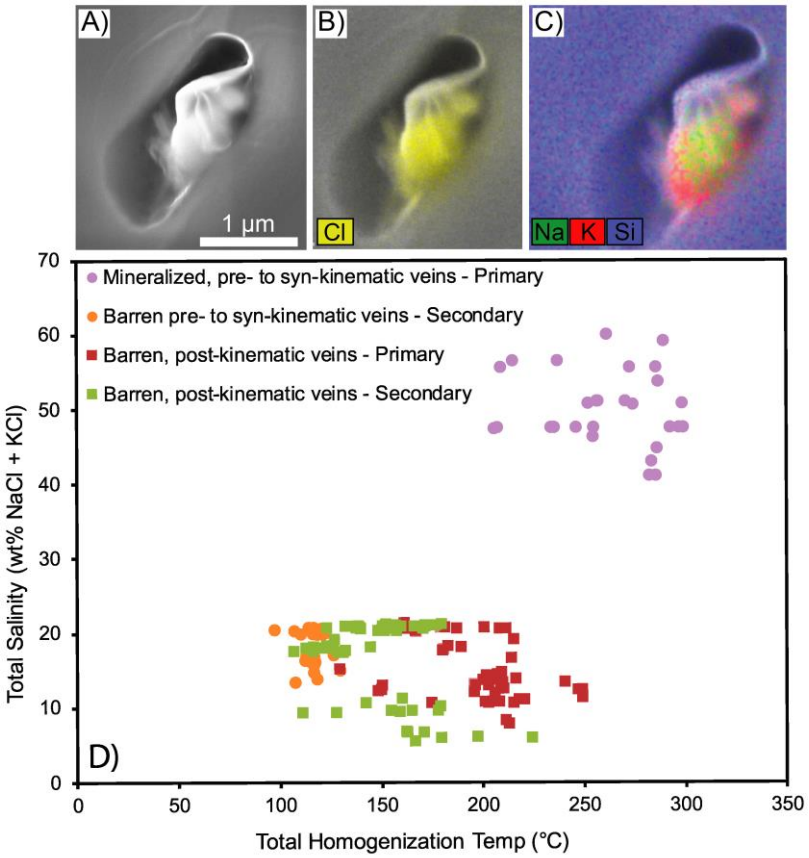

Fig. 4-2 Nkana fluid inclusion microthermometry and SEM images. A) Secondary electron image showing an indistinguishable anhedral salt mass. B-C) Element maps showing the relative masses of Cl and intergrown Na and K chloride salts. D) Plot of fluid temperature and salinity data derived from microthermometry. Salinity was estimated from the freezing point depression of ice, modelled in the NaCl-H_2O system for all two phase (undersaturated) inclusions and from halite dissolution temperatures and Na:K ratios, modelled in the NaCl-KCl-H_2O system for multiphase (saturated) inclusions. Primary inclusions associated with sulphides in pre- to syn-kinematic veins show distinctly higher temperature-salinity characteristics than both primary inclusions in discordant post-kinematic veins and secondary inclusions in a variety of kinematic settings (all of which are interpreted as later fluid overprints). Homogenisation temperatures represent minimum estimates of true trapping temperatures.

Laser ablation inductively-coupled-plasma mass spectrometry of individual, texturally-constrained inclusions with corresponding microthermometric analyses indicate that the earlier potassic brines are geochemically distinct from several populations of later, lower temperature NaCl-dominant solutions. In particular, Cu (5-1600 ppm), Co (<1-780 ppm), Pb (10-1940 ppm) and Zn (<40-3340 ppm) concentrations are typically one to two orders-of-magnitude higher in the early fluids; many inclusions representing later fluids did not return Cu or Co concentrations above their respective limits of detection. Plotting copper concentrations as a function of the K/Na ratio of individual

inclusions confirms the potassic nature of the metalliferous fluids (K/Na ≥1). Conversely, all metal-poor fluids show a simple, NaCl-dominant salt chemistry with K/Na <1. The metal-rich fluids also display distinct Ba and Li enrichment, averaging 1.5 ± 0.9 wt.% Ba (n = 26, 1σ) and 1100 ± 900 ppm Li (n=26, 1σ).

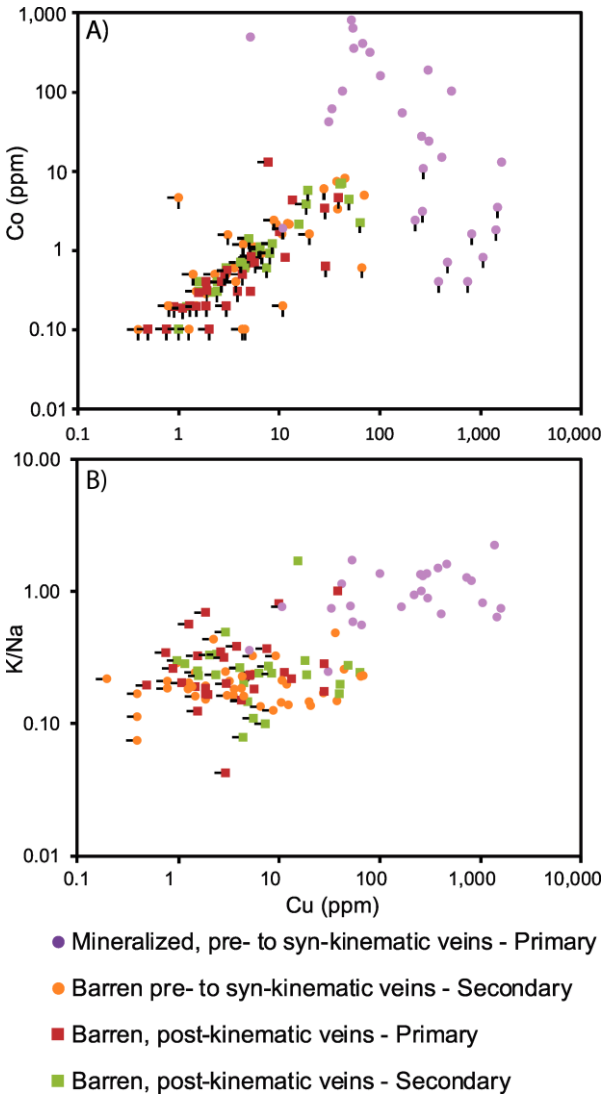

Fig. 4-3 Nkana-Mindola laser ablation ICP-MS data for individual inclusions. Colors and symbology match those in Fig. 2A) Concentrations of Cu and Co. B) Cu concentrations versus K/Na ratios. Comparing the major and trace element chemistries of fluid inclusion populations identified by petrographic and microthermometric properties shows a clear distinction between base metal-rich, higher temperature-salinity ore fluids in pre- to syn-kinematic veins and several kinematically later populations of base metal-poor, lower temperature-salinity fluids. Bars on symbols indicate that the value represents a maximum (limit of detection) value for that element in a given inclusion.

4.4 Discussion

Fluid inclusion homogenisation temperatures, solution major element chemistry and base metal budgets provide a clear geochemical distinction between pre- to syn-kinematic fluids associated with mineralisation and post-orogenic fluids in largely barren veins. Theoretical data suggesting that high temperature/high salinity chloride brines are capable of transporting appreciable quantities of Cu and Co (± Pb-Zn) (Brugger et al., 2016; Liu and McPhail, 2005) are confirmed here (up to 1600 ppm Cu and 800 ppm Co at >300°C and 40-60 wt.% NaCl + KCl). These are the most Cu-Co-rich fluids recorded from any sedimentary basin environment and overlap with the concentrations of Cu reported from magmatic-hydrothermal systems (e.g. Audetat et al., 2008). For the first time, we can be confident in suggesting that CACB ore fluids are significantly enriched in the principal ore metals compared to other basinal fluids (cf. Wilkinson et al., 2009).

4.4.1 Potassic brine origins

Most sedimentary basin fluids are low to moderate temperature, moderate salinity NaCl (± $CaCl_2$) solutions (e.g. Wilkinson, 2010). The anomalously elevated temperatures, salinities and base metal contents of the Nkana-Mindola ore fluids, as well as their distinctive potassic signature, indicate an atypical brine source or residence history in the Zambian Basin.

Fluids interpreted to be associated with mineralised rocks in several Zambian and Congolese Copperbelt deposits show distinct and low Cl/Br and Na/Br ratios which are characteristic of bittern brines produced by extensive evaporation in a restricted environment (Selley et al., 2018). Experimental studies of modern seawater evaporation indicate that highly evolved bitterns develop elevated K/Na ratios only after advanced degrees of evaporation (>65-70 (degree of evaporation [DE] defined as the ratio of given element concentrations per kg H_2O in a brine relative to bulk seawater), with K/Na ~2 prior to carnallite and kainite precipitation at DE = 75-90 (Bąbel and Schreiber; McCaffrey et al., 1987). Although Neoproterozoic seawater compositions remain relatively poorly constrained, halite-hosted fluid inclusions from the Amadeus and Officer Basins, Australia, as well as the Otavi Formation, Namibia, indicate a period of $CaCl_2$-rich, $MgSO_4$-poor seas for up to 200 million years during the middle Neoproterozoic, broadly coinciding with the breakup of Rodinia (Kah et al., 2004; Kovalevych et al., 2006; Spear et al., 2014). Theoretical evaporite crystallization sequences of such sulphate-deficient ancient seawaters replicate evaporite sequences observed in the Bonneville Salt Flats, Utah, where sylvite immediately followed halite, with the omission of significant $MgSO_4$ salts (Valyashko, 1962). This implies that high K/Na ratios can be developed at lower degrees of evaporation from seawater, when an initially low sulphate budget is almost entirely consumed through gypsum deposition during the earliest stages of

evaporation. The abundance of Ba in the ore fluids from Nkana-Mindola yet scarcity of barite in the basin successions can be reconciled if these brines had low SO_4^{2-} concentrations, consistent with an origin from $CaCl_2$ seawater.

4.4.2 Potassium exchange during subsequent fluid-rock interactions

Burial of the Lower Roan clastic sequence and its proposed bittern brine porewaters by up to 11 km of Upper Roan, Nguba and Kundelungu sediments would have led to significant elevated temperature fluid-rock reactions. The presence of up to 30% detrital potassium feldspar in these rocks provides a source for further enrichment of K(-Ba) in the brines, and detailed petrographic studies (Selley et al., 2005; Sutton and Maynard, 2005) indicate that pervasive partial breakdown and replacement of potassic minerals occurred throughout footwall clastic sequences (Fig. 4-4). It would not require significant K addition (/Na loss) during this stage to increase the K/Na ratio from evaporitic values (~1) to those measured in the Nkana-Mindola brines (average 1.1, n=26).

The intimate spatial and temporal relationships between Cu-Co sulphides and secondary (often Ba-rich) potassium feldspars observed in ore shale units in various Zambian deposits (Darnely, 1960; Sutton and Maynard, 2005) reflect the importance of potassium metasomatism during ore formation. This observation lends support to a model invoking mineralisation from unusually potassic fluids. Ore deposit metasomatism in the CACB is macroscopically partitioned, with Congolese deposits characterised by Mg metasomatism and many Zambian Copperbelt deposits characterised by pervasive K alteration. Extensive Mg metasomatism and the concomitant dissolution of primary alkali contents in basal clastic sequences in the central Congolese Copperbelt may indicate potassium remobilisation from the depocentre towards the basin margins (Zambian Copperbelt in the south and Kamoa in the north) (Selley et al., 2018).

4.4.3 Transition to halite dissolution brines

Primary fluid inclusions from discordant veins as well as secondary inclusions from all vein types at Nkana-Mindola represent moderate temperature, metal-poor, NaCl-dominant fluids. Similar fluids from post orogenic deposits such as Kipushi and Kansanshi have halogen chemistry consistent with a halite dissolution origin (Heijlen et al., 2008; Nowecki, 2014; Selley et al., 2018). Extensive dissolution breccias in the Upper Roan stratigraphy (Selley et al., 2005; Selley et al., 2018) implies that widespread exploitation of supra-salt levels by halite-undersaturated fluids occurred. The distinct chemistry of these lower temperature fluids compared with the high temperature potassic brines suggests that minimal mixing with deeper basinal fluids occurred prior to removal of the salt seals. The progressive penetration of shallower, halite-dissolution brines into the Lower Roan during the onset of orogenesis is consistent with the development of pervasive, structurally-

controlled sodic-calcic (albite ± scapolite) alteration that overprints stratiform mineralisation and earlier potassic alteration assemblages (Selley et al., 2005; Sweeney and Binda, 1989).

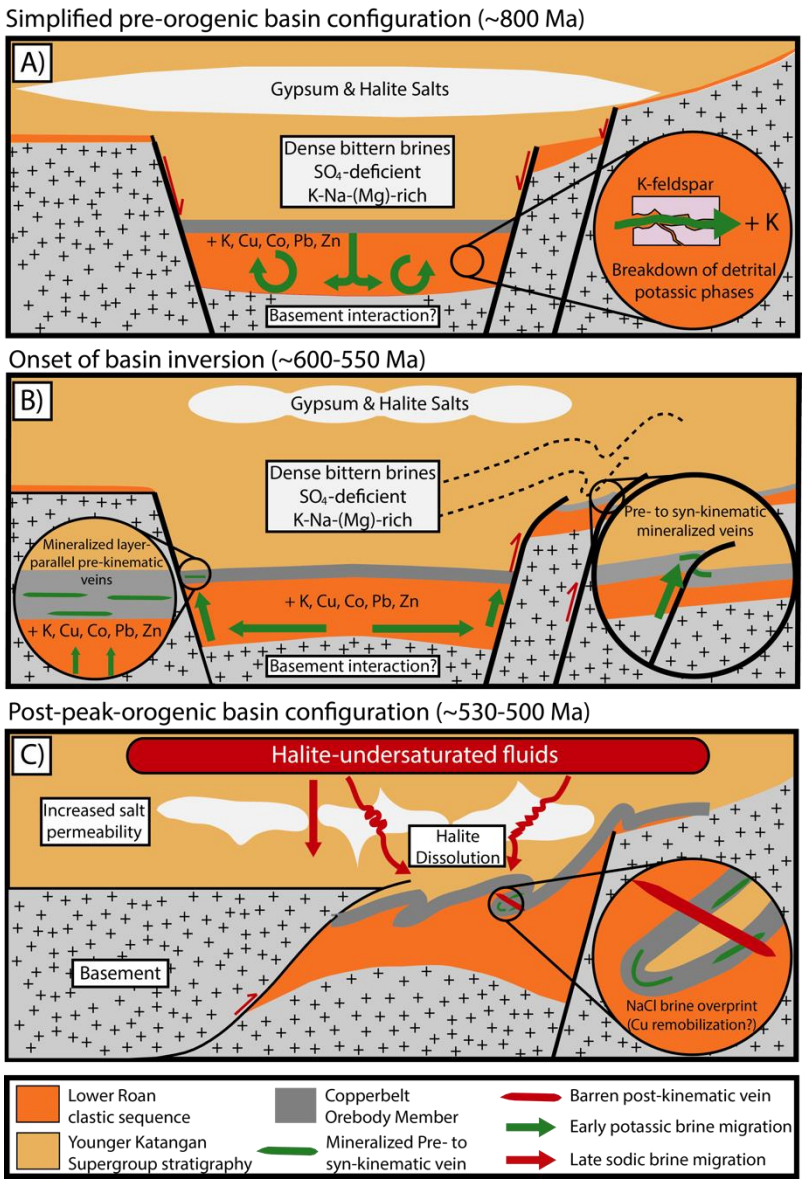

Fig. 4-4 Simplified schematic diagrams illustrating evolving fluid regimes from pre- to post-peak orogenic times in the Zambian Copperbelt. A) Having undergone high degrees of evaporation from $CaCl_2$-rich, $MgSO_4$-poor mid-Neoproterozoic seawater, dense, sulphate-deficient ultra-potassic bittern brines were resident in basal clastic sequences for extended durations. The fluids acquired high temperatures (>250°C), enhancing leaching of base metals from red bed (± basement) sequences as well as increasing fluid K/Na ratios and total salinities. B) Fluid migration along basin margins during the onset of basin inversion focussed ore fluids to structural and chemical trap sites where Cu and Co-sulphides were precipitated concomitantly with widespread potassic metasomatism. C) During basin inversion halite-undersaturated NaCl brines residing at supra-salt levels interacted with salt rafts, promoting salt dissolution. Following peak orogenesis,

largely barren NaCl-brines penetrated into the deep basin, forming discordant veins and associated structurally controlled sodic metasomatism.

4.4.4 Controls on copper-cobalt mineralisation in sedimentary basins

Fluids responsible for mineralisation in the Zambian Copperbelt were anomalously enriched in Cu, Co, Pb and Zn. Elevated base metal concentrations are attributed to enhanced leaching efficiencies by high-temperature, sulphate-deficient, ultra-potassic bittern brines residing in the basin at subsalt levels prior to Pan-African orogenesis. In addition to high degrees of evaporation, the supply of brines capable of evolving into Cu-Co-fertile ore fluids may be a function of sulphate-deficient, $CaCl_2$ seawater chemistry during the early stages of basin development. Such residual evaporitic, $CaCl_2$-rich brines have been proposed as proto-ore fluids in lower temperature sediment-hosted base metal systems (e.g. Wilkinson, 2014), thus there may be a secular control on the development of globally significant basin margin Cu-Co-(Pb-Zn) systems. Unusually low fluid pH is an unlikely factor given that a dominance of divalent cations (e.g. Ca^{2+}) over monovalent alkali species is unfavourable for increasing fluid acidity as salinity increases (Yardley, 2005). Oxidised basin sequences are likely to be important for limiting reduced sulphur availability which would otherwise suppress metal solubility (e.g. Cooke et al., 2000). Consequently, we conclude that the long residence of sulphate-deficient, high salinity, high temperature fluids in deep and potentially thermally-anomalous settings are critical characteristics for the generation of Cu-fertile basins.

Chapter 5 Were Zambian Copperbelt Fluids Anomalously Metal Enriched? A Geochemical Comparison of Basin Brines in the Pan-African Belt

ABSTRACT

The Pan-African mobile belt is one of the most well-endowed metallogenic provinces in Africa. In the northeast of the belt, the Lufilian Arc hosts the Central African Copperbelt which is the largest repository of sediment-hosted Cu and the most important source of Co on Earth. The Damaran Orogen forms the southwest of the belt and hosts the Kalahari Copperbelt; a smaller-scale, but highly prospective sediment-hosted Cu-Ag district. In the Central African Copperbelt, the nature and origin of ore fluids and relative timing of mineralisation have long been contentious. By comparing the compositions of hydrothermal fluids from three Cu-Co deposits in the Zambian Copperbelt and one prospect in the Kalahari Copperbelt, we show that the ore fluids analyzed from the Central African Copperbelt were anomalously enriched in base metals compared to basinal brines in analogous settings elsewhere along the Pan-African belt.

Microthermometry, scanning electron microscopy, stable isotope and laser ablation ICP-MS analysis of fluid inclusions hosted in suites of barren and mineralised veins from Zambia and Botswana show clear compositional distinctions between pre- to syn-kinematic and post-kinematic fluid populations. Base metal concentrations vary by one to two orders-of-magnitude between 'barren' and 'ore' fluids in the Zambian Copperbelt, with concomitant distinctions in the major salt chemistry of the fluids. Mineralised pre- to syn-kinematic veins in all three Zambian deposits were formed from high temperature brines (homogenisation temperatures >250°C and >40 wt % NaCl + KCl equiv.), characterised by K/Na ≥1, and with elevated metal concentrations (10^2 to 10^3 ppm Cu and Co). Typically barren, post-kinematic veins host lower temperature - lower salinity inclusions (homogenisation temperatures <250°C and <25 wt % NaCl equiv.), characterised by K/Na <1 and low metal contents (<10^2 ppm Cu and 10^1 ppm Co). Mineralised veins in the Kalahari Copperbelt are typically syn- to late-kinematic, exploiting the Damaran cleavage. Primary fluid inclusions from these veins are compositionally similar to post-kinematic inclusions in the Zambian deposits, with moderate homogenisation temperatures and salinity, and dominated by NaCl with relatively low base metal concentrations. Crush-leach analysis of fluids from several Central African Copperbelt deposits indicate that the early potassic ore fluids were bittern brines with an advanced evaporitic

origin, whereas later sodic fluids represent halite-dissolution brines which had interacted extensively with evaporites hosted within the Katangan stratigraphy.

These data indicate that bittern brines generated elevated K/Na ratios through advanced evaporation of sulfate-deficient seawater early in the basin's history. Burial beneath a thick succession of Katangan Supergroup sediments generated significantly elevated temperatures, promoting further increase in K/Na ratios and fluid salinity, as well as highly efficient mobilization of base metals through extensive fluid-rock interactions. Fertile solutions were then expelled along basin margins, basement highs and, in some cases, inversion structures. Pervasive fluid-rock interaction during mineralisation is evidenced by intimate associations between Cu-Co sulphides and secondary potassic phases. More soluble Pb and Zn were transported distally, outboard of the major Cu-Co accumulations. During basin closure, lower temperature halite-undersaturated brines were generated more widely along the Pan-African belt, with broadly comparable fluids measured in the Kalahari Copperbelt deposits and the late stages of the Zambian deposits. The distinct chemistry of these fluids implies that minimal mixing with deeper potassic brines occurred in the Zambian basin prior to removal of the salt seals. Salt rafts became increasingly permeable during basin inversion, promoting the progressive downward migration of late sodic brines into the Lower Roan stratigraphy, as evidenced by pervasive, structurally-controlled sodic metasomatism which often overprints earlier mineralised rocks and associated potassic assemblages. In the Kalahari copperbelt, where ultra-potassic ore fluids were absent, NaCl-undersaturated solutions formed the principal ore fluid, transporting relatively low concentrations of base metals into reducing sediments of the lower D'kar Formation. These new data suggest that the extended residence of sulfate-deficient, ultra-potassic, bittern brines within a high temperature depocentre was the critical factor in mobilizing anomalous concentrations of base metals in the Central African Copperbelt, relative to other basins along the Pan-African margin.

5.1 Introduction

The Pan-African mobile belt, including the Central African and Kalahari copperbelts, has the largest endowment of sediment-hosted Cu-Co on Earth. The orogenic belt formed through the collision of the Congo and Kalahari cratons during the Neoproterozoic assembly of Gondwana, and stretches ~2000 km from central Namibia in the southwest, to the Lufilian Arc and the Mozambique belt in the northeast. The Central African Copperbelt occurs within the Lufilian Arc which straddles the border between Zambia and the DRC and represents a mature exploration domain, with tens of producing mines hosting in excess of 220 Mt of contained Cu and the most significant Co resources in the world (Sillitoe et al., 2017). Further southwest, the Kalahari Copperbelt lacks "world class" sediment-hosted Cu discoveries and represents a relatively immature exploration province,

characterised by smaller, lower grade Cu-Ag deposits, typically covered by Cenozoic Kalahari sands and calcrete (Haddon and McCarthy, 2005).

Although the Pan-African belt hosts a diverse range of sediment-hosted Cu deposits which vary in size, geological characteristics and metal associations, numerous variables which may have affected the viability of forming an economic deposit are comparable between the Zambian and Kalahari Copperbelts. In both regions, the palaeotectonic setting, basin evolution, stratigraphy, palaeogeography and paleoclimate are broadly comparable. The geological evolution of the Zambian and Kalahari Copperbelts followed a similar path of basin formation, followed by closure and inversion during the Neoproterozoic to early Cambrian. Given these similarities, the contrast between the world class mineralisation of the Zambian Copperbelt and the smaller, lower grade systems of the Kalahari Copperbelt can be attributed to basin-specific geologic variables such as hydrothermal fluid compositions, fluid focussing structures and the efficiency of physical and chemical traps.

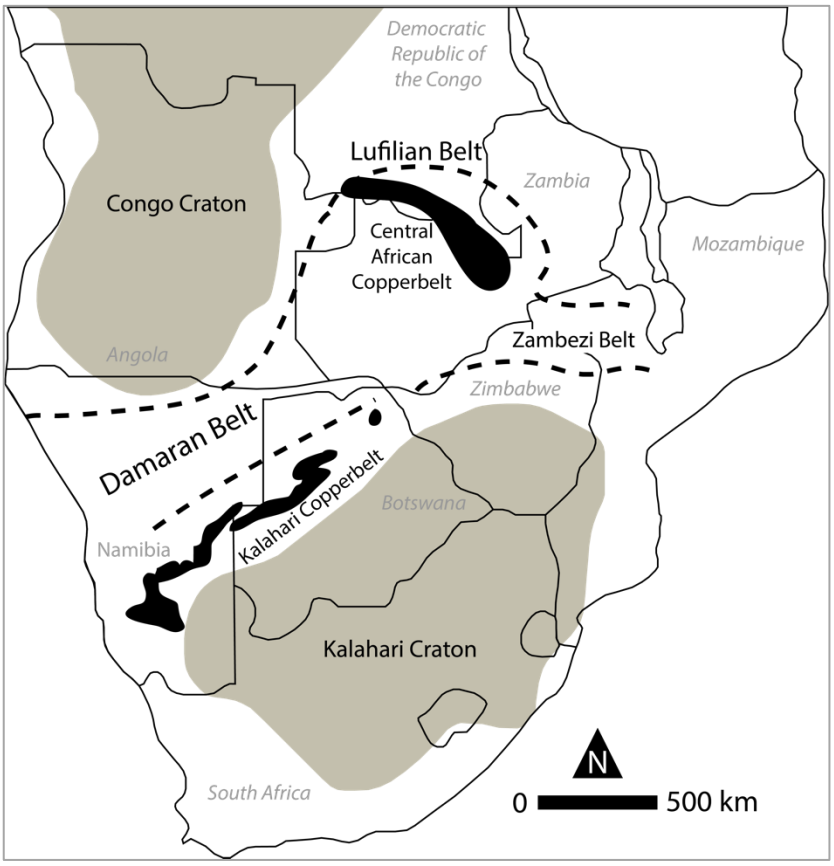

Fig. 5-1 Regional map showing the positions of the Lufilian and Damaran orogenic belts within the Pan-African collisional margin between the Congo and Kalahari cratons. The approximate extent of Neoproterozoic basinal metasedimentary packages that host mineralised rocks in the Central African and Kalahari Copperbelts are highlighted in black.

This study compares the physicochemical characteristics of hydrothermal ore fluids in the two copperbelts in order to test the hypothesis that the fluids responsible for mineralisation in the Central African Copperbelt were anomalously base metal enriched. Through fluid inclusion petrography, microthermometry, laser ablation ICP-MS and stable isotope systematics, the temperature, salinity, and major and trace element chemistry of ore fluids from three deposits in the Zambian Copperbelt and one prospect in the Kalahari Copperbelt are investigated. The results of our study suggest a significant role for highly evolved, potassic brines prior to basin inversion in the unique mineralisation of the Zambian Copperbelt, with voluminous lower temperature-salinity NaCl brines more prevalent throughout the Pan-African belt during peak- and post-orogenic times.

5.2 Geology and Geochemistry of the Pan-African Belt

The Pan-African belt comprises a series of mobile fold and thrust belts which stretch from the Damaran belt of northern Namibia and Botswana to the Mozambique belt along the east coast of southern Africa. This zone represents the suture along which the Angola-Kalahari and Congo-Tanzania plates rifted apart during the breakup of Rodinia, before again converging during the Neoproterozoic-earliest Paleozoic assembly of Gondwana (John et al., 2004; Johnson et al., 2005; Kampunzu and Cailteux, 1999).

5.2.1 Lufilian Belt

The Central African Copperbelt is located in the southeastern section of the 900 km-long Neoproterozoic Lufilian Arc which comprises Archaean to Mesoproterozoic granitic, metavolcanic and metasedimentary basement inliers, overlain by a thick succession of Neoproterozoic, Katangan Supergroup metasediments (Fig. 5-2). The maximum age of the unconformably overlying Katangan Supergroup sediments is constrained by the youngest granitic basement suite, the Nchanga Granite, to 883 ± 10 Ma (Armstrong et al., 2005). The Katangan sediments were deposited during two main rift phases, with phase one rifting leading to deposition of the Roan Group. The onset of phase two rifting is marked by the deposition of reduced, shale-dominant lithologies of the Mwashya Subgroup, along with broadly coeval mafic intrusives, and likely involved a greater degree of crustal thinning (Armstrong, 2000; Key et al., 2001; Selley et al., 2018).

The lowermost sediments of the Katangan Supergroup belong to the Lower Roan Subgroup and host the majority of Zambian Copperbelt Cu-Co deposits. These are predominantly terrigenous clastic sediments comprising conglomerates and subarkosic sandstones deposited in fluvial, alluvial fan and fan delta environments (Bull et al., 2011; Selley et al., 2005). Rift climax coincided with an abrupt marine transgression and the deposition of the Copperbelt Orebody Member – a reduced black shale averaging 25 m in thickness. This often hosts the majority of the Cu-Co mineralisation.

Evaporitic textures and desiccation cracks are common throughout the Lower Roan stratigraphy, indicating episodic sub-aerial exposure in an evaporitic environment (Selley et al., 2018). Upper Roan strata are dominated by siliciclastic and platformal carbonate facies with evaporitic nodules and massive dissolution breccias.

The second rift phase is represented by reduced rocks of the Mwashya Subgroup in the uppermost Roan Group, along with volumetrically minor, rift-related mafic intrusives emplaced at ~765 Ma (Kampunzu et al., 2000b; Key et al., 2001). The overlying Nguba and Kundelungu Groups comprise thick sequences of carbonate and siliciclastic rocks, along with the Grand and Petite Conglomérat. These are two matrix-supported diamictite intervals which some authors attribute to the Sturtian and Marinoan 'snowball earth' events (Batumike et al., 2007; Master et al., 2005). However, recent evidence suggests they may represent subaqueous debrites, produced through tectonic, rather than glacial, processes during Rodinian rifting (Kennedy et al., 2018).

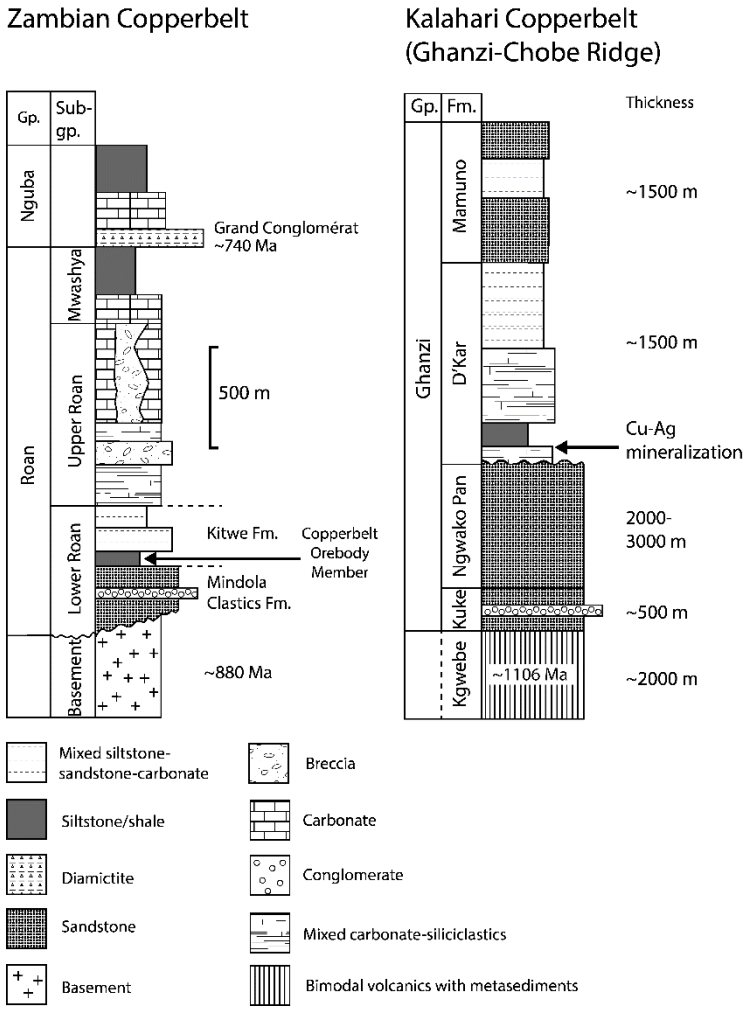

Fig. 5-2 Comparative stratigraphy of the Zambian and Kalahari Copperbelts. A) Simplified lithostratigraphy of the Katangan Supergroup in the Zambian Copperbelt. Maximum age of sedimentation is constrained by the Nchanga Red Granite (Armstrong et al., 2005); deposition of the Mwashya Subgroup and Nguba sediments is constrained by the age of Sturtian glaciation and

of mafic units in the western Zambian Copperbelt (Batumike et al., 2007; Kampunzu et al., 2000a; Key et al., 2001). Adapted from Selley et al. (2005). B) Simplified lithostratigraphy and average stratal thicknesses of the Kalahari Copperbelt Ghanzi Group and underlying Kgwebe Fm. in the Ghanzi-Chobe Ridge region. Maximum age of Ghanzi Group sedimentation is constrained by the unconformably underlying Kgwebe Volcanics (Schwartz et al., 1996).

Basin inversion commenced between ~600 and 560 Ma, with U-Pb dating of monazite indicating that peak orogenic conditions were reached between 545 and 530 Ma (John et al., 2004; Turlin et al., 2016). Orogenesis resulted in regional folding and reactivation of normal faults, with salt tectonics and pervasive dissolution playing a significant role in the kinematics of Lufilian deformation (Cailteux and Kampunzu, 1995; Jackson et al., 2003; Selley et al., 2018). The Zambian Basin typically underwent greenschist to subgreenschist facies metamorphism; however, the Domes Region records higher grade metamorphic assemblages (phlogopite, kyanite, Mg-chlorite) likely produced through metasomatism at P-T conditions approximating 700 Mpa and 600°C (Meighan, 2015).

The Zambian Copperbelt hosts six deposits with >2 Mt contained Cu (Konkola-Musoshi, Nchanga, Nkana-Mindola, Mufulira, Chambishi and Luanshya) and over twenty smaller deposits (Hitzman et al., 2012). Although historic exploration has focused on the Copperbelt Orebody Member in the Lower Roan sediments, recent studies and exploration success have promoted exploration higher in the stratigraphy, where deposits such as Kansanshi are located, as well as in basement units below the Lower Roan e.g. Lumwana (Bernau et al., 2013; Torrealday et al., 2000).

The largest deposits typically comprise multiple ore bodies, either structurally controlled and at different stratigraphic levels (e.g. Nchanga), or as mineralised pods separated by barren gaps along-strike (e.g. Nkana-Mindola and Konkola-Musoshi). Sulphides are typically disseminated (<0.1-2 mm) occupying pore spaces along stratiform layers and as coarser (1-40 mm) aggregates hosted within quartz-carbonate veins. Many deposits also display an oxidised cap, hosting supergene Cu enrichments. Pre- and syn-kinematic vein-hosted sulphides frequently share a common paragenesis with spatially associated disseminated sulphides, whereas post-kinematic veins are often barren or, where mineralised, are dominated by chalcopyrite (Sillitoe et al., 2010).

Vein kinematics can be assessed on a basin-wide scale at deposits situated at a range of stratigraphic levels from the pre-Katangan basement to the Lower Roan metasediments. A combination of detailed fluid inclusion petrography and laser ablation ICP-MS analysis of individual, texturally constrained inclusions, enables the base metal fertility of temporally and compositionally distinct fluid generations to be elucidated throughout the 350 m.y history of the Katangan Basin.

Fluid inclusion studies of individual deposits have outlined fluid P-T-X conditions across a range of stratigraphic and geographic domains, from relatively early in the basin history e.g. Chambishi (Greyling et al., 2005) through early, peak and post orogenic times e.g. Nchanga, Musoshi and Kansanshi (McGowan et al., 2006; Richards et al., 1988; Speiser et al., 1995). Primary fluid inclusions from a mineralised "lateral secretion" vein at Chambishi, interpreted by Greyling et al. (2005) to immediately postdate stratiform sulphides, have low homogenisation temperatures (T_{hTOT} = 86-129°C) and moderate salinities (11.9-23.1 wt % NaCl equiv.). These fluids are aqueo-carbonic with NaCl + $CaCl_2$ ± $MgCl_2$ salts and minor N_2 and CH_4. Inferred primary inclusions from nodules and sub-concordant veins within the ore shale at Chambishi have similar temperature-salinity ranges (T_{hTOT} = 110-180°C; 9-22 wt % NaCl equiv.) (Annels, 1989).

Fluid inclusions from veins controlled by early orogenic inversion structures at Nchanga show salinities of 31-38 wt % NaCl equiv. and modal T_{hTOT} of 185°C and 155°C for the Lower and Upper Orebodies, respectively (McGowan et al., 2006). Fluids interpreted to be orogenic in nature have also been recorded from Nkana, where Muchez et al. (2010) and Greyling (2009) reported H_2O-NaCl/KCl-$MgCl_2$ brines from layer-parallel veins with T_{hTOT} measurements of ~450°C. Later secondary inclusions yielded T_{hTOT} values of 100-250°C and salinities of 18.1-23.2 wt % NaCl equiv. Similar high temperature-salinity primary fluids are reported from Musoshi, a Zambian-type deposit located in the DRC, where high temperature (T_{hTOT} = 397 ± 5°C) fluid inclusions with ~39 wt % NaCl and ~15 wt % KCl ± minor CO_2 were measured in mineralised quartz veins cross-cutting the ore shale (Richards et al., 1988).

Recent studies of palaeofluid halogen systematics from the Central African Copperbelt suggest a dominant population of low Cl/Br and low Na/Br bittern brines from pre- to syn-kinematic veins in many Zambian and Congolese deposits. These compositions indicate Br enrichment from evaporation of seawater beyond the point of halite saturation and/or a component of sylvite dissolution (Nowecki, 2014; Selley et al., 2018). Conversely, post-kinematic veins from a variety of Zambian Copperbelt deposits, as well as all fluids from demonstrably post-kinematic deposits (e.g. Kipushi), show significantly higher Cl/Br values, typically above that of seawater, indicating Cl-enrichment through the dissolution of in situ evaporite deposits (Heijlen et al., 2008; Nowecki, 2014; Selley et al., 2018).

5.2.2 Ghanzi-Chobe Belt

The Kalahari Copperbelt is an 800 km-long terrane stretching from Klein Aub in central Namibia, to the Northwest province of Botswana (Fig. 5-1). The majority of active exploration and recent discoveries are located within the Ghanzi-Chobe belt, a ~500 km-long, ~100 km-wide tract from Mamuno, near the Namibian border, to the Goha and Shinamba Hills in northern Botswana. Historic

discoveries and broad comparisons with the world class Central African Copperbelt associated with the age-equivalent Lufilian Orogenic Belt have prompted continued interest in this underexplored domain.

The Kgwebe Volcanic Complex forms the base of the Ghanzi-Chobe Belt and comprises bimodal volcanics which were extruded into a northeast-trending basin in the late Mesoproterozoic (Modie, 2000). The volcanics are exposed as a series of inliers within younger Kalahari cover sediments, and attain a maximum thickness of 2500 m near the Kgwebe Hills, pinching out towards the southwest (Schwartz et al., 1996). A second phase of extension accommodated 5 to 10 km of siliciclastic and carbonate sediments of the Ghanzi Group and is constrained in age to younger than 1085.5 ± 4.5 Ma by U-Pb dating of rhyolite-hosted zircons from the Kgwebe Volcanics (Hall et al., 2018).

Copper-Ag mineralisation is developed in the metasediments of the Ghanzi Group, which is subdivided into the Kuke, Ngwako Pan, D'Kar and Mamuno Formations (Fig. 5-2). The Kuke and Ngwako Pan Formations are defined by a 2000-3500 m-thick sequence of basal clastics deposited in a continental fluvial system; these form the footwall to ore-bearing strata (Hall et al., 2018; Modie, 1996). The D'Kar Formation unconformably overlies this unit. It was deposited during an abrupt marine transgression, with a sharp transition to reduced facies siltstones and marlstones which host the majority of the Cu-Ag mineralised rocks. The D'Kar Formation grades upwards into Pb-Zn-bearing subarkosic sandstones, followed by 1500-2000 m of oxidised arkoses, siltstones and mudstones of the Mamuno Formation (Hall et al., 2018). Unconformably overlying the Ghanzi Group is the Okwa Group, constrained by a single detrital zircon U-Pb age to younger than ~579 ± 12 Ma (Ramokate et al., 2000), prior to basin inversion and Damaran orogenesis (~580 to 500 Ma; Gray et al. (2006)). Rocks of the Ghanzi Group underwent fold-and-thrust style deformation, peaking at ~530 Ma (Gray et al., 2006; Horstmann et al., 1990) along the southern foreland of the Damara Orogen, with major isoclinal fold axes typically trending northeast-southwest (Schwartz et al., 1995).

Mineralisation in the Ghanzi-Chobe belt is not strictly stratiform, being more closely controlled by Damaran structures and fabrics, with the highest grades restricted to areas of intense veining. In contrast to many deposits further southwest in Namibia, the sulphides often show a clear zonation from proximal chalcocite-bornite outwards to chalcopyrite, pyrite-sphalerite and galena (Borg, 1995). Recent studies have emphasized the importance of orogenic-related structures in sulphide distribution, with Maiden and Borg (2011) concluding that most copper was syn- to post-orogenic in timing. Recent Re-Os sulphide (molybdenite, chalcocite, arsenopyrite) and U-Pb xenotime

geochronology from several prospects in the Ghanzi Ridge area returned ages of 549.0 ± 11.2 Ma and 538 ± 8 Ma, respectively, supporting a peak-orogenic mineralisation age (Hall, 2017) .

5.2.3 Case study sites

The Nkana-Mindola and Nchanga deposits, located on the western flank of the Kafue Anticline (Fig. 5-3), represent significant Cu-Co accumulations (each hosting >13 Mt contained Cu) and together form the basis of our quantification of the base metal fertility of ore fluids in typical Lower Roan-hosted Zambian Copperbelt deposits. The Lumwana Cu-(Co-U) deposit is located within the Mwombezhi Dome, approximately 220 km northwest of the Kafue Anticline and represents a mineralised basement shear zone (Bernau et al., 2013). Due to its stratigraphic position, below the Katangan Supergroup sediments, as well as its geographic position in the Domes region, Lumwana serves as an intriguing comparison with the Lower Roan-hosted deposits of the Zambian Copperbelt.

The Zone 5 and Zone 5 North prospects are located ~90 km southwest of Maun, Botswana (Fig. 5-3), and exemplify the style of disseminated and vein-hosted Cu-Ag mineralisation typical of the Ghanzi-Chobe belt. Fluids associated with mineralisation here provide an excellent comparison with those from the broadly contemporaneous, but significantly larger Zambian Copperbelt deposits.

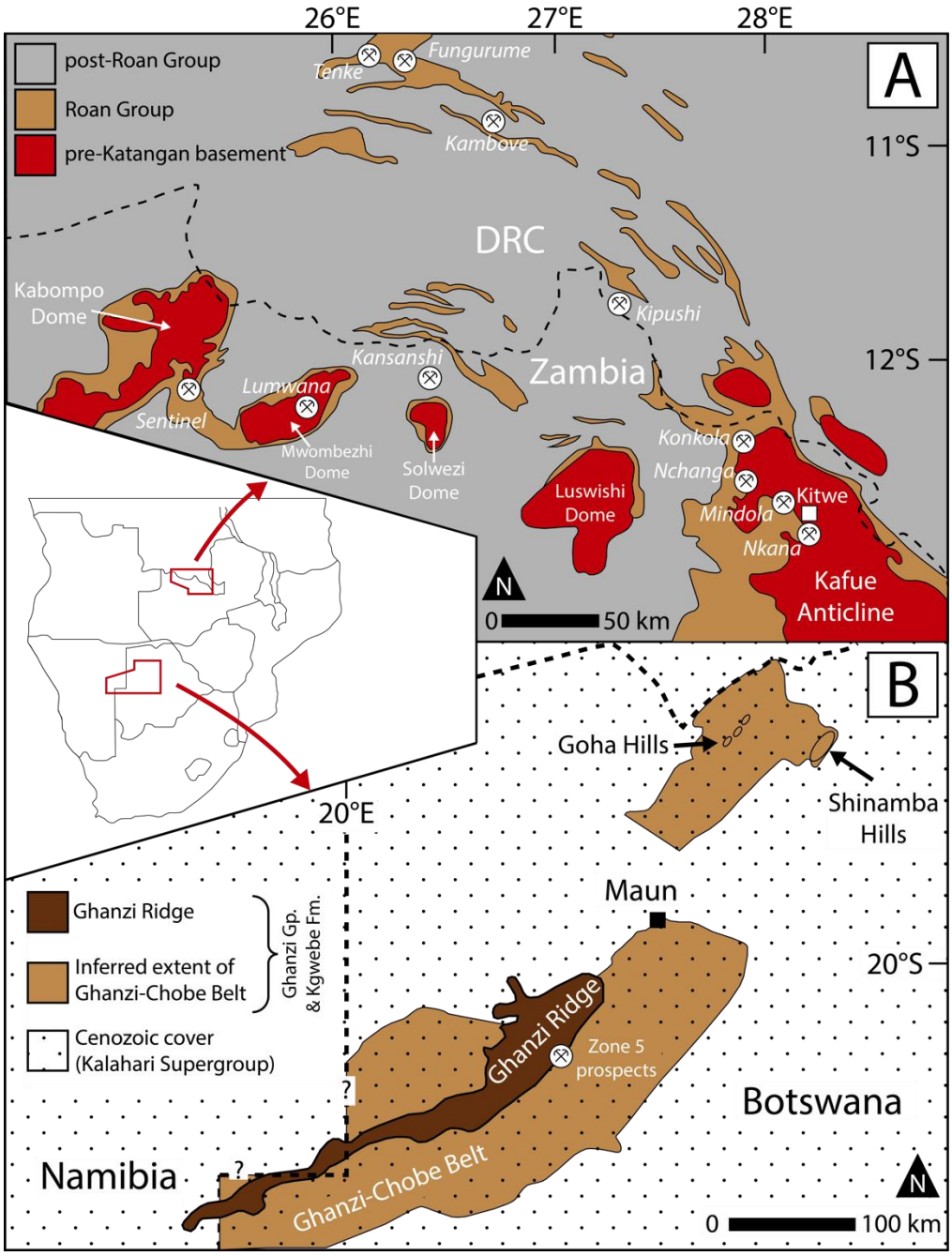

Fig. 5-3 Schematic geological maps of the Zambian Copperbelt (A) and the Ghanzi-Chobe Ridge region of the Kalahari Copperbelt (B). Inset shows the position of these maps in southern-central Africa. International borders are marked by dashed lines; geology compiled from Mendelsohn (1961); Lehmann et al. (2015); Modie (2000).

5.3 Methods

5.3.1 Sampling, petrography and microthermometry

Barren and mineralised quartz ± carbonate veins were sampled from the Nkana South, Central and Mindola North deposits in Zambia, as well as from twelve drillcores at the Zone 5 and Zone 5 North prospects in the Ghanzi-Chobe belt, Botswana. Vein material from the Nchanga and Lumwana deposits was sub-sampled from the suites of McGowan et al. (2006) and Bernau et al. (2013), respectively. Doubly-polished fluid inclusion wafers (200 µm thick) were studied under transmitted light using a fluid inclusion assemblage approach (Goldstein and Reynolds, 1994). Wherever possible, the temporal relationship between the fluid inclusion assemblages and their host mineral were classified as primary, pseudosecondary or secondary using conventional petrographic criteria (Roedder, 1972, 1984). A fundamental limitation of any fluid inclusion study in a metallogenic province dominated by disseminated sulphide mineralisation is an inability to sample fluids directly associated with fine grained disseminations. Although there is evidence to suggest a genetic relationship between disseminated sulphide assemblages and co-existing proximal vein-hosted sulphides in some Zambian Copperbelt deposits (Sillitoe et al., 2010), this study focuses primarily upon fluids associated with vein-hosted mineralisation events.

Microthermometry was conducted at the University of Southampton using a LinkamTM THMS600 heating-freezing stage. Stage calibration was carried out at -56.6, 0.0 and +30.4°C using in-house synthetic H_2O-CO_2 fluid inclusion standards, with a reproducibility of ±0.5°C (2σ); and at +308°C using a sodium nitrate standard, with a reproducibility of better than ±2°C (2σ). The temperatures of final ice melting and liquid-vapor homogenisation were measured in all two-phase inclusions; and final melting temperatures of solid daughter phases in multiphase inclusions. Eutectic, clathrate and hydrate melting temperatures were measured where applicable and in larger inclusions where phase transitions could be more easily observed. Estimates of Na concentrations were derived from final ice melting temperatures in two-phase inclusions, and from halite dissolution temperatures (and Na/K ratios, derived from laser ablation ICP-MS) in multiphase inclusions, assuming an NaCl-H_2O or NaCl-KCl-H_2O system, as appropriate (Bodnar et al., 1985; Sterner et al., 1988). Calculation of KCl and $CaCl_2$ concentrations for some FIAs were completed using the software package FLUIDS (Bakker, 2003).

5.3.2 Scanning electron microscopy

Selected fluid inclusion wafers were mounted in 400-600 µm-wide grooves cut into a standard 25 mm epoxy block and dried in an oven at 35°C for 48 hours. Samples were visually scanned for fluid inclusion cavities containing solid daughter phases using an FEI Quanta 650 FEG SEM at the Natural

History Museum (London). An acceleration voltage of 10 kV was applied for both spot analyses and semi-quantitative element mapping. Element maps were acquired at 2 microseconds per pixel, and deconvolved, background-subtracted net intensity maps were produced using the QUANTA X Bruker Esprit software (v2.1).

Selected wafers were also scanned automatically using a Zeiss EVO 15LS SEM with a cathodoluminescence (CL) detector. Samples were carbon coated (30 nm) and a probe current of 3 nA, with an accelerating voltage of 20 kV was applied at a working distance of 8.5 mm. Cathodoluminescence images were captured for 1-4 mm-sized areas at 250× magnification, with particular sites of interest imaged at greater magnifications.

5.3.3 Laser ablation ICP-MS

Laser ablation analyses were carried out in the LODE Laboratory at the Natural History Museum, London, using an ESI New-Wave NWR 213 nm laser system equipped with beam homogenisation optics and a two-volume cell. Ablated material was analysed by an Agilent 7700x ICP-MS, transported using gas flows of 1.1 l/min Ar and 450 ml/min He. Stable ablation was achieved by focusing the laser beam at the sample surface before gradually increasing the laser energy (fluence) at a constant repetition rate of 10 Hz. Where fluid inclusions were at a depth >20-25 µm, a stepwise opening procedure was utilised (Gunther et al., 1998), whereby initial coupling of the laser with the matrix was achieved using a small spot size (8-14 µm) in order to minimise 'sharding' at surface, with the spot size and laser energy then increased gradually in order to ablate the entire contents of the targeted inclusion. Targeted inclusions ranged in size from 6-50 µm, with the majority of the successfully analysed inclusions being 10-25 µm in maximum dimension.

Calibration using an external standard was carried out at the beginning and end of each experiment using NIST 610 and 612 glass standard reference materials. Although they are not matrix-matched to fluid inclusions, tests have shown that external calibration using NIST glasses provides accurate results and excellent reproducibility, with minimal error due to matrix effects when compared to other sources of error such as ablation quality, processing techniques and issues with internal standards (Heinrich et al., 2003; Sylvester, 2008).

Element ratios for 31 major and trace elements relative to an internal standard (Na) were determined following background correction of time-resolved signals. Absolute concentrations were determined from the element ratios using estimates of Na concentrations derived from microthermometry. These were estimated using the $NaCl\text{-}H_2O$ system for two-phase inclusions. Many three-phase inclusions appeared to host a single, anhedral daughter crystal during microthermometry, initially assumed to be halite. However, subsequent laser ablation ICP-MS and

SEM analysis revealed unusual intergrown masses of NaCl and KCl in these daughters. As such, wt % NaCl estimates derived only from halite dissolution temperatures assuming an NaCl-H_2O system were deemed unreliable. In such instances, the ternary H_2O-NaCl-KCl system was utilised and a Na estimate was made directly from the phase diagram (Sterner et al., 1988) using the final dissolution temperature and the Na/K ratio measured for each inclusion by laser ablation ICP-MS.

Processing was done using the Exlam2000 software package (Zacharias and Wilkinson, 2007). A limit of detection (LOD) was calculated for each element in every inclusion based on the 3σ variability of the background signal (Longerich et al., 1996). Precision and accuracy were assessed using a total of 122 measurements of NIST 610 standard reference material calibrated using NIST 612, with all elements showing good precision (RSD <10%). Relative error (accuracy) is excellent for all elements (<5%). Data quality was assessed by calculating charge balance based on inferred Cl content from microthermometric data and the cations determined using LA-ICP-MS. Charge balance was within ±10% for most samples and inclusions types (with the exception of some complex, multisalt brines, see Appendix A.1.4) indicating that analyses are robust. Full data are reported in Appendix C.4.

5.3.4 Stable isotopes

Oxygen and hydrogen stable isotope analyses were carried out at the Scottish Universities Environmental Research Centre (SUERC). Quartz separates were picked from fluid inclusion wafers to correlate oxygen isotope signatures with fluid inclusion results. Separates were analysed using a laser fluorination process involving complete sample reaction with ClF3 and combustion via CO_2 laser at >1500°C (Sharp, 1990). Oxygen released from the silica lattice was reacted with heated platinised graphite, producing CO_2 which was analysed by a VG SIRA 10 mass spectrometer. Repeat analyses of YP2 (16.4‰), GP147 (7.3‰), UWG2 (5.8‰) and JJB8 (30.3‰) standards showed reproducibility of better than ±0.2‰ (2σ). Results are reported in standard notation (δ18O) as per mil (‰) deviations from Standard Mean Ocean Water (V-SMOW).

For each hydrogen isotope analysis, approximately 1 g of quartz or carbonate separate was dried at 140°C in a vacuum overnight before being heated in a furnace at 700°C (quartz) or 400°C (carbonate) for sixty minutes to release inclusion fluids. Hydrogen gas was obtained from H_2O via reduction in a chromium furnace (Donnelly et al., 2001) and analysed by a VG-Micromass 602D mass spectrometer. Repeat analyses of the SUERC internal lab standard LT showed a reproducibility of ± 3‰ (2σ). Results are reported in standard notation (δD) as per mil deviation from V-SMOW.

5.4 Results

5.4.1 Vein kinematics and fluid Inclusion petrography

Many Zambian Copperbelt deposits host multiple generations of mineralised and barren veins from pre- to post-orogenic. Here, vein kinematics are divided into two broad temporal domains relative to peak Lufilian Orogenesis (~530-540 Ma). Typically layer-parallel veins within the primary ore horizons that are crosscut by orogenic structures or show high degrees of folding, shearing or boudinage are classified as pre- to syn-kinematic. Veins which clearly crosscut inversion structures and/or metamorphic fabrics and often can be observed to transgress stratigraphy are classified as post-kinematic.

At Nkana-Mindola, quartz-carbonate (± sulphide) veins are most abundant in the carbonaceous/graphitic shales of the Nkana South and Nkana Central orebodies, but are also present in more dolomitic lithologies in the Mindola North Open Pit. Mineralised pre- to syn-kinematic veins range from planar (Fig. 5-4A), to folded and boudinaged (Fig. 5-4B) and typically host abundant bn-cpy with lesser py-cc-po. These veins show temporally- and compositionally-distinct fluid populations, with volumetrically-dominant halite (±sylvite)-saturated primary inclusions and less common, two-phase, liquid-vapor secondary inclusions. Primary inclusions range from ~10 µm to 35 µm in length and typically display relatively low degrees of liquid fill (F = 0.60-0.80), with large solid daughter phases. They commonly host liquid CO_2 at room temperature (Fig. 5-5C and D). Secondary inclusions range in size from <1 µm to ~20 µm in length, have higher degrees of fill (F >0.95) and lack significant CO_2 (Fig. 5-5E). Post-kinematic discordant veins host abundant small (<15 µm), but volumetrically-dominant, secondary liquid-vapor inclusions with high degrees of fill (F >0.95), as well as rare assemblages of much larger (15-40 µm), CO_2-bearing, primary liquid-vapor inclusions with larger vapor bubbles (F = 0.75-0.90) (Fig. 5-5F).

Vein kinematics at Lumwana can be similarly subdivided into two broad classifications relative to peak Lufilian orogenesis. Mineralised veins are typically boudinaged and sheared within the ore schist and internal gneiss horizons, whereas post-kinematic veins crosscut the metamorphic fabric and transgress the hanging wall and footwall stratigraphy. Post-kinematic veins are typically barren, or host very minor chalcopyrite proximal to the ore schist horizons, suggesting remobilisation of earlier sulphides. Rare, primary inclusions from pre- to syn-kinematic veins at Lumwana typically host a single, anhedral salt crystal or multiple solid daughter phases and often contain liquid CO_2 (Fig. 5-5A). Primary inclusions were not evident in the Lumwana post-kinematic vein samples studied here. Secondary inclusions are volumetrically dominant in all vein types at Lumwana and

occur as linear trails of two-phase, liquid-vapor inclusions or assemblages of small (<10 µm) halite-saturated inclusions (Fig. 5-5G).

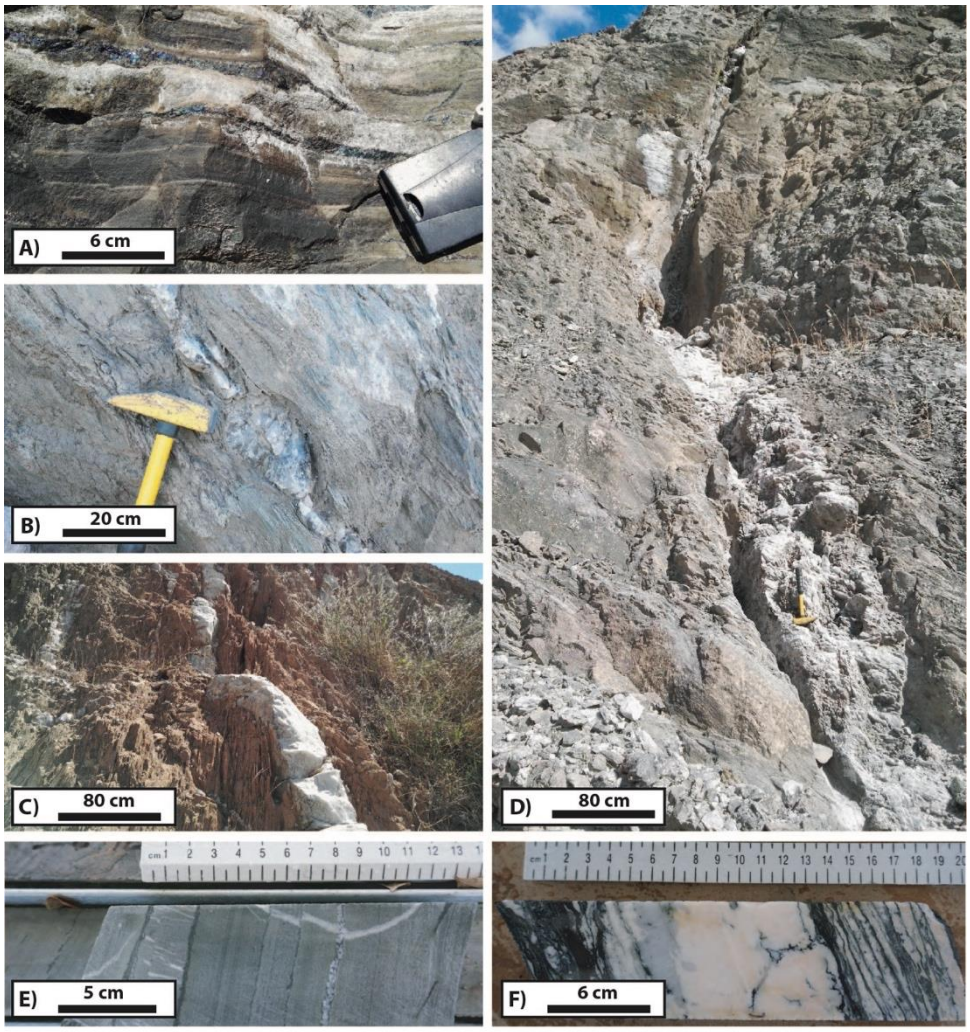

Fig. 5-4 Field evidence for contrasting vein kinematics. A) Layer-parallel quartz-carbonate-bornite veins hosted in partially silicified arenites in the Mindola North open pit. B) Boudinaged shale-hosted quartz-bornite-(chalcopyrite) vein in the Nkana South open pit. (A) and (B) are examples of pre- to syn-kinematic veins. C) Massive quartz vein cross-cutting the S_1 fabric in the hangingwall sediments at the Nkana Central open pit. D) Massive quartz-(carbonate) vein cross-cutting the footwall sediments at the Nkana Central open pit. (C) and (D) are examples of post-kinematic veins in the Zambian Copperbelt and are largely barren, with occasional minor chalcopyrite disseminations. E) Grey marlstone in the lower D'Kar Formation from the Zone 5 prospect in the Ghanzi Ridge region of the Kalahari Copperbelt. Millimeter- to centimeter-scale carbonate-bornite-chalcocite stringers exploit the Damaran S_1 cleavage and cross-cut and displace earlier discordant barren quartz-carbonate veinlets. Mineralised veinlets are interpreted as syn- to late-kinematic. Small-scale slip along cleavage planes accounts for significant cumulative displacement along fold limbs in the Ghanzi Ridge area. F) Siltstone-hosted

laminated quartz-carbonate-sphalerite vein in the middle-D'Kar stratigraphy at the Zone 5 prospect. Banded texture results from multiple fluid injections along slip planes on fold limbs. This vein is interpreted as syn-kinematic.

The vast majority of veins with workable inclusions from Nchanga are associated with Lufilian fabrics and early inversion structures and typically crosscut the earliest, bedding-parallel, pyritic veins. The Nchanga veins studied here are all classified as early- to syn-kinematic and are subdivided by their stratigraphic position in either the Cu-Co sulphide-dominant Upper Orebody or the Cu oxide-dominant Lower Orebody McGowan et al. (2006). Primary inclusions in Upper Orebody veins are typically halite (±sylvite)-saturated, multiphase CO_2-bearing brines ranging in length from ~10 µm to 90 µm (Fig. 5-5B). Solid daughter phases often occur as a single, large anhedral mass, or as multiple smaller anhedral crystals comprising >10% of the inclusion volume. Linear trails of smaller, secondary inclusions contain comparable daughter phases but host no appreciable CO_2. Similar, multiphase inclusion assemblages are present in the Lower Orebody veins, with additional secondary, CO_2-rich (liquid-vapor) and pure CO_2 inclusions present in some veins.

Veins at the Zone 5 and Zone 5 North prospects in the Ghanzi-Chobe belt show similar kinematics to those at Nchanga, with a strong association between mineralised quartz-carbonate veins and orogenic structures and fabrics. Small-scale veinlets (<1 cm) almost exclusively exploit the Damaran S_1 cleavage which is sub-parallel to bedding (Fig. 5-4E), whereas larger, laminated, mineralised veins formed due to repeated fluid injections along flexural slip planes on fold limbs (Fig. 5-4F). Inferred primary, aqueous liquid-vapor inclusions with high degrees of fill (F >0.95) are volumetrically dominant in most samples (Fig. 5-5H). A small number of sphalerite-hosted inclusions show identical petrographic properties to coexisting, primary quartz-hosted inclusions. Trails of small secondary inclusions (<8 µm) lacking CO_2 and with high degrees of fill (F >0.98) were sometimes observed.

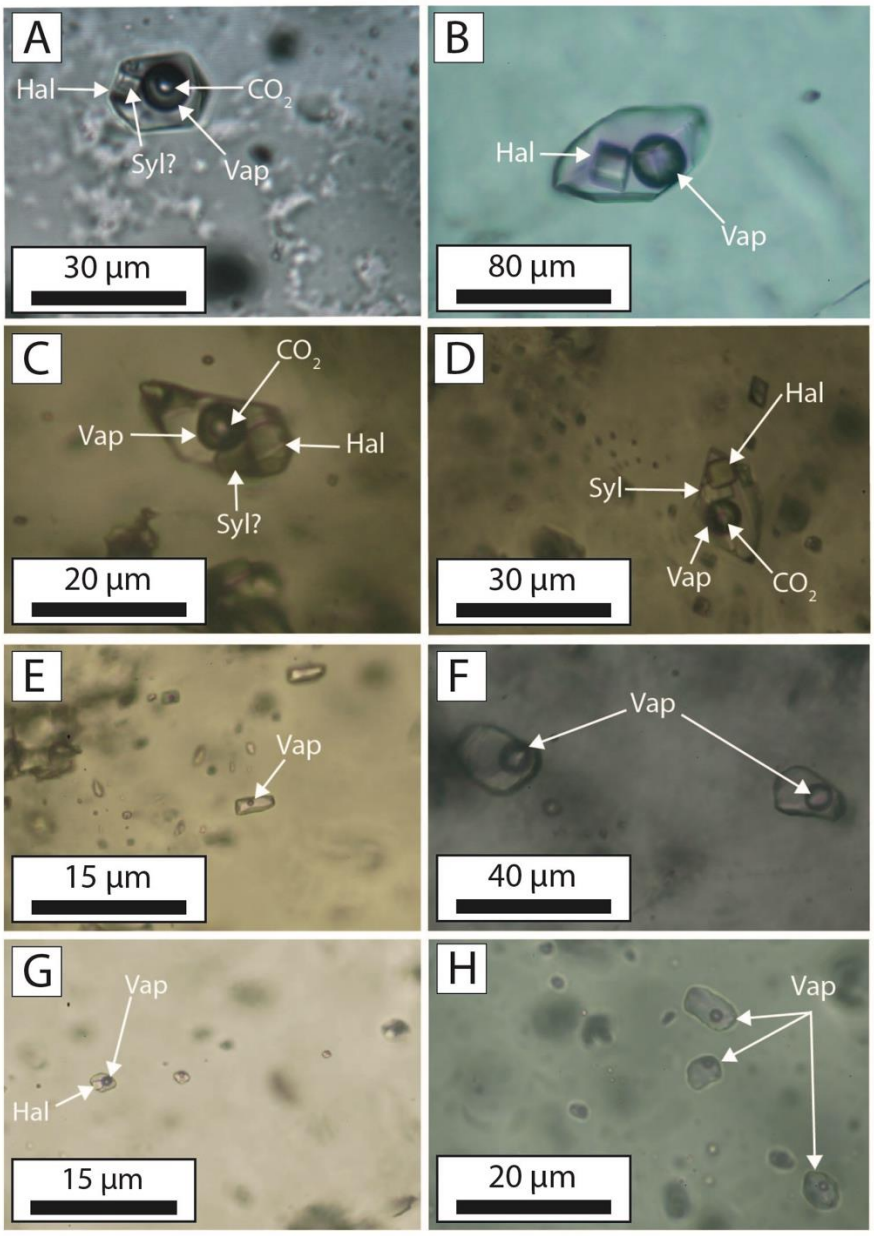

Fig. 5-5 Photomicrographs of quartz and carbonate-hosted fluid inclusions from the four deposits discussed in this study. A) Primary inclusion in a boudinaged and mineralised (bn-cpy) pre-kinematic vein hosted within the main ore schist horizon at Lumwana. The inclusion hosts liquid CO_2, a halite crystal and a possible sylvite daughter phase at room temperature (sample LUM1E-008). B) Primary halite-saturated inclusion within a mineralised syn-kinematic quartz vein in the 'Feldspathic Quartzite' (Upper Orebody) at Nchanga (sample NOP27). C) Primary quartz-hosted inclusion from a mineralised pre- to syn-kinematic vein within the siliceous dolomite ore in the Mindola North deposit. Liquid CO_2, as well as halite and sylvite(?) daughter phases are present at room temperature (sample JAZ55). D) A carbonate-hosted primary inclusion from Mindola North, with similar phase proportions and microthermometric properties to (C) (sample JAZ56). E) Two-phase liquid-vapor secondary inclusions typical of those hosted in weakly mineralised-to-barren syn-kinematic quartz veins at the Nkana-Mindola deposits (sample JAZ51). Primary

liquid-vapor inclusions with large vapor bubbles typical of those hosted in barren-to-weakly mineralised post-kinematic veins in the Nkana South and Central open pits (sample JAZ47). G) Halite-saturated secondary inclusion hosted in a barren post-kinematic vein cross-cutting the ore schist and hangingwall sediments at Lumwana (sample LUM1E-009). H) Primary liquid-vapor inclusions hosted within a mineralised syn-kinematic quartz-carbonate vein at the Zone 5 prospect (sample KCB-Z5-02).

Cathodoluminescence imaging of selected samples helped to better constrain the temporal context of fluid inclusion assemblages. In many samples, domains of primary quartz show bright luminescence and these were correlated with transmitted light images in order to confirm the primary origin of a given fluid inclusion assemblage (Fig. 5-6). Multiple generations of lower temperature secondary quartz with a darker CL response typically crosscut primary quartz domains and reflect the presence of later fluids, trapped as secondary inclusions, exploiting fractures and crystal boundaries.

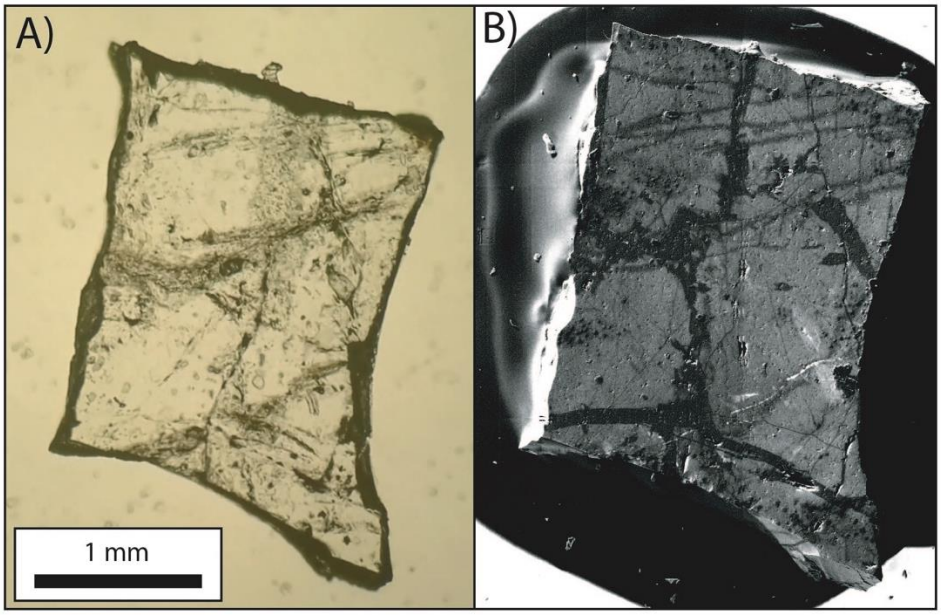

Fig. 5-6 Transmitted light photomicrograph (A) and corresponding scanning electron microscope-cathodoluminescence (SEM-CL) image (B) of sample NOP27 from the Upper Orebody at Nchanga. Domains of primary quartz show a brighter cathodoluminescence response (lighter gray), with cooler secondary quartz generations giving a lower cathodoluminescence intensity, forming at least two distinct cross-cutting darker grey quartz generations. Comparisons of the position of fluid inclusions precisely located under transmitted light with corresponding SEM-CL images which show distinct quartz generations provides increased confidence when establishing fluid inclusion paragenesis in a given sample or vein set.

5.4.2 Microthermometry

Total homogenisation temperatures (T_{hTOT}) and estimated salinities, subdivided according to host vein kinematics for the Nkana-Mindola and Lumwana deposits, by orebody at the syn-kinematic Nchanga deposit and by sulphide zones at the syn-kinematic Ghanzi-Chobe belt deposits, are shown in Fig. 5-7. Homogenisation temperatures represent a minimum estimate of the true trapping temperatures of inclusions and need to have a fluid pressure correction applied to infer fluid temperatures. Burial depths in the Zambian Copperbelt remain poorly constrained, with estimates ranging from 4.7 km to 40-50 km (Annels, 1989; Eglinger et al., 2016; Garlick, 1961). A substantial proportion of fluid inclusions analysed in this study are multiphase brines with significant KCl $\pm$ $CaCl_2$ components and as such, accurately constraining their true PVT relationships at the time of trapping remains problematic. Where assemblages of pure CO_2 and H_2O-CO_2 inclusions have been identified within the Lower Orebody at Nchanga, an estimate of the minimum trapping pressure can be made. Assuming an average lithostatic head of 2700 kg/m^3, along with a minimum trapping temperature equal to the average T_{hTOT} value of ~260°C measured for primary three-phase aqueous inclusions in the Lower Orebody Arkose, the average measured CO_2 inclusion density (0.972 $\pm$ 0.042 g cm^{-3}, n = 20) yields a minimum trapping pressure of ~225 MPa. This corresponds to a minimum trapping depth of ~8.5 km and a geothermal gradient of ~31°C/km. Imposing an upper lithostatic pressure threshold equivalent to the estimated pre-erosional overburden thickness towards the Katangan basin depocentre (~11 km; Selley et al. (2018)), a maximum possible pressure correction of ~90°C is estimated (trapping temperature ~350°C) (see Appendix A.1.2). Regardless of the magnitude of the pressure correction applied, many of the primary fluid inclusion homogenisation temperatures reported here indicate that fluids were unusually hot relative to analogous basins elsewhere in the world.

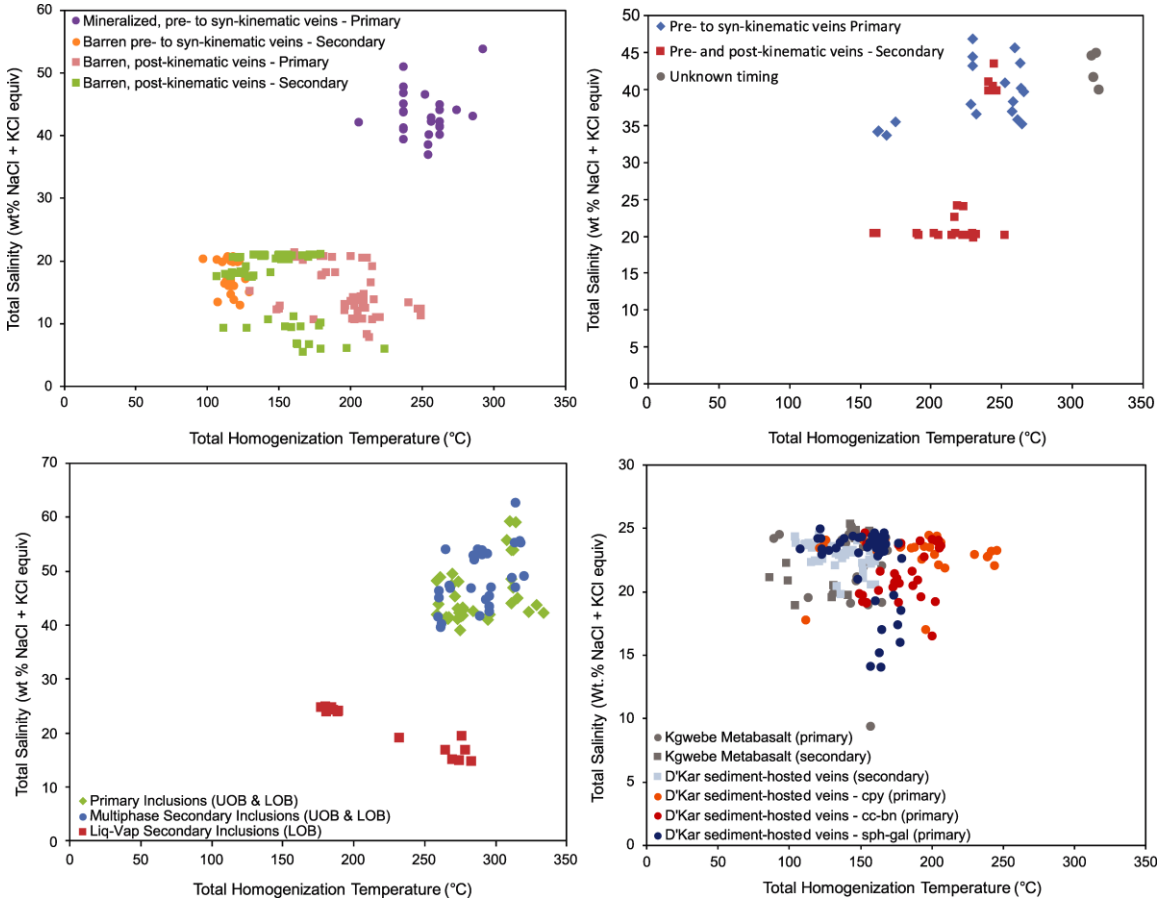

Fig. 5-7 Plots of total salinity (wt % NaCl + KCl equiv) versus T_{hTOT} (°C) for each of the four deposits discussed in this study. A) Nkana-Mindola - primary inclusions spatially associated with Cu-Co sulphides in pre- to syn-kinematic veins show distinctly higher temperature-salinity characteristics than both primary inclusions in discordant post-kinematic veins, or secondary fluid overprints. B) Lumwana – primary inclusions associated with sulphides in pre- to syn-kinematic veins show similar Th_{TOT} and total salinity characteristics to comparably timed inclusions at the Nkana-Mindola deposits. C) Nchanga – inclusions are categorised only as 'primary' or 'secondary', with the majority of veins in this deposit believed to have been emplaced during Lufilian orogenesis (UOB and LOB = Upper or Lower Orebody). Liquid-vapor secondary inclusions from LOB samples moderate-high Th_{TOT} and distinctly lower salinities, likely representing post-orogenic retrograde NaCl-dominant fluids. D) Zone 5 – Primary and secondary inclusions in all vein types display broadly consistent moderate salinities, with distinctly higher T_{hTOT} values for primary inclusions spatially associated with Cu sulphides than those stratigraphically higher in the D'Kar Fm. associated with Pb-Zn sulphides. Secondary inclusions in D'Kar-hosted sediments and all inclusions measured in a single vein sample from the underlying Kgwebe volcanics also display consistently lower T_{hTOT}. Salinities of all two-phase inclusions were derived from the freezing point depression of ice, modelled in the NaCl-H_2O system (Bodnar et al., 1985). Salinities for multi-phase inclusions were estimated from halite dissolution

temperatures, as well as Na:K ratios (derived from laser ablation ICP-MS analysis of inclusions), modelled in the NaCl-KCl-H_2O system (Sterner et al., 1988). All T_{hTOT} values represent minimum estimates of true trapping temperatures.

Multiphase primary inclusions from mineralised pre- to syn-kinematic veins at Nkana-Mindola show distinctly elevated temperature-salinity characteristics (modal T_{hTOT} = 280 - 290°C; salinity = 37 - 54 wt % NaCl + KCl equiv.) compared to two-phase, post-kinematic, vein-hosted primary inclusions (modal T_{hTOT} = 200 - 210°C; salinity = 7.8 - 20.6 wt % NaCl equiv.) and secondary inclusions from all vein types (modal T_{hTOT} = 110 - 120°C; salinity = 5.4 - 21.0 wt % NaCl equiv.). Significant CO_2 concentrations are restricted to primary inclusions in both pre- to syn-kinematic and post-kinematic veins, with CO_2 melting (T_{mCO2}) temperatures consistently indicating a near-pure CO_2 composition (T_{mCO2} = -56.6 to -57.1; n = 48).

Primary fluid inclusions hosted by mineralised pre- to syn-kinematic veins at Lumwana reflect similar temperatures and salinities to those at Nkana-Mindola (modal T_{hTOT} = 260 - 270°C; salinity = 34.0 - 47.4 wt % NaCl + KCl equiv.). Secondary inclusions, measured in both pre- to syn-kinematic and post-kinematic veins, fall into two broad populations: moderate temperature-salinity, two-phase, liquid-vapor inclusions (modal T_{hTOT} = 220 - 230°C; salinity = 18.9 - 23.6 wt % NaCl equiv.), and higher temperature-salinity, halite-saturated inclusions (modal T_{hTOT} = 330 - 340°C; salinity = 40.0 - 45.4 wt % NaCl equiv.) with no appreciable CO_2 content.

Syn-kinematic veins at Nchanga host similar, high temperature-salinity primary (modal T_{hTOT} = 270 - 280°C; salinity = 37.5 - 58.9 wt % NaCl + KCl equiv.) and secondary (modal T_{hTOT} = 260 - 270°C; salinity = 38.1 - 62.5 wt % NaCl + KCl equiv.) inclusions, with larger primary inclusions commonly containing near-pure CO_2 (T_{mCO2} = 56.6 – 58.7; n = 58). Assemblages of secondary CO_2-rich (liquid-vapor) and pure CO_2 inclusions present in several Lower Orebody veins have significantly lower homogenisation temperatures and salinities (modal T_{hTOT} = 180° - 190°C; salinity = 22.7 - 23.8 wt % NaCl equiv.). Secondary inclusions from a single syn-kinematic vein sample in the Nchanga Granite have higher homogenisation temperatures and moderate salinities (modal T_{hTOT} = 270 - 280°C; salinity = 12.8 - 17.9 wt % NaCl equiv.).

Fluid inclusion populations from the Kalahari Copperbelt Zone 5 and Zone 5 North prospects show relatively consistent salinities (typically 20-25 wt % NaCl equiv.) and a range of T_{hTOT}, from a mode of 210°C for primary inclusions associated with copper sulphide mineralisation in the lower D'Kar stratigraphy, to a mode of 160°C for primary fluids associated with sphalerite at higher levels. Secondary inclusions, measured in all vein types, have moderate salinity (19.6 - 24.4 wt % NaCl equiv.) and lower homogenisation temperatures (modal T_{hTOT} = 130°C). Primary inclusions from a single, metabasite-hosted quartz vein in the underlying Kgwebe Volcanics show comparable

salinities (18.9 - 25.4 wt % NaCl equiv.) and modal T_{hTOT} = 170°C, whereas secondary inclusions have lower homogenisation temperatures (modal T_{hTOT} = 140°C).

5.4.3 Elemental fluid inclusion analysis

Approximately 300 fluid inclusions were successfully analysed for their cationic composition by LA-ICP-MS (Appendix C.4). In most inclusions, Na, K and Ca are the dominant cations, with variable concentrations and ratios of each. These differences define a first-order compositional distinction between pre- to syn-kinematic fluids and post-kinematic fluids within the Pan-African belt.

Nkana-Mindola:

Primary inclusions from pre- to syn-kinematic mineralised veins at Nkana-Mindola are dominated by Na and K (subordinate Ca), with an average K/Na ratio of 1.0. Lithium, Ba and base metal concentrations are consistently relatively high in most pre- to syn-kinematic primary fluids, with Pb and Zn concentrations typically in the 102 - 103 ppm range; Cu concentrations ranging from 5 - 1560 ppm; and Co ranging from <10 – 770 ppm (Fig. 5-8). Late fluids are present as primary inclusions in post-kinematic veins as well as secondary inclusions in all vein types and these always have Na as the dominant cation, with mean K/Na ratios of 0.26. Base metal concentrations are one to two orders-of-magnitude lower than those in the earlier brines, with Pb-Zn concentrations typically in the 100 - 102 ppm range and many inclusions failing to return Cu or Co concentrations above their respective limits of detection (typically <10 ppm).

Lumwana:

Pre- to syn-kinematic veins at Lumwana host primary fluid inclusions with a distinct Na-K-Ca-(±Fe) cation chemistry. The absence of data for modelling these fluids in a suitable quaternary H_2O-salt system results in increased errors when estimating Na concentrations and in their subsequent application as an internal standard for cation quantification. Thus, although absolute cationic concentrations in such fluids are less certain than those from other deposits, order-of-magnitude distinctions in the concentrations of major cations and base metals between different fluid populations reveals similar trends in the kinematic evolution of fluid compositions at Lumwana to those observed at Nkana-Mindola. Primary fluid inclusions, hosted by pre- to syn-kinematic veins, display a mean K/Na ratio of 1.0 and elevated Ca concentrations (mean = 11.1 ± 5.2 wt %; n=15, 1σ). Base metal concentrations are consistently relatively high, with Pb and Zn on the order of 102 - 103 ppm and Cu and Co concentrations ranging from 85 - 1580 ppm and 37 - 380 ppm, respectively (Fig. 5-8).

Secondary fluids in pre- to syn-kinematic veins, as well as primary fluids in discordant veins, are NaCl-dominant, with a mean K/Na ratio of 0.5 and Ca concentrations (where above detection limits) of 2.0 ± 1.6 wt % (n=11, 1σ). Base metal concentrations are lower relative to earlier fluids, with Cu ranging from 49 - 540 ppm and Co from <1 - 55 ppm. Many inclusions from Lumwana display a cation charge excess, assuming that Cl- is the dominant anion, which can be accounted for by the presence of an unquantified component of divalent anions. Addition of ~8% of divalent anions (e.g. CO_3^{2-}) achieves charge-balance for all the Lumwana inclusions reported here. The presence of carbonate daughter phases in fluid inclusions (Fig. 5-10), together with elevated Ca and Ba concentrations, suggests they interacted with host rocks which contrast with the Lower Roan-hosted Zambian Copperbelt deposits bordering the Kafue Anticline.

Nchanga:

Primary inclusions hosted by syn-kinematic veins in the Upper and Lower orebodies at Nchanga share Na and K as dominant cations, with mean K/Na ratios of 1.1 and 0.9, respectively. Base metal concentrations are analogous to early fluids at Lumwana and Nkana-Mindola, with Pb and Zn typically in the 102 - 103 ppm range; detected Cu averaging 310 ± 260 ppm (n=24, 1σ); and mean Co concentrations of 94 ± 72 ppm (n=33, 1σ). Barium and Li concentrations are similar to those measured in early metalliferous fluids at Lumwana (typically 102 - 103 ppm) (Fig. 5-9). Multiphase secondary inclusions share similar cationic compositions to their primary counterparts, with reduced concentrations only present in secondary trails of two-phase, halite-undersaturated inclusions. Where present, these CO_2-rich inclusions are Na-dominant, with an average K/Na ratio of 0.24 and maximum Cu and Co concentrations of 110 ppm and 24 ppm, respectively.

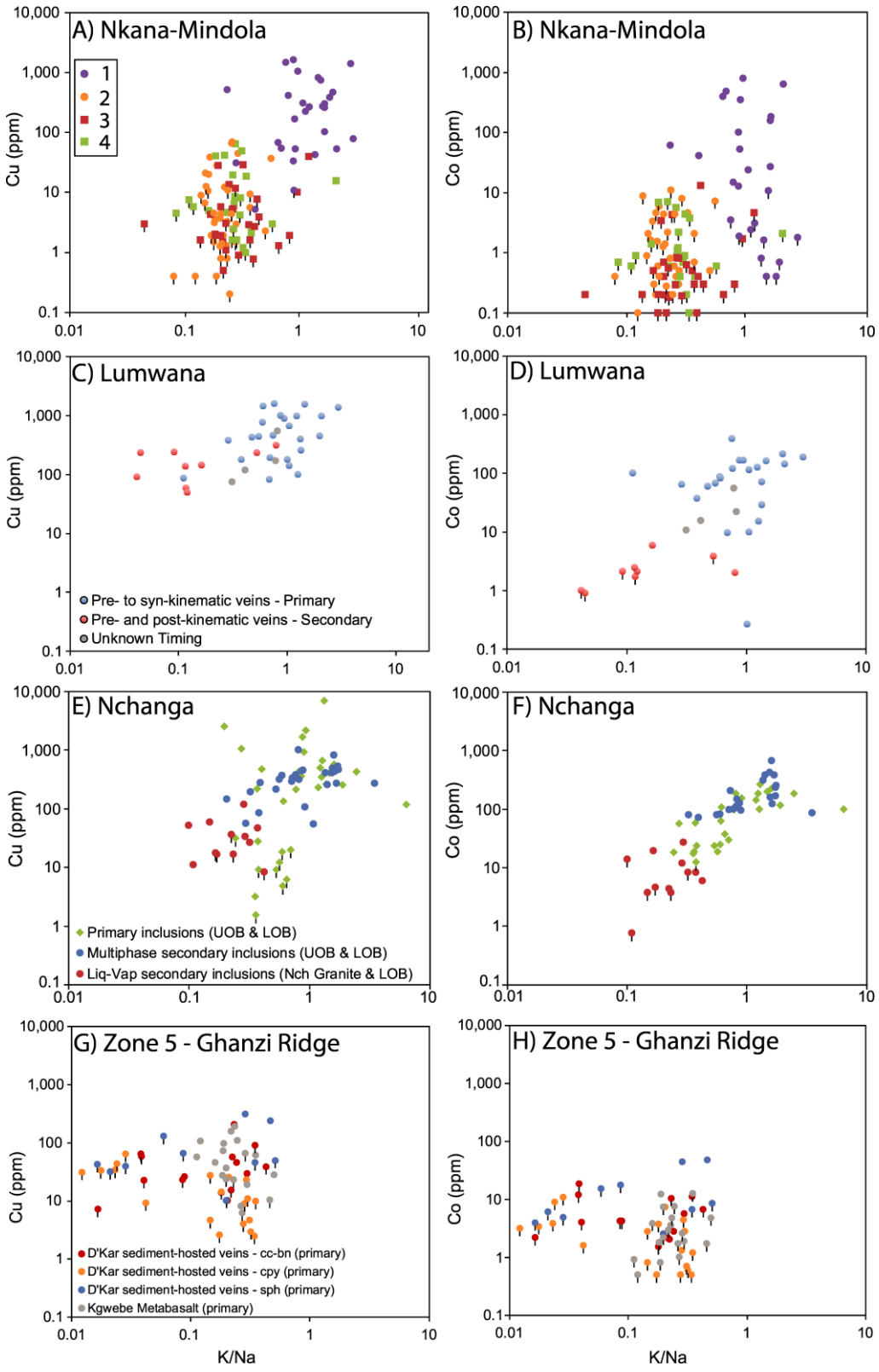

Fig. 5-8 Concentrations of Cu and Co versus K/Na ratios for individual fluid inclusions from each of the four deposits discussed in this study. Symbology remains consistent with Fig. 5-7. Bars on symbols indicate that the plotted value is a maximum value for that element (limit of detection). A and B) Nkana-Mindola: 1 = primary inclusions in mineralised, pre- to syn-kinematic veins; 2 = Secondary inclusions in weakly mineralised-to-barren, pre- to syn-kinematic veins; 3 = primary

inclusions in barren, post-kinematic veins; 4 = secondary inclusions in barren, post-kinematic veins. Fluids from all three Zambian deposits show a potential relationship between K/Na and Cu-Co concentrations. Primary inclusions spatially associated with sulphides in early veins at both Nkana-Mindola and Lumwana (C and D) show elevated K/Na ratios and 1-2 orders-of-magnitude higher Cu and Co concentrations than post-peak orogenic fluids. E and F) Nchanga - primary and secondary multiphase inclusions together show a potential relationship between Cu-Co and K/Na, with little distinction between the base metal content of the two populations. G and H) Zone 5 – all fluid inclusions from the Kalahari Copperbelt prospect show significantly lower absolute concentrations of Cu and Co when compared to the multiphase potassic brines measured from all three Zambian deposits, with most inclusions returning Cu and Co measurements below their respective limits of detection.

Ghanzi-Chobe Belt Deposits:

Syn- to late-orogenic, vein-hosted primary inclusions spatially associated with Cu-(Pb-Zn)-sulphides in the Zone 5 and Zone 5 North deposits show comparable cationic compositions to kinematically late, two-phase solutions from all three Zambian Copperbelt deposits. Solutions are Na-dominant, with lesser Ca and K and a mean K/Na of 0.17. Lead and Zn concentrations are consistently in the 10^1 - 10^2 ppm range, with most inclusions failing to return Cu or Co concentrations above their respective limits of detection. Primary inclusions hosted within a quartz-haematite vein in the footwall Kgwebe Volcanics shared similar cationic compositions but with a higher number of detectable Cu analyses (mean = 73 ± 53 ppm; n=14, 1σ).

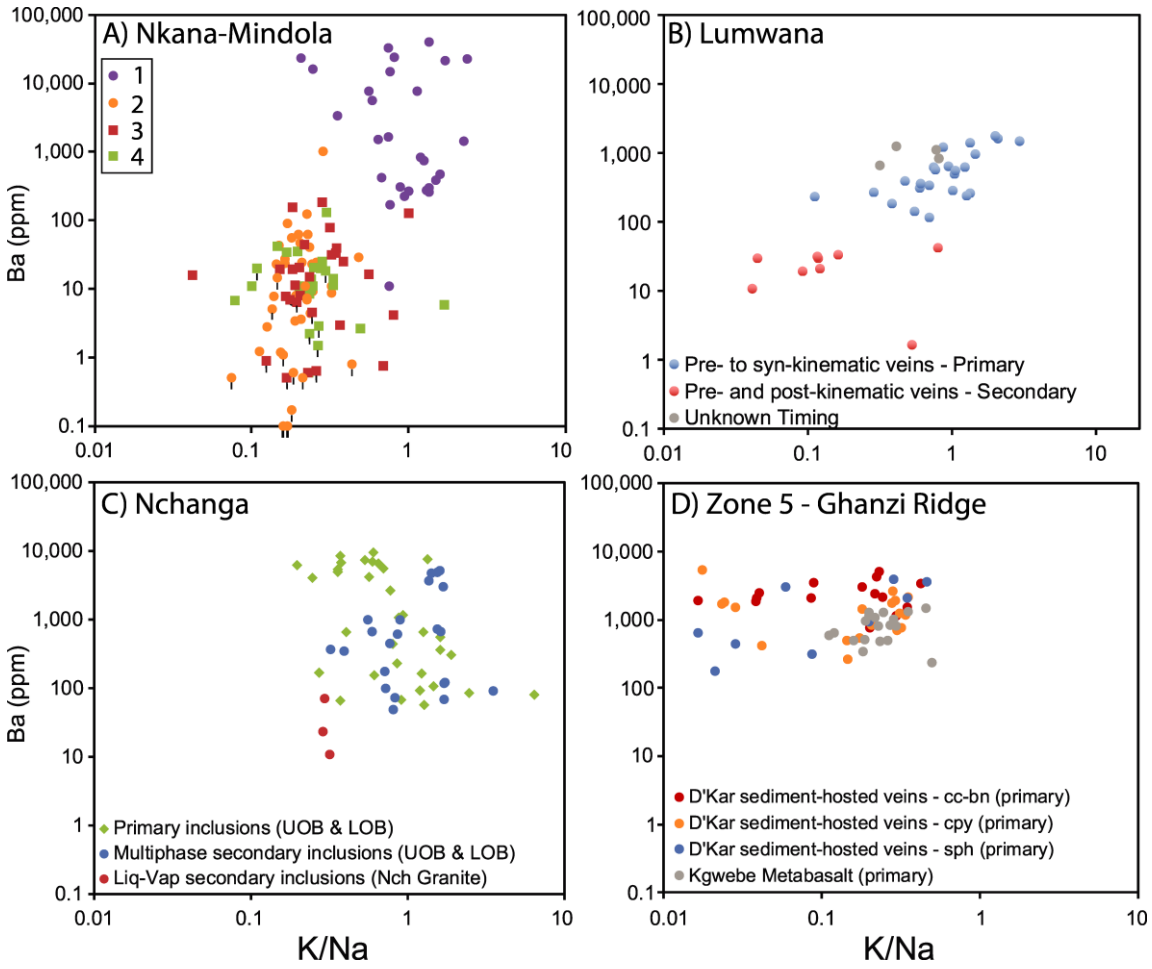

Fig. 5-9 Barium concentrations versus K/Na of individual inclusions from each of the four deposits discussed in this study. Bars on symbols indicate that the plotted value is a maximum value for that element (limit of detection). Inclusions from Nkana-Mindola (A) and Lumwana (B) show a potential relationship between Ba and K/Na, with metalliferous potassic brines consistently hosting elevated Ba concentrations. The majority of syn-kinematic potassic multiphase brines from Nchanga (C) also show elevated Ba concentrations (>100 ppm). D) All fluids from the Zone 5 prospect in the Kalahari Copperbelt show moderately elevated Ba concentrations, with no systematic variation between fluid populations or as a function of their major cation chemistry.

5.4.4 SEM imaging

Secondary and back-scattered electron SEM imaging was used alongside element mapping in order to semi-quantitatively assess the composition of solid daughter phases hosted by various fluid inclusion assemblages identified from Nkana-Mindola, Lumwana and Nchanga. Element maps of base metal-rich, primary inclusions hosted by pre- to syn-kinematic veins with elevated K/Na ratios reveal ubiquitous KCl, occurring either as a cubic phase associated with halite, or as unusual intergrowths, forming anhedral salt masses with distinct NaCl and KCl compositional domains (Fig. 5-10 A, B). Elevated Ba concentrations measured in these fluids are reflected by the presence of

BaCO3 (Fig. 5-10 D, E, G). Sulfur-deficient Fe-phases were also imaged in three inclusions (Fig. 5-10 E), indicating the presence of iron-oxide or oxyhydroxide species in some early fluids. A small number of salt-saturated secondary inclusions with low K/Na ratios from Lumwana were imaged, in most cases revealing only halite as a daughter phase, with rare Ca and Ba sulfate daughters (Fig. 5-10 H).

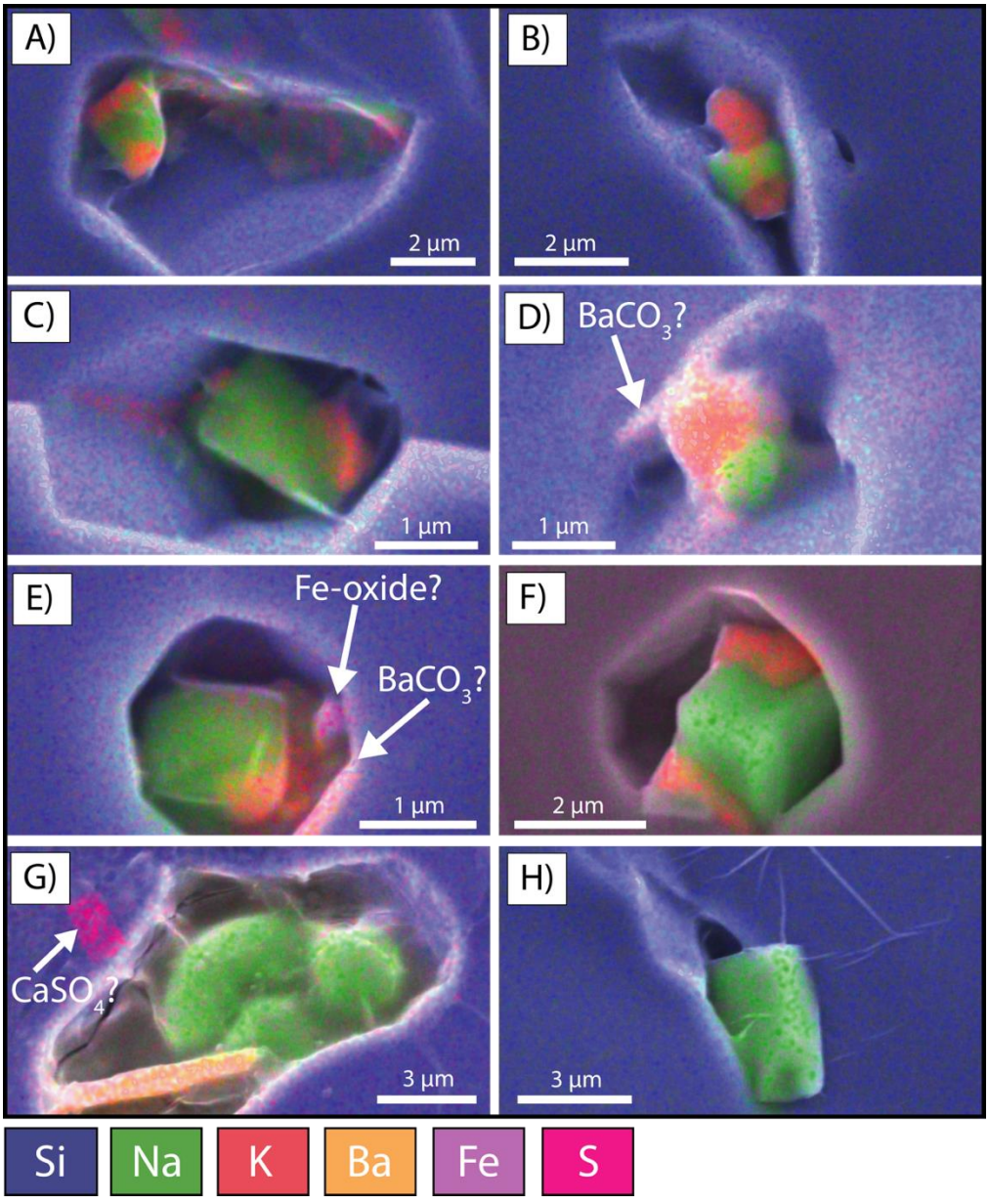

Fig. 5-10 Scanning electron microscope images of fluid inclusion cavities. Net intensity element maps display the relative masses of various solid daughter phases using backscattered electron imagery. A-C) Intergrown halite and sylvite forming anhedral salt masses in primary fluid inclusions hosted by two mineralised syn-kinematic veins in the Nchanga Upper Orebody. D) Primary inclusion in a mineralised pre- to syn-kinematic vein from the ore shale at Nkana. Sylvite and halite form the primary solid phases, with a minor Ba(CO_3?) phase (left). E) Intergrown halite and sylvite with minor Ba(CO_3?) and Fe-oxide phases (right) in a primary includion from a

mineralised vein in the Nchanga Upper Orebody. Large intergrown halite and sylvite cubes in a dolomite-hosted inclusion from a mineralised pre-kinematic quartz-carbonate vein at Nkana-Mindola. G) Halite-dominant brine inclusion within a post-kinematic quartz vein at the Lumwana deposit. The inclusion also shows a large Ba(CO_3?) crystal and likely hosted a $CaSO_4$ daughter phase imaged on the left periphery of the inclusion cavity. H) Large halite cube within a late sodic brine inclusion from a secondary trail in a quartz vein from Lumwana.

5.4.5 Oxygen and hydrogen stable isotope analysis

Samples from mineralised pre- to syn-kinematic vein quartz and dolomite from the Nkana Central and Mindola North open pits have $\delta^{18}O$ values of +15.2‰ to +18.9‰. In contrast, barren, post-kinematic vein quartz from the Nkana South, Central and Mindola North open pits has $\delta^{18}O$ ranging from +12.1‰ to +15.3‰ (Fig. 5-11 A). Using the modal T_{hTOT} for primary fluid inclusion assemblages belonging to each of the vein samples, estimates of minimum $\delta^{18}O$fluid values for the earlier fluids range from +6.7‰ to +9.0‰ (mean = 7.8 ± 0.9‰; n=5, 1σ and from -3.8 to 4.1 for post-orogenic fluids (mean = +0.4 ± 3.0‰; n=7, 1σ).

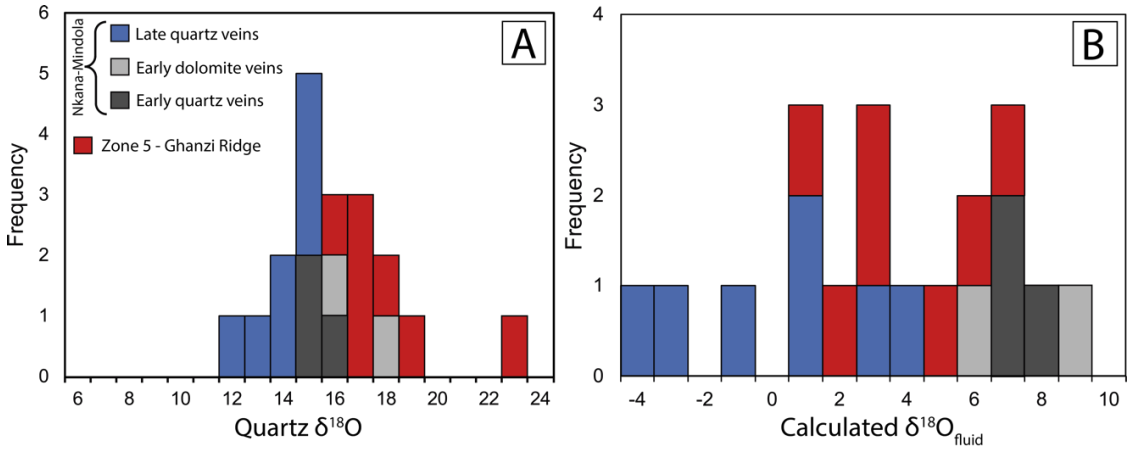

Fig. 5-11 Oxygen isotope data for quartz and carbonate vein material from the Nkana-Mindola deposit and the Zone 5 prospect (A). 'Early' veins comprise quartz and carbonate pre- to syn-kinematic veins which show slightly higher $\delta^{18}O$ values than post-kinematic quartz veins from Nkana-Mindola. Veins hosted within the D'Kar Formation sediments at Zone 5 show a narrow range of $\delta^{18}O$ values, with a single vein hosted in the underlying Kgwebe Formation volcanic sequence returning a higher $\delta^{18}O$ value. B) $\delta^{18}O_{fluid}$ values calculated using fluid inclusion fluid inclusion T_{hTOT} measurements and the fractionation factors from Matsuhisa et al. (1979) and Zheng (1999). Kinematically early veins at Nkana-Mindola show distinctly higher $\delta^{18}O_{fluid}$ estimates than post-kinematic veins.

Only six samples from Nkana-Mindola hosted a sufficiently homogeneous fluid inclusion population to return a reliable hydrogen isotope signature. One mineralised pre- to syn-kinematic quartz vein from the Mindola North deposit yielded a δD value of -45‰, whereas five barren, post-kinematic quartz veins from Nkana South, Central and Mindola North show values ranging from -50‰ to -26‰ (mean = -37 ± 9‰; n=5, 1σ) (Fig. 5-12).

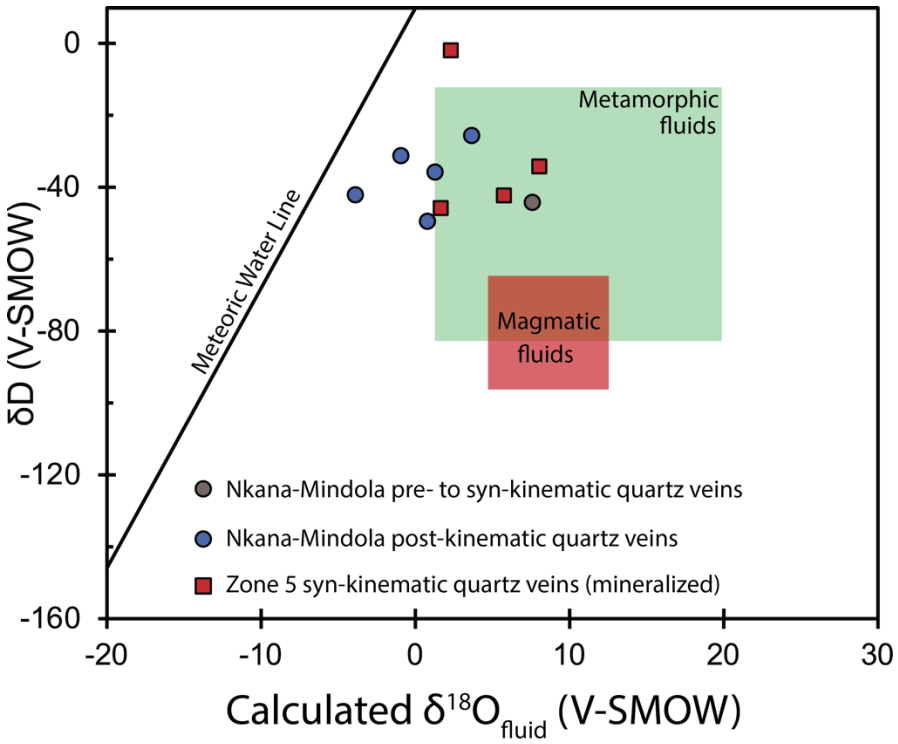

Fig. 5-12 Hydrogen and oxygen isotope data for fluid inclusions and their host veins from the Nkana-Mindola and Zone 5 deposits. Typical fields for metamorphic and magmatic fluids are indicated (Taylor, 1997). There are no systematic variations in the hydrogen isotope signatures of any of the fluid inclusions analysed here, with consistent δD values of ~ -30 to -45‰ for both datasets.

Six mineralised syn-orogenic quartz vein samples from the Zone 5 prospect gave δ^{18}O values ranging from +16.9 to +19.1‰, whilst a single barren quartz-haematite vein hosted by the basal Kgwebe Volcanics returned a δ^{18}O value of +23.7‰. Calculated minimum $\delta^{18}O_{fluid}$ values based upon modal T_{hTOT} values for corresponding primary fluid inclusion assemblages in the six mineralised veins average +3.9‰ (± 1.9‰, 1σ) (Fig. 5-11 B). Three quartz vein samples returned δD values ranging from -46 to -34‰ (mean = -41‰).

5.5 Discussion

5.5.1 Characterising Zambian Copperbelt ore fluids

Pre- to syn-kinematic veins at Nkana-Mindola and Lumwana host geochemically distinct fluids from those occurring in later, post-kinematic veins, or as secondary inclusion trails in all vein types. Primary fluids in early kinematic structures typically display higher homogenisation temperatures, K/Na ≥1 and one to two orders-of-magnitude higher base metal concentrations than their post-orogenic counterparts. At Nchanga, where vein-hosted mineralisation is syn-kinematic (McGowan et al., 2006), all multiphase inclusions studied represent high temperature, metalliferous, potassic brines, analogous to the early fluids associated with mineralisation at Nkana-Mindola and Lumwana. Copper and Co concentrations in the potassic brines are amongst the highest reported from any sedimentary basin environment, supporting the hypothesis that Zambian Copperbelt ore fluids were anomalously base metal enriched.

Elevated Ca-(±Fe) concentrations and cation excesses in early fluid inclusions from Lumwana are indicative of a contrasting ore fluid chemistry in the Domes region when compared to the more typical Lower Roan-hosted deposits peripheral to the Kafue Anticline. Barium carbonate daughter phases imaged in these inclusions (Fig. 5-10) indicate a significant CO_3^{2-} component, and the addition of ~5-15 wt % divalent anions achieves charge-balance for all such inclusions measured in this study. These fluids appear to have retained the elevated K/Na ratio bittern brine signature observed in ore fluids at Nkana-Mindola and Nchanga, whilst attaining additional Ca through interaction with contrasting lithologies to those in the Lower Roan-hosted deposits which fringe the Kafue Anticline. Whole rock geochemical analyses of ore schists at Lumwana indicate Ca depletion relative to hangingwall gneiss units, which Bernau et al. (2013) attribute to the replacement of feldspars by biotite during syn- or pre-peak metamorphism. This process may explain concomitant Ca depletions in whole rock samples, alongside Ca enrichment of proximal vein-hosted fluid inclusions interpreted to have been trapped at a similar time.

5.5.2 Cobalt distribution

The three Zambian Copperbelt deposits discussed here are variably endowed with Co, with Nkana-Mindola containing approximately four times as much Co as Nchanga or Lumwana (Taylor et al., 2013). Early ore fluid compositions reflect this distinction, with primary quartz-hosted fluid inclusions in pre- to syn-kinematic veins at Nkana-Mindola averaging 340 ppm Co, compared with 92 ppm and 130 ppm Co for primary potassic ore fluids at Nchanga and Lumwana, respectively. Notably, carbonate-hosted, pre- to syn-kinematic veins at Nkana-Mindola appear to have formed from fluids with much lower Co content, averaging only 21 ppm Co. Cobalt mineralisation was not

as clearly fluid-controlled at Nchanga, where it is decoupled between orebodies, with Cu only in the Lower Orebody and Cu-Co in the Upper Orebody (McGowan et al., 2006). This is not a distinction that is reflected in the base metal concentrations of fluids recovered from the respective orebodies, indicating that Co enrichment in the Upper Orebody is not a function of the fluid composition or source, but instead reflects the efficiency of Co precipitation within the contrasting stratigraphic intervals.

5.5.3 Generation of a potassic bittern brine

Consistent K/Na ratios of 0.9 to 1.1 for metalliferous brines from Nkana-Mindola, Lumwana and Nchanga suggest a widespread association between ultra-potassic brines and base metal fertility, and an atypical brine source or residence history. Comparisons of the halogen ratios of kinematically distinct vein generations across a series of Central African Copperbelt deposits indicate a dominant population of highly evaporated bittern brines early in the basin history, with pre- to syn-kinematic veins from many Zambian and Congolese deposits displaying average Cl/Br values below that of seawater (Nowecki, 2014; Selley et al., 2018). Development of large volumes of bittern brines with low Cl/Br and Na/Br and high K/Na ratios at source requires extended periods of evaporation in a restricted marine setting.

At high degrees of evaporation (a measure of the ratio of element concentrations per kg H_2O in a brine relative to bulk seawater [DE]), the precipitation of NaCl, coupled with the more conservative behaviour of K, results in K/Na ratios reaching ~1 to 2 prior to saturation of any major K-bearing phases (kainite and carnallite precipitation commences at DE >75). Progressive removal of NaCl from solution from DE ~10 onwards therefore results in both K enrichment relative to Na as well as the low Na/Br and Cl/Br ratios characteristic of these brines.

Neoproterozoic ocean compositions are primarily constrained by halite-hosted fluid inclusions that are believed to have preserved original seawater compositions. Inclusions from the Amadeus and Officer Basins (Australia) indicate a period of $CaCl_2$-rich, $MgSO_4$-poor seas for up to 200 million years during the middle Neoproterozoic, broadly coinciding with the breakup of Rodinia (Kovalevych et al., 2006; Spear et al., 2014). Thus, during the proposed time period that early, ultra-potassic bittern brines were sourced in the Zambian Basin (ca. 800 Ma), marine sulfate concentrations may have been ~10% of modern seawater values, increasing to ~20-35% of present concentrations during the deposition of the Vazante Fm. (Brazil) at ca. 750 Ma and the Otavi Fm. (Namibia) at ca. 740 Ma (Kah et al., 2004). Theoretical evaporite crystallization sequences of such sulfate-deficient ancient seawaters replicate evaporite sequences observed in the Bonneville Salt Flats, Utah, where sylvite precipitated immediately after halite, with the omission of significant $MgSO_4$ salts (Valyashko, 1962). This indicates that elevated fluid K/Na ratios can be developed at lower degrees of

evaporation from such seawater, where an initially low sulfate budget is entirely consumed through gypsum deposition during the earliest stages of evaporation. The abundance of Ba in the metalliferous bittern brines from all three Zambian deposits (Fig. 5-9), yet scarcity of barite as daughter phases within brine inclusions or more widely in the Katangan stratigraphy, can also be reconciled if these brines had low SO_4^{2-} concentrations, consistent with the proposed $CaCl_2$-rich, $MgSO_4$-deficient middle Neoproterozoic seawater source.

5.5.4 Fluid-rock interaction

Ore fluids in sediment-hosted Cu systems are typically low-moderate temperature solutions, ranging from ~100°C (White Pine, Dzhezkazgan, Kupferschiefer) to a maximum of ~250°C (Coates Lake, Redstone) (Box et al., 2012; Brown, 2018; Jowett, 1986; Milton, 2015). However, in the Zambian Basin, the fluid inclusions in pre- to syn-kinematic veins indicate brines were in excess of 275°C and 40 wt % NaCl + KCl equiv. over a prolonged period of the basin history, representing long-lived, highly efficient solvents. This was presumably due to burial of the Lower Roan clastic sequences by up to 11 km of Katangan Supergroup sediments. Leaching experiments targeting variably crystallized secondary iron oxides in a variety of diagenetically 'reddened' siliclastic rocks from Baja California mobilized ~44% Cu and 47% Co in a series of low temperature (<100°C) saline solutions (Zielinski et al., 1983). At higher temperatures (350°C), halite-saturated brines have been shown to leach ~73% of the initial Cu and >90% of Pb and Zn from greywackes (Bischoff et al., 1981). Together, these data suggest that provided intergranular porosity and permeability were maintained through the deep burial history, leaching and mobilization of base metals on a basin-wide scale could have been highly efficient.

Oxygen stable isotope signatures of pre- to syn-kinematic and post-kinematic vein quartz and carbonate reflect differing residence histories in the Katangan Basin, with early mineralised veins showing higher $\delta^{18}O$ values than barren discordant veins. Similarly, in a study of carbonate veins from Nkana, Muchez et al. (2010) reported higher $\delta^{18}O$ values for pre- to syn-kinematic nodules, 'layer-parallel' and 'irregular' veins than post-peak orogenic 'massive' discordant veins. In both cases, this distinction is attributed to contrasting fluid sources and degrees of water-rock interactions, with earlier brines having undergone greater degrees of interaction with host metasediments during more prolonged residence times in the deep basin. Fluid interaction with Roan sediments also likely modified the total salinity and K/Na ratio of resident brines through the breakdown of primary potassic phases. Red beds of the Mindola Clastics Formation typically comprise 20-30% detrital potassium feldspar and could provide a supplementary source of K for further enrichment of pre-kinematic bittern brines. Petrographic studies of footwall sediments at various Zambian deposits indicate extensive breakdown and replacement of detrital potassium

feldspar by secondary feldspars and mica (Fig. 5-13) (Selley et al., 2005; Sutton and Maynard, 2005), suggesting that the potassium budget of primary/detrital sediment grains was mobile during interactions with anomalously high temperature hypersaline brines. Whilst unusually high K/Na ratios are generated through advanced evaporative processes during bittern brine production, the thermally anomalous nature of resident pre-kinematic brines in the Katangan Basin ultimately enabled the generation of significantly elevated total fluid salinities (>50 wt % NaCl + KCl equiv.).

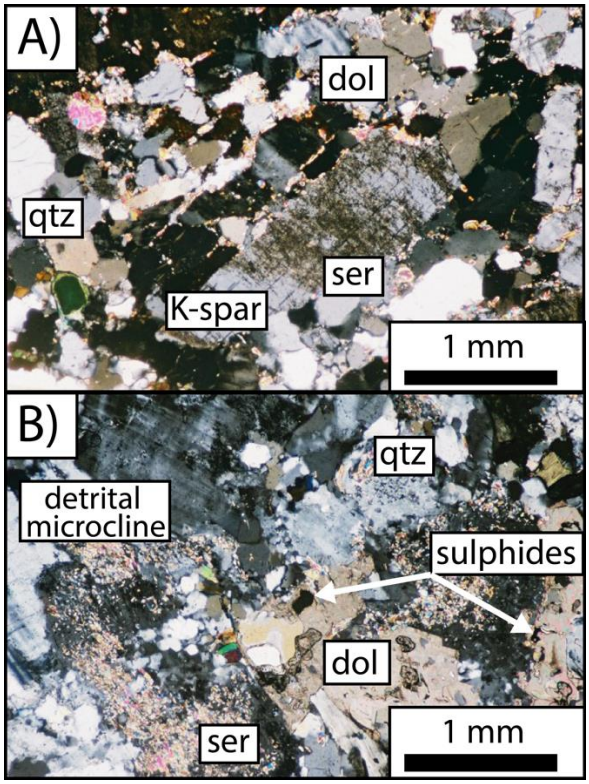

Fig. 5-13 Cross-polarised transmitted light images of altered arkose from the footwall of the Lower Orebody at Nchanga. Both images show interlocking aggregates of primary quartz, microcline and feldspar, variably replaced by dolomite, sericite and lesser phlogopite (primarily along grain boundaries and feldspar cleavage). Image B also shows disseminated Cu-Co sulphides (cpy, bn, carr).

5.5.5 Mineralisation

In addition to direct sampling and analysis of palaeofluids, mineralisation of Zambian Copperbelt deposits by potassic brines is evidenced in several deposits by secondary alteration phases which are spatially and temporally associated with Cu-Co sulphides. Potassic alteration, principally in the form of potassium feldspar and biotite/phlogopite, is intensely developed in Lower Roan footwall rocks (Darnley, 1960), most closely associated with shale-hosted mineralisation. Textures including clotted intergrowths of K-feldspar (± biotite) with sulphides in Konkola North, and partitioning of K-feldspar, chalcopyrite and carrollite into microfracture-controlled linear arrays at the Mwambashi

B deposit (Selley et al., 2005), reflect the presence of potassic fluids during ore formation. At Konkola North, secondary K-feldspar grains in the ore shale and its immediate footwall are Ba-enriched (typically 1-4% BaO) (Sutton and Maynard, 2005), consistent with the elevated Ba concentrations measured in this study.

Subsalt metasomatism across the Central African Copperbelt is macroscopically partitioned, with the "classic Congolese Copperbelt" deposits characterised by Mg-dominant metasomatism, whereas deposits in the Zambian Copperbelt and the Domes region are characterised by pervasive K metasomatism (Hitzman et al., 2012; Selley et al., 2018). Extensive Mg metasomatism and the concomitant absence of alkali metals in basal clastic sequences in the central Congolese Copperbelt may imply potassium remobilisation from the depocentre towards the basin margins (Zambian Copperbelt in the south and Kamoa in the north) (Selley et al., 2018). Analyses of palaeofluids from a more diverse range of temporal, straigraphic and geographic settings across the Central African Copperbelt are required to more confidently establish the major salt chemistry of bittern brines throughout the Katangan Basin.

The sulfate-deficient nature of the proposed ore fluids at the deposits studied here necessitates an independent source of reduced sulfur at mineralisation sites. A variety of such sulfur sources have been proposed across the Zambian Copperbelt, ranging from in situ diagenetic pyrite at Nkana (Brems et al., 2009), to thermochemical reduction of sulfate $\pm$ metal-enriched fluids at Nchanga (McGowan et al., 2006). The presence of significant Zn and Pb in the ore fluids but their general absence from the deposits can perhaps be accounted for by a limited sulfur supply that was exhausted by Cu-Co sufide precipitation at higher temperature resulting in onward transport of these metals to distal basin margins, outboard of the major Cu-Co accumulations.

5.5.6 Development of Pan-African NaCl-dominant brines

Primary fluid inclusions from discordant veins at Nkana-Mindola and Lumwana, as well as most secondary inclusions from all three Zambian deposits, represent moderate temperature, metal-poor, NaCl-dominant solutions. Where saturated, SEM element maps of these inclusions show that chloride daughter minerals are restricted to halite, with rarer Ba and Ca sulfate (± carbonate) phases. Such fluids could have been produced by interaction between halite-undersaturated fluids and gypsum-halite-dominant salt rafts during basin inversion, a process evidenced by pervasive dissolution breccias in the Upper Roan stratigraphy. The distinct chemistry of these lower temperature fluids compared with the high temperature potassic brines suggests that minimal mixing with deeper basinal fluids occurred prior to removal of the salt seals. Destruction of salt seals and progressive penetration of shallower, halite-dissolution brines into the deep basin is evidenced by their presence as primary inclusions in late, discordant veins in the basement-hosted

Lumwana deposit. Their passage through the Katangan stratigraphy during orogenesis is consistent with the development of pervasive, structurally-controlled sodic-calcic (albite ± scapolite) alteration that overprints stratiform mineralisation and earlier potassic alteration assemblages across the copperbelt (Selley et al., 2005; Sweeney and Binda, 1989). This process was potentially enhanced by halite extraction during the development of salt walls, as well as the development of permeable inversion structures.

Bulk crush-leach analysis of post-kinematic veins from Lumwana, as well as vein material from demonstrably post-kinematic deposits in Zambia such as Kipushi and Kansanshi reveal Cl/Br and Na/Br ratios in excess of typical seawater values, consistent with an origin via halite dissolution (Heijlen et al., 2008; Nowecki, 2014; Selley et al., 2018). Determining the exact timing of entrapment of these sodic brines is difficult, however, their residence at suprasalt levels in the stratigraphy prior to widespread salt dissolution implies they developed after deposition of the upper Katangan stratigraphy. Halite-hosted seawater inclusions from upper Neoproterozoic evaporite deposits in Oman and Pakistan suggest that ocean chemistry transitioned from sulfate-deficient $CaCl_2$ seas prior to ~650 Ma, to a period of $MgSO_4$-rich 'aragonite' seas between ~650 and 530 Ma (Horita et al., 2002; Kovalevych et al., 2006; Lowenstein et al., 2001). In marked contrast to the early potassic brines, the presence of $CaSO_4$ as daughter phases in some secondary NaCl-dominant inclusions at Lumwana (Fig. 5-10 G) supports an origin from relatively sulfate-enriched seawater during this period.

Primary fluid inclusions in syn-kinematic mineralised veins at the Zone 5 and Zone 5 North prospects in the Ghanzi-Chobe belt share comparable homogenisation temperatures, salinities and base metal concentrations with the late, NaCl-dominant fluids identified in the Zambian Copperbelt (Fig. 5-14). Mineralised veins are primarily hosted within the Damaran cleavage and other orogenic structures, constraining the timing of mineralisation to peak or post-peak orogenesis, which was broadly synchronous with Lufilian orogenesis in the Central African Copperbelt (Gray et al., 2006). The geochemical similarities between the fluids responsible for relatively small-scale and low grade mineralisation in the Kalahari Copperbelt prospects and for the widespread sodic fluid overprint prevalent in the Zambian Copperbelt are striking (Fig. 5-14). Thus, in contrast to the hydrologically restricted ultra-potassic bittern brines responsible for mineralisation in the Zambian Copperbelt, moderate temperature-salinity NaCl-dominant fluids having undergone varying degrees of halite-dissolution appear to have been widely sourced in large volumes during inversion of the Pan-African margin in the upper Neoproterozoic. Significant volumes of fluid sourced from an extensive marine basin during the closure of the Pan-African margin likely possessed relatively homogeneous initial $\delta^{18}O$ and δD signatures. Although fluid $\delta^{18}O$ values are easily modified by fluid-rock interactions, at high fluid:rock ratios, the lack of significant mineral-hosted hydrogen ensures δD values remain

relatively unaltered. A comparison of δD signatures of mineralised veins from the Ghanzi-Chobe belt prospects (average δD = -41‰, n=3) and barren post-kinematic veins at Nkana-Mindola (average δD = -37‰, n=5) shows relatively homogeneous values, supporting their derivation from a common fluid reservoir prior to peak orogenesis. More variable δ^{18}O signatures, both within, and between the deposits studied, reflect differing degrees of equilibration with metasediment host rocks.

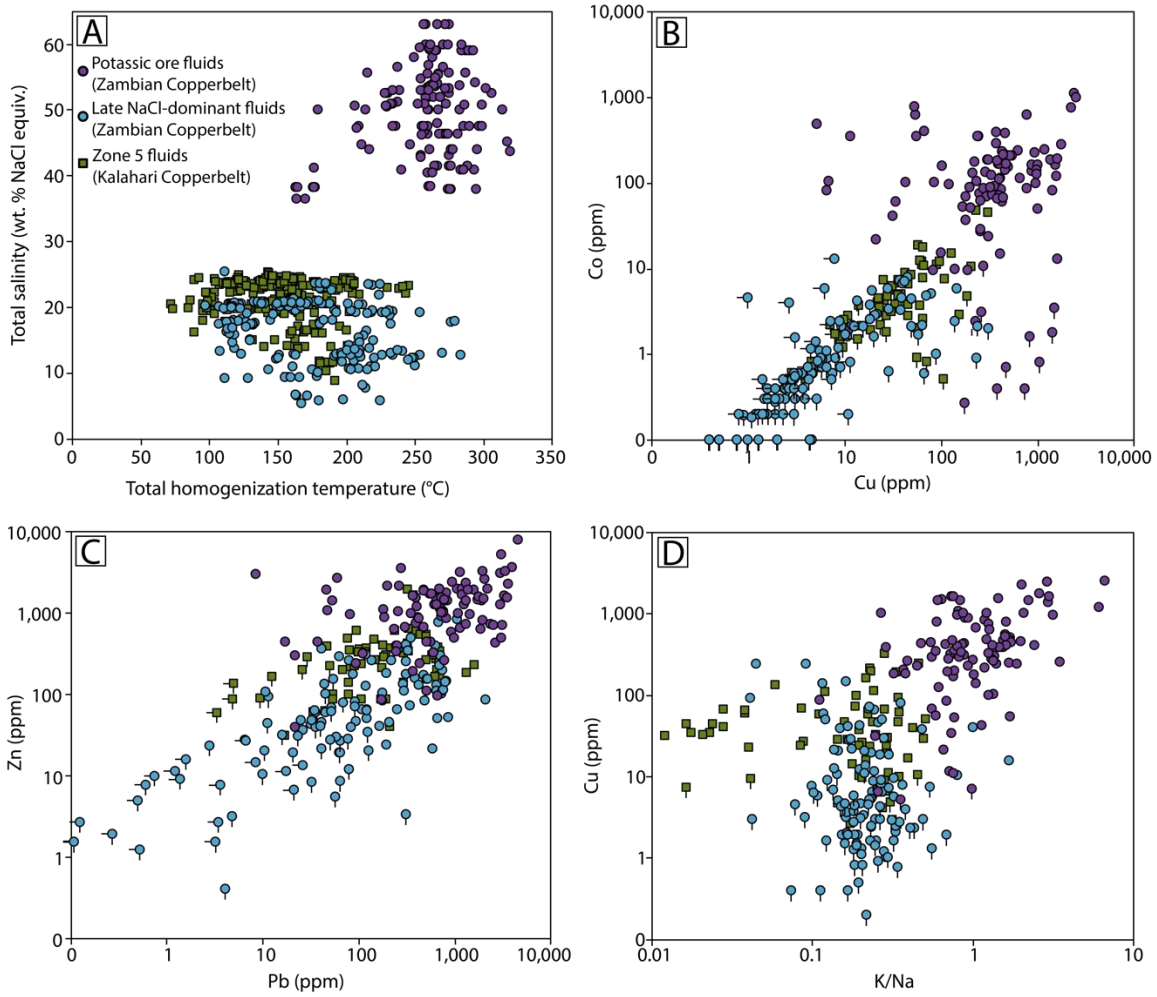

Fig. 5-14 Comparison of the microthermometric and major and trace element properties of Zambian Copperbelt metalliferous potassic bittern brines; Zambian Copperbelt post-kinematic NaCl-dominant fluids; and all measured fluids from the Kalahari Copperbelt Zone 5 prospect. Bars on symbols indicate that the plotted value is a maximum value for that element (limit of detection). A) Total salinity (wt % NaCl + KCl equiv) versus T_{hTOT}. B) Co versus Cu concentrations. C) Zn versus Pb concentrations. D) K/Na versus Cu concentration.

5.6 Summary

Investigation of the composition and base metal content of fluid inclusions in mineralised and barren veins from several prospects and deposits throughout the Pan-African collisional belt provides important insights into the evolution of hydrothermal fluids during basin development, from early extension, through basin closure, to peak orogenesis during the assembly of Gondwana at ca. 530 Ma. Inclusions trapped prior to peak orogenesis show distinct temperature, salinity, compositional and stable isotopic characteristics from those interpreted as post-kinematic. Early fluids are characterised by relatively high temperatures and total salinities, K/Na ratios ≥1 and one to two orders-of-magnitude higher Cu, Co, Pb and Zn concentrations than later fluids. Halogen systematics of analogous fluids from several Central African Copperbelt deposits indicate an advanced evaporitic origin, with bittern brine signatures. Elevated Ba concentrations together with an absence of barite imply early ore fluids were sulphate-deficient and encountered an independent source of reduced sulphur where significant mineralisation is developed. Interaction of metalliferous, potassic brines with host rocks is evidenced by pervasive potassic metasomatism associated with many Zambian orebodies, and intimate intergrowths of sulphides with secondary potassic phases. Fluids trapped during or after peak orogenesis in both the Lufilian and Damaran belts show contrasting compositional characteristics to the earlier Zambian brines. Late fluids are lower temperature-salinity NaCl-dominant brines with K/Na <1 and lack significant base metal enrichment. Halogen systematics of fluid inclusions from Lumwana, as well as demonstrably post-kinematic deposits in the Zambian Copperbelt indicate that late fluids underwent halite-dissolution and acquired distinctly higher Na/Br and Cl/Br ratios than earlier bittern brines (Heijlen et al., 2008; Nowecki, 2014; Selley et al., 2018).

These data are consistent with the trapping of two compositionally distinct brines, perhaps sourced during periods of contrasting global ocean chemistry (Fig. 5-15). Earlier potassic brines were likely expelled along basin margins and basement highs (± early inversion structures) following an extended residence period, with fluid-rock interaction during mineralisation evidenced by attendant potassic metasomatism. Later, NaCl-undersaturated brines were derived from $MgSO_4$-rich, $CaCl_2$-poor seas and expelled in large volumes during the closure of a series of basins along the Pan-African margin. The distinct chemistry of these lower temperature fluids implies minimal mixing with deeper bittern brines occurred in the Zambian basin prior to the removal of salt seals. Salt dissolution during basin inversion promoted the progressive penetration of late fluids into the Lower Roan stratigraphy, forming pervasive, structurally-controlled sodic (albite ± scapolite) alteration that overprints stratiform mineralised rocks and earlier potassic alteration assemblages. Where earlier potassic bittern brines were absent in the Ghanzi-Chobe belt, NaCl-undersaturated solutions formed the primary ore fluid, transporting relatively low base metal concentrations from

the Ngwako Pan red beds and Kgwebe Volcanics towards variably reduced, structurally-controlled traps within the lower D'kar Formation (Fig. 5-15). Ultimately, the extended residence of ultra-potassic bittern brines within a high temperature depocentre was crucial in transporting anomalously high concentrations of base metals in the Central African Copperbelt, relative to other Pan-African basins.

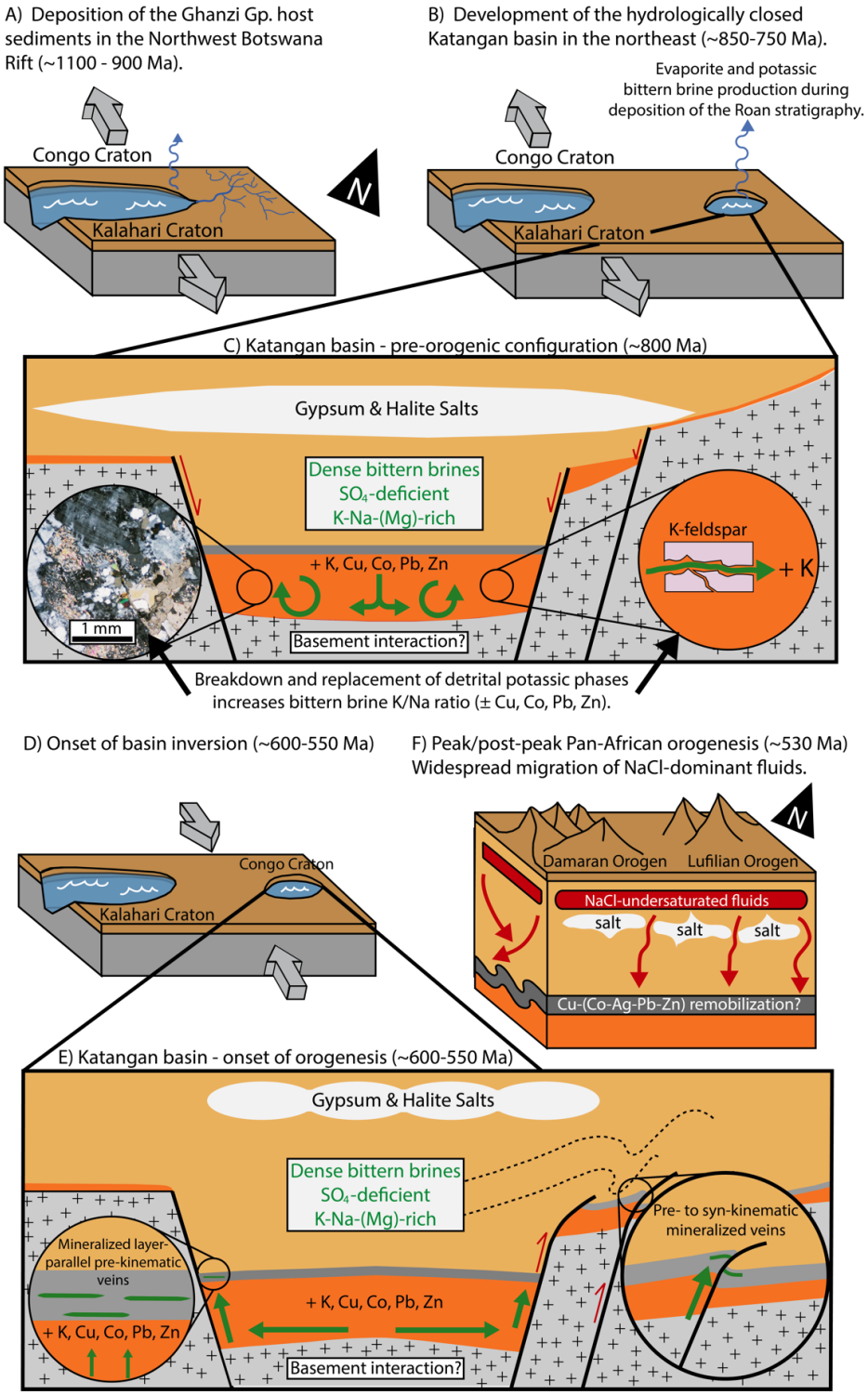

Fig. 5-15 Simplified schematic model illustrating brine generation and compositional evolution during the development of Neoproterozoic basins and their subsequent closure between the

Congo and Kalahari cratons during the Pan-African orogeny. A) Initial development of the late Mesoproterozoic to early Neoproterozoic Northwest Botswana rift, including deposition of the fluvial/alluvial Ngwako Pan red bed sequence and the overlying shallow marine D'Kar Group sediments. B) Development of the Katangan basin approximately 1000 km northeast of the Northwest Botswana Rift. Deposition of the Roan Group sediments in a periodically subaerial and highly evaporitic environment generated high salinity, high K/Na and low Cl/Br bittern brines in a hydrologically closed basinal setting. C) Simplified cross-section showing the pre-orogenic configuration of the Katangan basin, including the circulation of bittern brines. Inset (left) is a photomicrograph showing the breakdown of detrital potassic phases and replacement by sericite, dolomite and phlogopite, further increasing resident brine K/Na ratios. D) Convergent tectonics during the assembly of Gondwana invert Neoporterozoic basins, generating the Pan-African age Damaran and Lufilian collisional belts. Orogenesis peaked between ~540-530 Ma. E) During peak and post-peak orogenesis, the remaining evaporitic strata was chemically and mechanically disaggregated, with NaCl-undersaturated basinal brines acquiring moderate to high temperatures and salinities during progressive penetration into Pan-African depocentres and along the intercratonic margin. This likely represented the most voluminous fluid event recorded throughout the entire Pan-African belt, forming a variety of syn- to post-kinematic veins in the Zambian and Kalahari Copperbelts and widely remobilising pre-kinematic Cu-(Co-Ag-Pb-Zn) sulphides.

Chapter 6 Sediment-hosted Copper Mineralisation in the Munster Basin: Characterising ore fluid chemistry at the Allihies deposits

ABSTRACT

Multiple generations of barren and mineralised veins are present in clastic sequences of the Devonian Old Red Sandstone across the Munster Basin in southwest Ireland. Fluid inclusions hosted by temporally distinct barren and mineralised vein sets towards the basin depocentre at Allihies are analysed, alongside a comparable barren vein set from the northern margin of the basin, at Inch. Microthermometric and laser ablation ICP-MS analyses of inclusion fluids reveal that pre-peak orogenic barren fluids at Allihies represent medium temperature and salinity solutions (150-190°C and 13 wt % NaCl equiv.) and are compositionally comparable to those analysed in similar veins at Inch. In both cases, fluid cation concentrations reflect extensive interaction with clastic sequences in Devonian palaeoaquifers. Proposed ore fluids show distinctly higher homogenisation temperatures (~260°C), lower salinities (~9 wt % NaCl equiv.) and host slightly increased Cu concentrations. Cation concentrations and oxygen stable isotope signatures indicate that ore fluids did not undergo extensive interaction with clastic sequences and instead suggest a short-lived residence during ongoing Variscan metamorphism. Negative sulphide δ^{34}S signatures and the absence of *in situ* reduced sulphur sources at Allihies implies ore fluids remobilised limited concentrations of Cu and S together, likely from small-scale syngenetic mineralisation elsewhere in the basin. Although the fundamental components for sediment-hosted Cu mineralisation were present at Allihies, the timing and composition of ore fluids were not optimal for large-scale mobilisation and efficient precipitation of base metals in the Munster Basin.

6.1 Introduction

Copper mineralisation in the Devonian Munster Basin of southwest Ireland remains a little-studied component of the wider middle- to Upper Paleozoic basin margin terranes of central and southern Ireland. In contrast to many of the sediment-hosted Pb-Zn deposits of the Irish Midlands Basin, the sediment-hosted Cu mineralisation at Allihies in the Munster Basin represents a small-scale system, unlikely to be economically viable for commercial production in the 21st century. In a risk-averse exploration climate, where the largest 20% of global Cu deposits account for over 92% of the total Cu metal budget (Singer, 2017), it is critical to understand what geologic factors differentiate small-scale systems like Allihies, from the giant deposits in globally significant sediment-hosted copper provinces such as the Central African Copperbelt.

Here, a detailed fluid inclusion study of the vein-hosted copper mineralisation at Allihies, in the west of the Munster Basin, is presented. Fluid inclusion homogenisation temperatures, salinities and major and trace element chemistry are reported alongside insights from stable isotope systematics, in order to characterise the mineralising fluids and elucidate ore-forming processes in a small-scale, vein-dominated sediment-hosted Cu system. Fluids are compared to compositional data for fertile brines in several much larger Zambian Copperbelt systems in an attempt to assess the relative importance of key processes and geochemical variables in the formation of a world-class system. It is suggested that barren or low grade (± tonnage) systems such as Allihies represent far more typical basin margin hydrothermal systems, whereas the anomalously high grade/tonnage Zambian deposits are the product of a series of coinciding anomalous geological conditions and are a rarity through geologic time.

6.2 Geological Setting

The Munster Basin is dominated by Mid- to Late Devonian rocks, outcropping over an area of >12,500 km^2 (Williams et al., 1997). Following the Early- to Mid Devonian Acadian Orogeny, the Mid- to Late Devonian was a period of lithospheric stretching and basin formation across the south of Great Britain and Ireland (James and Graham, 1995). During this period of wider intra-continental basin development, the Munster Basin developed as a half graben structure in response to reactivation of Caledonian lineaments – notably the Killarney-Mallow Fault system to the north and the antithetic Bantry Fault to the south (Meere and Banks, 1997; Pracht, 2000). The basin was filled with continental clastic sediments, typically comprising fluvial and alluvial facies of the Old Red Sandstone Supergroup throughout the Late Devonian, followed by a major marine transgression in the early Carboniferous (MacCarthy, 1990, 2007). The abundance of distinct braided fluvial and alluvial sedimentary regimes in the Munster Basin during the Late Devonian produced highly variable lateral facies changes across the basin and as such, the reported stratigraphic succession in the Allihies area (Fig. 6-2) remains uncertain. A series of tholeiitic dolerite sills in the Valentia Harbour area towards the northwest of the basin show a mid-ocean ridge basalt (MORB) geochemical signature, indicating extension peaked during the Middle- to Late Devonian (Pracht, 2000).

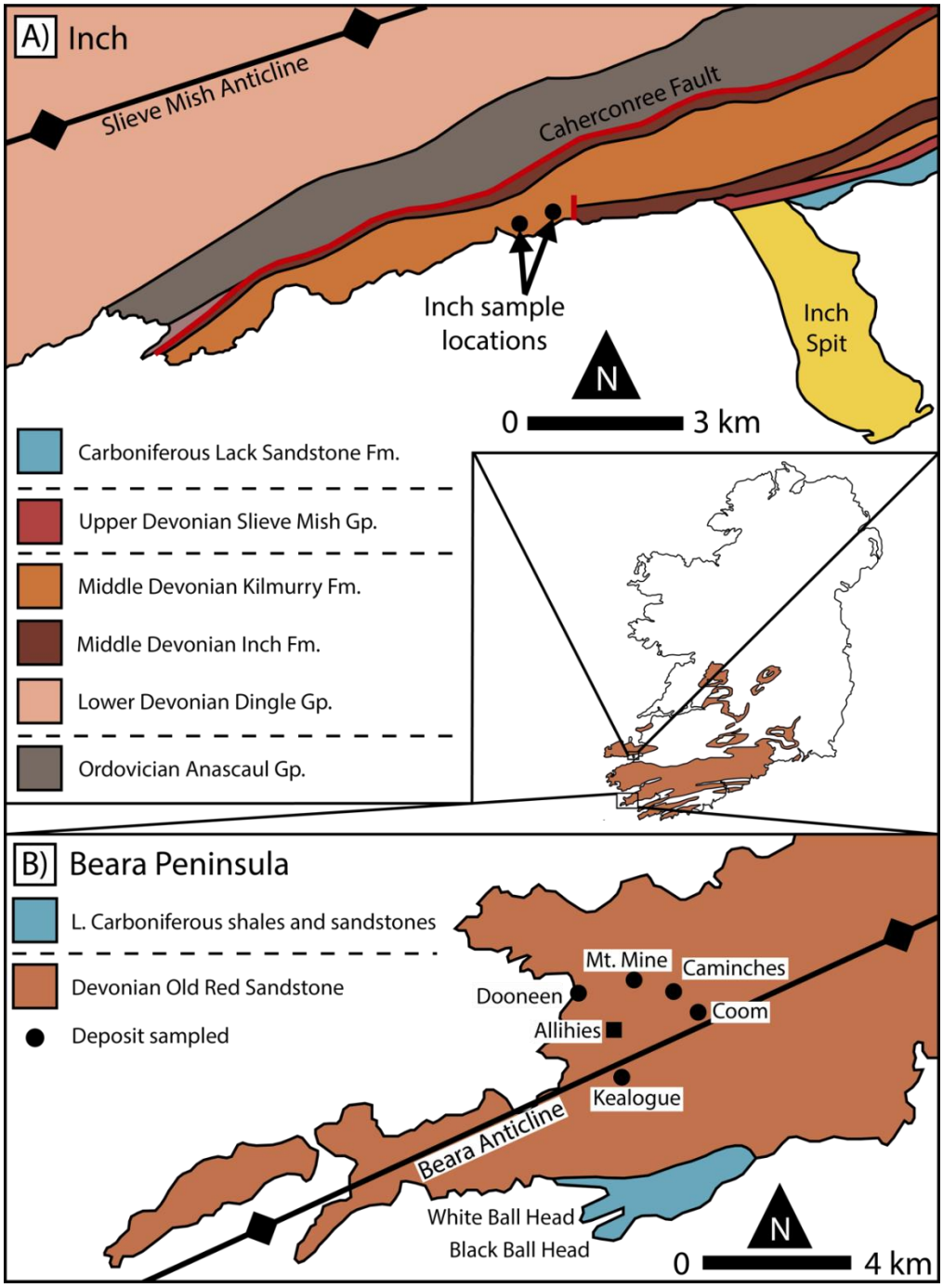

Fig. 6-1 Simplified geology maps of the Inch and Allihies sampling areas. The inset shows the locations of (A) and (B) in southwest Ireland. Modified after Graham (2009) and Pracht (2000).

Following a period of relative tectonic quiescence and widespread shallow marine sedimentation throughout much of the Carboniferous Period, inversion of the Munster Basin commenced in response to Variscan convergence during the late Carboniferous. The Variscan Orogeny resulted from the collision of Gondwana and Laurussia, forming the Pangaea supercontinent. The convergence event entrained several Gondwana-derived microcontinents including eastern Avalonia, which hosted the Munster Basin, largely along the Cornwall-Rhenish Terrane (Spinks et al., 2016).

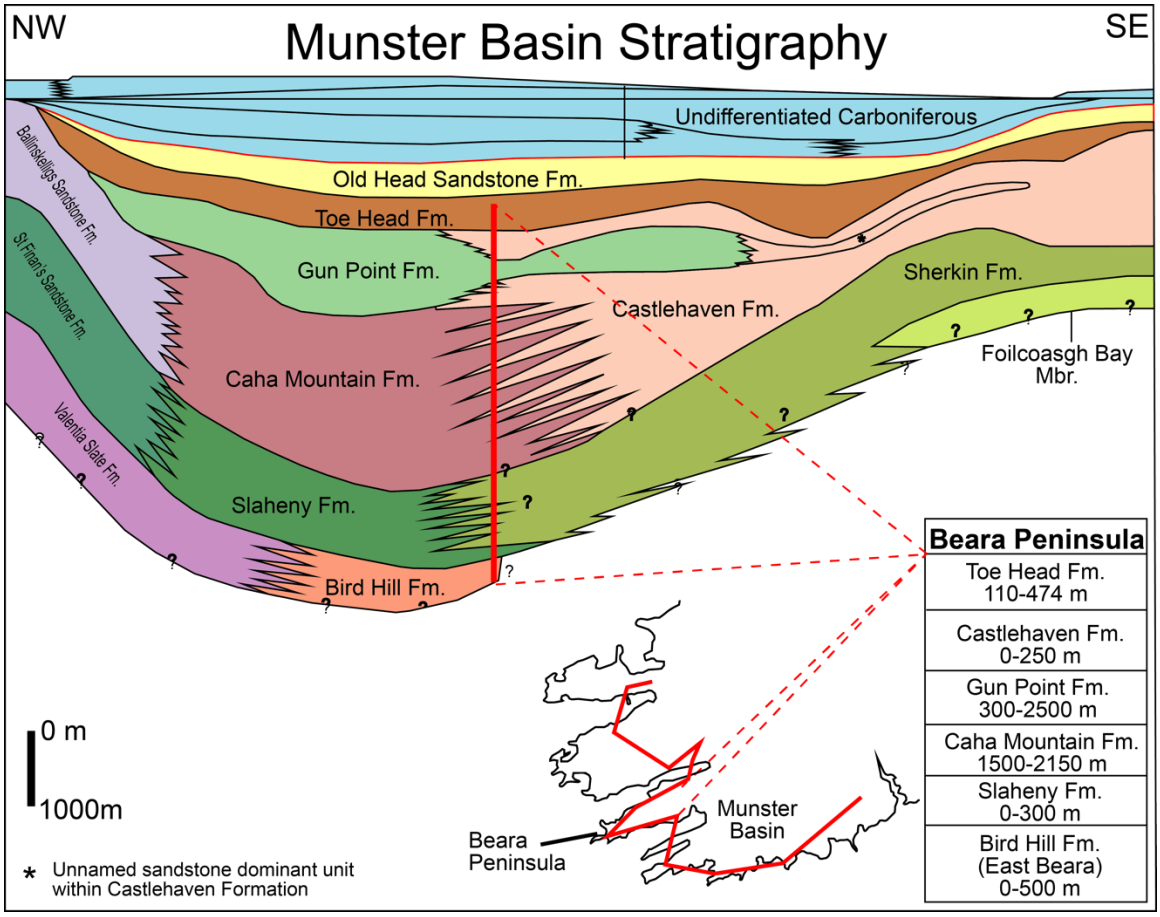

Fig. 6-2 Devonian and Carboniferous stratigraphy of the Munster Basin. The approximate line of section is marked on the map of south-west Ireland (inset), alongside estimated stratigraphic thicknesses in the Beara Peninsula area (approximate position along the line of section is marked by the vertical red line through the section). Veins sampled at Allihies in this study are hosted in the Caha Mountain Formation. Modified after MacCarthy (2007).

Variscan orogenesis resulted in significant N-S shortening across southern Ireland as far north as County Clare. South of the Killarney-Mallow Fault, Munster Basin sediments underwent layer-parallel shortening, cleavage development and buckling, along with reactivation of Caledonian faults and lineaments which resulted in 30% to 50% north-south shortening (Meere, 1995; Quin, 2008). The alternating deep bays and peninsulas of southwest Ireland represent macroscopic first-order Variscan folds, with axial traces striking ENE-WSW (Fig. 6-1) and amplitudes and wavelengths on the order of several kilometres (Todd, 2014). The first-order Beara Peninsula anticlinorium has an approximately ENE-WSW axial trace and plunges towards the southwest (James and Graham, 1995). Smaller, second-order folds commonly display decametre-scale amplitudes and wavelengths, whilst centimetre-scale parasitic folds are common across the Munster Basin (Graham, 2009). Folding is much less apparent north of the Killarney-Mallow Fault, with only first-order undulating kilometre-scale folds present. Within the Munster Basin, pelitic lithologies have

developed a slaty cleavage with steep, axial planar attitudes, whereas coarser siltstones and sandstones have developed more widely spaced cleavage sets which tend not to be axial planar. Much of the large-scale Variscan faulting took place along reactivated Caledonian age structures, with mineralised lodes often associated with high-angle east-west-trending structures displaying significant normal dip-slip displacements (up to 2500 m).

6.2.1 Allihies mineralisation

The Allihies copper deposit is located at the western tip of the Beara Peninsula in southwest Co. Cork (Fig. 6-1). The predominantly vein-hosted copper mineralisation was first worked in 1812, with small-scale mining operations active until the late 19th Century. Ore production totalled approximately 0.3 Mt (Williams, 1993), with later exploratory drilling delineating a further 2.35 Mt of ore at 2% Cu remaining in situ (McMahon, 1965).

Numerous vein sets have been identified at Allihies, representing a multistage process of hydrothermal fluid activity spanning pre- to post-orogenic times. Ubiquitous narrow barren veins have been recognised as pre-peak Variscan structures, whereas massive, gossanous, mineralised quartz lodes have typically been interpreted as post-kinematic (Sheridan, 1964). Radiometric dating (K-Ar) of clays ostensibly associated with mineralisation support this paragenesis, with barren 'regional' veins dated at 307-331 Ma and mineralised lodes at ca 290 Ma (Halliday and Mitchell, 1983). Whilst it remains uncertain whether these clays are temporally associated with primary mineralisation or whether they represent later Permian heating events, the relative age of the two vein sets is evident from field relations, with massive mineralised lodes generally cross-cutting Variscan structures and fabrics whilst the barren 'regional' veins occur as infill within joints and fractures. Veins at Allihies are hosted by two main units within the Caha Mountain Fm. – the Upper Allihies Sandstone and the Ballydonegan Slates. During Varsican deformation, competency contrasts between the two lithologies resulted in contrasting deformation styles, with argillaceous units of the Ballydonegan Slates undergoing ductile deformation and developing a strong cleavage, whereas more competent, blocky arenites of the Upper Allihies Sandstone show evidence of brittle deformation, particularly towards fold hinges. Some of the primary lodes at Mountain Mine occur along the contact between these two lithologies (trending approximately east-west), indicating the contact played a significant role in focussing local hydrothermal fluid flow during the Variscan orogeny.

Mineralisation typically occurs as a pyrite + chalcopyrite + bornite ± chalcocite ± secondary malachite assemblage in quartz lodes which have been worked extensively across the western tip of the Beara Peninsula. The main 'Mountain Mine' workings exploit a 1-2 m-wide lode trending east-west, to a depth of approximately 400-500 m below surface. Further significant lodes have

been worked at Coom, Caminches, Kealogue and most notably, at Dooneen, where an 8-10 m wide quartz vein propagates in an approximately east-west direction out to sea.

Previous efforts to characterise the ore fluids at Allihies have been limited in scope but do provide some microthermometric constraints on Variscan fluids from three vein samples which hosted two-phase liquid-vapour fluid inclusions with eutectic melting values indicative of a $CaCl_2$ composition (< -45°C) (Meere and Banks, 1997). Bulk fluid homogenisation temperatures (T_h) and salinities ranged from 150°C to 290°C and 4-14 wt % NaCl equiv. A fourth sample, interpreted to represent post-orogenic extensional fault fill, yielded T_h and salinity values ranging from 120°C to 155°C and 22-27 wt % NaCl equiv., respectively. Crush-leach analysis of the same samples indicated that all of the fluids shared a marine origin, with Br/Cl values close to the seawater evaporation trend. Cation ratios, which are more easily altered by fluid-rock interactions, show Na depletion relative to seawater, perhaps indicating albitisation of wallrocks. Fluids also showed enrichments in elements indicative of pervasive breakdown of primary K-feldspar, including K, Pb and Sr (Meere and Banks, 1997).

A more detailed fluid inclusion study of mineralised veins accompanying sediment-hosted disseminated sulphides at Dhurode, approximately 25 km south-east of Allihies and hosted within the Old Head Sandstone Fm., showed the presence of CO_2-bearing, low salinity (<4 wt% NaCl equiv.), high temperature (T_h = 283°C to 348°C) fluids (Wen et al., 1996). However the relationship between these mineralised rocks and the Cu-bearing lodes at Allihies remains unclear.

6.2.2 Inch

Inch is located in the south-east of the Dingle Peninsula, approximately 55 km north of Allihies, and 15 km north of the traditional Irish Variscan Front (Gill, 1962) (Fig. 6-1). The geology of the area is characterised by clastic sediments of the Middle Devonian Caherbla Group which comprises alluvial fan conglomerates of the Inch Fm., overlain by aeolian red beds of the Kilmurry Fm. Regular fracture sets host barren quartz veins in the Kilmurry sandstones, with fluids established as dense, marine-derived brines, likely trapped in clastic paleoaquifers during the early Carboniferous marine transgression which occurred across southwest Ireland and the Munster Basin (Meere and Banks, 1997). These fluids therefore provide a useful independent control, representing pre-orogenic, evaporated seawater brines which were sourced regionally across the Munster Basin, residing in Devonian clastic sequences prior to Variscan Orogenesis. In this study, fluids from Inch are compared to those in barren vein sets within sandstones of the Caha Mountain Fm. at Allihies, where rocks were subjected to more intense Variscan deformation (± metasomatism), in order to address the hypothesis that fluids associated with Cu mineralisation of east-west-trending lodes at

Allihies are physicochemically distinct from those hosted in earlier, regionally abundant barren vein sets.

6.3 Samples and Analytical Methods

A total of 20 samples were collected from veins associated with a series of abandoned mine workings in the Allihies area (Mountain Mine, Coom, Caminches, Dooneen and Kealogue). Of these, 12 samples represent Cu-mineralised lodes, typically trending approximately east-west (or their north-south intersections) and 8 samples represent narrower, barren, chloritic quartz veins which are common across the western tip of the Beara Peninsula. Three additional samples were taken from barren, regular joint-fill quartz veins in blocky sandstones of the Middle Devonian Kilmurry Fm. on the northern side of the R561 road cutting at Inch (Fig. 6-1). Further samples of host rock alteration haloes and millimetre-scale mineralised veinlets along the margins of mineralised lodes were also collected for petrographic study.

Microthermometric analysis was carried out on doubly polished fluid inclusion wafers (~200 µm thick) using a Linkam^{TM} THMS 600 heating-freezing stage. Stage calibration was carried out using in-house synthetic H_2O-CO_2 fluid inclusion standards, with a reproducibility of ±0.5°C (2σ) at low temperature and at +308°C using a sodium nitrate standard (reproducibility of better than ±2°C, 2σ). The freezing point depression and liquid-vapor homogenisation temperatures were measured in all inclusions, alongside the eutectic, clathrate and hydrate melting temperatures where observable. Sodium concentrations were estimated from final ice melting temperatures using the NaCl-H_2O system (Bodnar et al., 1985).

Fluid inclusion laser ablation analyses were carried out using an ESI New-Wave NWR 213 nm laser system equipped with beam homogenisation optics and a two-volume cell. Ablated material was transported by gas flows of 1.1 l/min Ar and 450 ml/min H and analysed using an Agilent 7700x ICP-MS. Calibration using an external standard was conducted at the beginning and end of each experiment using NIST 610 and 612 glass standard reference materials. Element ratios to the internal standard (Na) were determined following background correction of a time-resolved signal, with absolute concentrations determined using Na concentration estimates for individual inclusions. Time resolved ablation profiles were processed using the Exlam2000 software package (Zacharias and Wilkinson, 2007). A limit of detection (LOD) was calculated for each element in every inclusion using 3σ of the background signal variation (Longerich et al., 1996). Precision and accuracy are assessed using repeat measurements of the NIST 610 standard reference material, with all elements yielding %RSD values of <10%. Relative error (accuracy) is excellent for all elements (<5%). Full data are reported in Appendix C.4.

Oxygen stable isotope analyses were carried out on quartz separates picked from fluid inclusion wafers in order to best correlate results with fluid inclusion populations. Oxygen was liberated from the SiO_2 lattice through the laser fluorination process of Sharp (1990) and reacted with heated platinised graphite, producing CO_2 which was analysed by a VG SIRA 10 mass spectrometer. The standards employed were YP2 (16.4‰), GP147 (7.3‰), UWG2 (5.8‰) and JJB8 (30.3‰), which showed reproducibility of better than ±0.2‰ (2σ). Results are reported in standard notation ($\delta^{18}O$) as per mil (‰) deviations from Standard Mean Ocean Water (V-SMOW).

Approximately 1g of quartz separates were picked for hydrogen isotope analysis and dried at 140°C in a vacuum overnight before being heated at 700°C for sixty minutes to release inclusion fluids. Hydrogen gas was obtained from H_2O via reduction in a chromium furnace (Donnelly et al., 2001) and analysed by a VG-Micromass 602D mass spectrometer. The SUERC internal lab standard LT showed a reproducibility of ± 4‰ (2σ). Results are reported in standard notation (δD) as per mil deviations from V-SMOW.

Sulphur isotope analyses were carried out on sulphide separates using minor modification of the method of Robinson and Kusakabe (1975). Sulphur dioxide gas was analysed using a Thermo Fisher MAT 253 dual inlet mass spectrometer, and then $\delta^{66}SO_2$ converted to $\delta^{34}S$ by calibration with two international standards (NBS 123 and IAEA-S-3) as well as an in-house standard (CP1). Reproducibility was better than ±0.4‰ (2σ) and data is reported in standard notation ($\delta^{34}S$) as per mil deviations from the Vienna Canyon Diablo Troilite (V-CDT) standard.

6.4 Results

Three main vein generations were recognised across the western Beara Peninsula and are summarised in Table 6-1, with structural measurements presented in Fig. 6-3. The most ubiquitous veins are narrow (<5 cm) barren quartz structures, commonly displaying chloritic alteration along their margins. These veins, hereafter referred to as 'barren regional veins', are widespread and laterally continuous, often exploiting regular fractures and joints, forming conjugate sets within the arenaceous units of the Upper Allihies Sandstone (Fig. 6-4 A-B).

Table 6-1 Key characteristics of Allihies quartz veins

	Barren regional veins	**Massive E-W lodes**	**Cross-cutting N-S lodes**
Width:	<5 cm	0.5 – 2 m	0.5 – 2 m
Mineralisation:	Unmineralised	Visible cpy-py-bn-cc. Secondary malachite	Occasional cpy-py-bn
Alteration:	Fine chlorite within veins and country rock margins	Chlorite-muscovite	Chlorite-muscovite. Wallrock alteration along margins
Structural relationships:	Fills pre- to syn-orogenic joints and fractures	Obliquely cross-cuts Variscan fabric	Cross-cuts Variscan fabric. Intersects massive E-W lodes

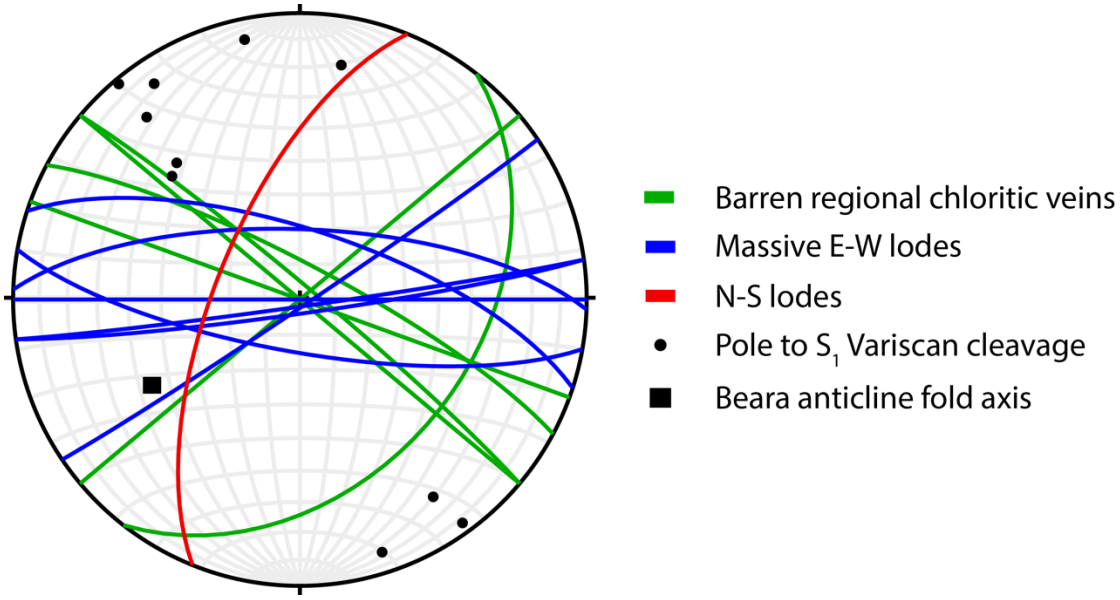

Fig. 6-3 Equal area stereonet showing orientations of the three vein sets sampled at Allihies, as well as the S_1 fabric and Beara Anticline fold axis in the Allihies area.

The second most abundant vein generation is characterised by wider east-west-trending massive quartz lodes, forming obliquely to the fold axis of the Beara Anticline. These veins frequently host visible chalcopyrite and bornite, with abundant secondary malachite (Fig. 6-4). Lodes can be up to 8-10 m wide at Dooneen, but are more typically 0.5-2 m wide, often displaying wallrock alteration/bleaching along both margins. Transmitted light petrography of millimetre-scale veinlets within the immediate wallrock alteration halo of these veins shows co-existing Cu-sulphide minerals and greenschist facies metamorphic assemblages (Fig. 6-5A). Similar veinlets also show evidence of sub-millimetre-scale deformation, with shear zones characterised by intergrowths of chlorite and muscovite (Fig. 6-5B). The least common type of veins observed at Allihies are sub-vertical north-south trending mineralised structures which typically intersect the main east-west-trending lodes and cross-cut the Variscan S_1 fabric. These veins share a similar mineralogy and gossanous appearance to the main lodes but occur along much shorter strike lengths. Only one of these veins was sampled in this study.

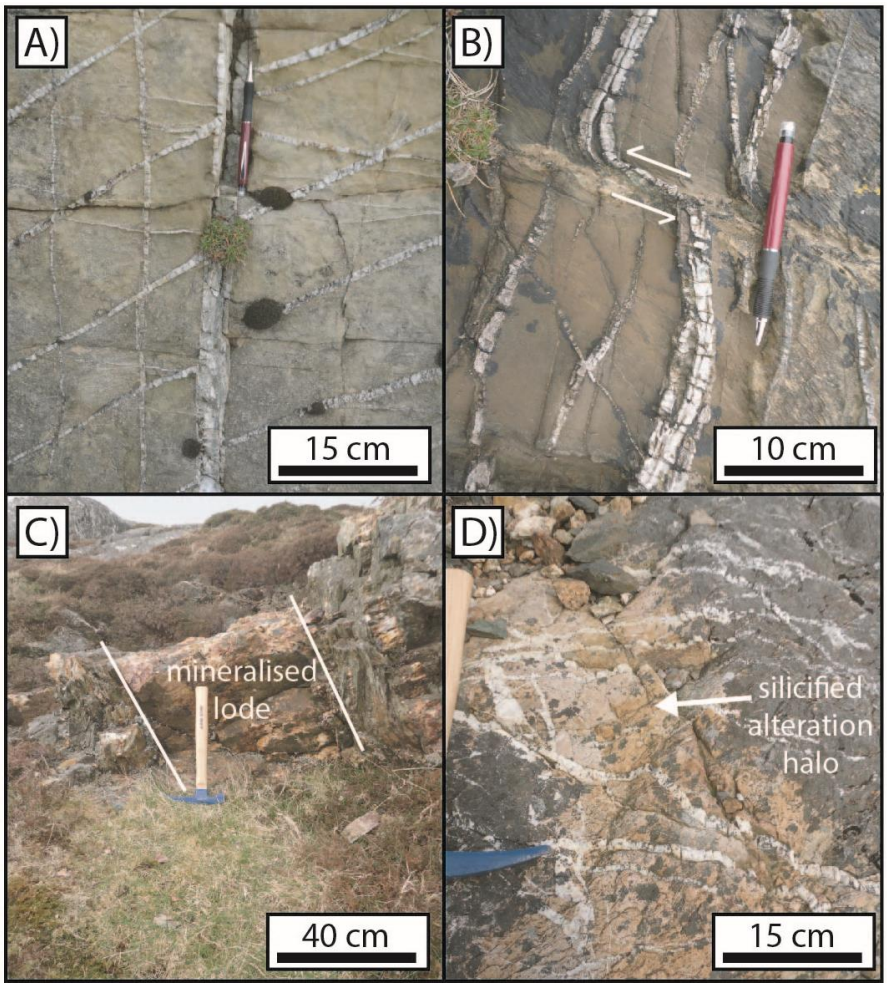

Fig. 6-4 Images of vein sets sampled at Allihies. A) Barren regional veins forming conjugate sets within chloritic arenite of the Upper Allihies Sandtones. B) Barren regional veins showing sinistral displacement along a small shear zone within the Upper Allihies Sandtones. C) East-west trending gossanous vein parallel to the primary lode worked at the Mountain Mine in Allihies. Vein hosts visible chalcopyrite, bornite and secondary malachite. D) Zone of bleaching and silicification of host argillites around a small stockwork of veins nearby an intersection between east-west and north-south trending mineralised veins.

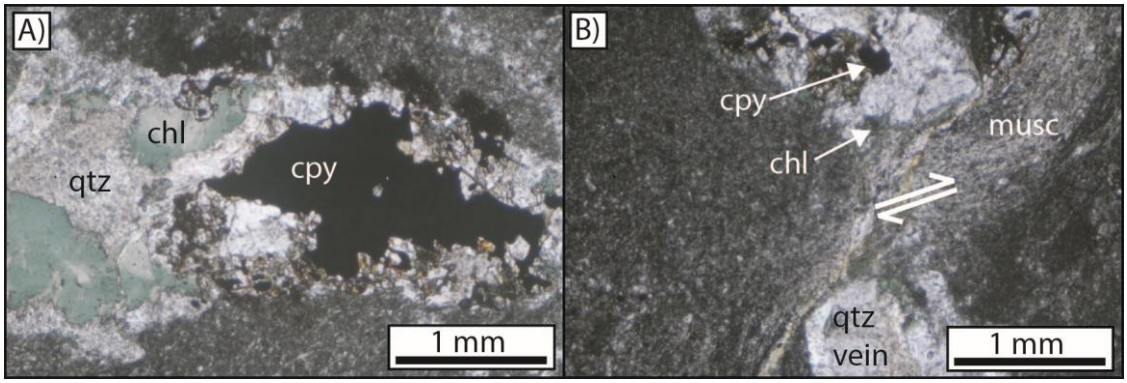

Fig. 6-5 Plane polarised photomicrographs of mineralised veinlets located along the margins of massive east-west trending lodes at the Allihies Mountain Mine. A) Displays close spatial relationship between quartz-hosted copper sulphides and chlorite. B) Small-scale dextral shearing of a mineralisaed veinlet. The shear zone predominantly consists of muscovite intergrown with fine grained chlorite.

6.4.1 Fluid inclusions

All 23 vein samples collected underwent petrographic inspection, with 15 samples hosting fluid inclusion populations considered suitable for further work. From this sample subset, a total of 268 fluid inclusions underwent microthermometric analysis (results summarised in Table 6-2) and 78 inclusions were successfully analysed for major and trace element concentrations by laser ablation ICP-MS. Inclusions from Allihies and Inch are aqueous two-phase (liquid-vapour), ranging in size from <1 to 22 µm and typically display a high degree of fill (F ≥0.9). Primary inclusions are larger and form the volumetrically dominant population in most samples, with less frequent secondary trails characterised by <2 µm inclusions.

Eutectic melting temperatures (T_e) for all inclusions hosted in veins from Allihies show a strong mode of -22°C (n = 73), indicating a near-pure H_2O-NaCl composition, whereas primary inclusions from Inch show a distinctly higher modal T_e value of -46°C (n = 17), indicating a greater $CaCl_2$ component (Fig. 6-6).

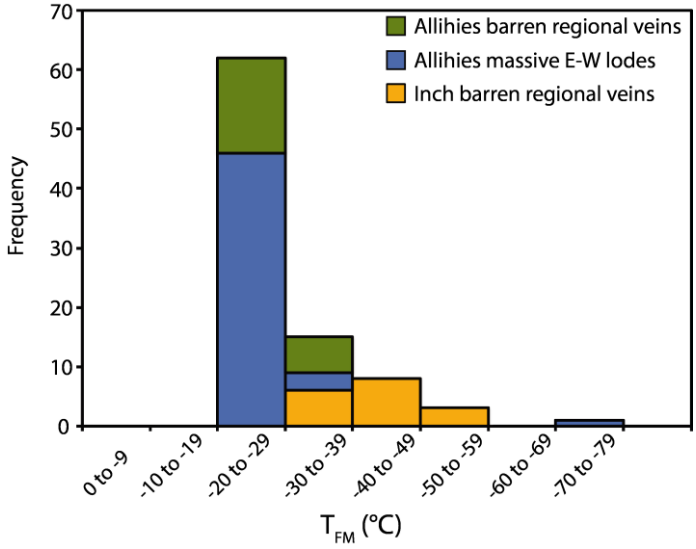

Fig. 6-6 Histogram of fluid inclusion eutectic melting temperatues categorised by vein sets at Allihies and Inch.

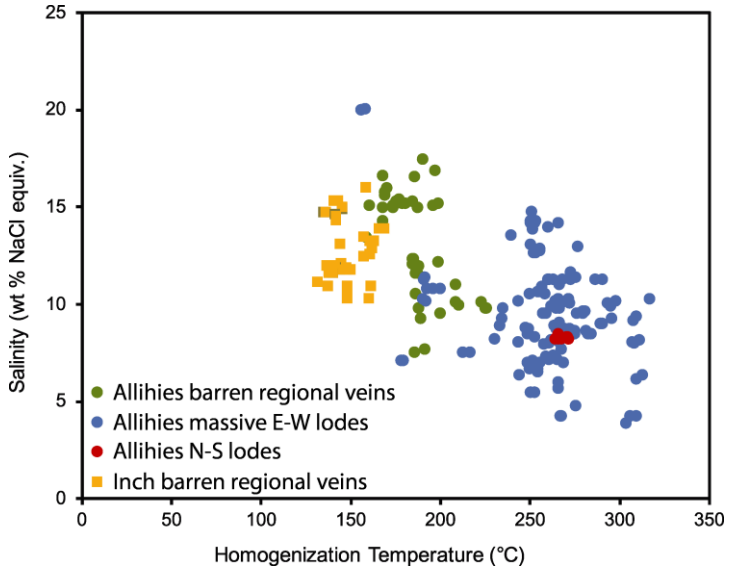

Fig. 6-7 Salinity versus bulk homogenisation temperature (T_h) of primary fluid inclusions observed in barren and mineralised veins from Allihies and Inch. Proposed ore fluids show distinctly higher T_h and moderately lower salinities than those measured in barren veins. Fluids from barren veins at both Inch and Allihies share similar salinities, with those recovered from closer to the basin depocentre (Allihies) displaying slightly higher homogenisation temperatures.

Salinities derived from final ice melting temperatures (T_{mICE}) show a distinction between inferred primary inclusions in barren regional veins which show a mean of 13.0 $\pm$ 2.8 wt % NaCl equiv. (1σ, n = 50) and those hosted in mineralised lodes with a mean of 9.4 $\pm$ 2.5 wt % NaCl equiv. (1σ, n = 162). Primary inclusions hosted in veins from Inch share similar salinities to barren regional veins from Allihies, with a mean value of 12.7 $\pm$ 1.5 wt % NaCl equiv. (1σ, n = 41). Temperatures of bulk

homogenisation to the liquid phase (T_h) more clearly record the distinction between fluid populations, with barren regional vein inclusions showing a mean T_h of 186 ± 16°C (1σ, n = 44) and those from mineralised lodes averaging 260 ± 33°C (1σ, n = 145). Homogenisation temperatures of fluid inclusions from Inch are comparable with those from barren regional veins at Allihies, with a mean T_h of 149 ± 10°C (1σ, n = 41). Together, fluid inclusion homogenisation temperatures and salinities provide a clear distinction between moderate homogenisation temperature and salinity brines hosted in regionally abundant, barren, chloritic veins and high homogenisation temperature, lower salinity fluids perhaps responsible for mineralisation at Allihies (Fig. 6-7).

Table 6-2 Summary of vein samples analysed, along with their stable isotope signatures and the microthermometric properties of volumetrically-dominant fluid populations

Location	Sample	Description	Mean T_h (°C)	Mean salinity*	$\delta^{18}O_{qtz}$	$\delta^{18}O_{fluid}$	$\delta^{18}O_{fluid}{}^{\Psi}$	δD
Inch Q 060510, 000285	ALH-JD-11	Barren vein in massive blocky sandstone	152	14	15.9	0.8	-	-26
Inch Q 059955, 000173	ALH-JD-12	Barren vein in massive blocky sandstone	147	10.9	15.8	0.2	-	-
Inch Q 059955, 000173	ALH-JD-13	Druzy vein quartz from massive blocky sandstone	144	11.9	16.5	0.6	-	-25
Allihies V 059093, 046013	ALH-JD-03	Barren, chloritic vein in folded massive sandstone	190	9.3	13.0	0.8	-	-
Allihies V 057674, 045985	ALH-JD-17	Barren, cross-cutting conjugate veins in Allihies Sst. Fm.	218	10	12.3	1.8	-	-
Allihies V 057734, 046256	ALH-JD-19	Barren vein along NE-SW-trending fold (Allihies Sst. Fm.)	178	15.4	12.8	-0.2	-	-21
Allihies V 057769, 046269	ALH-JD-20	Barren, chloritic vein in folded Allihies Sst. Fm.	172	15.6	10.8	-2.7	-	-19
Allihies V 058902, 046123	ALH-JD-04	1-2m wide massive E-W lode near Mt. Mine engine house	246	9.6	12.6	3.5	5.0	-
Allihies V 058884, 045842	ALH-JD-06	Massive E-W lode south of Mt. Mine engine house	267	9.8	13.4	5.3	6.6	-22
Allihies V 059772, 045490	ALH-JD-09	Massive weakly mineralised E-W vein (Coom)	304	6.6	13.8	7.1	8.2	-
Allihies V 057696, 045918	ALH-JD-14	Weakly mineralised vein quartz from main Dooneen lode	279	11.3	13.2	5.6	6.8	-
Allihies V 058938, 045830	ALH-JD-01	Discrete N-S lode intersecting mineralised E-W vein (Mt. Mine)	245	8.3	13.0	3.9	5.4	-
Allihies V 059495, 045582	ALH-JD-07	Mineralised vein quartz (py, cpy, bn and malachite) (Caminches)	266	9	13.6	5.4	6.8	-
Allihies V 059765, 045542	ALH-JD-08	Mineralised vein quartz (py, cpy, bn and malachite) (Coom)	238	6.8	13.0	3.5	5.1	-30
Allihies V 057696, 045918	ALH-JD-16	Mineralised vein quartz (py, cpy, bn) (Dooneen)	249	9.6	12.7	3.8	5.3	-25

*Salinity derived from the freezing point depression of ice and is reported in wt. % NaCl equiv.

$^{\Psi}$Calculated based on the pressure-corrected average T_h for fluid inclusions in each mineralised vein sample.

Laser ablation ICP-MS analysis of individual, texturally constrained fluid inclusions indicates that Na (± Ca) is the dominant cation in most fluids from both Allihies and Inch. Inclusions from mineralised lodes at Allihies returned values below their respective LOD for the majority of cations due to the dominance of small, low salinity inclusions (often <6 μm). Inclusion fluids from barren regional veins

at Allihies and Inch show consistently elevated Ca concentrations (mean = 1.2 wt % Ca, n = 32) compared to those in mineralised lodes where all Ca measurements fell below the LOD. Fluids hosted in barren quartz veins also show consistently elevated concentrations of cations susceptible to mobilisation through fluid-rock interactions such as Sr, Ba and Pb (Table 6-3). The concentrations of different base metals are not uniformly distributed within fluid populations. For example, high temperature, low salinity solutions in mineralised lodes typically show relative Cu (± Fe) enrichment, whereas lower temperature, moderate salinity brines hosted in barren, regional quartz veins display distinct enrichments in Pb (Fig. 6-8). Only three out of a total of 23 'ore fluid' analyses returned Mn concentrations above their respective LOD values, averaging 40 ppm, whereas higher salinity, regionally extensive, barren fluids averaged 126 ppm Mn.

Table 6-3 Average concentrations (ppm) of selected cations in fluid inclusions from Allihies and Inch

	Total n	Na*	Mg	K	Ca	Mn	Fe	Cu	Zn	As	Sr	Ba	Pb
Barren regional veins	33	46,880	170	2,340	7,726	120	140	10	76	220	462	43	190
		(33)	(31)	(31)	(21)	(30)	(2)	(9)	(11)	(27)	(33)	(30)	(33)
Inch regional veins	22	52,140	120	5,280	19,793	140	-	13	120	920	1126	180	220
		(22)	(15)	(21)	(11)	(11)	(0)	(2)	(7)	(22)	(22)	(21)	(21)
Massive E-W lodes	18	36,800	120	1,560	-	40	1470	26	99	1340	184	25	57
		(18)	(9)	(9)	(0)	(3)	(2)	(5)	(2)	(17)	(18)	(9)	(17)
N-S lodes	5	32,340	110	650	-	-	-	20	-	370	144	14	39
		(5)	(2)	(4)	(0)	(0)	(0)	(2)	(0)	(5)	(5)	(4)	(5)

*Estimated from T_{mICE} measurements

** Values in brackets represent the number of inclusions with concentrations above the LOD for the given element which were used to calculate averages

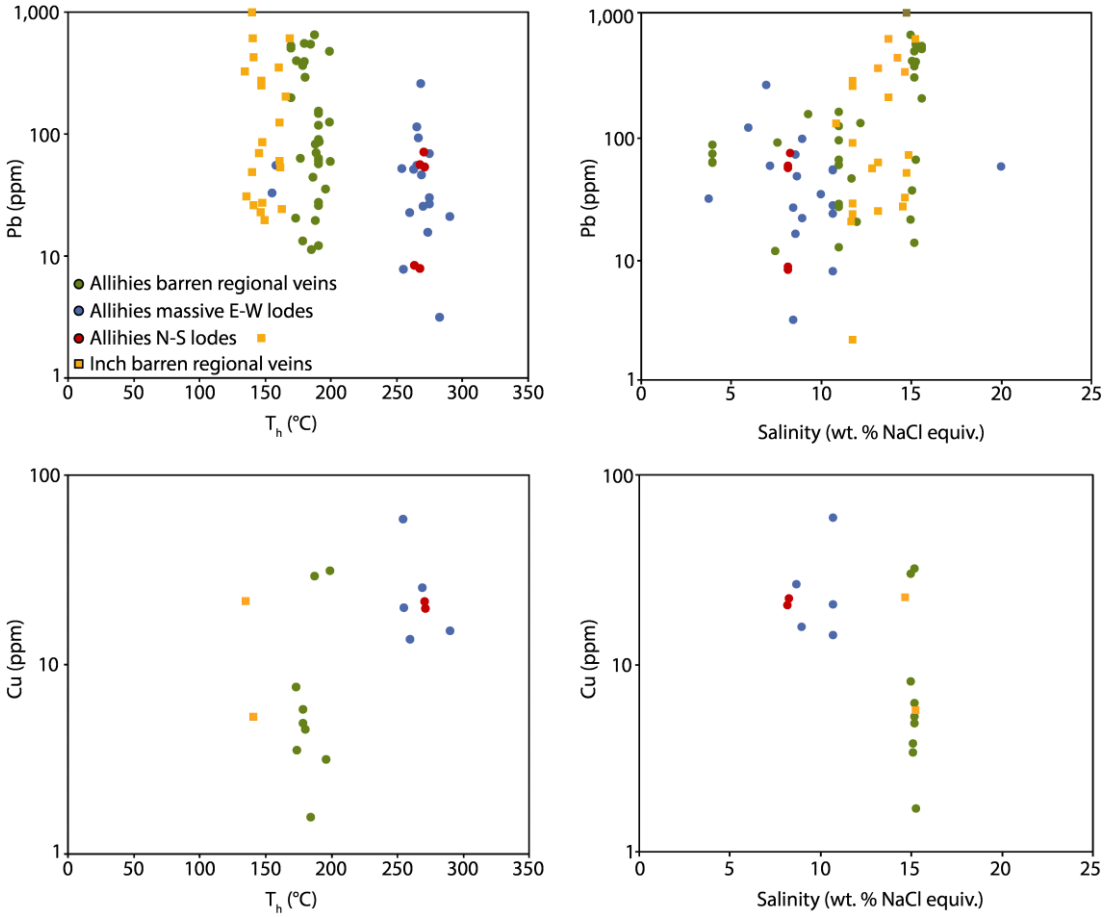

Fig. 6-8 Concentrations of Pb and Cu versus T_h and total salinity for individual fluid inclusions from Allihies and Inch veins. Due to small inclusion sizes and low salinities, LODs often show a large range within fluid inclusion assemblages and their inclusion in calculated averages significantly skews the relatively small number of data points above their respective LOD. As such, only concentrations above the respective limit of detection (LOD) for each element in a given inclusion are plotted. Where measured, Pb and Cu show an antithetic relationship, with Pb concentrations seemingly a function of salinity and not T_h, whereas Cu shows a potential relationship with T_h but not with fluid salinity.

6.4.2 Stable isotopes

Veins from Allihies show consistent $\delta^{18}O$ isotope signatures which are distinctly lower than those for barren veins from Inch (Fig. 6-9 A). Quartz from barren regional veins at Allihies have $\delta^{18}O$ values of 10.8 to 13.0‰, with mineralised lodes showing a similar range, from 12.6 to 13.8‰. Vein quartz from Inch yields $\delta^{18}O$ values ranging from 15.8 to 16.5‰. Although quartz $\delta^{18}O$ values are consistent between vein sets at Allihies, these signatures are a function of the vein formation temperature as well as its inherent isotopic ratio; as such, the minimum $\delta^{18}O$ signature of a fluid in equilibrium with quartz in each sample has been estimated using the average fluid inclusion

homogenisation temperature and quartz $\delta^{18}O$ value from each vein, alongside the fractionation factor of Matsuhisa et al. (1979). Minimum $\delta^{18}O_{fluid}$ values clearly differentiate barren, regional chloritic veins at both Allihies and Inch (averaging -0.1 and 0.5‰, respectively), from mineralised veins at Allihies, with a mean $\delta^{18}O_{fluid}$ of 4.8‰ (Fig. 6-9 B).

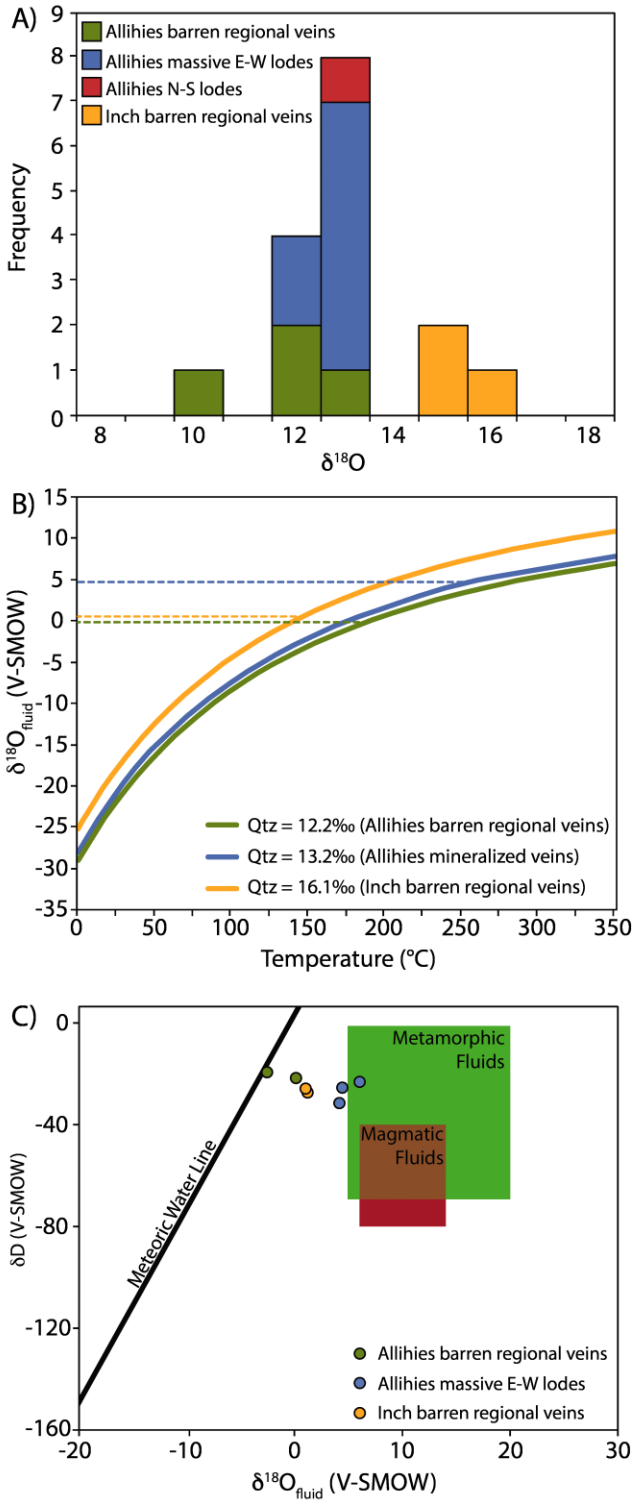

Fig. 6-9 Oxygen and hydrogen isotope data for quartz vein material from Allihies and Inch. A) Quartz $\delta^{18}O$ values categorised by vein set. B) Calculated curves based on the average quartz $\delta^{18}O$ signature for each vein set and the fractionation factor of Matsuhisa et al. (1979). The

average T_h of primary fluid inclusions in each vein set is used to estimate the average $\delta^{18}O_{fluid}$ of corresponding fluid populations (marked by dashed lines). C) Fluid δD versus calculated minimum $\delta^{18}O_{fluid}$ for seven samples covering the three major vein sets from Allihies and Inch. Pre-peak orogenic barren regional fluids display isotopic signatures close to the meteoric water line whereas the proposed ore fluids show more evidence for isotopic equilibration with metamorphic host rocks.

Hydrogen isotopic signatures (δD) for inclusion fluids from seven vein samples range from -19 to -30‰. Sulphur isotope signatures of ore-stage pyrite, often intergrown with Cu sulphides, from five mineralised veins across four mine sites at Allihies show a narrow range of -12.4 to -17.7‰, with a mean $\delta^{34}S$ value of -14.1‰ (Fig. 6-10).

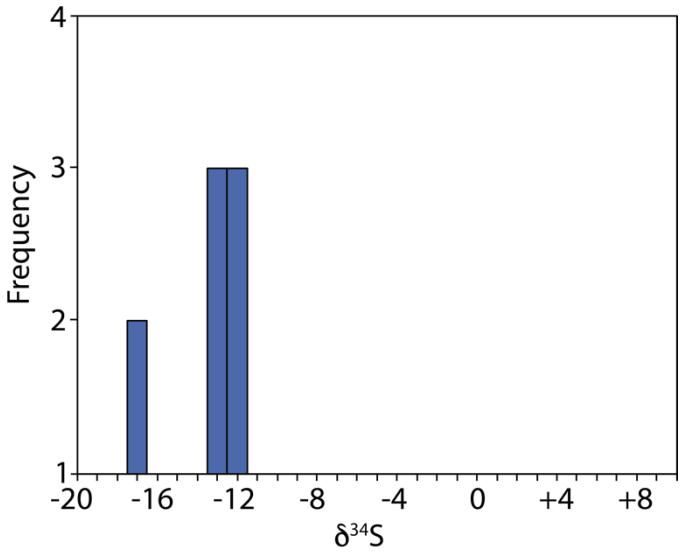

Fig. 6-10 Ore-stage pyrite $\delta^{34}S$ signatures from mineralised veins at the Dooneen, Caminches, Coom and Kealogue mine sites near Allihies.

6.5 Discussion

6.5.1 Barren vein sets

Regional, barren, chloritic vein sets at Allihies host geochemically and isotopically distinct fluids from those in co-existing mineralised veins but share many similarities with palaeofluids hosted in barren veins within Devonian red beds at Inch, on the northern margin of the Munster Basin. Barren quartz veins at Allihies fill joints and fractures that predate or are directly associated with Variscan deformation (Meere and Banks, 1997) and frequently display chloritic overprints, indicating emplacement prior to peak metamorphic conditions. Moderate fluid inclusion homogenisation temperatures support a pre-peak metamorphic entrapment model, with a likely maximum

overburden thickness of c. 6.7 km in the Munster Basin depocentre prior to basin inversion (Coe and Selwood, 1963; Sheridan, 1964). Veins hosted within Devonian red beds of the northern marginal horst block at Inch record lower fluid inclusion homogenisation temperatures, reflecting a reduced overburden thickness, thought to be in the region of 5 to 5.5 km (Clayton et al., 1989; Hudson et al., 1966). Leachate analysis of the same vein sets from Allihies and Inch indicate an evaporated seawater fluid source, with Br/Cl ratios lying close to the seawater evaporation trend (Meere and Banks, 1997).

Salinities of pre-peak metamorphic fluids are consistent between Allihies and Inch, with major and trace element data indicating enrichments in various cations relative to evaporated seawater. Elevated concentrations of K, Pb, Sr and Ba (Table 6-3) indicate pervasive breakdown of K-feldspars – a common constituent mineral in pre-diagenetic terrestrial clastic sequences. Notably, copper concentrations in these fluids are low (typically <15 ppm, where measured above the LOD). Given the suitability of medium temperature-salinity fluids for Cu transport (Brown, 2017; Brugger et al., 2016), this implies that voluminous, widespread pre-orogenic seawater evaporation brines did not sufficiently interact with cupriferous source rocks to mobilise appreciable quantities of copper towards structural or chemical trapping sites. The apparent non-involvement of these brines in Cu mobilisation in the Munster Basin, yet close spatial relationship of their host veins with mineralised lodes at Allihies serves to further evidence the temporal distinction between these regionally ubiquitous brines and later fertile ore fluids. Oxygen isotopic signatures estimated for fluids in equilibrium with quartz in barren veins from both Allihies and Inch are consistently below that of fluids in equilibrium with metamorphic host rocks (Fig. 6-9 B), lending further support to our interpretation of pre-peak metamorphic barren vein emplacement across much of the Munster Basin.

Fluid inclusion salinities and major and trace element chemistry indicate that regionally ubiquitous brines which formed fracture-controlled vein systems within Devonian red beds were broadly homogenous throughout the Munster Basin prior to peak Variscan metamorphism. The brines shared an evaporated seawater origin and were likely tapped during the early Carboniferous marine incursion across south-west Ireland (Meere and Banks, 1997). These data suggest that fluids underwent a moderate degree of interaction with clastic sedimentary rocks within Devonian palaeoaquifers and acquired higher temperatures within the basin depocentre than along basin margin highs. Veins were emplaced along structurally-controlled domains prior to peak orogenesis and, south of the main Variscan front, were subject to chloritic overprints during greenschist facies Variscan metamorphism.

6.5.2 Mineralised vein sets

Primary fluid inclusions spatially associated with Cu sulphides in mineralised veins at Allihies are lower salinity, but significantly higher homogenisation temperature solutions than those measured in earlier barren veins. Oblique cross-cutting relations between massive east-west lodes and the S_1 cleavage indicate veins were emplaced during or after Variscan fabric development, with intersecting north-south-trending lodes later still. Chlorite intergrown with primary vein quartz and associated with sulphides, as well as small-scale deformation of veins, indicate ongoing greenschist facies metamorphism during vein crystallisation.

Independent estimates of peak *P-T* conditions in the Munster Basin during Variscan inversion made using illite crystallinity, chlorite geothermometry and conodont alteration indices indicate maximum temperatures of ~275 to 400°C (Jones, 1992; Meere, 1995). Average fluid inclusion homogenisation temperatures of 260°C from mineralised veins represent a minimum estimate, with the true fluid trapping temperature being dependent on its pressure at the time of entrapment. A maximum overburden thickness of ~6.7 km has been estimated in the Allihies area (Coe and Selwood, 1963; Sheridan, 1964), giving maximum fluid pressures of ~67 MPa, assuming fluids were trapped in a dominantly hydrostatic regime (Meere and Banks, 1997). Given a fluid homogenisation pressure of ~4.4 MPa for a 10 wt % NaCl fluid homogenising at ~260°C (Haas, 1976) and an isochoric dP/dT for similar fluids of ~1.8 MPa $°C^{-1}$, a maximum pressure correction of +34.7°C is estimated. Application of this correction to ore fluids at Allihies gives an average estimated fluid trapping temperature of ~295°C, consistent with late orogenic *P-T* profiles for mineralised vein emplacement.

With a few notable exceptions (Cu, Fe, As), major and trace cation concentrations are lower in fluids associated with Cu sulphides than those in earlier barren vein sets (Table 6-3). Lower concentrations of K, Ca, Pb, Ba, Sr reflect lower total salinities but also indicate reduced breakdown of primary detrital mineral phases through fluid-rock interaction. This is likely the result of shorter fluid residence times and/or interaction with recrystallised rocks with significantly reduced intrinsic permeability compared to pre-diagenetic sediments. The average estimated minimum $\delta^{18}O_{fluid}$ signature for fluids in equilibrium with the mineralised quartz veins presented in Fig. 6-9, at an average pressure-corrected temperature of 295°C, is 6.1‰ (see Table 6-2). This value indicates that ore fluids at Allihies underwent a significant degree of interaction with metamorphic host rocks during or after Variscan metamorphism.

6.5.3 Sources of copper and sulphur

Through extensive fluid-rock interaction, ore-forming fluids associated with mineralised rocks in some of the world's largest sediment-hosted copper deposits have been shown in this study to host anomalously elevated Cu concentrations. Fluids associated with sulphide mineralisation at Allihies are significantly lower salinity solutions and are shown here to host concomitantly low Cu concentrations, with many inclusions from all veins at Allihies returning values below their respective LOD for Cu. Where Cu has been quantified, concentrations are slightly higher than those in regionally extensive, barren veins across the Munster Basin (Table 6-3). A comparison of Cu and Pb concentrations versus fluid inclusion salinity and bulk homogenisation temperature indicates that in contrast to Pb, copper concentrations are not a function of salinity but instead co-vary with fluid temperature. In other systems, fluid inclusion Cu concentrations show a strong correlation with salinity, directly reflecting the complexing capabilities of chloride-rich brines (e.g. Yardley, 2005). Here, elevated Pb concentrations in barren, regional fluids are interpreted to reflect high degrees of interaction with host sediments; as such, low Cu concentrations in these solutions suggests relatively low quantities of copper were 'available' to medium temperature-salinity solutions in Devonian Old Red Sandstone palaeoaquifers. Modest Cu enrichment of relatively small volumes of localised hydrothermal fluids at Allihies, along with elevated fluid temperatures, an absence of sediment-hosted disseminated mineralisation and $^{18}O_{fluid}$ signatures indicative of interaction with metamorphic rocks all indicate a more spatially constrained, singular source of copper, rather than pervasive leaching of metals from recrystallised Devonian clastic sequences.

In the West Carbery district, approximately 25 km south-east of Allihies, cupriferous veins locally accompany more pervasive disseminated sulphides within the Castlehaven Fm. of the Devonian Old Red Sandstone. Here, Wen et al. (1996) showed that fluids associated with vein-hosted Cu sulphides had a metamorphic origin, and locally remobilised Cu ($\pm$ S) from syngenetic disseminated mineralisation during vein emplacement in late orogenic times. Such examples of localised diagenetic mineralisation provide viable sources of Cu for high temperature fluids migrating in a predominantly fracture-controlled flow regime during the latter stages of Variscan orogenesis.

Ore sulphide assemblages at both Allihies and the West Carbery deposits show consistently negative $\delta^{34}S$ signatures (Wen et al., 1996), indicating bacterial reduction of sulphate, likely during diagenesis, played a key role in the supply of reduced sulphur for mineralisation. Effective transport of Cu requires an oxidised, sulphur-deficient hydrothermal fluid, thereby precluding the formation of a high tonnage deposit through large-scale mobilisation of reduced sulphur and ore metals together in a single fluid. Without an apparent *in situ* source of reduced sulphur at Allihies, Cu sulphide mineralisation was likely dependent on either fluid mixing with a distinct, reduced fluid,

the presence of which has not been evidenced in this study, or small-scale remobilisation of S and Cu by oxidised, high temperature fluids. Argillaceous units within the Caha Mountain Fm. form localised redox traps, likely capable of reducing such ore fluids. However, the inability of relatively low salinity fluids to co-transport large quantities of Cu and S, combined with a relatively inefficient, laterally discontinuous reductant at Allihies ultimately resulted in a low tonnage deposit.

6.6 A Comparative Approach to System Fertility

Allihies represents a relatively small sediment-hosted Cu deposit when compared with some of the giant systems of the Central African Copperbelt which often individually host >10 Mt contained Cu. Such systems result from the temporal and spatial alignment of various key elements, the variability of which are discussed here.

6.6.1 Brine generation

Unlike Allihies ore fluids, the brines responsible for the majority of vein-hosted mineralisation in many Zambian Copperbelt deposits were hypersaline bittern fluids with complex salt chemistries developed through advanced evaporation in a restricted marine environment (Nowecki, 2014; Selley et al., 2018). Bittern brine salinities in excess of 30 wt % NaCl equiv. promoted the formation of metal chloride complexes for more effective Cu transportation, as evidenced by their anomalous enrichments in Cu, Co, Pb and Zn. Ore fluid homogenisation temperatures at the Nkana-Mindola deposit in Zambia average 280-290°C – a similar order of magnitude to ore fluids at Allihies, however significantly reduced salinities in Allihies ore fluids played a substantial role in correspondingly low base metal concentrations.

6.6.2 Metal sources and fluid-rock interaction

High temperature-salinity brines in the Zambian Copperbelt were highly efficient solvents with extremely long residence times in the basal clastic sequences of the Katangan Basin prior to basin inversion. Burial of bittern brines in palaeoaquifers early in basin history likely maintained the intrinsic permeability of clastic sequences, allowing long-term hydrothermal fluid regimes to be sustained. In basins where fluids with appropriate physicochemical conditions for Cu mobilisation do not circulate until peak or post-peak metamorphic conditions are reached, clastic sequences have largely been recrystallised and permeability is dominated by brittle deformation structures, significantly reducing the intrinsic permeability and therefore availability of Cu in source regions. Although pre-peak orogenic, regionally extensive fluids in the Munster Basin were likely capable of transporting moderate concentrations of Cu - and modified cation signatures indicate they did

undergo a significant degree of fluid-rock interaction (Fig. 6-8), they clearly did not leach appreciable quantities of Cu from a fertile source region.

6.6.3 Mineralisation

In addition to possessing favourable temperature-salinity characteristics, in order to transport appreciable quantities of Cu, an oxidised, sulphur-deficient solution is favourable. Fertile pre- to syn-kinematic Zambian Copperbelt fluids were sulphate-deficient and therefore highly effective base metal transport agents, typically hosting 10^2 to 10^3 ppm Cu. Most mineralised rocks in the Zambian Copperbelt are associated with the laterally extensive Copperbelt Orebody Member, a pyritic black shale unit (Selley et al., 2005); or, where Cu sulphides are hosted in other clastic sequences, there is evidence for the presence of reducing hydrocarbon accumulations in structural trap sites (McGowan et al., 2006). At Allihies, reducing argillaceous units are discontinuous and show no evidence of providing a source of *in situ* reduced sulphur (e.g. diagenetic pyrite). Delivery of copper and sulphate to relatively weak redox traps along fracture-controlled permeability pathways is not favourable for large-scale ore formation. Ore tonnages were perhaps further limited by a small source region, with evidence suggesting Cu and S were remobilised from an area of existing mineralisation as opposed to large volumes of fertile clastic sequences.

6.7 Summary

Multiple vein sets at Allihies and Inch record an extended history of hydrothermal fluid activity in the Munster Basin, from moderate temperature-salinity evaporated seawater-derived brines residing in Devonian Old Red Sandstone aquifers prior to basin inversion, to higher temperature, lower salinity ore fluids emplaced during late orogenic times. Major and trace element analysis of palaeofluids indicates that pre-peak orogenic fluids present in veins at both Allihies and Inch did not carry appreciable quantities of Cu, with cation concentrations reflecting the breakdown and dissolution of detrital feldspars. Later fluids associated with Cu sulphides in the main lodes at Allihies host marginally higher Cu concentrations but show less evidence for extensive interaction with clastic sequences. Oxygen stable isotope signatures support a model whereby barren fluids were emplaced prior to peak Variscan metamorphism whereas later ore-forming solutions comprised a metamorphic fluid component. A lack of apparent *in situ* reduced sulphur sources at Allihies implies that ore fluids likely remobilised limited concentrations of Cu and S together from small-scale sediment-hosted mineralisation elsewhere in the basin.

A comparison of ore fluids from Allihies and the Zambian Copperbelt highlights several physicochemical properties which reflect fundamentally contrasting fluid histories, from source to vein emplacement, resulting in considerably different scales of metal endowment in the respective

regions. Fertile ore fluids in the Zambian basin acquired significantly higher salinities at source, and underwent far greater degrees of interaction with permeable, cupriferous clastic sequences over an extended period of geologic time during basin development. Base metals were transported as chloride complexes in sulphur-deficient, highly oxidised brines, before precipitating in extremely efficient chemical traps. Ore fluids recovered from Allihies were significantly lower salinity solutions, generated much later in basin history when the intrinsic permeability of base metal source regions was significantly reduced and fluid residence times considerably shorter. Clastic sequences likely hosted pre-existing small-scale syngenetic mineralisation, meaning Cu and S were remobilised simultaneously, thereby reducing the efficiency of metal transport. Copper was precipitated along brittle deformation structures associated with thin, discontinuous reduced intervals, representing relatively inefficient chemical traps. The Allihies Cu deposits provide an excellent example of a basin margin system whereby multiple physicochemical properties of an ideal ore fluid were not generated, resulting in significantly reduced metal transport, concentration and precipitation efficiencies when compared to an idealised sediment-hosted Cu system such as the Central African Copperbelt.

Chapter 7 Implications of fluid chemistry on the metal endowment of the Zambian Copperbelt

Chapters 4 to 6 have quantified base metal concentrations in a variety of sediment-hosted Cu-(Co-Ag-Pb-Zn) systems which formed at distinct times and in different settings. The contrasting base metal contents of separate fluid populations within, and between deposits highlights the quantity of physicochemical variables which contribute to the relative fertility of a particular fluid generation. Section 7.1 draws on the data presented in previous chapters in order to address the hypothesis that anomalously metal-enriched brines were responsible for mineralisation in the Central African Copperbelt.

7.1 Anomalous Base Metal Enrichment of Zambian Copperbelt Brines?

Estimates of brine Cu concentrations in the Zambian Copperbelt have hitherto been based on the assumption that mineralising fluids were compositionally comparable to those present in other globally significant sediment-hosted Cu districts, with Hitzman (2000) estimating approximately 100 ppm Cu, based on estimates of fluid Cu endowments (50 ppm) at White Pine (White, 1971) and the Polish Kupferschiefer (127 ppm) (Cathles et al., 1993), as well as theoretical and experimental work on Cu solubility and transport (Rose, 1976, 1989). However, ore fluid Cu concentrations reported from two 'classical' Zambian Copperbelt deposits and one Domes Region deposit in this study suggest that the fluids responsible for mineralisation in at least some of the Zambian Copperbelt were anomalously enriched in Cu when compared to published estimates, as well as other sediment-hosted Cu-(Ag-Pb-Zn) systems investigated here (Fig. 5-14). Additionally, numerous physicochemical factors, including fluid temperature, total salinity, major cation ratios and anion chemistry were all to some extent, anomalous in the Zambian Copperbelt, owing to a unique evaporative origin and a prolonged residence time with high degrees of fluid-rock interaction in a thermally anomalous basin setting.

In section 1.2, temperature and chlorinity were established as the two first-order controls on base metal concentrations of any crustal fluid, and as such, where these two key variables are distinctly elevated as a result of unusual fluid origins or residence history, correspondingly elevated base metal concentrations are anticipated. Using measured base metal concentrations and homogenisation temperatures for individual fluid inclusions, along with chlorinities derived from total salinity estimations, the degree of control imposed on base metal concentrations by temperature and chlorinity alone, is here compared with predictions presented in Chapter 1.

Estimations were made for Fe, Mn, Pb and Zn concentrations based on the modified dataset of crustal fluid compositions published by Yardley (2005) (Fig. 1-12).

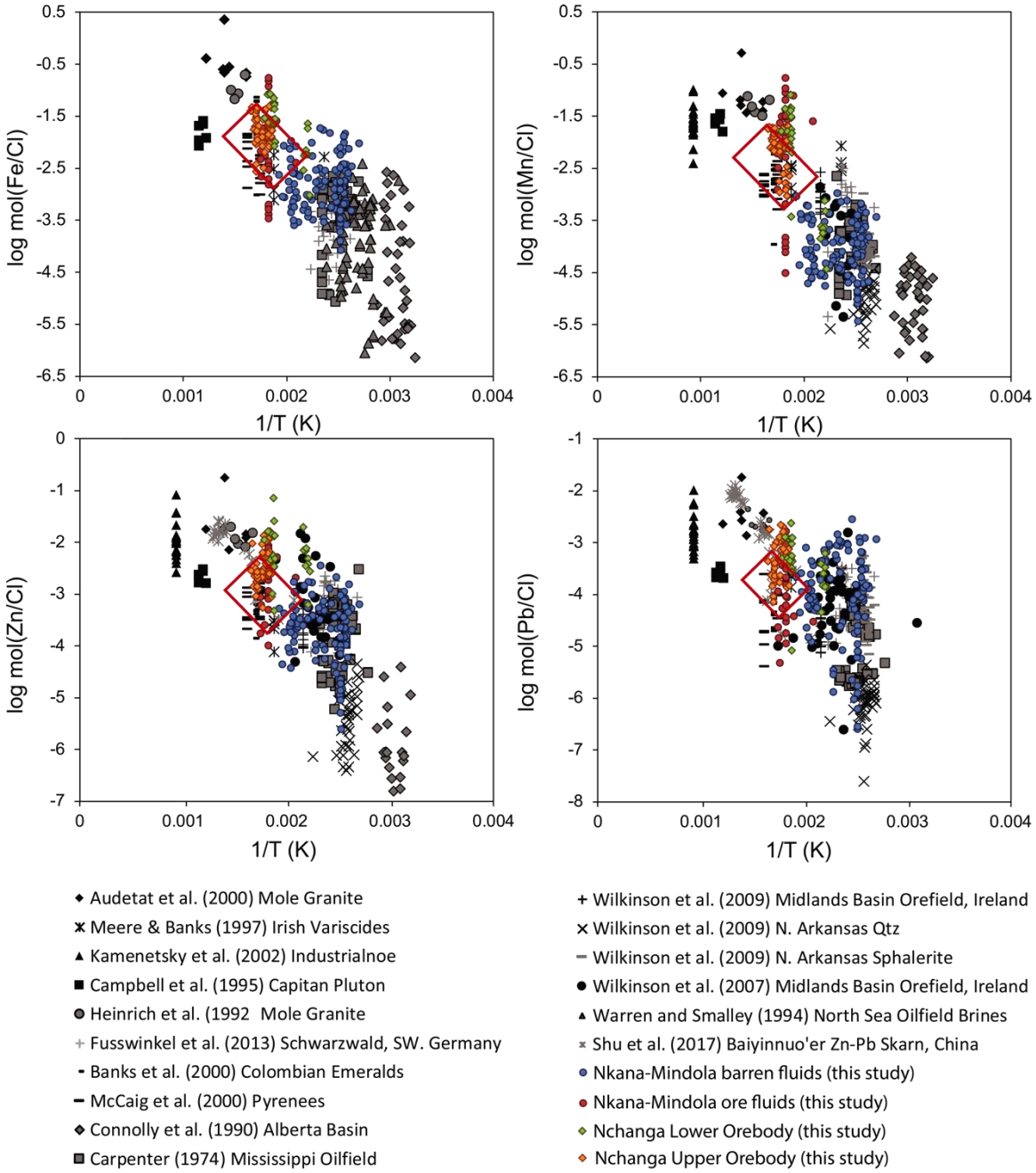

Fig. 7-1 Predicted and measured Fe, Mn, Zn and Pb concentrations of Zambian Copperbelt palaeofluids as a function of estimated fluid temperature and chlorinity. Red boxes denote predicted fields presented in Fig. 1-12, constructed using fluid temperature and chlorinity alone. Coloured data points represent measured values from the Nkana-Mindola and Nchanga deposits. Greyscale background dataset is expanded from Yardley (2005).

Within the order-of-magnitude spread around a best fit line through each dataset, the relationship between Fe, Mn, Zn and Pb concentrations in Zambian Copperbelt ore fluids conforms to predicted fields, indicating that base metal concentrations are broadly comparable to those expected for any

crustal fluid with the temperature-salinity characteristics of those measured in the copperbelt. Although a paucity of Cu data in published crustal fluid datasets precluded accurate predictions of concentrations in Zambian Copperbelt ore fluids, analyses for the metal in fluids from Nkana-Mindola and Nchanga significantly increase the quantity of available data, and begin to better constrain its relationship with temperature and salinity (Fig. 7-2). Although temperature and chlorinity still represent the first-order controls on Cu mobility, its ability to be complexed and transported by sulphur species in high temperature fluids, as well as in S-rich, Cl-poor lower temperature solutions, is likely responsible for increased degrees of scatter in Fig. 7-2, particularly in higher temperature crustal fluids.

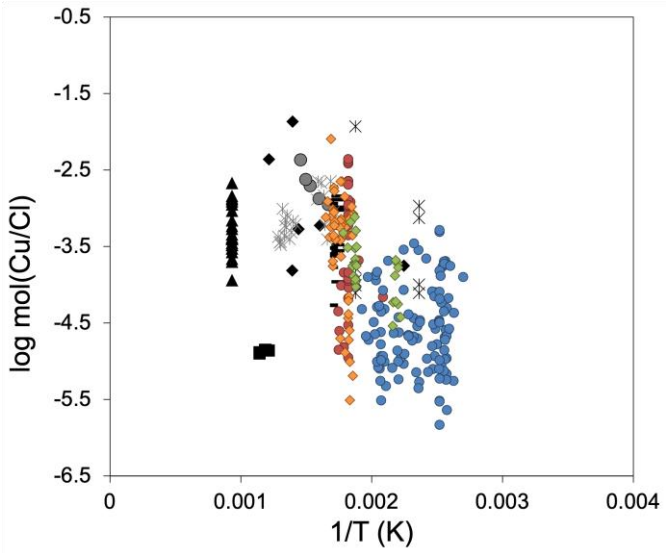

Fig. 7-2 Relationship between temperature, chlorinity and Cu concentrations in a selection of crustal fluids, including those measured in this study from the Nkana-Mindola and Nchanga deposits. Symbology replicated from Fig. 7-1.

Ultimately, although Katangan Basin palaeofluids hosted demonstrably elevated base metal concentrations relative to other analogous systems elsewhere in the world, Fig. 7-1 and Fig. 7-2 show that such enrichments in ore-forming metals are primarily a function of fluid temperature and salinity, and that Zambian Copperbelt ore fluids were, first and foremost, temperature-salinity anomalies. The following section discusses the effects of such brines on base metal mobility over a prolonged residence period in a basin environment.

7.2 Metal Sources and Mobilisation in the Zambian Copperbelt

Although some authors have speculated that mafic intrusives within the Katangan stratigraphy acted as significant sources of Cu in the Zambian Copperbelt (Annels, 1974, 1984; Key et al., 2001), it remains likely that oxidised clastic sequences (red beds) underlying the Copperbelt Orebody

Member formed the primary source of the main ore-forming metals. Previous efforts at reconciling red bed volumes with known and extrapolated tonnages of Cu mineralisation in the Zambian Copperbelt concluded, based on the assumption that basin brines were similar to those in better characterised districts such as White Pine and the Kupferschiefer, that insufficient volumes of red beds were available to source the quantity of metals observed in Zambia (Hitzman, 2000). Given the findings of this study, which suggest that many Zambian Copperbelt ore fluids were appreciably higher temperature-salinity solutions than other sediment-hosted Cu systems, and that these brines underwent high degrees of interaction with clastic sequences, it is appropriate that such estimates are revisited. Additionally, recent drilling and geophysical surveys indicate that red bed sequences are often considerably thicker than previously reported, thereby significantly increasing the volume of potential source material (Selley et al., 2018; Woodhead, 2018).

Here, Monte Carlo simulations are used in order to assess the significance of each of the selected variables through thousands of iterations, randomly sampling from a specified range for each input. Two models are presented in Fig. 7-3 in order to demonstrate the significant impact on the degree of remobilisation of metals as a result of brine composition and temperature. The minimum and maximum values for each input variable in both models are listed in Table 7-1 and justifications for these ranges are provided in the following paragraphs.

Table 7-1 Minimum and maximum input variables used to generate Monte Carlo simulations presented in Fig. 7-3.

	Red bed length (km)	Red bed width (km)	Red bed thickness (km)	Red bed volume (m^3)	Red bed density (kg m^{-3})	Red bed Cu content (ppm)	Efficiency of leaching (%)
Model 1:							
Min	100	50	0.25	1.25×10^{12}	2200	45	25
Max	125	60	2	1.50×10^{13}	2600	425	75
Model 2:							
Min	100	50	0.25	1.25×10^{12}	2200	45	1
Max	125	60	2	1.50×10^{13}	2600	425	15

Red bed volume:

The dimensions of source material in the Zambian basin are difficult to accurately quantify, partly due to erosion and poor outcrop, but also because the lateral extent of hydrothermal fluid systems remains unknown. Mapped extents of Lower Roan clastic sequences allow estimates of the basin length and width to be made (~100 x 50 km). Average thicknesses have traditionally been reported as ~300 m, although more recent drilling and geophysical surveys have suggested thicknesses of up to 2000 m in the basin depocentre, north of the Domes region (Selley et al., 2018). A range of 0.25 to 2 km has been used in both models.

Red bed Cu content:

Due to the long-lived, widespread hydrothermal fluid activity throughout the Zambian basin, it is difficult to sample red beds that are neither leached, or mineralised and therefore representative of 'fresh', unaltered protolith compositions. Bulk rock analyses of thirteen samples of relatively unaltered footwall arkose material from the Nchanga deposit (collected, archived and analysed by McGowan (2003)) returned an average Cu content of 232 ppm, with a minimum of 55 ppm Cu. In order to more confidently assess the potential Cu budget of fresh, unleached, diagenetically reddened sandstones, analyses of modern-day red beds forming in the northern foreland basin of Iraq (Hassan et al., 2016) are here used to conservatively estimate the upper threshold of likely red bed Cu concentrations in unaltered Neoproterozoic red beds (425 ppm). Based on examples of modern and ancient red beds in Zambia and elsewhere, a red bed Cu concentration range of 45 to 425 ppm is used in both models.

Red bed density:

Typical arkose densities range from 2200 to 2600 kg m^{-3} (Manger, 1963), but are highly variable depending on degrees of compaction, porosity and mineralogy. A pure quartzite with zero porosity would have a density of 2650 kg m^{-3} (bulk density = grain density), meaning that an arkose retaining a moderate degree of porosity, but with a minor detrital mafic mineral component would likely fall within the typical bulk density range stated above.

Efficiency of leaching:

The efficiency of leaching Cu from red beds by hydrothermal fluids is here used as a holistic metric by which to account for numerous variables which might all affect mobilisation potential. This includes the physicochemical conditions of fluids, average host rock grain sizes and the degree of crystallisation of oxide grain coatings, as well as the residence times of fluids in clastic reservoirs – many of which are almost impossible to individually quantify in the Zambian Copperbelt and likely varied, both temporally and spatially. Minimum and maximum leaching efficiencies used in this model are based upon experimental work investigating the degree of mobilisation of ore metals from different lithologies using a range of solutions at differing temperatures (Bischoff et al., 1981; Zielinski et al., 1983). Zielinski et al. (1983) found that an average of 44% of the total Cu hosted in Holocene-Pliocene red bed sequences from Baja California was leachable by a series of weakly- to moderately acidic, oxidised brines of various salinities at low temperatures (<150°C). At higher temperatures, Bischoff et al. (1981) showed a significant difference in the leachable fraction of Cu hosted by fresh greywackes from the Irish Midlands Basin as a function of fluid salinity, with seawater mobilising 2% of total Cu at 350°C, compared to 73% mobilisation by a NaCl-saturated

brine at the same temperature. Given the temperature-salinity characteristics of proposed ore fluids in the Zambian basin, a lower estimate of 25% leaching efficiency is particularly conservative, with the upper threshold set at 75% to reflect the experimental findings of Bischoff et al. (1981), at broadly analogous temperatures. In order to demonstrate the magnitude of the influence of this so-far largely neglected factor in mass balance calculations, model 1 (Fig. 7-3) uses a range of leaching efficiencies deemed relevant to the Zambian Copperbelt (25-75%), whereas model 2 uses significantly reduced leaching efficiencies (1-15%) in an otherwise identical model.

Using Equations 7.1, 7.2 and 7.3, the total mass of leached copper was calculated 20,000 times for each model, with each iteration using a randomly sampled set of variables from the ranges outlined in Table 7-1.

$$Red\ bed\ mass\ (m) = \rho V \qquad \text{Equation 7.1}$$

$$Contained\ Cu = m \times Cu\ conc. \qquad \text{Equation 7.2}$$

$$Leached\ Cu\ (kg) = Contained\ Cu\ \times\ LE. \qquad \text{Equation 7.3}$$

Where:

ρ = red bed density (kg m^{-3}); V = red bed volume (m^3); $Cu\ conc.$ = wt. % (/100); $LE.$ = Leaching efficiency (%)

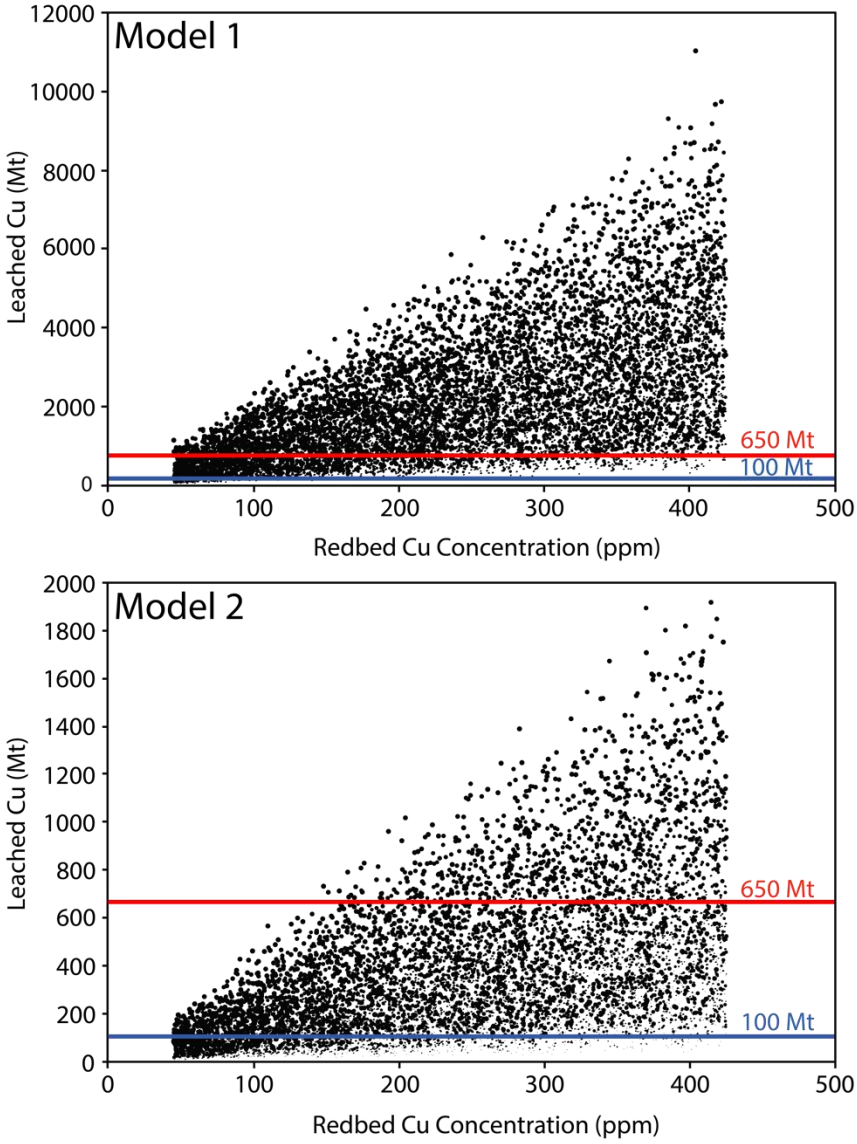

Fig. 7-3 Plots of total leached Cu versus fresh red bed Cu concentrations for 20,000, randomly sampled sets of variables from. Point sizes are graded according to leaching efficiency, with larger points representing increased efficiencies. Blue lines represent 100 Mt leached Cu – approximating the quantity of contained Cu in known deposits in the Zambian Copperbelt (Hitzman et al., 2012). Red lines represent 650 Mt Cu – an estimate of the total Cu content, including sub-economic mineralisation, of the Zambian Copperbelt (Hitzman, 2000). A) Model 1 – range of leaching efficiencies = 25% to 75%. B) Model 2 – range of leaching efficiencies = 1 to 15%.

Using leaching efficiencies considered appropriate for Zambian Copperbelt ore fluids characterised in this study, model 1 shows that with an unaltered red bed Cu concentration of >150 ppm, the lower end of the outcome distribution is capable of producing the total mass of Cu estimated in the Zambian Copperbelt. In other words, use of the most conservative end members of each input variable (e.g. smallest red bed volume, lowest leaching efficiency etc.) are sufficient to meet the

estimated total Cu budget of the region. Using the lowest red bed Cu concentrations considered in this model (45 ppm), only the upper quartile of simulations produced total leached Cu masses in excess of the 650 Mt threshold, meaning that almost every other variable in the model would have to be sampled at the highest ends of their respective ranges (Table 7-1) in order to meet the required total contained Cu threshold (650 Mt).

Model 2 demonstrates the significant effect of decreasing leaching efficiencies (manifested in most cases as significantly lower temperature/salinity fluids, or interaction with older, recrystallised red beds) on total leached Cu masses. With a leaching efficiency range of 1 to 15%, the extraction of >650 Mt Cu becomes significantly less likely, and would have probably required unaltered red bed Cu concentrations >350 ppm, along with a total red bed volume significantly greater than that proposed by Hitzman (2000).

These simulations are by no means exhaustive. Arguably the two greatest sources of error are the uncertainty regarding average red bed thicknesses and the leaching efficiencies used in these calculations. Further exploratory work to better constrain average thicknesses of clastic sequences, along with experimental studies to more accurately establish the leaching efficiency of very high temperature-salinity brines within red bed aquifers will be fundamental in quantifying the likelihood that all of the Cu present in the Zambian Copperbelt was sourced from autochthonous red bed sequences. Nevertheless, the models presented in Fig. 7-3 provide an insight into the potentially substantial effects of physicochemically anomalous brines on Cu leaching efficiencies in the Zambian Basin when compared to much lower temperature-salinity systems such as White Pine. These data suggest that such anomalous brines, held resident in a hydrologically closed system for long periods of geologic time, may be capable of mobilising significantly greater quantities of base metals than previously appreciated.

Chapter 8 Conclusions

The primary objective of this thesis was to investigate palaeofluid compositions and quantify base metal concentrations through the analysis of fluid inclusions associated with world-class mineralisation in the Zambian Copperbelt and draw comparisons with fluids from smaller deposits in the Kalahari Copperbelt and the Munster Basin. This chapter first summarises the key findings of the study and then addresses the main research questions individually.

Oxidised, chloride-dominant brines are known to play a crucial role in the liberation and transport of base metals in sediment-hosted Cu-(Co-Ag-Pb-Zn) systems (Hitzman et al., 2005; Jowett, 1991; Rose, 1976). Palaeofluids from the Zambian Copperbelt, Kalahari Copperbelt and Munster Basin show some clear distinctions in their temperature, total salinity, major cation chemistry and base metal content, all of which play an important role in the relative prospectivity of each basin. Fluid inclusions from the Nkana-Mindola, Nchanga and Lumwana deposits in Zambia can be divided into two broad populations based on their relative timing of trapping, along with concomitant distinctions in major salt chemistry and base metal budgets. Kinematically early fluids are characterised by anomalously high temperatures and total salinities, K/Na ratios ≥1 and one to two orders-of-magnitude higher Cu, Co, Pb and Zn concentrations than later fluid populations. Cl/Br and Na/Br ratios for similar fluids from several Central African Copperbelt deposits indicate these fluids represented bittern brines, generated through advanced evaporation of a potentially sulphate-deficient middle Neoproterozoic seawater source. Interaction of metalliferous potassic brines with clastic sequences is evidenced by widespread potassic metasomatism associated with high grade mineralised rocks across much of the Zambian Copperbelt. Further analysis of fluids associated with mineralised rocks in predominantly Mg-metasomatised deposits in the central Congolese Copperbelt may help to elucidate the geochemical evolution of bittern brines between the basin depocenter and the basin margin deposits studied here.

Fluids trapped during or after peak orogenesis in both the Zambian Copperbelt and the Kalahari Copperbelt contrast with earlier Zambian brines, showing lower homogenisation temperature and salinity characteristics, significantly reduced base metal concentrations, and K/Na <1. Halogen systematics of post-kinematic fluid inclusions from Lumwana, as well as demonstrably late palaeofluids from elsewhere in the Zambian Copperbelt show elevated Cl/Br and Na/Br (Heijlen et al., 2008; Nowecki, 2014; Selley et al., 2018), indicating a halite dissolution origin and a distinct fluid source from earlier ore fluids. NaCl-undersaturated solutions likely represented the primary ore fluid in the Ghanzi-Chobe belt, transporting relatively low base metal concentrations from the

Ngwako Pan red beds and Kgwebe Volcanics towards variably reduced, structurally-controlled traps within the lower D'Kar Formation during Damaran Orogenesis.

Mineralised and barren vein sets at Allihies and Inch record a protracted history of palaeofluid activity in the Munster Basin, with moderate homogenisation temperature and salinity evaporated seawater-derived brines likely residing in Devonian Old Red Sandstone aquifers prior to peak Variscan orogenesis. Later ore fluids were higher temperature, lower salinity solutions, likely emplaced during late orogenic times. Although none of the fluids from the Munster Basin analysed in this study hosted anomalously elevated Cu concentrations, the cation chemistry of contrasting fluid populations does indicate that earlier fluids underwent a greater degree of interaction with clastic host rocks, whereas proposed ore fluids show little evidence for extensive fluid-rock interaction and were likely channelled and emplaced within recrystallised rocks in a brittle deformation regime. Proposed ore fluids yield $\delta^{18}O$ signatures indicative of a metamorphic fluid component or equilibration of marine-derived fluids with metamorphic host rocks. A lack of apparent *in situ* reduced sulphur sources at Allihies implies that ore fluids may have remobilised low quantities of Cu and S together from small-scale sediment-hosted mineralisation elsewhere in the Munster Basin.

8.1 Research Questions

1. *Were the fluids responsible for mineralisation in the world's largest repository of sediment-host copper and cobalt, the Central African Copperbelt, anomalously metal enriched or are they chemically indistinguishable from the fluids present in smaller-scale systems?*

Palaeofluids hosted by mineralised veins at all three Zambian Copperbelt deposits studied here yielded Cu-Co-(Pb-Zn) concentrations 1-2 orders-of-magnitude higher than all fluids analysed from smaller deposits in the Kalahari Copperbelt and the Munster Basin (Fig. 5-14) and as such, may be considered particularly fertile. However, Fig. 7-1 demonstrates that based on their temperature and salinity characteristics, base metal concentrations in these 'ore fluids' remain predictable when compared more broadly with a wide range of crustal fluids. Ultimately, through a unique origin and residence history, Katangan Basin ore fluids generated unusually elevated temperatures and salinities, enabling the mobilisation of base metals at concentrations considered anomalous relative to analogous basins elsewhere in the world.

2. *Were fluids in the Zambian Copperbelt equally fertile over the entire duration of basin history or were certain fluid generations and periods of basin history responsible for punctuated mineralisation events?*

The base metal content of high temperature and salinity potassic brines measured in pre- to syn-kinematic veins at Nkana-Mindola, Nchanga and Lumwana is distinctly higher than post-orogenic brines recovered from the same deposits, indicating the expulsion of fertile brines largely occurred prior to, or in some cases, at the onset of basin inversion. Barren, lower temperature and salinity post-orogenic brines share similar characteristics with some fluids associated with atypical mineralisation styles (Pb-Zn; Cu-Au) in demonstrably post-Lufilian age deposits (e.g. Kansanshi and Kipushi)

3. *How does the major cation chemistry of palaeofluids differ between deposits, both within and outside of the Zambian Copperbelt, and how does this relate to the metal tenor and ratios of the associated mineralised rocks?*

Elevated base metal concentrations in Zambian palaeofluids show a strong association with particularly potassic brines (K/Na $\geq$1). Additionally, fertile brines at the Lumwana deposit in the Domes Region contain a significant Ca component, likely accompanied by increased carbonate concentrations and resulting from fluid-rock interactions in a contrasting stratigraphy to that present in more conventional Lower Roan-hosted deposits. Across all three Zambian deposits studied here, ratios of the principal ore-forming metals in fluid inclusions do not reflect the metal ratios reported from bulk ore. For example, at Nchanga, where Cu:Co ratios differ significantly between orebodies, palaeofluid metal concentrations from each orebody do not reflect this distinction, perhaps indicating that the contrasting stratigraphic intervals controlled different Co precipitation efficiencies. Palaeofluid compositions do, however, broadly reflect the relative abundance of Co in each system, with the most cobaltiferous deposit (Nkana-Mindola) yielding significantly more Co-enriched ore fluids than those analysed from Nchanga and Lumwana.

All fluids recovered from smaller-scale systems in Ireland and Botswana display more typical basin brine compositions, with cation budgets dominated by Na, and subordinate Ca reflecting differing degrees of cation exchange with the host rocks.

8.2 Key Factors in the Formation of Giant Deposits

Although basin architecture, stratigraphy, tectonics and the timing of geodynamic triggers such as basin inversion and brine expulsion all play significant roles in the relative success or failure of a prospective sediment-hosted Cu system, this section is centred on the role of hydrothermal fluids and how their varying temperatures, compositions, volumes and residence times affect the fertility of a basin.

The production of bittern brines capable of acquiring high salinities during advanced evaporation is fundamental to increasing base metal leaching and transport efficiencies. Although salinities may be commonly enhanced through the dissolution of evaporitic strata, this often breaches hydrological seals and significantly inhibits the longevity of a high temperature hydrothermal system. The Zambian Copperbelt provides an excellent example of a system where bittern brines with elevated salinities were trapped in large volumes at sub-salt levels. Deep burial and further heating over a prolonged period promoted fluid-rock interaction, cation exchange, and the development of anomalously saline, fertile brines in a relatively closed system. Should a basin fail to generate all of these components in the appropriate order or fail to maintain them over prolonged periods of geologic time, mineralising systems will be absent or short-lived, producing low quality deposits.

The presence of sufficient red beds (± volcanic units) or basement-hosted Cu sources is clearly a prerequisite for the generation of large-scale sediment-hosted Cu mineralisation. However, initial simulations suggest that relatively modest volumes of red beds may be sufficient to source significant quantities of Cu where the resident brines possess the appropriate physicochemical conditions to maintain high leaching efficiencies. In basins where lower temperature-salinity fluids reside in red bed aquifers for much shorter time periods, no volume of red beds will compensate for inefficient mobilisation of Cu by a single fluid generation. This concept is demonstrated in the Northwest Botswana rift, where red bed packages often exceed 2000 m in thickness and are typically underlain by the bimodal Kgwebe Volcanic Complex. Here, potential Cu sources likely exceeded the capacity of relatively short-lived, moderate temperature-salinity fluids to leach, mobilise and concentrate metals into high grade/tonnage accumulations. Ultimately, the extended residence of hypersaline brines within high temperature red bed aquifers is crucial in liberating and transporting anomalously high concentrations of base metals and the subsequent formation of giant, high grade deposits.

8.3 Future Work

8.3.1 Hydrothermal fluids in the Central African Copperbelt

- Metasomatic mineral assemblages are macroscopically partitioned across the Central African Copperbelt, from predominantly Mg assemblages associated with Congolese deposits near the basin depocentre, to K-dominant metasomatism associated with basin margin deposits in the Zambian Copperbelt (Selley et al., 2018). As such, it is possible that ore fluids remobilised the primary alkali content of basal clastic sequences from the basin depocentre towards basin margins, and that the potassic brines analysed in this study

represent these modified solutions. Broadening the scope of this study to assess fluid chemistries in some classic Congolese deposits would likely help to elucidate whether 'parental' ore fluids were in fact Mg-bittern brines, or whether the fluids characterised from several Zambian deposits in this study are representative of ore fluids more widely across the Central African Copperbelt.

- At deposits where palaeofluid compositions have been linked with particular alteration phases with a sufficient degree of confidence, dating of such phases (e.g. Rb-Sr dating of K-feldspar) may be a more reliable geochronometer than more traditional Re-Os dating of sulphide phases (Sillitoe et al., 2015; Sillitoe et al., 2017). Similarly, where alteration phases have themselves been geochemically linked with mineralising events, such as distinct REE signatures of ore-stage carbonates at Nchanga (Roberts et al., 2009), these phases could also provide more accurate dating solutions.
- Expansion of the scope of fluid inclusion laser ablation work to deposits with alternative mineralisation styles, metal associations and geochronology such as Kansanshi and Kipushi would be of particular merit when making assessments of the longevity of potassic versus dominantly sodic brines in the Zambian Copperbelt. Additionally, analysis of fluids from these deposits would provide a greater insight into the metal transporting capabilities of lower temperature-salinity post-kinematic brines.
- The difficulties described in Appendix A.1.4 regarding accurate quantification of absolute cation concentrations in complex, multisalt brines ultimately require a better understanding of the anion content of such fluids. Although both laser ablation ICP-MS and bulk crush leach analysis are destructive methods, obtaining anion and cation concentrations for the same fluid generation will be key in fully understanding the major salt chemistry of the brines and subsequent quantification of their base metal contents.

8.3.2 Ore genesis in the Munster Basin

- Microthermometric and stable isotope studies of vein-hosted Cu mineralisation in the West Carbery District (Wen et al., 1996) suggest a possible temporal and genetic relationship with mineralisation at Allihies. Investigation of the major and trace element chemistry of these fluids, as well as further sulphur isotope analyses of Cu sulphides from both deposits would help to elucidate whether they share a common history.

8.3.3 Exploration for high quality sediment-hosted Cu deposits

- This study has highlighted the importance of generating anomalously high fluid temperatures and salinities in a long-lived, closed system. As such, these variables should

be attributed high importance in ranking systems aimed at defining highly prospective regions during global basin fertility analysis.

- If the applicability of key fluid fertility indicators such as elevated K/Na ratios can be proven more widely across the Central African Copperbelt then relatively cheap, bulk crush-leach analysis of vein samples from prospective regions may be employed to assess fluid signatures and inform drilling decisions during exploration programmes.

Appendix A Methodology, Sample Lists and Drillcore Logs

A.1 Methodology

A.1.1 Linkam THMS 600 heating-freezing stage calibration

Calibration curves were constructed from repeat measurements of CO_2 melting (-56.6°C), pure H_2O melting (0.0°C), CO_2 homogenisation (31.1°C) and $NaNO_3$ melting (306.8°C) during Spring 2016, 2017 and 2018. Correction factors were calculated from the equation of each of the calibration curves and applied to the data offline (retrospectively).

Spring 2016:

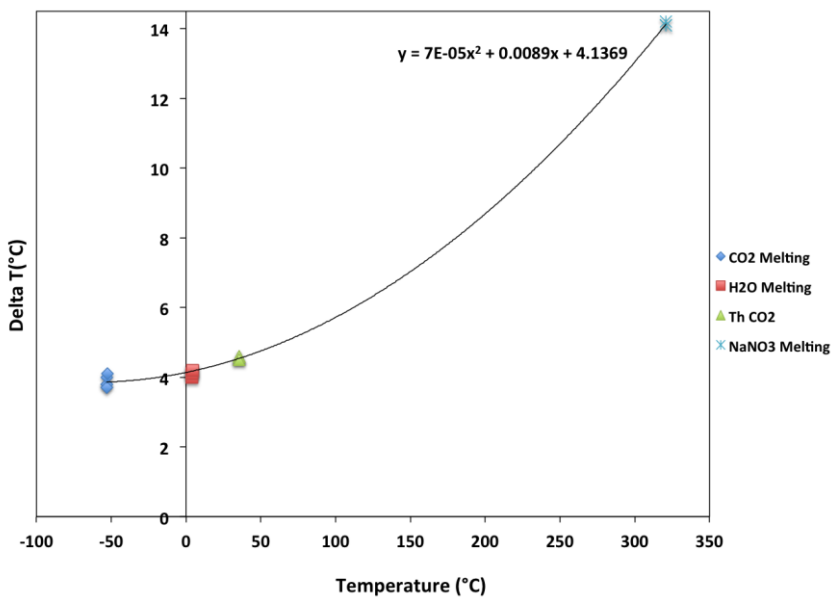

Spring 2017:

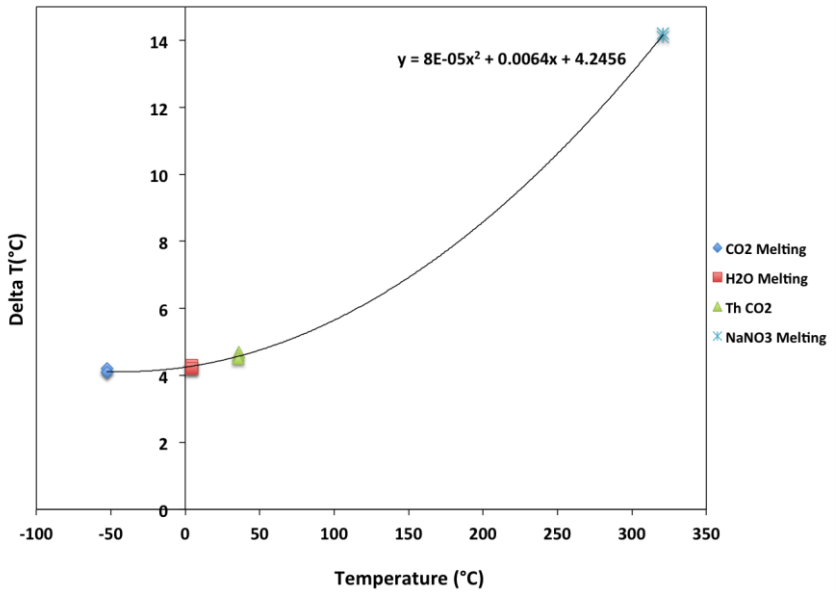

Spring 2018:

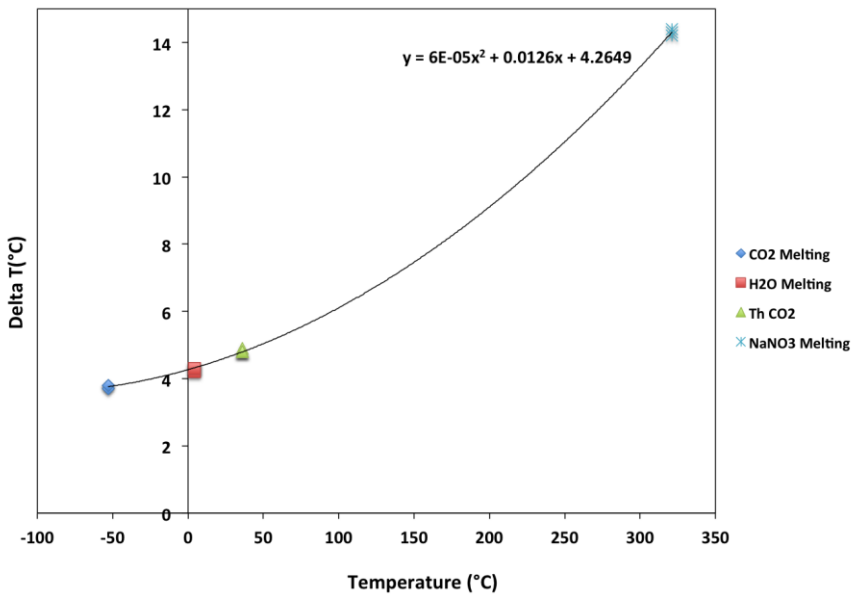

Fig. A.1. Calibration curves used for offline correction of microthermometry data.

A.1.2 Estimating minimum trapping depths of fluid inclusions

Allihies:

The pressure correction applied in Section 6.5.2 to high temperature, moderate salinity fluid inclusions hosted by mineralised veins at Allihies is based upon the assumption that hydrostatic conditions prevailed during fluid trapping. This assumption was first justified for similar fluids analysed by Meere and Banks (1997) and is confirmed here through the calculation of an isochoric plot (Fig. A.2).

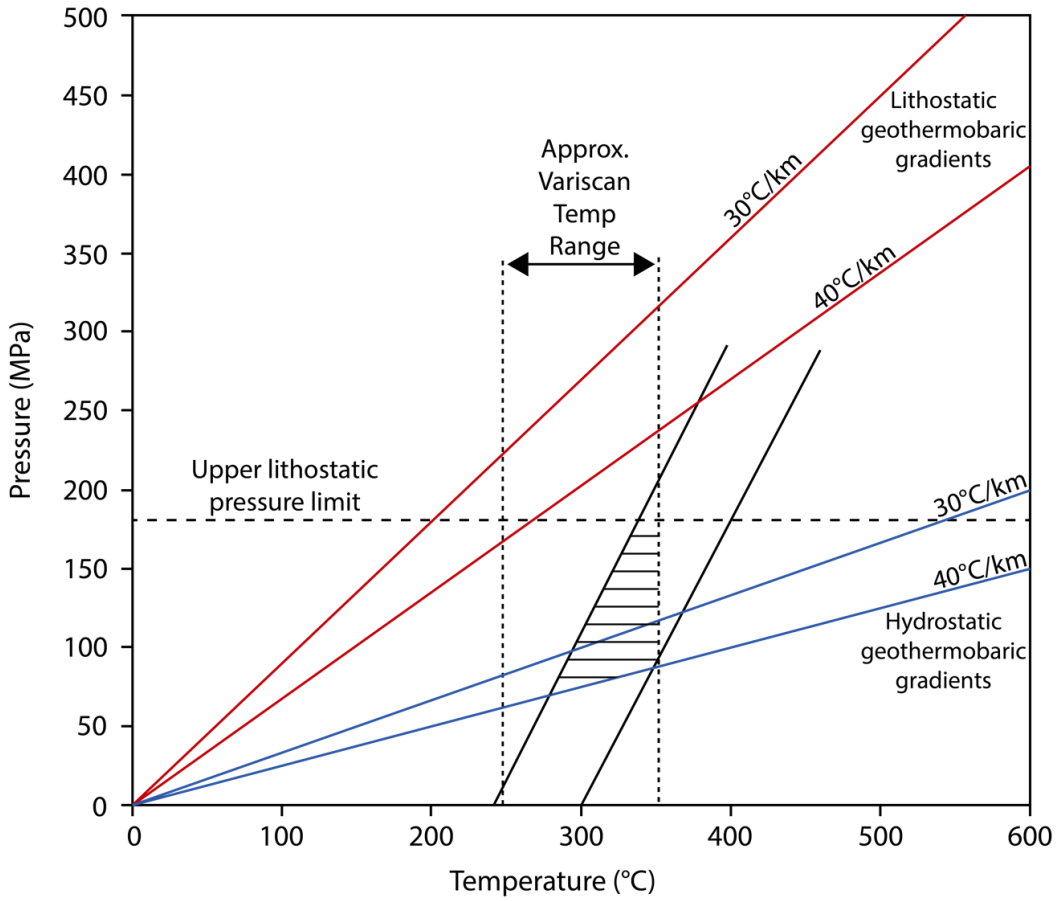

Fig. A.2. Isochore plot for high temperature (240-300°C), moderate salinity fluid inclusion populations hosted by mineralised veins at Allihies. The shaded area represents likely fluid trapping conditions constrained by the estimated maximum overburden thickness and the approximate Variscan Orogenesis temperature range derived from multiple sources (Jones, 1992; Meere, 1995).

The plot shows that these fluid inclusions were likely trapped near hydrostatic conditions at all geologically reasonable pressure conditions. Based on this assumption, the pressure correction applied to the average T_{hTOT} measurement of all proposed ore fluids (260°C) was calculated as follows:

$$Pressure\ Correction\ (°C) = \frac{(max\ fluid\ pressure - fluid\ homog.pressure)}{isochoric\ \frac{dP}{dT}}$$

$$Pressure\ Correction\ (°C) = \frac{(67 - 4.4)[MPa]}{1.8\ [\frac{MPa}{°C}]}$$

Appendix A

Zambian Copperbelt:

Relatively recent models have allowed the calculation of minimum trapping pressure estimates for halite-saturated inclusions in the H_2O-NaCl system across a broad temperature range (Lecumberri-Sanchez et al., 2012). However, a significant proportion of fluid inclusions analysed in this study are multiphase brines with significant KCl $\pm$ $CaCl_2$ components and as such, accurately constraining their true PVT relationships at the time of trapping remains problematic. Where assemblages of pure CO_2 and H_2O-CO_2 inclusions have been identified and undergone microthermometric experiments, an estimate of the minimum trapping pressure has been made.

Calculations made using the "FLUIDS" software package (Bakker, 2003) and the equation of state of Span and Wagner (1996) utilise CO_2 densities (derived from T_{hCO2}), along with an independent approximation of temperature to estimate the minimum trapping pressure (depth) of pure CO_2 inclusions in two samples from the Lower Orebody at Nchanga (L128-11 and L128-12). Assuming an average lithostatic head of 2700 kg/m^3, along with a minimum trapping temperature equal to the average T_{hTOT} value of ~260°C measured for co-existing primary three-phase aqueous inclusions in the Lower Orebody Arkose, the average measured CO_2 inclusion density (0.972 $\pm$ 0.042 g cm^{-3}, n = 20) yields a minimum trapping pressure of ~225 MPa. This corresponds to a minimum trapping depth of ~8.5 km and a geothermal gradient of ~31°C/km (Fig. A.3). Imposing an upper lithostatic pressure threshold equivalent to the estimated pre-erosional overburden thickness towards the Katangan basin depocentre (~11 km; Selley et al. (2018)), a maximum possible pressure correction of ~90°C is estimated (trapping temperature ~350°C), broadly consistent with a fluid in thermal equilibrium with greenschist facies rocks. Although the inherent errors associated with such calculations are not insignificant, they do indicate that more recent estimates of burial depths of up to 10-12 km prior to, and at the onset of basin inversion (Selley et al., 2018) are more accurate than historical estimates of <7 km (Annels, 1989; Garlick, 1961).

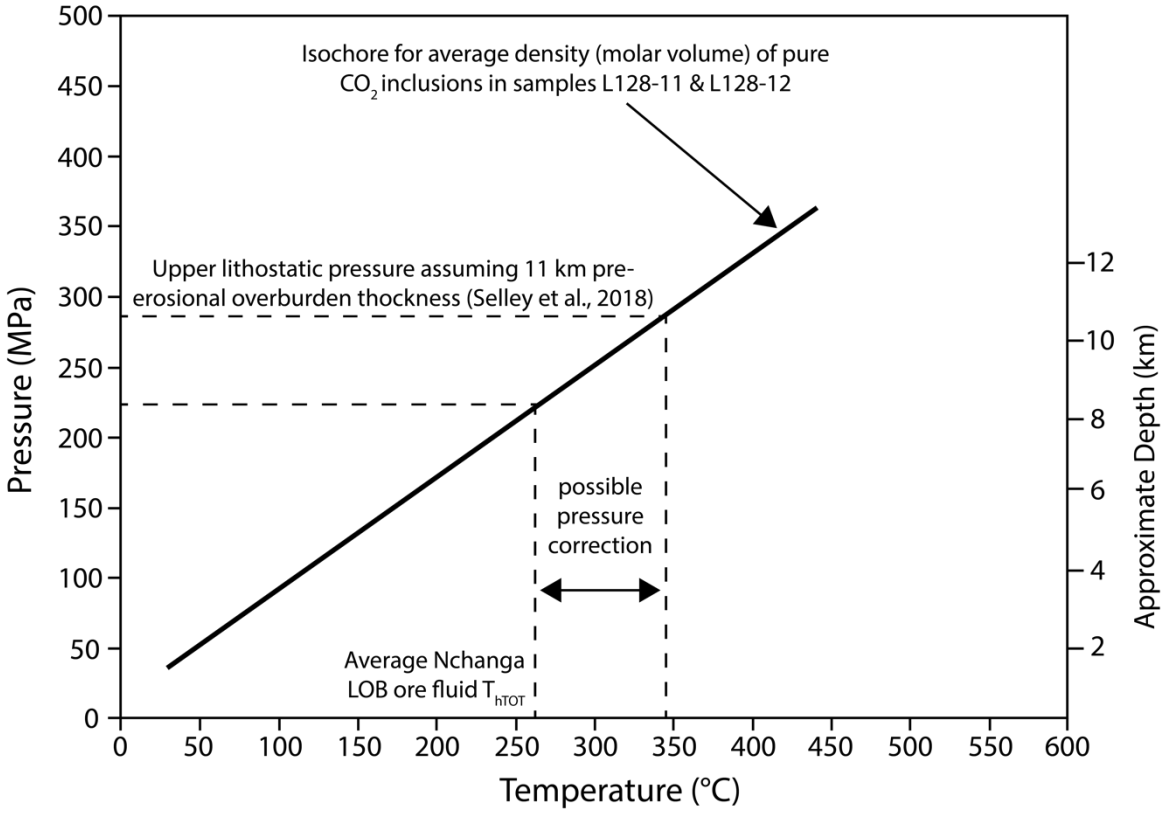

Fig. A.3. Isochore plot for CO_2 inclusions in samples L128-11 and L128-12 from Nchanga. CO_2 densities were calculated using the average T_{hCO2} of 20 inclusions (-8.4°C) and equations 3.14 and 3.15 of (Span and Wagner, 1996). The isochore is modelled using the equation of state of Sterner and Pitzer (1994) and the "FLUIDS" software package (Bakker, 2003).

Although these minimum pressure estimates for CO_2-bearing inclusions provide a useful insight into approximate trapping conditions prior to peak orogenesis, similar estimates cannot be made for the majority of multiphase fluid inclusions reported in this study and as such, it should be noted that reported T_{hTOT} values represent minimum estimates of true trapping temperatures.

A.1.3 Accuracy and precision of fluid inclusion laser ablation ICP-MS data

Table A.1 gives a full breakdown of instrumental precision (measured as %RSD and 2σ) and accuracy (measured as % relative error). The results are for 122 measurements of NIST 610 and 96 measurements of NIST 612. Note the poor precision of S and Cl (NIST 610 only). Poor Cl precision is likely due to inconsistent ionization during laser ablation and would require specific optimisation for halogen analysis (long dwell times etc). Sulphur data is not considered reliable and as such, has not been discussed in this study.

Graphs A.4 and A.5 show the data from Table A.1 in graphical format.

Appendix A

Table A.1. Summary of the accuracy and precision of fluid inclusion laser ablation ICP-MS data. Measured values are compared with those used by the SILLS fluid inclusion laser ablation data reduction programme, based on concentrations reported by Pearce et al. (1997).

	NIST 610 (n = 122)					**NIST 612 (n = 96)**				
	Mean (ppm)	σ	%RSD	2σ (%)	Relative Error (%)	Mean (ppm)	σ	%RSD	2σ (%)	Relative Error (%)
6Li	484.0	10.1	2.1	4.2	-0.1	42.9	4.2	9.7	19.5	3.2
7Li	483.8	5.7	1.2	2.4	-0.2	42.9	1.2	2.9	5.7	3.4
24Mg	466.3	13.5	2.9	5.8	0.2	60.5	3.2	5.3	10.6	-21.9
27Al	10780.0	151.6	1.4	2.8	-0.1	10399.8	832.6	8.0	16.0	-6.9
29Si	326953.4	3154.6	1.0	1.9	0.0	345338.4	9306.2	2.7	5.4	2.7
34S	594.8	97.5	16.4	32.8	4.4	474.4	167.2	35.2	70.5	35.5
35Cl	441.4	85.5	19.4	38.8	-6.1	413.1	134.8			
39K	466.3	8.0	1.7	3.4	0.3	60.4	3.0	5.0	10.0	-8.9
43Ca	81892.7	1132.5	1.4	2.8	0.1	80525.5	4847.4	6.0	12.0	-5.6
49Ti	437.1	12.7	2.9	5.8	0.7	36.2	2.6	7.1	14.2	-24.8
51V	442.1	5.2	1.2	2.3	0.1	38.7	1.0	2.6	5.2	-1.4
53Cr	406.0	6.4	1.6	3.2	0.2	36.3	1.2	3.4	6.8	-8.9
55Mn	433.7	5.5	1.3	2.6	0.1	37.4	1.1	3.0	6.1	-2.8
57Fe	451.3	24.3	5.4	10.7	-1.3	87.1	20.3	23.3	46.5	54.7
59Co	405.1	4.9	1.2	2.4	0.0	35.2	0.8	2.3	4.5	-0.1
60Ni	444.5	6.1	1.4	2.7	0.1	38.4	1.3	3.3	6.7	-0.1
65Cu	431.8	14.1	3.3	6.5	0.3	37.3	1.3	3.4	6.7	1.6
66Zn	456.8	10.3	2.2	4.5	0.1	39.0	2.6	6.6	13.2	2.8
75As	323.7	59.5	18.4	36.8	2.0	32.5	1.9	5.8	11.5	-13.0
85Rb	426.2	5.1	1.2	2.4	0.0	32.2	1.0	3.0	5.9	1.9
88Sr	516.0	6.5	1.3	2.5	0.0	73.8	4.3	5.8	11.6	-3.1
89Y	458.8	7.7	1.7	3.4	0.2	33.9	3.4	10.0	19.9	-11.5
95Mo	379.6	10.1	2.7	5.3	0.8	33.4	1.0	2.9	5.9	-12.8
107Ag	240.3	4.4	1.8	3.7	0.4	21.4	1.0	4.5	8.9	-2.6
111Cd	259.9	7.4	2.8	5.7	0.2	28.2	2.2	7.7	15.4	-0.4
118Sn	397.9	7.7	1.9	3.9	0.4	38.7	2.5	6.6	13.2	1.9
121Sb	371.6	10.6	2.9	5.7	0.8	31.6	1.1	3.4	6.9	-17.8
133Cs	357.9	5.7	1.6	3.2	0.2	40.7	1.1	2.7	5.3	-2.4
137Ba	453.9	6.4	1.4	2.8	0.0	38.0	2.1	5.5	11.0	0.8
140Ce	458.0	6.6	1.4	2.9	0.0	37.2	1.3	3.6	7.2	-3.0
175Lu	441.0	9.5	2.1	4.3	0.3	31.9	3.1	9.8	19.6	-15.3
182W	446.2	6.9	1.5	3.1	0.2	38.3	1.0	2.5	5.1	-3.3
197Au	22.7	0.5	2.3	4.6	0.7	4.5	0.2	4.7	9.5	-12.3
208Pb	426.5	5.4	1.3	2.5	0.1	38.8	1.3	3.5	6.9	-0.3
209Bi	358.7	7.7	2.1	4.3	0.3	32.1	1.1	3.5	7.1	7.6
232Th	457.8	7.3	1.6	3.2	0.2	33.2	2.9	8.9	17.7	-10.7
238U	461.6	4.3	0.9	1.9	0.0	37.2	1.1	2.8	5.7	0.2

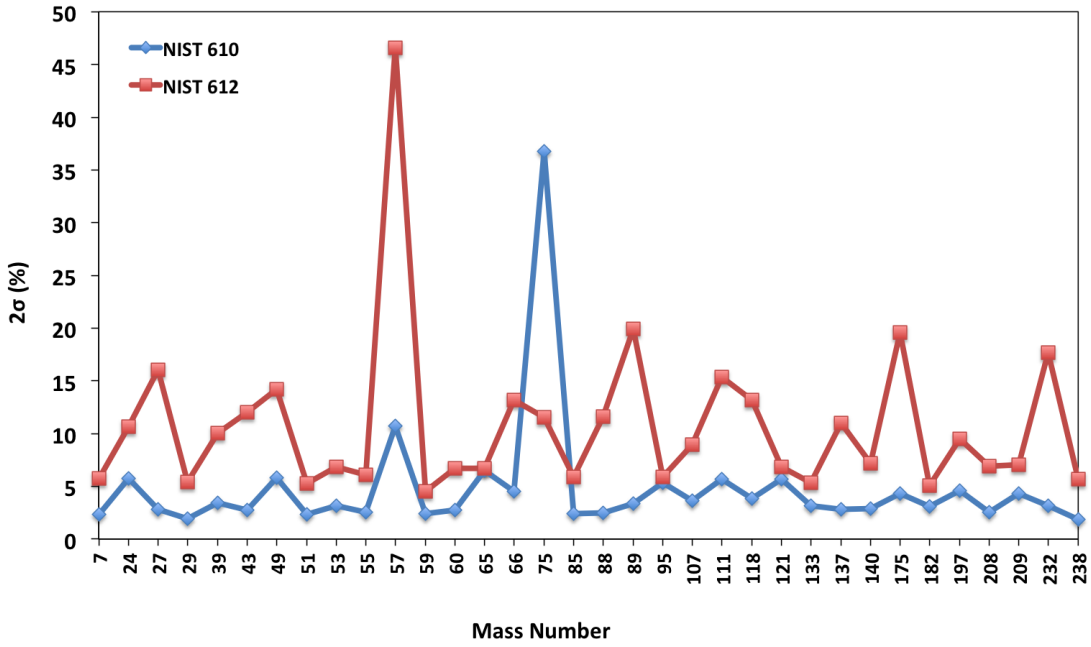

Fig. A.4. Instrumental precision (2σ as a percentage of the mean) for 122 analyses of NIST 610 and 96 analyses of NIST 612.

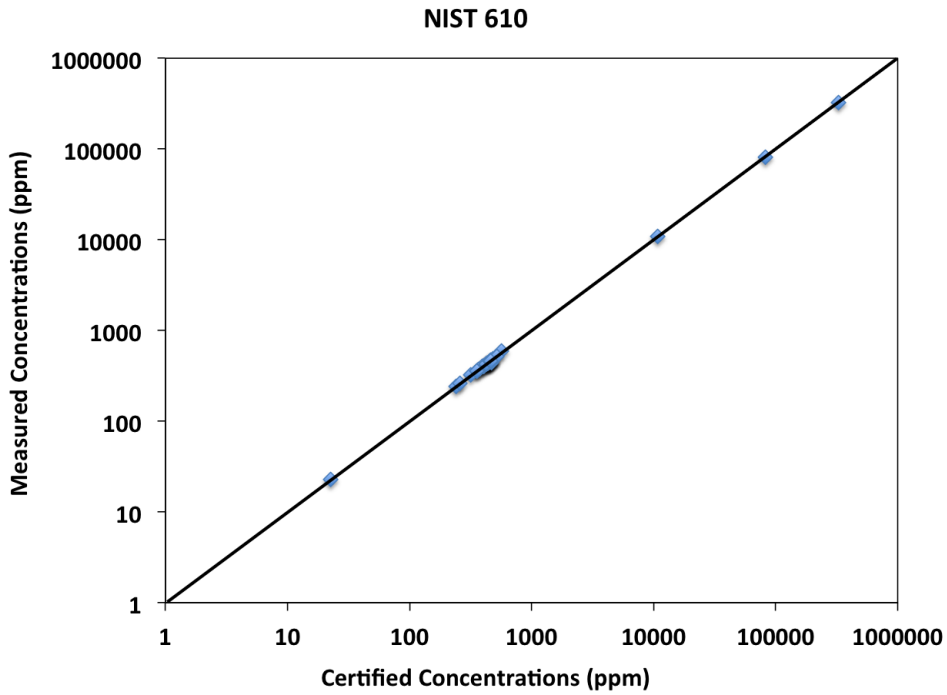

Fig. A.5. Instrumental accuracy, expressed as relative error (%) for 122 analyses of NIST 610 and 96 analyses of NIST 612.

A.1.4 Proposed method for scaling down cation concentrations (Lumwana laser ablation ICP-MS data)

In the absence of a reliable method of interpreting a 3-salt system, quantification of absolute elemental concentrations in such inclusions results in an overestimation of Na as an internal standard and an associated overestimation of total cations. A potential method to treat such data involves the use of visual estimates of phase proportions in each inclusion to estimate the total dissolved solid (TDS) content and scale down cation concentrations accordingly. Table A.2 shows an example of the process for 3 inclusions from Lumwana.

Table A.2 Example calculations for scaling down cation concentrations in fluid inclusions

Sample	Finc	L	V	S	Solids mass	H_2O mass	Solids mass (%)	H_2O mass (%)	TDS (ppm)	Estimated cations	Measured cations	Correction factor	Charge balance (before)	Charge balance (after)
MLW0291 28.00 (B)	7	0.8	0.08	0.12	0.50	0.72	40.9	59.1	409448	159685	239441	0.67	+10.3	-10.0
MLW0291 28.00 (C)	3	0.8	0.08	0.12	0.50	0.72	40.9	59.1	409448	159685	220446	0.72	+8.3	-7.9
MLW0287 59.75 (C)	1	0.8	0.1	0.1	0.46	0.72	38.8	61.2	387755	151224	275927	0.55	+15.5	-14.4

A comparison of charge balance calculations before and after this process shows that the method typically overcorrects cation concentrations, resulting in a cation deficit. Given that only Cl^- can be estimated and accounted for, the presence of any other anion species will result in a further increased anion surplus. Additionally, the method is considered to include the following sources of error:

1. Visual estimation of phase proportions in a 3D inclusion from a 2D perspective.
2. Excludes ion content of vapour phase.
3. Assumes entire anion budget is Cl^-.
4. Includes all other laser ablation ICP-MS analytical error.

Laser ablation ICP-MS results for multiphase inclusions from all three Zambian Copperbelt deposits show a strong relationship between the Ca content of an inclusion and its total cation surplus (Fig. A.6). Addition of Ca salts to a NaCl-dominant brine will raise the melting temperature of halite, and so in theory, will be accounted for when estimating total salinity. However, the addition of a significant concentration of Ca^{2+} is unlikely to be entirely corrected for and such inclusions likely host elevated concentrations of non-chloride anions (e.g. carbonate) which have not been quantified. The presence of unquantified concentrations of 2^- anions likely causes an indirect coupling between Ca concentrations and cation excesses, as demonstrated in Fig. A.6. The inherent errors included in the above method for scaling down cation concentrations, in addition to the likely presence of an unquantified contribution of 2^- anions in the fluid inclusions which display the

highest cation surpluses, indicates that the correction method underestimates true cation concentrations by a greater degree than initial overestimations. As such, the correction is not applied to the results presented in this study. Inclusion populations with a significant component of more than two salts remain challenging to accurately characterise without knowledge of both the anion and cation contents of the same population.

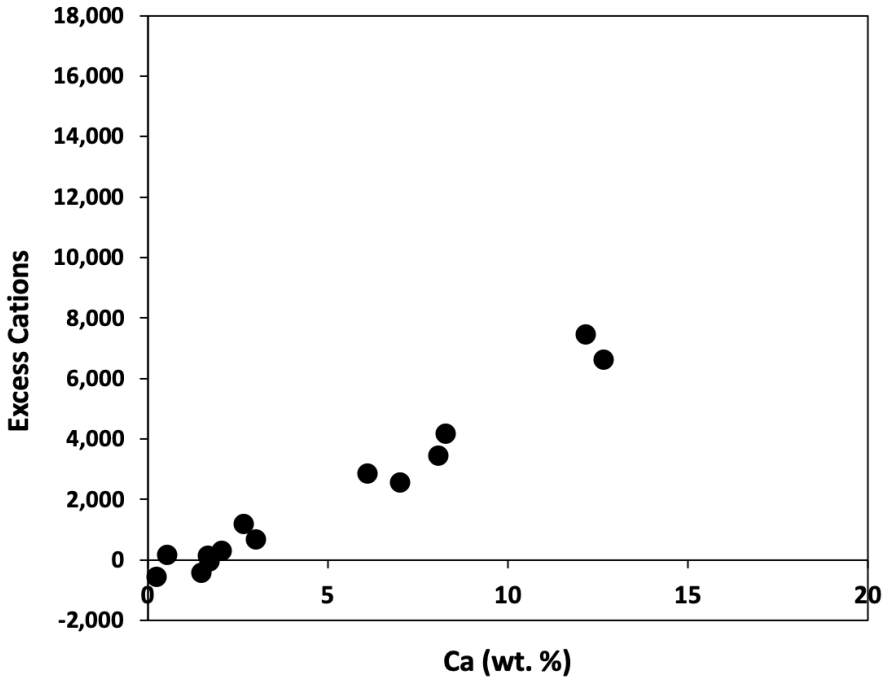

Fig. A.6. Plot of excess cations versus Ca concentration in a population of multiphase fluid inclusions from the Zambian Copperbelt.

A.1.5 Choice of $\delta^{18}O_{fluid}$ fractionation factor

In order to assess the relative significance of the choice of fractionation factor used to calculate $\delta^{18}O_{fluid}$ values from measured $\delta^{18}O$ signatures of quartz, two contrasting equations were applied to average $\delta^{18}O$ signatures of quartz vein sets from the Munster Basin (Matsuhisa et al., 1979; Sharp et al., 2016). Although the equation of Sharp et al. (2016) is valid over a wider temperature range (0-800°C), the Matsuhisa et al. (1979) fractionation equation is valid over the temperature range of interest in this study and allows a representative comparison of the data presented in this study with those in the literature which have historically used this older equation. Both equations produce almost identical fractionation factors at temperatures >150°C (Fig. A.7).

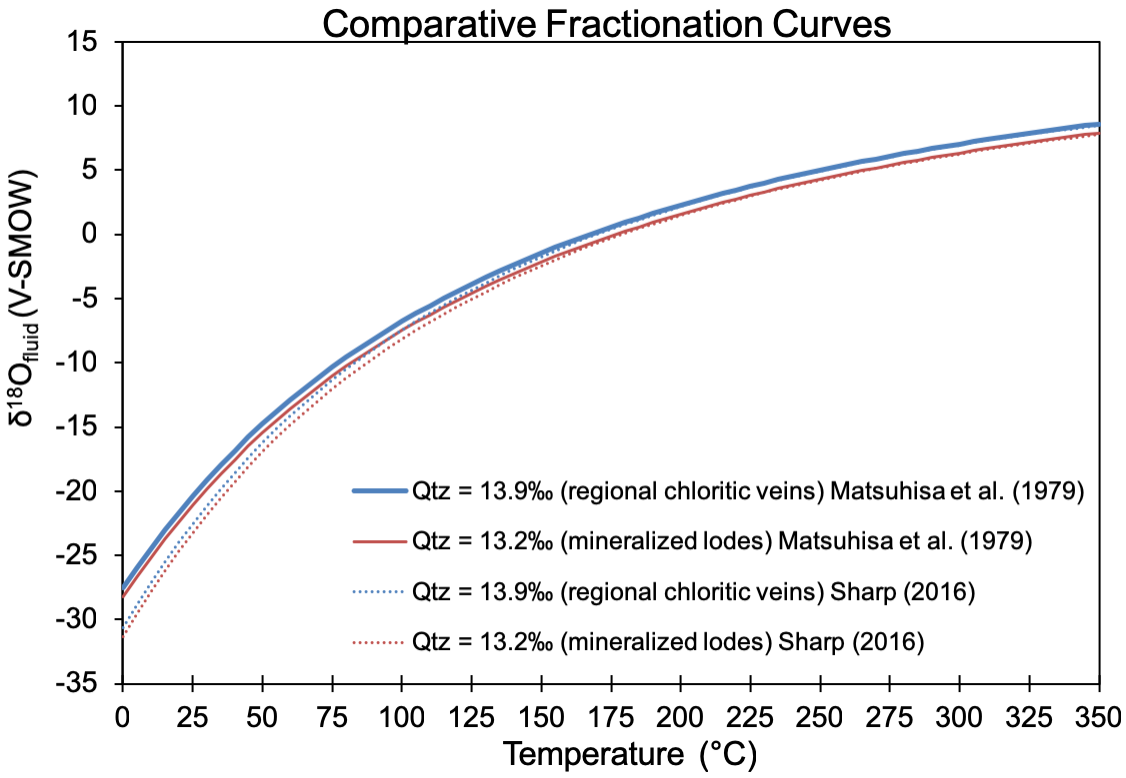

Fig. A.7. Fractionation curves for two example vein populations (+13.2 and +13.9‰) using the equations of Matsuhisa et al. (1979) and Sharp et al. (2016).

A.2 Sample lists

A.2.1 Nkana-Mindola

Table A.3 List of samples from Nkana-Mindola, including drillcore and open pit (OP) samples.

Sample	Source	Location	Borehole	Depth	Strike/Dip	Description
JAZ_35	Mopani Mines, Nkana	Mindola North Pit	OP			Silt/fine sandstone w/ malachite. No visible sulphides.
JAZ_36	Mopani Mines, Nkana	Mindola North Pit	OP			Malachite-rich siltstone.
JAZ_37	Mopani Mines, Nkana	Mindola North Pit	OP			Qtz-hosted mixed sulphides (siltstone host).
JAZ_38	Mopani Mines, Nkana	Mindola North Pit	OP			Bedding-parallel bn-rich qtz-carb vein in ore shale.
JAZ_39	Mopani Mines, Nkana	Mindola North Pit	OP			Euhedral QV along fault plane.
JAZ_40	Mopani Mines, Nkana	Mindola North Pit	OP			Qtz-hosted carrollite?
JAZ_41	Mopani Mines, Nkana	Nkana 'J' Pit	OP			Massive, barren, post-orogenic QV cutting S_1 in HW strata.
JAZ_42	Mopani Mines, Nkana	Nkana 'J' Pit	OP			Deformed mineralised QV within ore shale.
JAZ_43	Mopani Mines, Nkana	Nkana 'J' Pit	OP			Basement schist (actinolite).
JAZ_44	Mopani Mines, Nkana	Nkana 'J' Pit	OP			Barren QV tension gash array in FW sediments. Post-kinematic?
JAZ_45	Mopani Mines, Nkana	Nkana 'J' Pit	OP			QV w/ malachite in FW sediments. Pinches out along cleavage. Syn-kin?
JAZ_46	Mopani Mines, Nkana	Nkana 'J' Pit	OP			Massive sulphide + malachite (FW seds).
JAZ_47	Mopani Mines, Nkana	Nkana 'J' Pit	OP			Massive, barren QV cross-cutting S_1 fabric in FW seds.
JAZ_48	Mopani Mines, Nkana	Nkana 'Nose' Pit	OP			Barren, boudinaged syn-kin QV. Specular haematite?
JAZ_49	Mopani Mines, Nkana	Nkana 'Nose' Pit	OP			Basement schist.
JAZ_50	Mopani Mines, Nkana	Nkana 'Nose' Pit	OP			Ore shale w/ mineralised (bn-cpy), boudinaged carbonate veins.
JAZ_51	Mopani Mines, Nkana	Nkana 'Nose' Pit	OP			Boudinaged QV - syn-kin (barren?).
JAZ_52	Mopani Mines, Nkana	Mindola North Pit	MX 0236	190.5		Barren, discordant QV in siliceous dolomite.
JAZ_53	Mopani Mines, Nkana	Mindola North Pit	MX 0236	200.8		Spotted siliceous dolomite ore.
JAZ_54	Mopani Mines, Nkana	Mindola North Pit	MX 0236	219.1		Mineralised qtz-carb veins in siliceous rock
JAZ_55	Mopani Mines, Nkana	Mindola North Pit	MX 0236	224.2		Mineralised (bn-cpy) QV in siliceous dolomite ore (pre- to syn-kin).
JAZ_56	Mopani Mines, Nkana	Mindola North Pit	MX 0236	237.4		Mineralised (bn-cpy) QV in siliceous dolomite ore (pre- to syn-kin).
JAZ_57	Mopani Mines, Nkana	Mindola North Pit	MX 0236	197.2		Anhydrite-qtz-carb nodule in siliceous dolomite.
JAZ_58	Mopani Mines, Nkana	Mindola North Pit	MX 0236	266.2		Mineralised, banded siliceous dolomite and anhydrite.
JAZ_59	Mopani Mines, Nkana	Mindola North Pit	MX 0236	236.1		Pre- to syn-kin mineralised (bn-cpy) QV in siliceous dolomite ore.
JAZ_60	Mopani Mines, Nkana	Mindola North Pit	MX 0236	24		Conglom w/ anhydrite clasts.

Open pit locations: Mindola North: -12.77520, 28.16040; Nkana Central: -12.85433, 28.20853; Nkana South: -12.87708, 28.22500.

A.2.2 Nchanga and Lumwana

Table A.4 List of samples from the Nchanga and Lumwana deposits

Sample	Location	Description
	Nchanga	
NOP769 16	DDH (Nchanga OP)	Mineralised QV within 'The Feldspathic Quartzite' (UOB)
NOP27	Nchanga OP	Mineralised QV within 'The Feldspathic Quartzite' (UOB)
L128-11	DDH (Nchanga OP)	QV in footwall arkoses beneath the 'Lower Banded Shale' (lower part of LOB)
L128-12	DDH (Nchanga OP)	QV in footwall arkoses beneath the 'Lower Banded Shale' (lower part of LOB)
NOP21	Nchanga OP	Mineralised QV within arkoses of the LOB
NOP122	Nchanga OP	Barren QV within Nchanga Granite
NOP52	Nchanga OP	Barren QV within Nchanga Granite
	Lumwana	
1E-002	Lumwana OP	Massive discordant barren QV cross-cutting ore schist and hanging wall
1E-008	Lumwana OP	Boudinaged QV in weathered ore schist (bn-cpy)
1E-005	Lumwana OP	Discordant barren QV cross-cutting hanging wall sediments
1E-003	Lumwana OP	Discordant bifurcating barren QV cross-cutting hanging wall sediments
1E-009	Lumwana OP	Discordant QV cross-cutting hanging wall gneiss (local specular haematite)
MLW0291 52.9	Malundwe DDH	Weakly mineralised boudinaged QV parallel to fabric in ore schist footwall
MLW0291 50.85	Malundwe DDH	Discordant glassy QV w/ chl-bio alteration (footwall)
MLW0291 28.00	Malundwe DDH	Mineralised (bn-cpy) deformed QV in ore schist
EQMAL 083 94.43	Malundwe DDH	Mineralised (bn-cpy) deformed QV in ore schist
LUM0287 80.82	Lumwana DDH	Massive barren deformed QV in footwall
LUM0287 59.75	Lumwana DDH	Deformed QV with recrystallised sulphides (py-cpy) within ore schist

Nchanga samples from the suite of McGowan (2003). Open pit location: -12.511202, 27.858987.
Lumwana samples from the suite of Bernau (2007) and Nowecki (2014). Open pit location: -12.232733, 25.820063.
DDH = Diamond Drillhole
OP = Open Pit

A.2.3 Other Zambian samples

Table A.5. List of samples from the Mafuta prospect (Luswishi Dome)

Sample	Borehole	Depth (m)	Description
JAZ_17	CZSE0001	396.7	Chloritised gabbro (base of hole)
JAZ_18	CZSE0001	318.3	Qtz-sulphide (py) vein in chloritised gabbro
JAZ_19	CZSE0001	294.0	QV w/ py in fine gabbro
JAZ_20	CZSE0001	289.0	QV in silicified lithology (uppermost gabbro)
JAZ_21	CZSE0001	277.5	Mineralised carbonate veins in black shale (py-po-cpy?)
JAZ_22	CZSE0001	219.0	Spotted black shale
JAZ_23	CZSE0001	208.0	Massive sulphide (py-po)
JAZ_24	CZSE0001	186.0	Massive sulphide (py-po)
JAZ_25	CZSE0001	166.55	Silicified/altered shale
JAZ_26	CZSE0001	155.5	Unknown ("amphibolite schist"?)
JAZ_27	CZSE0014	289.8	Conglomerate-marble contact (thrust?)
JAZ_28	CZSE0014	269.6	QV in shale/fault zone
JAZ_29	CZSE0014	249.0	Pyritic laminated marble
JAZ_30	CZSE0014	196.2	Mineralised QV in marble (py-cpy)
JAZ_31	CZSE0014	180.1	Mineralised QV in marble (py-cpy)
JAZ_32	CZSE0014	167.2	Mineralised QV in marble (py-cpy)
JAZ_33	CZSE0014	136.0	Mineralised quartz-carbonate vein w/ dolomite (py-cpy)
JAZ_34	CZSE0014	58.0	Massive sulphide (py-po)

A.2.4 Zone 5 and Zone 5 North

Table A.6 List of samples from the Zone 5 and Zone 5 North prospects in Northwest Botswana

Sample	Borehole	Depth (m)	Description
KCB-Z5-01	HA-989-D	802.30	Ngwako Pan red sandstone
KCB-Z5-02	HA-989-D	795.05	S_1-parallel boudinaged qtz-carb vein with cc-bn
KCB-Z5-03	HA-989-D	770.00	40 cm wide S_1-parallel qtz-carb vein with cc-bn-cpy along margins
KCB-Z5-04	HA-989-D	762.90	15 cm wide mineralised qtz-carb vein with py-sph ± cpy
KCB-Z5-05	HA-929-D	654.95	6 cm wide qtz-carb-cpy-py vein in lower marl
KCB-Z5-06	HA-929-D	632.40	Intersection between 2 cross-cutting qtz-carb veins with bn-cc. Associated with cleavage-hosted mineralisation
KCB-Z5-07	HA-929-D	632.25	Laminated marl and carbonates with cleavage-hosted bn. Strong permeability control (less bn in silty layers)
KCB-Z5-08	HA-1049-D	1126.40	Pink boudinaged qtz-carb vein along S_1. Hosts minor bn-cc
KCB-Z5-09	HA-1049-D	1103.80	25 cm wide S_1-parallel qtz-carb vein with massive cc-bn along margins (in carb)
KCB-Z5-10	HA-1049-D	1077.05	12 cm wide zone of qtz-carb-sph veining in dark siltstone. Veins refolded/sheared along S_1
KCB-Z5-11	HA-1020-D	1190.90	Qtz-bn vein with irregular structure in dark siltstone
KCB-Z5-12	HA-1020-D	1172.90	Qtz-cpy vein approx S_1-parallel
KCB-Z5-13	HA-981-D	489.60	Carb-qtz-bn vein along marl-silt contact. Mineralised margins. Top of bn zone
KCB-Z5-14	HA-969-D	535.64	Barren QV in marker sandstone. Brittle tensional fracture during folding/deformation?
KCB-Z5-15	HA-957-D	645.34	6 cm wide qtz-carb-bn-cc parallel with fabric
KCB-Z5-16	HA-957-D	637.10	Qtz-carb-cpy-(bn) vein in dilational jog along cleavage plane in silt unit.
KCB-Z5-17	HA-957-D	633.20	8 cm wide qtz-carb-bn-(cc) vein in silt unit. Mineralised along margins. Boudinaged along fabric.
KCB-Z5-18	HA-1107-D	199.88	6 cm wide barren QV approx 200-250 m below D'Kar contact in sterilisation hole. Vein cross-cuts bedding
KCB-Z5-19	HA-929-D	552.50	Qtz-carb-sph-gal vein higher up in D'Kar strat. Hosted by fine grey fine sandstone. Possible conjugate pair = late extensional relaxation. 75 m above Cu-mineralised package.
KCB-Z5-20	HA-981-D	462.50	Qtz-carb massive veining with galena in tension gashes associated with parasitic fold approx. 23 m above Cu-mineralised package
KCB-Z5-21	HA-957-D	590.50	Qtz-carb-gl-py-sph vein in silty package separating marker sandstone (below) and another sandstone above. Vein is deformed and boudinaged - poss related to creation of permeability by shearing/strain accommodated by silty layer
KCB-Z5-22	HA-1049-D	970.00	Qtz-carb-sph vein in grey sandstone approx. 97 m above Cu-mineralisation
KCB-Z5-23	HA-1049-D	980.50	Qtz-carb-sph vein in grey sandstone approx. 107 m above Cu-mineralisation
KCB-Z5-24	HA-1049-D	988.00	Qtz-carb breccia inc. grey sandstone clasts/xenoliths approx. 115 m above Cu mineralisation
KCB-Z5N-01	HA-1099b-D	1096.42	FW qtz-carb vein in Ngwako Pan red sandstone. Minor cpy along margin
KCB-Z5N-02	HA-1085-D	412.00	0.50 m wide footwall qtz-carb vein. Contains hm & poss cc hosted in Ngwako Pan red sandstone. Approx. 8 m below D'Kar contact
KCB-Z5N-03	HA-1087-D	410.15	Qtz-carb vein in silt unit with cpy-hm. Some K-spar alteration along margins. Vein is folded with no obvious structure and includes wall rock xenoliths
KCB-Z5N-04	HA-1077-D	259.20	10 cm wide barren qtz-carb vein along S_0 in marl below mineralisation.
KCB-Z5N-05	HA-1077-D	240.85	Vuggy qtz-hm vein approx. 2 m above mineralisation in the marker sandstone
KCB-KH-01	Outcrop	718537, 7722260*	Dark grey fine grained metabasite. Abundant fractures & secondary epidote.
KCB-KH-02	Outcrop	714051, 7722923*	Fine grained metarhyolite from Kgwebe Hills
KCB-Ster-01	HA-1112-D	802.30	S_1-parallel 8 cm wide qtz-carb vein. Vuggy along upper contact. Hosted by altered metabasite

*co-ordinates reported in WGS84 / UTM zone 34S

A.2.5 Munster Basin

Table A.7 List of samples from the Munster Basin, Ireland

Sample	Location	Grid Ref*	Strike/Dip	Description
ALH-JD-01	Mt. Mine	V 58938, 45830	022/66 E	N-S lode intersecting large E-W vein S of the main Mt. Mine lode
ALH-JD-02	Mt. Mine	V 58977, 45831	-	Unaltered sandstone host rock with qtz veinlets hosting cpy
ALH-JD-03	Mt. Mine	V 59093, 46013	130/90	Regional chlorotic QV in folded blocky sandstone N of the main Mt. Mine
ALH-JD-04	Mt. Mine	V 58902, 46123	034/32 SE	1-2 m wide barren regional QV in core of anticline to the W of Mt. Mine
ALH-JD-05	Mt. Mine	V 58902, 46123	-	Bleached host sandstone from margin of vein sampled at same location
ALH-JD-06	Mt. Mine	V 58884, 45842	108/70 N	VQ from western end of large E-W lode, south of the main Mt. Mine lode
ALH-JD-07	Caminches	V 59495, 45882	-	VQ from spoil heap at adit entrance. Abundant py, cpy, bn & malachite
ALH-JD-08	Coom	V 59765, 45542	-	VQ from spoil heap by adit entrance. Py, cpy, bn & malachite.
ALH-JD-09	Coom	V 59772, 45490	100/75 N	Weakly mineralised VQ from large ~E-W vein running across hilltop
ALH-JD-10	Muckross Lake	V 94840, 85970	038/68 SE	Mineralised carbonate vein in Carboniferous limestone (cpy ± tenantite)
ALH-JD-11	Inch	Q 60510, 00285	126/42 N	VQ from massive blocky sandstone (N side of road cutting)
ALH-JD-12	Inch	Q 59955, 00173	134/50 NE	VQ from massive blocky sandstone (N side of road cutting)
ALH-JD-13	Inch	Q 59955, 00173	130/48 NE	Druzy VQ from massive blocky sandstone (N side of road cutting)
ALH-JD-14	Dooneen	V 57696, 48918	236/88 N	White-pink sugary VQ from main Dooneen lode (minor oxidised sulphides)
ALH-JD-15	Dooneen	V 57696, 48918	242/90	Grey-white VQ from main Dooneen lode (abundant cpy)
ALH-JD-16	Dooneen	V 57696, 48918	232/80 N	Mineralised VQ from Dooneen lode
ALH-JD-17	Dooneen	V 57674, 45985	130/86 S	Barren, cross-cutting conjugate veins in Allihies Sandstone Fm.
ALH-JD-18	Dooneen	V 57770, 46015	-	VQ from Dooneen spoil tip (abundant py + cpy + tenantite)
ALH-JD-19	Dooneen	V 57734, 46256	090/90	Barren chlorotic VQ along NE-SW trending fold (Allihies Sandstone Fm.)
ALH-JD-20	Dooneen	V 57769, 46269	108/58 S	Barren chlorotic vein in folded Allihies Sandstone Fm.
ALH-JD-21	Dooneen	V 57560, 45822	110/90	~SE-NW-trending barren VQ from coastal cliff section (Allihies Sandstone Fm.)
ALH-JD-22	Dooneen	V 57533, 45802	050/90	NE-SW-trending conjugate pair with ALH-JD-21
ALH-JD-23	Kealogue	V 58914, 44512	-	Glassy VQ from Kealogue spoil heap. Abundant cpy + py + bn

*Irish grid, squares V and Q

Appendix B Mafuta Fluid Study

The Mafuta prospect is located in the eastern part of Rio Tinto Exploration's (RTX) 'Copperzone' study area on the Luswishi Dome, approximately 100 km west of Kitwe, Zambia. The prospect is centred around a 7.8 × 3.4 km NNW-SSE-trending ellipsoidal structure, first delineated using airborne geophysical datasets and subsequently drilled by First Quantum Minerals and then RTX during 2014 and 2015. Upper Roan subgroup, Mwashya shales (and overlying Grand Conglomerate) and lower Nguba Group siltstones are present in the study area, all intruded by a series of variably altered gabbroic bodies. Based upon interpretations of geophysical datasets, along with drilling data, the 'Mafuta structure' has been interpreted by RTX geologists as a shallow-angle, flattened, NW-vergent recumbent sheath fold, bound by several high-angle fault zones. Elevated Cu grades correlate with magnetic susceptibility (pyrrhotite content) in Mwashya carbonaceous shales as well as lower Nguba strata in some boreholes, although pyrrhotitic Grand Conglomerate units in several boreholes show no mineralisation.

Fluid inclusion study:

Two boreholes, drilled by RTX in 2015, were logged and sampled during this study, with the aim of characterising palaeofluid conditions and comparing major cation and base metal concentrations with palaeofluids analysed from known deposits in the Zambian Copperbelt. Samples are listed in Table A.5.

After petrographic study, only two samples were found to host workable fluid inclusions (JAZ30 and JAZ33), both from borehole CZSE0014, located towards the SE of the Mafuta structure. Although the majority of multiphase primary fluid inclusions in both samples leaked at high temperatures, solid daughter phases were still present at temperatures up to 500°C, with rare intact inclusions undergoing total homogenisation between ~460-510°C. Based on these T_{hTOT} values, total salinities likely exceed 60 wt % NaCl + KCl equiv., however no inclusion population provided a sufficient quantity of consistent T_{hTOT} values to be deemed reliable for use as an internal standard during laser ablation ICP-MS analysis. As such, these fluid compositions are reported as ratios to Na in Table B.1. Sample JAZ_33 hosted several secondary fluid inclusion assemblages, characterised by the presence of a single, small halite cube, with typical phase proportions of 0.85:0.05:0.1 (L:V:S). These inclusions typically returned T_{hTOT} values of ~160-190°C and approx. 30 wt % NaCl equiv. (Fig. B.1).

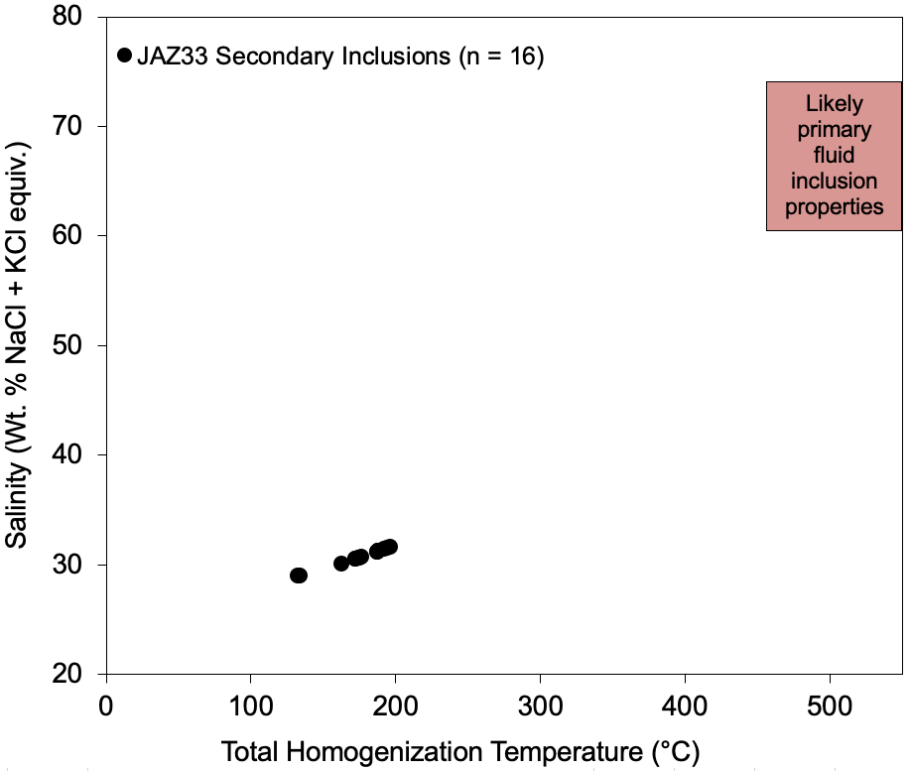

Fig. B.1. Salinity versus total homogenisation temperatures for secondary fluid inclusions from sample JAZ_33 at the Mafuta prospect. The majority of multiphase primary inclusions leaked at temperatures between ~300 and 500°C, prior to total homogenisation. Total homogenisation temperatures for four intact inclusions were used to estimate the likely field of temperature-salinity conditions applicable to primary fluid inclusion populations.

Net intensity element maps of daughter phases in the dried cavities of high temperature primary inclusion assemblages showed similar salt species to other ore fluids measured in this study, commonly consisting of coexisting halite and sylvite (Fig. B.2). Additionally, the presence of iron sulphide in several inclusions supports rare T_{hTOT} measurements which suggest these fluids were unusually high temperature (>450°C).

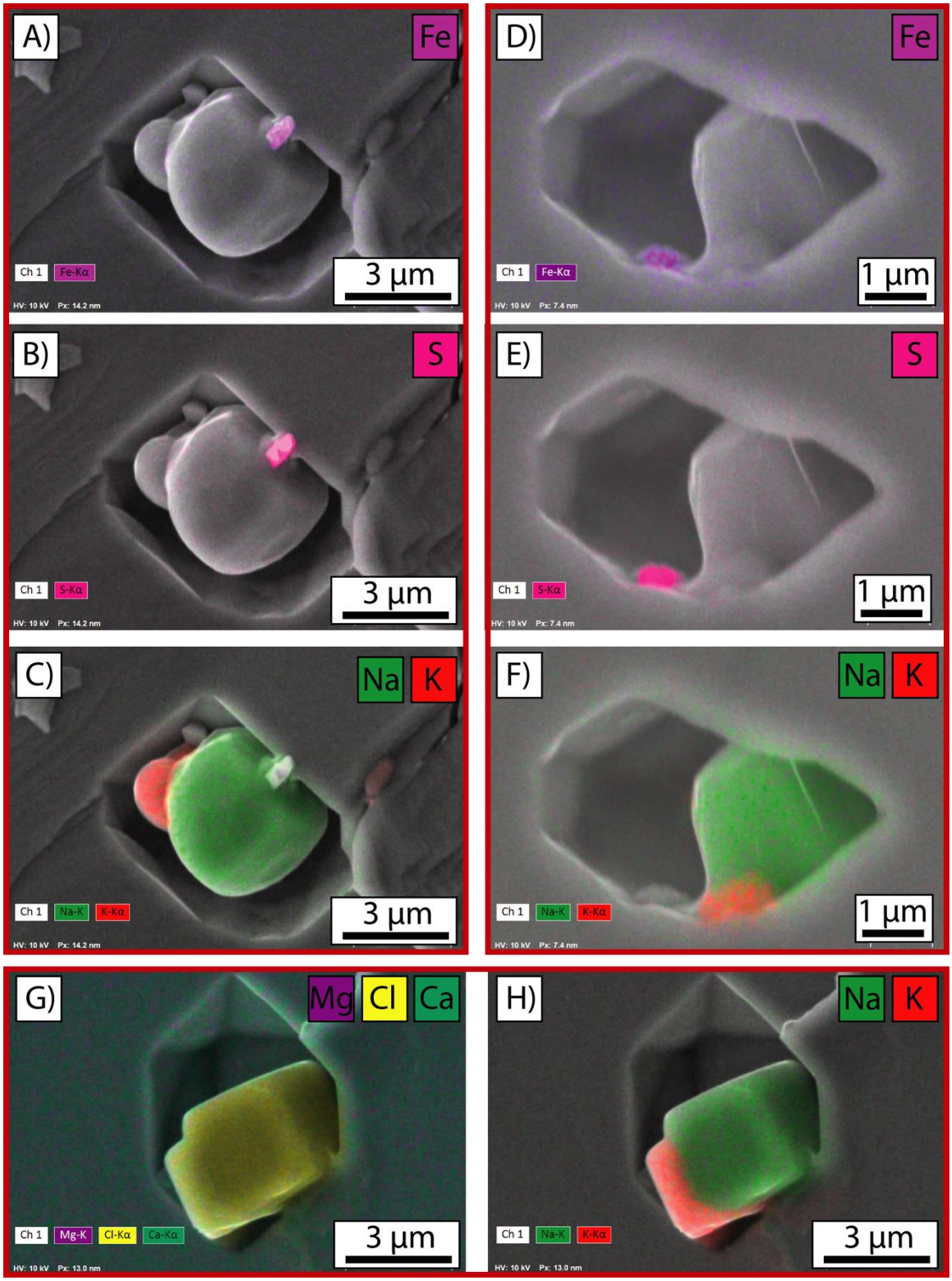

Fig. B.2. SEM net intensity element maps of daughter phases in high-temperature-salinity primary inclusions from sample JAZ_33 (Mafuta). Images A-C show an inclusion cavity hosting halite, sylvite, Fe-sulphide and a small aluminosilicate phase; D-F show a cavity hosting halite, sylvite and Fe-sulphide; G-H show a euhedral inclusion hosting euhedral halite and sylvite cubes.

Appendix B

Laser ablation ICP-MS:

The paucity of reliable T_{hTOT} measurements for high temperature-salinity primary fluid inclusion assemblages from Mafuta vein samples restricts the availability and reliability of salinity estimates which would ideally be used for internal standardisation of laser ablation ICP-MS results. As such, element abundances in these fluids are reported as ratios to Na in Table B.1. Element abundances in lower temperature-salinity secondary inclusions are reported as absolute concentrations in Table B.1, using Na as an internal standard.

Table B.1. Selected element concentrations in fluid inclusions from sample JAZ_33 (Mafuta)

Sample	Finc	^{7}Li	^{24}Mg	^{39}K	^{43}Ca	^{55}Mn	^{57}Fe	^{65}Cu	^{66}Zn	^{85}Rb	^{88}Sr	^{133}Cs	^{137}Ba	^{208}Pb
Absolute element concentrations in secondary fluid inclusions:														
JAZ33 Chip A	2	< 342.7	185.8	8725.6	< 26300.2	< 113.7	< 3096.6	< 33.1	< 101.1	29.7	223.9	6.7	94.8	< 7.9
JAZ33 Chip A	3	< 26	99.7	10179.4	6594.0	44.0	261.6	< 5.6	40.0	60.4	206.2	2.2	71.1	1.2
JAZ33 Chip A	4	< 283.2	110.3	2931.1	16171.8	< 85.3	< 2216	< 35.8	< 100.6	< 14	71.7	< 4.9	25.2	< 11.6
JAZ33 Chip A	5	< 213.2	211.6	10120.1	< 18366.9	< 86.4	< 2061.6	< 26.6	< 104.5	< 20.2	270.0	< 4	41.0	< 9.9
JAZ33 Chip A	7	24.5	17.9	10822.0	2477.4	15.7	< 310.1	< 3.8	30.6	29.8	143.6	< 0.5	67.9	< 1.3
JAZ33 Chip A	8	< 50.4	5050.3	7821.6	6585.3	156.0	< 466.3	< 6.9	373.6	35.1	119.0	< 1.3	42.8	12.9
JAZ33 Chip A	9	< 140	143.3	11300.0	13008.2	< 53.3	< 1192	< 16.8	< 53.6	40.0	224.6	3.7	106.8	< 5.4
JAZ33 Chip C	1	311.0	-	46224.9	-	9328.2	47651.1	100.2	1433.6	130.4	5434.5	18.6	4480.6	340.9
JAZ33 Chip C	1a	153.6	-	40763.8	-	4187.0	22300.2	26.6	367.7	72.0	2357.3	5.1	2146.9	336.7
JAZ33 Chip C	11	586.5	-	67361.2	-	16746.9	75351.5	124.8	2113.1	149.8	8858.1	9.2	6282.7	670.9
JAZ33 Chip D	1	< 591.8	278.2	12567.2	< 74786.2	< 261.7	< 7342.8	57.0	< 465.3	< 33.1	199.5	< 14	< 55.6	< 21.8
JAZ33 Chip D	2	70.9	121.6	14079.6	8929.5	< 18.5	< 435.6	< 3.8	< 39.9	52.2	289.1	2.8	33.6	< 1.5
JAZ33 Chip D	4	< 320.7	251.4	12609.6	< 38484.1	< 170.6	< 4454.2	< 56	< 341	< 30.3	478.0	17.0	82.5	< 26.8
JAZ33 Chip D	5	59.5	182.9	86943.0	6775.5	190.2	< 539.8	< 6.1	< 39.6	87.1	309.0	2.2	74.6	< 1.9
JAZ33 Chip D	6	< 213.5	69.3	13886.5	< 22976.9	< 86	< 2620	< 40	< 107.7	40.6	187.5	< 5.6	28.9	< 6
JAZ33 Chip D	6a	< 109.6	66.4	8832.7	< 11795.9	< 44.2	< 1345.1	< 20.5	57.6	45.7	197.4	3.5	25.3	< 3.1
Element ratios to Na in high-temperature-salinity primary fluid inclusions:														
JAZ33 Chip C	2	0.03	-	1.90	-	0.57	2.66	0.01	0.40	0.02	0.61	0.00	0.37	0.04
JAZ33 Chip C	3	0.01	-	1.82	-	-	-	0.00	0.05	0.01	0.04	0.00	0.04	0.02
JAZ33 Chip C	4	0.26	-	4.95	-	1.25	-	0.02	0.44	0.06	1.41	0.00	0.27	0.01
JAZ33 Chip C	6	0.14	-	8.17	-	2.54	7.61	0.01	1.02	0.04	1.31	0.01	0.15	0.07
JAZ33 Chip C	6a	0.15	-	5.41	-	1.67	3.16	0.00	0.47	0.04	1.48	0.01	0.16	0.03
JAZ33 Chip C	8	0.02	-	1.66	-	0.13	0.49	0.00	0.14	0.01	0.15	0.00	0.06	0.00
JAZ33 Chip C	9	0.08	-	5.36	-	0.60	1.32	0.01	0.23	0.04	0.77	0.01	0.24	0.05
JAZ33 Chip C	10	0.09	-	5.09	-	1.06	0.98	0.01	0.45	0.04	1.15	0.01	0.22	0.08
JAZ33 Chip C	11	0.00	-	0.56	-	0.14	0.63	0.00	0.02	0.00	0.07	0.00	0.05	0.01
JAZ33 Chip C	12	0.10	-	4.68	-	0.93	2.78	0.03	0.57	0.04	0.87	0.01	0.37	0.01
JAZ33 Chip C	13	0.09	-	3.02	-	0.41	-	0.01	0.34	0.03	0.92	0.01	0.55	0.02

*Ca and Mg not reported for dolomite-hosted inclusions. Co below LOD in all inclusions analysed.

Appendix B

The major cation budget of secondary fluid inclusions in sample JAZ_33 is dominated by Na, with lesser K and relatively minor Ca contributions. K/Na ratios average 0.19 (n = 16), which is comparable to those measured in post-kinematic fluids from Nkana-Mindola and Nchanga and shows no indication of interaction with earlier fertile ore fluids shown to have been present at lower stratigraphic levels across the Zambian Copperbelt. Base metal concentrations show no significant enrichment, despite the inclusions being hosted in a mineralised vein.

Primary inclusions from the same vein show distinct cation compositions, with a mean K/Na ratio of 3.9. This is significantly higher than can be realistically generated by evaporative processes and must, to some degree, reflect fluid-rock interactions. With an average Mn/Fe ratio of 0.4 (similar to ore fluids at Lumwana), these brines also show indications of being more reduced than ore fluids measured at Nkana-Mindola and Nchanga, which typically show Mn/Fe >0.6. Relatively reducing conditions and anomalously elevated fluid temperatures are further supported by the presence of Fe sulphide as a saturated daughter phase in several inclusions.

Although absolute concentrations of base metals cannot be reliably quantified, primary fluid inclusions in sample JAZ_33 returned a mean Cu/Na value of 0.01, indicating that at all reasonable estimates of salinity ($\sim 10^1$ wt % Na), Cu concentrations are on the order-of-magnitude of 10^2-10^3 ppm; broadly comparable to the most well-endowed ore fluids measured from Zambian Copperbelt deposits in this study. Interestingly, given the proximity of mineralised veins to several mafic intrusions, Co concentrations remained below the LOD in all primary inclusions from the Mafuta prospect.

Weak mineralisation of gabbroic bodies, as well as replacement of metamorphic 'spotting' in sediments proximal to intrusive bodies by Fe-(Cu)-sulphides indicates that mineralisation occurred after the emplacement of mafic intrusions through reduction of an oxidised brine, perhaps by *in situ* magmatic sulphides. Anomalously elevated homogenisation temperatures (>450°C), salinities (>60 wt % NaCl + KCl equiv.) and base metal concentrations, as well as the presence of Fe-sulphide daughter phases all indicate that primary fluids in mineralised veins at Mafuta are atypical sedimentary basin brines, perhaps implying a degree of interaction with previously emplaced mafic intrusions.

Although the scope of this fluid inclusion study was limited by the number of 'workable' samples obtained, as well as limitations on accurately estimating fluid salinities, initial findings suggest that primary fluid compositions share some similarities with proposed pre-orogenic bittern ore fluids present elsewhere in the Zambian Copperbelt. Further work on fluid inclusions, as well as trace element analyses of sulphides, is, however required in order to confirm a genetic relationship between the abundant gabbroic intrusive bodies and mineralisation at Mafuta.

Appendix C Digital Data Tables

Appendix C consists of digital data tables stored on a CD, the contents of which are detailed below:

C.1 Microthermometry Results

C.2 Microthermometry Calibration

C.3 Laser Raman Results

C.4 Laser Ablation ICP-MS Results

C.5 Stable Isotope Results

C.6 SEM-CL Images

C.7 Drillcore logs

List of References

Annels, A.E. 1974. Some aspects of the stratiformore deposits of the Zambian Copperbelt and their genetic significance. *In:* Bartholome, P. (ed.) *Gisements stratiformes et provinces cupriferes.* Liege: Centenaire Societe Geologique Belgique.

Annels, A.E. 1984. The geotectonic environment of Zambian copper-cobalt mineralization. *Journal of the Geological Society,* 141, 279-289.

Annels, A.E. 1989. Ore genesis in the Zambian Copperbelt, with particular reference to the northern sector of the Chambishi Basin. *Geological Association of Canada,* Special Paper 36, 427-452.

Anthony, E.Y., Reynolds, T.J. & Beane, R.E. 1984. Identification of daughter minerals in fluid inclusions using scanning electron microscopy and energy dispersive analysis. *American Mineralogist,* 69, 1053-1057.

Armstrong, R., Robb, L.J., Master, S., Kruger, F.J. & Mumba, P. 1999. New U-Pb age constraints on the Katangan sequence, Central African Copperbelt [abs]. *Journal of African Earth Sciences,* 28, 6-7.

Armstrong, R.A. 2000. Ion microprobe (SHRIMP) dating of zircons from granites, granulites and volcanic samples from Zambia. *Unpub. Rep.* Canberra.

Armstrong, R.A., Master, S. & Robb, L.J. 2005. Geochronology of the Nchanga Granite, and constraints on the maximum age of the Katanga Supergroup, Zambian Copperbelt. *Journal of African Earth Sciences,* 42, 32-40.

Audetat, A., Gunther, D. & Heinrich, C.A. 1998. Formation of a Magmatic-Hydrothermal Ore Deposit: Insights with LA-ICP-MS Analysis of Fluid Inclusions. *Science,* 279, 2091-2094.

Audetat, A., Gunther, D. & Heinrich, C.A. 2000. Causes for Large-Scale Metal Zonation around Mineralized Plutons: Fluid Inclusion LA-ICP-MS Evidence from the Mole Granite, Australia. *Economic Geology,* 95, 1563-1581.

Audetat, A., Pettke, T., Heinrich, C.A. & Bodnar, R.J. 2008. The Composition of Magmatic-Hydrothermal Fluids in Barren and Mineralized Intrusions. *Economic Geology,* 103, 877-908.

Bąbel, M. & Schreiber, B.C. 2014. Geochemistry of Evaporites and Evolution of Seawater. *In:* Turekian, K. & Holland, H. D. (eds.) *Treatise on Geochemistry (2nd Ed.).* Elsevier.

Bakker, R.J. 2003. Package FLUIDS; 1. Computer programs for analysis of fluid inclusion data and for modelling bulk fluid properties. *Chemical Geology,* 194, 3-23.

Banks, D.A., Green, R., Cliff, R.A. & Yardley, B.W.D. 2000. Chlorine isotopes in fluid inclusions: Determination of the origins of salinity in magmatic fluids. *Geochimica et Cosmochimica Acta,* 64, 1785-1789.

Barnes, H.L. 1979. Solubilities of ore minerals. *In:* Barnes, H. L. (ed.) *Geochemistry of hydrothermal ore deposits.* 2nd ed. New York: Wiley.

Barra, F., Broughton, D., Ruiz, J. & Hitzman, M.W. Multi-stage mineralization in the Zambian Copperbelt based on Re-Os isotope constraints. Geological Society of America, Abstracts with Program, 2004 Denver.

Bateman, A.M. 1930. Ores of the Northern Rhodesian Copperbelt. *Economic Geology,* 25, 365-418.

Batumike, M.J., Cailteux, J. & Kampunzu, A.B. 2007. Lithostratigraphy, basin development, base metal deposits, and regional correlations of the Neoproterozoic Nguba and Kundelungu rock successions, central African Copperbelt. *Gondwana Research,* 11, 432-447.

Behr, H.J., Ahrendt, H., Martin, H., Porada, H., Rohrs, J. & Weber, K. 1983. Sedimentology and Mineralogy of Upper Proterozoic Playa-Lake Deposits in the Damara Orogen. *In:* Martin, H. & Eder, F. W. (eds.) *Intracontinental Fold Belts.* Berlin-Heidelberg: Springer.

Benham, D.G., Greig, D.D. & Vink, B.W. 1976. Copper Occurrences of the Mwombezhi Dome Area, Northwestern Zambia. *Economic Geology,* 71, 433-442.

Bernau, R. 2007. *The Geology and Geochemistry of the Lumwana Basement Hosted Copper-Cobalt (Uranium) Deposits, NW Zambia.* Unpublished PhD thesis, University of Southampton.

Bernau, R., Roberts, S., Richards, M., Nisbet, B., Boyce, A. & Nowecki, J. 2013. The geology and geochemistry of the Lumwana Cu (± Co ± U) deposits, NW Zambia. *Mineralium Deposita,* 48, 137-153.

Binda, P.L. 1994. Stratigraphy of Zambian Copperbelt Orebodies. *Journal of African Earth Sciences,* 19, 251-264.

Bischoff, J.L., Radtke, A.S. & Rosenbauer, R.J. 1981. Hydrothermal Alteration of Graywacke by Brine and Seawater: Roles of Alteration and Chloride Complexing on Metal Solubilization at 200° and 350°C. *Economic Geology,* 76, 659-676.

Bodnar, R.J. 1993. Revised equation and table for determining the freezing point depression of H2O-NaCl solution. *Geochimica et Cosmochimica Acta,* 57, 683-684.

Bodnar, R.J., Burnham, C.W. & Sterner, S.M. 1985. Synthetic IIuid inclusions in natural quartz. III. Determination of phase equilibrium properties in the system H,O-NaCl to 1000°C and 1500 bars. *Geochemical Perspectives,* 49, 1861-1873.

Borg, G. 1995. Metallogenesis of Neoporterozoic basins in Namibia and Botswana. *Communications of the Geological Survey of Namibia,* 10, 109-119.

Borg, G. & Maiden, K. 1987. Alteration of late Middle Proterozoic volcanics and its relation to stratabound copper-silver mineralization along the margin of the Kalahari Craton in SW A/Namibia and Botswana. *Geochemistry and Mineralization of Proterozoic Volcanic Suites.* Geological Society Special Publication.

Borg, G., Piestrzynski, A., Bachmann, G.H., Puttmann, W., Walther, S. & Fiedler, M. 2012. An Overview of the European Kupferschiefer Deposits. *Economic Geology,* Special Publication 16, 455-486.

Bowers, T.S. & Helgeson, H.C. 1983. Calculation of the thermodynamic and geochemical consequences of nonideal mixing in the system H2O-CO2-NaCl on phase relations in geologic systems: metamorphic equilibria at high pressures and temperatures. *American Mineralogist,* 68, 1059-1075.

Box, S.E., Syusyura, B., Seltmann, R., Creaser, R.A., Dolgopolova, A. & Zientek, M.L. 2012. Dzhezkazgan and Associated Sandstone Copper Deposits of the Chu-Sarysu Basin, Central Kazakhstan. *Economic Geology,* Special Publication 16, 303-328.

Brems, D., Muchez, P., Sikazwe, O. & Mukumba, W. 2009. Metallogenesis of the Nkana copper–cobalt South Orebody, Zambia. *Journal of African Earth Sciences,* 55, 185-196.

Broughton, D.W., Hitzman, M.W. & Stephens, A. 2002. Exploration histroy and geology of the Kansanshi Cu(-Au) deposit, Zambia. *In:* Goldfarb, R. & Nielson, R. (eds.) *Integrated Methods for Discovery: Global Exploration in the 21st Century. Society of Economic Geologists Special Publication 9.* London: Society of Economic Geologists.

Broughton, D.W., Valorose, C.P., Coker, S.A., Spera, L., Venendaal, J.F. & Hitzman, M.W. 2004. Congolese-style hypogene and supergene copper mineralizationat the Kalengwa deposit, Zambia. *Geological Society of America Abstracts with Programs,* 36, 517.

Brown, A. 2017. Constraints on Conceptual and Quantitative Modeling of Early Diagenetic Sediment-Hosted Stratiform Copper Mineralization. *Minerals,* 7, 192.

Brown, A.C. 2009. A process-based approach to estimating the copper derived from red beds in the sediment-hosted stratiform copper deposit model. *Economic Geology,* 104, 857-868.

Brown, A.C. 2018. Latent volcanic heat and further unique aspects of early diagenetic stratiform copper mineralization in the White Pine-Presque Isle District, northern Michigan. *Mineralium Deposita,* 53, 721-728.

Brugger, J., Liu, W., Etschmann, B., Mei, Y., Sherman, D.M. & Testemale, D. 2016. A review of the coordination chemistry of hydrothermal systems, or do coordination changes make ore deposits? *Chemical Geology,* 447, 219-253.

Buckroyd, C.C. 2008. *Development of the 213nm UV Laser Ablation ICP-MS Technique for Fluid Inclusion Microanalysis and Application to Contrasting Magmatic-Hydrothermal Systems.* Unpublished PhD thesis, Imperial College London.

Bull, S., Selley, D., Broughton, D., Hitzman, M., Cailteux, J., Large, R. & Mcgoldrick, P. 2011. Sequence and carbon isotopic stratigraphy of the Neoproterozoic Roan Group strata of the Zambian copperbelt. *Precambrian Research,* 190, 70-89.

Burke, E.J. 2001. Raman microspectrometry of fluid inclusions. *Lithos,* 55, 139-158.

Cailteux, J. & Kampunzu, A.B. 1995. The Katangan tectonic breccias in the Shaba province (Zaire) and their genetic significance. *In:* Wendorff, M. & Tack, L. (eds.) *Late Proterozoic Belts in Central Africa.* Tervuren, Belgique: Musee Royal de lAfrique Centrale.

Campbell, A.R., Banks, D.A., Phillips, D. & Yardley, B.W.D. 1995. Geochemistry of Th-U-REE Mineralizing Magmatic Fluids, Capitan Mountains, New Mexico. *Economic Geology,* 90, 1271-1287.

Candela, P.A. & Holland, H.D. 1984. The partitioning of copper and molybdenum between silicate melts and aqueous fluids. *Geochimica et Cosmochimica Acta,* 48, 373-380.

Carpenter, A.B., Trout, M.L. & Pickett, E.E. 1974. Preliminary Report on the Origin and Chemical Evolution of Lead-and Zinc-Rich Oil Field Brines in Central Mississippi. *Economic Geology,* 69, 1191-1206.

Cathles, L.M., Oszczepalski, S. & Jowett, E.C. 1993. Mass balance evaluation of the late diagenetic hypothesis for Kupferschiefer Cu mineralization in the Lubin Basin of southwestern Poland. *Economic Geology,* 88, 948-956.

Catterall, D. 2017. *Personal Communication*.

Clayton, G., Haughey, N., Sevastopulo, G.D. & Burnett, R.D. 1989. *Thermal maturation levels in the Devonian and carboniferous of Ireland,* Dublin: Geological Survey of Ireland.

Clemmey, H. 1974. Sedimentary Geology of a Late Precambrian Copper Deposit at Kitwe, Zambia. *In:* Bartholome, P., De Magnee, I., Evrard, P. & Moreau, J. (eds.) *Gisements Stratiformes et Provinces Cuprifères.* Liège: Société Géologique de Belgique.

Coe, K. & Selwood, E.B. 1963. The Stratigraphy and Structure of Part of the Beara Peninsula, Co. Cork. *Proceedings of the Royal Irish Academy. Section B: Biological, Geological, and Chemical Science,* 63, 33-59.

Connolly, K.A., Walter, L.M., Baadsgaard, H. & Longstaffe, F.J. 1990. Origin and evolution of formation waters, Alberta Basin, Western Canada Sedimentary Basin. I. Chemistry. *Applied Geochemistry,* 5, 375-395.

Cooke, D.R., Bull, S., Large, R. & Mcgoldrick, P. 2000. The Importance of Oxidized Brines for the Formation of Australian Proterozoic Stratiform Sediment-hosted Pb-Zn (Sedex) Deposits. *Economic Geology,* 95, 1-18.

Cosi, M., De Bonis, A., Gosso, G., Hunziker, J., Martinotti, G., Moratto, S., Robert, J.P. & Ruhlman, F. 1992. Late Proterozoic thrust tectonics, high pressure metamorphism and uranium mineralization in the Domes Area, Lufilian Arc, northwestern Zambia. *Precambrian Research,* 58, 215-240.

Croaker, M.R.D. 2011. *Nkana-Mindola Sediment-hosted Cu-Co Deposit.* Unpublished PhD thesis, University of Tazmania.

Cupric Canyon Capital. 2019. *Zone 5 Resources and Exploration* [Online]. Available: https://www.cupriccanyon.com/development-exploration/zone-5-resources [Accessed 04/01/2019 2019].

Daly, M.C., Chakraborty, S.K., Kasolo, P., Musiwa, M., Mumba, P., Naidu, B., Namateba, C., Ngambi, O. & Coward, M.P. 1984. The Lufilian arc and Irumide belt of Zambia: results of a geotraverse across their intersection. *Journal of African Earth Sciences,* 2, 311-318.

Darnley, A.G., 1960, Petrology of some Rhodesian Copperbelt orebodies and associated rocks: Institute of Mining and Metallurgy Transactions, v. 69, p 137-173.

Davidson, D.M. 1931. The geologyand ore deposits of Chambishi, Northern Rhodesia. *Economic Geology,* 26, 131-152.

De Swardt, A.M.J. & Drysdall, A.R. 1964. Precambrian geology and structure in central Northern Rhodesia. *Memoirs Geological Survey of Northern Rhodesia,* 2, 82.

De Waele, B. & Fitzsimons, I.C.W. The age and detrital fingerprint of the Muva Supergroup of Zambia: molassic deposition to the southwest of the Ubendian Belt. Geoscience Africa conference, 2004, University of the Witwatersrand, Johannesburg, South Africa. 162-163.

Dewaele, S., Muchez, P., Vets, J., Fernandez-Alonzo, M. & Tack, L. 2006. Multiphase origin of the Cu–Co ore deposits in the western part of the Lufilian fold-and-thrust belt, Katanga (Democratic Republic of Congo). *Journal of African Earth Sciences,* 46, 455-469.

Donnelly, T., Waldron, S., Tait, A., Dougans, J. & Bearhop, S. 2001. Hydrogen isotope analysis of natural abundance and deuterium-enriched waters by reduction over chromium on-line to a dynamic dual inlet isotope-ratio mass spectrometer. *Rapid Communications in Mass Spectrometry,* 15, 1297-1303.

Duffett, M., Sebagenzi, S. & Selley, D. 2010. Gravity and Magnetics of the Central African Copperbelt: AMIRA P872 Sediment-hosted copper deposits of Congolese, Zambian and central Australian basin systems, Final Report, July 2010. 49-78.

Eglinger, A., Vanderhaeghe, O., André-Mayer, A.-S., Goncalves, P., Zeh, A., Durand, C. & Deloule, E. 2016. Tectono-metamorphic evolution of the internal zone of the Pan-African Lufilian orogenic belt (Zambia): Implications for crustal reworking and syn-orogenic uranium mineralization. *Lithos,* 240-243, 167-188.

El Desouky, H.A., Muchez, P. & Cailteux, J. 2009. Two Cu–Co sulfide phases and contrasting fluid systems in the Katanga Copperbelt, Democratic Republic of Congo. *Ore Geology Reviews,* 36, 315-332.

Etschmann, B.E., Liu, W., Testemale, D., Müller, H., Rae, N.A., Proux, O., Hazemann, J.L. & Brugger, J. 2010. An in situ XAS study of copper(I) transport as hydrosulfide complexes in hydrothermal solutions (25–592°C, 180–600bar): Speciation and solubility in vapor and liquid phases. *Geochimica et Cosmochimica Acta,* 74, 4723-4739.

F., Q.M. 2019. *First Quantum Minerals Ltd. - Our Business - Operating Mines - Kansanshi* [Online]. Available: http://www.first-quantum.com/Our-Business/operating-mines/Kansanshi/ [Accessed 30/01/2019 2017].

Fleischer, V.D., Garlick, W.G. & Haldane, R. 1976. Geology of the Zambian Copperbelt. *In:* Wolf, K. H. (ed.) *Handbook of strata-bound and stratiform ore deposits - II Regional studies and specific deposits.* Amsterdam, Netherlands.

Frelinger, S.N., Ledvina, M.D., Kyle, J.R. & Zhao, D. 2015. Scanning electron microscopy cathodoluminescence of quartz: Principles, techniques and applications in ore geology. *Ore Geology Reviews,* 65, 840-852.

Frezzotti, M.L., Tecce, F. & Casagli, A. 2012. Raman spectroscopy for fluid inclusion analysis. *Journal of Geochemical Exploration,* 112, 1-20.

Fusswinkel, T., Wagner, T., Walle, M., Wenzel, T., Heinrich, C.A. & Markl, G. 2013. Fluid mixing forms basement-hosted Pb-Zn deposits: Insight from metal and halogen geochemistry of individual fluid inclusions. *Geology,* 41, 679-682.

Fyfe, W.S., Price, N.J. & Thompson, A.B. 1978. *Fluids in the Earth's crust,* Amsterdam: Elsevier.

Garlick, W.G. 1961. The syngenetic theory. *In:* Mendelsohn, F. (ed.) *The geology of the Northern Rhodesian Copperbelt.* London: MacDonald & Co. (publishers) Ltd.

Gill, W.D. 1962. The Variscan fold belt in Ireland. *In:* Coe, K. (ed.) *Some Aspects of the Variscan Fold Belt.* Manchester: Manchester University Press.

Goldstein, R.H. & Reynolds, T.J. 1994. Systematics of fluid inclusions in diagenetic minerals. *Sepm Short Course,* 32, 199.

Gorman, A. 2013. *Constraining a genetic model for copper - silver mineralisation in the Kalahari Copperbelt, Botswana - mineralogy, geochemistry and structure.* Unpublished MGeol thesis, University of Leicester.

Gotze, J., Plotze, M. & Habermann, D. 2001. Origin, spectral characteristics and practical applications of the cathodoluminescence (CL) of quartz - a review. *Mineralogy and Petrology,* 71, 225-250.

Graham, J.R. 2009. Devonian. *In:* Holland, C. H. & Sanders, I. S. (eds.) *The Geology of Ireland (2nd ed.).* Edinburgh: Dunedin Academic Press.

Gray, D.R., Foster, D.A., Goscombe, B., Passchier, C.W. & Trouw, R.a.J. 2006. 40Ar/39Ar thermochronology of the Pan-African Damara Orogen, Namibia, with implications for tectonothermal and geodynamic evolution. *Precambrian Research,* 150, 49-72.

Greyling, L.N. 2009. *Fluid evolution and characterisation of mineralising solutions in the Central African Copperbelt.* Unpublished PhD thesis, University of the Witwatersrand.

Greyling, L.N., Robb, L.J., Master, S., Boiron, M.C. & Yao, Y. 2005. The nature of early basinal fluids in the Zambian Copperbelt: A case study from the Chambishi deposit. *Journal of African Earth Sciences,* 42, 159-172.

Gunther, D., Audetat, A., Frischknecht, R. & Heinrich, C.A. 1998. Quantitative analysis of major, minor and trace elements in fluid inclusions using laser ablation– inductively coupled plasma mass spectrometry. *Journal of Analytical Atomic Spectrometry,* 13, 263-270.

Gunther, D., Frischknecht, R. & Muschenborn, H.J. 1997. Direct liquid ablation: a new calibration strategy for laser ablation-ICP-MS microanalysis of solids and liquids. *Fresenius Journal of Analytical Chemistry,* 359, 390-393.

Haas, J.L. 1976. Physical properties of the coexisting phases and thermochemical properties of the H2O component in boiling NaCl solutions. (Preliminary steam tables for NaCl solutions). *U.S. Geological Survey Bulletin,* 1421-A.

Haddon, I.G. & Mccarthy, T.S. 2005. The Mesozoic–Cenozoic interior sag basins of Central Africa: the Late-Cretaceous–Cenozoic Kalahari and Okavango basins. *Journal of African Earth Sciences,* 43, 316-333.

Hall, W.S. 2013. *Geology and Paragenesis of the Boseto Copper Deposits, Kalahari Copperbelt, Northwest Botswana.* MSc thesis, Colorado School of Mines.

Hall, W.S. 2017. *Geochronology, magnetic lithostratigraphy, and the tectonostratigraphic evolution of the late Meso- to Neoproterozoic Ghanzi Basin in Botswana and Namibia, and implications for Cu-Ag mineralization in the Kalahari Copperbelt.* PhD thesis, Colorado School of Mines.

Hall, W.S., Hitzman, M.W., Kuiper, Y., Kylander-Clark, A.R.C., Holm-Denoma, C.S., Moscati, R.J., Plink-Bjorklund, P. & Enders, S. 2018. Igneous and detrital zircon U-Pb and Lu-Hf geochronology of the late Meso- to Neoproterozoic northwest Botswana rift: Maximum depositional age and provenance of the Ghazi Group, Kalahari Copperbelt, Botswana and Namibia. *Precambrian Research,* 318, 133-155.

Halliday, A.N. & Mitchell, J.G. 1983. K-Ar ages of clay concentrations from Irish orebodies and their bearing on the timing of mineralisation. *Transactions of the Royal Society of Edinburgh,* 74, 1-14.

Hanson, R.E., Martin, M.W., Bowring, S.A. & Munyanyiwa, H. 1998. U-Pb zircon age for the Umkondo dolerites, eastern Zimbabwe: 1.1Ga large igneous province in southern Africa-East Antarctica and possible Rodinia correlations. *Geology,* 26, 1143-1146.

Hardie, L.A. 1996. Secular variation in seawater chemistry: An explanation for the coupled secular variation in the mineralogies of marine limestones and potash evaporates over the past 600 my. *Geology,* 24, 279-283.

Hassan, A., Jamshid, S. & Balandeh, A. 2016. Metallogenesis of the sediment-hosted stratiform Cu deposits of the Ravar Copper Belt (RCB), Central Iran. *Ore Geology Reviews,* 81, 369-395.

Hegenberger, W. & Burger, A.J. 1985. The Oorlogsende Porphyry Member, South West Africa/Namibia: its age and regional setting. *South West Africa/Namibia Geol. Surv. Commun.,* 1, 23-29.

Heijlen, W., Banks, D.A., Muchez, P., Stensgard, B.M. & Yardley, B.W.D. 2008. The Nature of Mineralizing Fluids of the Kipushi Zn-Cu Deposit, Katanga, Democratic Republic of Congo: Quantitative Fluid Inclusion Analysis using Laser Ablation ICP-MS and Bulk Crush-Leach Methods. *Economic Geology,* 103, 1459-1482.

Heinrich, C.A., Pettke, T., Halter, W.E., Aigner-Torres, M., Audétat, A., Günther, D., Hattendorf, B., Bleiner, D., Guillong, M. & Horn, I. 2003. Quantitative multi-element analysis of minerals, fluid and melt inclusions by laser-ablation inductively-coupled-plasma mass-spectrometry. *Geochimica et Cosmochimica Acta,* 67, 3473-3497.

Heinrich, C.A., Ryan, C.G., Mernagh, T.P. & Eadington, P.J. 1992. Segregation of Ore Metals between Magmatic Brine and Vapor: A Fluid Inclusion Study Using PIXE Microanalysis. *Economic Geology,* 87, 1566-1583.

Helgeson, H.C. 1970. Description and Interpretation of Phase Relations in Geochemical Processes Involving Aqueous Solutions. *American Journal of Science,* 268, 415-438.

Hitzman, M.W. 2000. Source basins for sediment-hosted stratiform Cu deposits: implications for the structure of the Zambian Copperbelt. *Journal of African Earth Sciences,* 30, 855-863.

Hitzman, M.W. 2010. The basement-hosted Samba copper prospect, Zambian Copperbelt. In: Selley, D., Bull, S. & Hitzman, M.W. 2010. *Sediment-hosted copper deposits of Congolese,*

Zambina and central Australian basin systems. CODES-CSM/AMIRA P872 Final Report, 325-336.

Hitzman, M.W., Broughton, D., Selley, D., Woodhead, J., Wood, D. & Bull, S. 2012. The Central African Copperbelt: Diverse Stratigraphic, Structural, and Temporal Settings in the World's Largest Sedimentary Copper District. *Economic Geology,* Special Publication 16, 487-514.

Hitzman, M.W., Kirkham, R., Broughton, D., Thorson, J. & Selley, D. 2005. The Sediment-Hosted Stratiform Copper Ore System. *Economic Geology,* 100, 609-642.

Hitzman, M.W., Selley, D. & Bull, S. 2010. Formation of Sedimentary Rock-Hosted Stratiform Copper Deposits through Earth History. *Economic Geology,* 105, 627-639.

Hoffmann, K.H., Condon, D.J., Bowring, S.A. & Crowley, J.L. 2004. U-Pb zircon date from the Neoproterozoic Ghaub Formation, Namibia: Constraints on Marinoan glaciation. *Geology,* 32, 817.

Hoffmann, P.F. & Li, Z.X. 2009. A palaeogeographic context for Neoproterozoic glaciation. *Palaeogeography, Palaeoclimatology, Palaeoecology,* 277, 158-172.

Horita, J., Zimmermann, H. & Holland, H.D. 2002. Chemical evolution of seawater during the Phanerozoic: Implictions from the record of marine evaporites. *Geochimica et Cosmochimica Acta,* 66, 3733-3756.

Horstmann, U.E., Ahrendt, H., Clauer, N. & Porada, H. 1990. The metamorphic history of the Damaran Orogen based on K/Ar data of detrital white micas from the Nama Group, Namibia. *Precambrian Research,* 48, 41-61.

Hudson, R.G.S., Clarke, M.J. & Brennand, T.P. 1966. The Lower Carboniferous (Dinantian) stratigraphy of the Castleisland area, Co. Kerry. *Scientific Proceedings of the Royal Dublin Society,* A2, 297-317.

Jackson, M., Warin, O., Woad, G. & Hudec, M. 2003. Neoproterozoic allochthonous salt tectonics during the Lufilian orogeny in the Katangan Coppebelt, central Africa. *Geological Society of America Bulletin,* 115, 314-330.

Jackson, S.E. 2008. Calibration Strategies for Elemental Analysis by LA-ICP-MS. *In:* Sylvester, P. J. (ed.) *Laser Ablation ICP-MS in Earth Sciences: Current Practices and Outstanding Issues.* Mineralogical Association of Canada Short Course Volume 40.

James, A. & Graham, J.R. 1995. Stratigraphy and structure of Devonian fluvial sediments, western Beara Peninsula, south-west Ireland. *Geological Journal,* 30, 165-182.

Jochum, K.P., Weis, U., Stoll, B., Kuzmin, D., Yang, Q., Raczek, I., Jacob, D.E., Stracke, A., Birbaum, K., Frick, D.A., Günther, D. & Enzweiler, J. 2011. Determination of Reference Values for NIST SRM 610-617 Glasses Following ISO Guidelines. *Geostandards and Geoanalytical Research,* 35, 397-429.

John, T., Schenk, V., Haase, K., Scherer, E. & Tembo, F. 2003. Evidence for a Neoproterozoic ocean in south-central Africa from mid-oceanic-ridge–type geochemical signatures and pressure-temperature estimates of Zambian eclogites. *Geology,* 31, 243.

John, T., Schenk, V., Mezger, K. & Tembo, F. 2004. Timing and PT Evolution of Whiteschist Metamorphism in the Lufilian Arc–Zambezi Belt Orogen (Zambia): Implications for the Assembly of Gondwana. *The Journal of Geology,* 112, 71-90.

Johnson, S.P., Rivers, T. & De Waele, B. 2005. A review of the Mesoproterozoic to early Palaeozoic magmatic and tectonothermal history of south-central Africa: implications for Rodinia and Gondwana. *Journal of the Geological Society,* 162, 433-450.

Jones, G.L. 1992. Irish Carboniferous conodonts record maturation levels and the influence of tectonism, igneous activity and mineralization. *Terra Nova,* 4, 238-244.

Jordaan, J. 1961. Nkana. *In:* Mendelsohn, F. (ed.) *The Geology of the Northern Rhodesian Copperbelt.* London: MacDonald.

Jowett, E.C. 1986. Genesis of Kupferschiefer Cu-Ag deposits by convective flow of Rotliegends brines during Triassic rifting. *Economic Geology,* 81, 1823-1837.

Jowett, E.C. 1991. The evolution of ideas about the genesis of stratiform copper-silver deposits. *Economic Geology Monograph 8,* 117-132.

Kah, L.C., Lyons, T.W. & Frank, T.D. 2004. Low marine sulphate and protracted oxygenation of the Proterozoic beosphere. *Nature,* 431, 834-838.

Kamenetsky, V.S., Achterbergh, E., Ryan, C.G., Naumov, V.B., Mernagh, T.P. & Davidson, P. 2002. Extreme chemical heterogeneity of granite-derived hydrothermal fluids: An example from inclusions in a single crystal of miarolitic quartz. *Geology,* 30, 459-462.

Kampunzu, A.B., Akanyang, P., Mapeo, R.B.M., Modie, B.N. & Wendorff, M. 1998. Geochemistry and tectonic significance of the Mesoproterozoic Kgwebe metavolcanic rocks in northwest

Botswana: implications for the evolution of the Kibaran Namaqua-Natal Belt. *Geological Magazine,* 135, 669-683.

Kampunzu, A.B., Armstrong, R.A., Modisi, M.P. & Mapeo, R.B.M. 2000a. Ion Microprobe U-Pb ages on detrital zircon grains from the Ghanzi Group: implications for the identification of Kibaran-age crust in northwest Botswana. *Journal of African Earth Sciences,* 30, 579-587.

Kampunzu, A.B. & Cailteux, J. 1999. Tectonic Evolution of the Lufilian Arc (Central Africa Copper Belt) During Neoproterozoic Pan African Orogenesis. *Gondwana Research,* 2, 401-421.

Kampunzu, A.B., Tembo, F., Matheis, G., Kapenda, D. & Huntsman-Mapila, P. 2000b. Geochemistry and Tectonic Setting of Mafic Igneous Units in the Neoproterozoic Katangan Basin, Central Africa: Implications for Rodinia Break-up. *Gondwana Research,* 3, 125-153.

Kelly, W.C. & Burgio, P.A. 1983. Cryogenic scanning electron microscopy of fluid inclusions in ore and gangue minerals. *Economic Geology,* 78, 1262-1267.

Kennedy, K., Eyles, N. & Broughton, D. 2018. Basinal setting and origin of thick (1.8 km) mass-flow dominated Grand Conglomerat diamictites, Kamoa, Democratic Republic of Congo: Resolving climate and tectonic controls during Neoproterozoic glaciations. *Sedimentology, DOI: 10.1111/sed.12494*.

Key, R.M., Liyungu, A.K., Njamu, F.M., Somwe, V., Banda, J., Mosley, P.N. & Armstrong, R.A. 2001. The western arm of the Lufilian Arc in NW Zambia and its potential for copper mineralization. *African Earth Sciences,* 33, 503-528.

Key, R.M. & Mapeo, R.B.M. 1999. The Mesoproterozoic history of Botswana and the relationship of the NW Botswana Rift to Rodinia. *Episodes,* 22, 118-122.

Kovalevych, V., Marshall, T., Peryt, T., Petrychenko, O. & Zhukova, S. 2006. Chemical composition of seawater in Neoproterozoic: Results of fluid inclusion study of halite from Salt Range (Pakistan) and Amadeus Basin (Australia). *Precambrian Research,* 144, 39-51.

Koziy, L., Bull, S., Large, R. & Selley, D. 2009. Salt as a fluid driver, and basement as a metal source, for stratiform sediment-hosted copper deposits. *Geology,* 37, 1107-1110.

Large, R., Mukherjee, I., Gregory, D.D., Steadman, J.A., Maslennikov, V.V. & Meffre, S. 2017. Ocean and Atmosphere Geochemical Proxies Derived from Trace Elements in Marine Pyrite: Implications for Ore Genesis in Sedimentary Basins. *Economic Geology,* 112, 423-450.

Lecumberri-Sanchez, P., Steele-Macinnis, M. & Bodnar, R.J. 2012. A numerical model to estimate trapping conditions of fluid inclusions that homogenize by halite disappearance. *Geochimica et Cosmochimica Acta,* 92, 14-22.

Lehmann, J., Master, S., Rankin, W., Milani, L., Kinnaird, J.A., Naydenov, K.V., Saalmann, K. & Kumar, M. 2015. Regional aeromagnetic and stratigraphic correlations of the Kalahari Copperbelt in Namibia and Botswana. *Ore Geology Reviews,* 71, 169-190.

Litherland, M. 1982. The geology of the area around Mamuno and Kalkfontein, Ghanzi District, Botswana. Lobatse, Botswana: Geological Survey Department, Ministry of Mineral Resources and Water Affairs.

Liu, W. & Mcphail, D.C. 2005. Thermodynamic properties of copper chloride complexes and copper transport in magmatic-hydrothermal solutions. *Chemical Geology,* 221, 21-39.

Longerich, H.P., Jackson, S.E. & Günther, D. 1996. Inter-laboratory note. Laser ablation inductively coupled plasma mass spectrometric transient signal data acquisition and analyte concentration calculation. *Journal of Analytical Atomic Spectrometry,* 11, 899-904.

Lowenstein, T.K., Hardie, L.A., Timofeeff, M.N. & Demicco, R.V. 2003. Secular variation in seawater chemistry and the origin of calcium chloride basinal brines. *Geology,* 31, 857-860.

Lowenstein, T.K., Timofeeff, M.N., Brennan, S.T., Hardie, L.A. & Demicco, R.V. 2001. Oscillations in Phanerozoic Seawater Chemistry: Evidence from Fluid Inclusions. *Science,* 294, 1086-1088.

Maccarthy, I.J. 1990. Alluvial sedimentation patterns in the Munster Basin, Ireland. *Sedimentology,* 34, 685-712.

Maccarthy, I.J. 2007. The South Munster Basin of southwest Ireland. *Journal of Maps,* 3, 149-172.

Maiden, K. & Borg, G. 2011. The Kalahari Copperbelt in Central Namibia: Controls on Copper Mineralization. *Society of Economic Geologists Newsletter,* 87, 14-19.

Manger, G.E. 1963. Porosity and Bulk Density of Sedimentary Rocks. Washington: United States Department of the Interior and the US Geological Survey.

Marshall, D.J. 1988. *Cathodoluminescence of geological materials,* Boston: Unwin Hyman.

Master, S., Rainaud, C., Armstrong, R.A., Phillips, D. & Robb, L.J. 2005. Provenance ages of the Neoproterozoic Katanga Supergroup (Central African Copperbelt), with implications for basin evolution. *Journal of African Earth Sciences,* 42, 41-60.

Matsuhisa, Y., Goldsmith, J.R. & Clayton, R.N. 1979. Oxygen isotopic fractionation in the system quartz-albite-anorthite-water. *Geochimica et Cosmochimica Acta,* 43, 1131-1140.

Mccaffrey, M.A., Lazar, B. & Holland, H.D. 1987. The Evaporation Path of Seawater and the Coprecipitation of Br- and K+ with Halite. *SEPM Journal of Sedimentary Research,* 57, 928-938.

Mccaig, A.M., Tritlla, J. & Banks, D.A. 2000. Fluid mixing and recycling during Pyrenean thrusting: Evidence from fluid inclusion halogen ratios. *Geochimica et Cosmochimica Acta,* 64, 3395-3412.

Mcgowan, R.R. 2003. *The Origin of the Nchanga Copper-Cobalt Deposits of the Zambian Copperbelt.* PhD thesis, University of Southampton, UK.

Mcgowan, R.R., Roberts, S. & Boyce, A.J. 2006. Origin of the Nchanga copper–cobalt deposits of the Zambian Copperbelt. *Mineralium Deposita,* 40, 617-638.

Mcgowan, R.R., Roberts, S., Foster, R.P., Boyce, A. & Coller, D. 2003. Origin of the copper-cobalt deposits of the Zambian Copperbelt: An epigenetic view from Nchanga. *Geology,* 31, 497-500.

Mcmahon, A.D. 1965. Copper: A Materials Survey. Washington: U. S. Dept. of the Interior Bureau of Mines.

Meere, P.A. 1995. Sub-greenschist facies metamorphism from the Variscides of SW Ireland: an early syn-extensional peak thermal event. *Journal of the Geological Society,* 152, 511-521.

Meere, P.A. & Banks, D.A. 1997. Upper crustal fluid migration: an example from the Variscides of SW Ireland. *Journal of the Geological Society,* 154, 975-985.

Mei, Y., Sherman, D.M., Liu, W. & Brugger, J. 2013. Ab initio molecular dynamics simulation and free energy exploration of copper(I) complexation by chloride and bisulfide in hydrothermal fluids. *Geochimica et Cosmochimica Acta,* 102, 45-64.

Meighan, C.J. 2015. PT Evolution of Sentinel Cu Deposit, Northwestern Zambia. PhD thesis, Colorado School of Mines.

Meighan, C.J., Kelly, N.M., Hitzman, M.W. & Wood, D. 2012. Low P-T kyanite growth associated with aluminium metasomatism and quartz-sulfide veining, Sentinel Cu deposit, northwestern Zambia. *Abstracts with Programs - Geological Society of America, 44, 525.*

Mendelsohn, F. 1961. *The geology of the Northern Rhodesian Copperbelt,* London: MacDonald.

Metzger, F.W., Kelly, W.C., Nesbitt, B.E. & Essene, E.J. 1977. Scanning Electron Microscopy of Daughter Minerals in Fluid Inclusions. *Economic Geology,* 72, 141-152.

Miller, R. 1983. The Pan-African Damara Orogen of Southwest Africa/Namibia. *Geological Society of South Africa,* Special Publication 11, 431-515.

Milton, J.E. 2015. *Sedimentary rock hosted copper mineralization in the Neoproterozoic Redstone Copperbelt, MacKenzie Mountains, Northwest Territories, Canada.* PhD thesis, The University of British Columbia

Modie, B.N. 2000. Geology and mineralisation in the Meso- to Neoproterozoic Ghanzi-Chobe belt of northwest Botswana. *Journal of African Earth Sciences,* 30, 467-474.

Modie, B.N., Akanyang, P. & Ramokate, L.V. 1998. Formalisation of the lithostratigraphic units of the Ghanzi-Chobe belt. *Geological Survey of Botswana Bulletin,* 45, 32.

Modie, B.N.J. 1996. Depositional environments of the Meso- to Neoproterozoic Ghanzi-Chobe belt, northwest Botswana. *Journal of African Earth Sciences,* 22, 255-268.

Muchez, P., Brems, D., Clara, E., De Cleyn, A., Lammens, L., Boyce, A., De Muynck, D., Mukumba, W. & Sikazwe, O. 2010. Evolution of Cu–Co mineralizing fluids at Nkana Mine, Central African Copperbelt, Zambia. *Journal of African Earth Sciences,* 58, 457-474.

Muchez, P., Vanderhaeghen, P., El Desouky, H., Schneider, J., Boyce, A., Dewaele, S. & Cailteux, J. 2008. Anhydrite pseudomorphs and the origin of stratiform Cu–Co ores in the Katangan Copperbelt (Democratic Republic of Congo). *Mineralium Deposita,* 43, 575-589.

Nowecki, J. 2014. *Tracing seawater evaporation and its role in the formation of sediment-hosted stratiform copper deposits.* Unpublished PhD thesis, University of Southampton, UK.

Pearce, N.J.G., Perkins, W.T., Westgate, J.A., Gorton, M.P., Jackon, S.E., Neal, C.R. & Chenery, S.P. 1997. A Compilation of New and Published Major and Trace Element Data for NIST SRM 610 and NIST SRM 612 Glass Reference Materials. *Geostandards and Geoanalytical Research,* 21, 115-144.

Pearson, R.G. 1963. Hard and soft acids and their bases. *Journal of the American Chemical Society,* 85, 3533-3539.

Pettke, T., Audétat, A., Schaltegger, U. & Heinrich, C.A. 2005. Magmatic-to-hydrothermal crystallization in the W–Sn mineralized Mole Granite (NSW, Australia). *Chemical Geology,* 220, 191-213.

Pettke, T., Oberli, F., Audétat, A., Guillong, M., Simon, A.C., Hanley, J.J. & Klemm, L.M. 2012. Recent developments in element concentration and isotope ratio analysis of individual fluid inclusions by laser ablation single and multiple collector ICP-MS. *Ore Geology Reviews,* 44, 10-38.

Pfurr, N., Ahrendt, H., Hansen, B.T. & Weber, K. 1991. U-Pb and Rb-Sr isotopic study of granitic gneisses and associated metavolcanic rocks from the Rostock massifs, southern margin of the Damara Orogen: implications for lithostratigraphy of this crustal segment. *Namibian Geological Survey Communications,* 7, 35-48.

Porada, H. 1989. Pan-African Rifting and Orogenesis in Southern to Equatorial Africa and Eastern Brazil. *Precambrian Research,* 44, 103-136.

Porada, H. & Berhorst, V. 2000. Towards a new understanding of the Neoproterozoic-Early Palaeozoic Lufilian and northern Zambezi Belts in Zambia and the Democratic Republic of Congo. *Journal of African Earth Sciences,* 30, 727-771.

Pracht, M. 2000. Controls on magmatism in the Munster Basin, SW Ireland. *Geological Society, London, Special Publication,* 180, 303-317.

Quin, J.G. 2008. The evolution of a thick shallow marine succession, the South Munster Basin, Ireland. *Sedimentology,* 55, 1053-1082.

Rainaud, C., Master, S., Armstrong, R.A. & Robb, L.J. 2005. Geochronology and nature of the Palaeoproterozoic basement in the Central African Copperbelt (Zambia and the Democratic Republic of Congo), with regional implications. *Journal of African Earth Sciences,* 42, 1-31.

Ramokate, L.V., Mapeo, R.B.M., Corfu, F. & Kampunzu, A.B. 2000. Proterozoic geology and regional correlation of the Ghanzi-Makunda area, western Botswana. *Journal of African Earth Sciences,* 30, 453-466.

Ramsay, C. & Ridgway, J. 1977. Metamorphic patterns in Zambia and their bearing on problems of Zambian tectonics history. *Precambrian Research,* 4, 321-337.

Richards, J.P., Krogh, T.E. & Spooner, E.T.C. 1988. Fluid Inclusion Characteristics and U-Pb Rutile Age of Late Hydrothermal Alteration and Veining at the Musoshi Stratiform Copper Deposit, Central African Copper Belt, Zaire. *Economic Geology,* 83, 118-139.

Roberts, S., Palmer, M.R., Cooper, M.J., Buchaus, P. & Sargent, D. 2009. REE and Sr isotope characteristics of carbonate within the Cu–Co mineralized sedimentary sequence of the Nchanga Mine, Zambian Copperbelt. *Mineralium Deposita,* 44, 881-891.

Robinson, B.W. & Kusakabe, M. 1975. Quantitative Preparation of Sulfur Dioxide, for 34S/32S Analyses, from Sulfides by Combustion with Cuprous Oxide. *Analytical Chemistry,* 47, 1179-1181.

Roedder, E. 1972. Composition of fluid inclusions. *US Geological Survey Professional Paper 440JJ.*

Roedder, E. 1984. Fluid inclusions: an introduction to studies of all types of fluid inclusions, gas, liquid, or melt, trapped in materials from earth and space. *Reviews in Mineralogy Volume 12.* Washington D.C: Mineralogical Society of America.

Rose, A.W. 1976. The Effect of Cuprous Chloride Complexes in the Origin of Red-Bed Copper and Related Deposits. *Economic Geology,* 71, 1036-1048.

Rose, A.W. 1989. Mobility of copper and other heavy metals in sedimentary environments. *In:* Boyle, R. W., Brown, A. C., Jefferson, C. W., Jowett, E. C. & Kirkham, R. (eds.) *Sediment-hosted Stratiform Copper Deposits.* Geological Association of Canada.

Rusk, B.G., Lowers, H.A. & Reed, M.H. 2008. Trace elements in hydrothermal quartz: Relationships to cathodoluminescent textures and insights into vein formation. *Geology,* 36, 547.

Schneider, G.I.C. & Seeger, K.G. 1992. The Mineral Resources of Namibia. Windhoek, Republic of Namibia: Ministry of Mines and Energy.

Schwartz, M.O., Akanyang, P., Trippler, K. & Ngwisanyi, T.H. 1995. The sediment-hosted Ngwako Pan copper deposit, Botswana. *Economic Geology,* 90, 1118-1147.

Schwartz, M.O., Kwok, Y.Y., Davis, D.W. & Akanyang, P. 1996. Geology, geochronology and regional correlation of the Ghanzi Ridge, Botswana. *South African Journal of Geology,* 99, 245-250.

Selley, D., Broughton, D., Scott, R., Hitzman, M., Bull, S., Large, R., Mcgoldrick, P., Croaker, M., Pollington, N. & Barra, F. 2005. A New Look at the Geology of the Zambian Copperbelt. *Economic Geology,* 100th Anniversary Volume, 965-1000.

Selley, D., Scott, R., Emsbo, P., Koziy, L., Hitzman, M.W., Bull, S., Duffett, M., Sebagenzi, S., Halpin, J. & Broughton, D. 2018. Structural Configuration of the Central African Copperbelt: Roles of Evaporites in Structural Evolution, Basin Hydrology, and Ore Location. *SEG Special Publication,* 21, 115-156.

Seward, T.M., Williams-Jones, A.E. & Migdisov, A.A. 2014. The Chemistry of Metal Transport and Deposition by Ore-Forming Hydrothermal Fluids. *In:* Holland, H. D. & Turekian, K. (eds.) *Treatise on Geochemistry.* 2nd ed.: Elsevier.

Sharp, Z.D. 1990. A laser-based microanalytical method for the in situ determination of oxygen isotope ratios of silicates and oxides. *Geochimica et Cosmochimica Acta,* 54, 1353-1357.

Sharp, Z.D., Gibbons, J.A., Maltsev, O., Atudorei, V., Pack, A., Segupta, S., Shock, E.L. & Knauth, L.P. 2016. A calibration of the triple oxygen isotope fractionation in the SiO2-H2O system and applications to natural samples. *Geochimica et Cosmochimica Acta,* 186, 105-119.

Shepherd, T.J., Rankin, A.H. & Alderton, D.H.M. 1985. *A Practical Guide to Fluid Inclusion Studies,* London: Blacki.

Sheridan, D.J. 1964. The structure and mineralisation of the Mountain Mine area, Allihies, West Cork, Ireland. *Scientific Proceedings of the Royal Dublin Society,* A2, 21-27.

Shu, Q., Chang, Z., Hammerli, J., Lai, Y. & Huizenga, J.-M. 2017. Composition and Evolution of Fluids Forming the Baiyinnuo'er Zn-Pb Skarn Deposit, Northeastern China: Insights from Laser Ablation ICP-MS Study of Fluid Inclusions. *Economic Geology,* 112, 1441-1460.

Sillitoe, R.H. 2010. Porphyry Copper Systems. *Economic Geology,* 105, 3-41.

Sillitoe, R.H., Perello, J., Creaser, R.A., Wilton, J. & Dawborn, T. 2015. Two Ages of Copper Mineralization in the Mwombezhi Dome, Northwestern Zambia: Metallogenic Implications for the Central African Copperbelt. *Economic Geology,* 110, 1917-1923.

Sillitoe, R.H., Perelló, J., Creaser, R.A., Wilton, J., Wilson, A.J. & Dawborn, T. 2017. Age of the Zambian Copperbelt. *Mineralium Deposita,* 52, 1245-1268.

Sillitoe, R.H., Perello, J. & Garcia, A. 2010. Sulfide-bearing Veinlets Throughout the Stratiform Mineralization of the Central African Copperbelt: Temporal and Genetic Implications. *Economic Geology,* 105, 1361-1368.

Singer, D.A. 2017. Future copper resources. *Ore Geology Reviews,* 86, 271-279.

Singletary, S.J., Hanson, R.E., Martin, M.W., Crowley, J.L., Bowring, S.A., Key, R.M., Ramokate, L.V., Direng, B.B. & Krol, M.A. 2003. Geochronology of basement rocks in the Kalahari Desert, Botswana, and implications for regional Proterozoic tectonics. *Precambrian Research,* 121, 47-71.

Span, R. & Wagner, W. 1996. A New Equation of State for Carbon Dioxide Covering the Fluid Region from the Triple-Point Temperature to 1100 K at Pressures up to 800 MPa. *Journal of Physical and Chemical Reference Data,* 25, 1509-1596.

Spear, N., Holland, H.D., Garcia-Veigas, J., Lowenstein, T.K., Giegengack, R. & Peters, H. 2014. Analyses of fluid inclusions in Neoproterozoic marine halite provide oldest measurement of seswater chemistry. *Geology,* 42, 103-106.

Speiser, A., Hein, U.F. & Porada, H. 1995. The Kansanshi copper mine (Solwezi area, northwestern Zambia): Geology, wall-rock alteration and fluid inclusions. *In:* Pasava, J., Kribek, B. & Zak, K. (eds.) *Mineral Deposits: From their origin to their environmental impacts.* Rotterdam: A. A. Balkema.

Spinks, S.C., Parnell, J., Bellis, D. & Still, J. 2016. Remobilization and mineralization of selenium–tellurium in metamorphosed red beds: Evidence from the Munster Basin, Ireland. *Ore Geology Reviews,* 72, 114-127.

Sterner, S.M., Hall, D.L. & Bodnar, R.J. 1988. Synthetic fluid inclusions. V. Solubility relations in the system NaCl-KCl-H2O under vapor-saturated conditions. *Geochimica et Cosmochimica Acta,* 52, 989-1005.

Sterner, S.M. & Pitzer, K.S. 1994. An equation of state for carbon dioxide valid from zero to extreme pressures. . *Contributions to Mineralogy and Petrology,* 117, 362-374.

Stoffell, B. 2007. *Metal Transport and Deposition Hydrothermal Fluids - Insights from Laser Ablation Microanalysis of Individual Fluid Inclusions.* PhD thesis, Imperial College London.

Stoffell, B., Appold, M.S., Wilkinson, J.J., Mcclean, N. & Jeffries, T. 2008. Geochemistry and Evolution of Mississippi Valley-Type Mineralizing Brines from the Tri-State and Northern Arkansas Districts Determined by LA-ICP-MS Microanalysis of Fluid Inclusions. *Economic Geology,* 103, 1411-1435.

Sutton, S.J. & Maynard, J.B. 2005. A fluid mixing model for copper mineralization at Konkola North, Zambian Copperbelt. *Journal of African Earth Sciences,* 42, 95-118.

Sweeney, M.A. & Binda, P.L. 1989. The role of diagenesis in the formation of the Konkola Cu-Co orebody of the Zambian Copperbelt. *Geological Association of Canada,* 36, 499-518.

Sylvester, P.J. 2008. Matrix Effects in Laser Ablation-ICP-MS. *In:* Sylvester, P. J. (ed.) *Laser Ablation ICP-MS in Earth Sciences: Current Practices and Outstanding Issues.* Mineralogical Association of Canada Short Course Volume 40.

Sylvester, P.J. & Eggins, S.M. 1997. Analysis of Re, Au, Pd, Pt and Rh in NIST GLass Certified Reference Materials and Natural Basalt Glasses by Laser Ablation ICP-MS. *Geostandards and Geoanalytical Research,* 21, 215-229.

Taylor, C.D., Causey, J.D., Denning, P.D., Hammarstrom, J.M., Hayes, T.S., Horton, J.D., Kirschbaum, M.J., Parks, H.L., Wilson, A.B., Wintzer, N.E. & Zientek, M.L. 2013. Descriptive models, grade-tonnage relations, and databases for the assessment of sediment-hosted copper deposits - With emphasis on deposits in the Central African Copperbelt, Democratic Republic of the Congo and Zambia. *U.S. Geological Survey Scientific Investigations Report 2010-5090-J.* USGS.

Taylor, H. 1997. Oxygen and hydrogen isotope relationships in hydrothermal mineral deposits *In:* Barnes, H. (ed.) *Geochemistry of hydrothermal ore deposits.* New York: Wiley.

Thode, H. 1991. Sulphur isotopes in nature and the environment: An overview. *In:* Krause, H. & Grinenko, V. (eds.) *Stable Isotopes: Natural and anthropogenic sulpur in the environment (Scope 43).* New York: Wiley and Sons.

Todd, S.P. 2014. Structure of the Dingle Peninsula, SW Ireland: evidence for the nature and timing of Caledonian, Acadian and Variscan tectonics. *Geological Magazine,* 152, 242-268.

Torrealday, H.I., Hitzman, M.W., Stein, H., Markley, R.J., Armstrong, R. & Broughton, D. 2000. Re-Os Dating of the Vein-hosted Mineralization at the Kansanshi Copper Deposit, Northern Zambia. *Economic Geology,* 95, 1165-1170.

Torremans, K., Muchez, P. & Sintubin, M. 2014. Mechanisms of flexural flow folding of competent single-layers as evidenced by folded fibrous dolomite veins. *Journal of Structural Geology,* 69, 75-90.

Turlin, F., Eglinger, A., Vanderhaeghe, O., André-Mayer, A.-S., Poujol, M., Mercadier, J. & Bartlett, R. 2016. Synmetamorphic Cu remobilization during the Pan-African orogeny: Microstructural, petrological and geochronological data on the kyanite-micaschists hosting the Cu(–U) Lumwana deposit in the Western Zambian Copperbelt of the Lufilian belt. *Ore Geology Reviews,* 75, 52-75.

Valyashko, M.G. 1962. *Geochemical Rules of the Potassium Salt Deposits Formation.* Izdatelstvo Moskovskovo Universiteta.

Van Der Heever, D., Arengi, J. & Van Rensburg, J. 2009. Technichal report for Hana Mining: Ghanzi Copper-Silver Project, Ghanzi District, Botswana. GeoLogix Mineral Resource Consultants (Pty) Ltd.

Van Wilderode, J., Debruyne, D., Torremans, K., Elburg, M.A., Vanhaecke, F. & Muchez, P. 2015. Metal sources for the Nkana and Konkola stratiform Cu–Co deposits (Zambian Copperbelt): Insights from Sr and Nd isotope ratios. *Ore Geology Reviews,* 67, 127-138.

Vanko, D.A., Bodnar, R.J. & Sterner, S.M. 1988. Synthetic fluid inclusions: VIII. Vapor-saturated halite solubility in part of the system NACl-CaCl2-H2O, with application to fluid inclusions from ocenic hydrothermal systems. *Geochimica et Cosmochimica Acta,* 52, 2451-2456.

Vry, V.H. 2010. *Geological and Hydrothermal Fluid Evolution at El Teniente, Chile.* PhD thesis, Imperial College London.

Wakefield, J. 1978. Samba: a deformed porphyry-type copper deposit in the basement of the Zambian Copperbelt. *Transactions of the Institution of Mining and Metallurgy,* 87, 43-52.

Warren, E.A. & Smalley, P.C. 1994. *North Sea Formation Waters Atlas*: Geological Society of London Memoir 15.

Warren, J. 2016. Evaporites. *In:* White, W. M. (ed.) *Encyclopedia of Geochemistry.* Springer International Publishing.

Warren, J.K. 2006. *Evaporites: Sediments, Resources and Hydrocarbons,* Berlin-Heidelberg: Springer.

Wen, N., Boyce, A., Fallick, A.E., Ashworth, J.R. & Ixer, R.A. 1996. The genesis of Cu-bearing quartz veins by metamorphic remobilization from stratiformred bed deposits, SWCounty Cork, Ireland. *Mineralogy and Petrology,* 57, 73-89.

White, W.S. 1971. A Paleohydrologic Model for Mineralization of the White Pine Copper Deposit, Northern Michigan. *Economic Geology,* 66, 1-13.

Wilkinson, J.J. 2010. A Review of Fluid Inclusion Constraints on Mineralization in the Irish Ore Field and Implications for the Genesis of Sediment-Hosted Zn-Pb Deposits. *Economic Geology,* 105, 417-442.

Wilkinson, J.J. 2014. Sediment-Hosted Zinc-Lead Mineralization: Processes and Perspectives. *In:* Holland, H. D. & Turekian, K. (eds.) *Treatise on Geochemistry (2nd Ed.).* Elsevier.

Wilkinson, J.J., Chang, Z., Cooke, D.R., Baker, M.J., Wilkinson, C.C., Inglis, S., Chen, H. & Bruce Gemmell, J. 2015. The chlorite proximitor: A new tool for detecting porphyry ore deposits. *Journal of Geochemical Exploration,* 152, 10-26.

Wilkinson, J.J., Collins, S.J. & Jeffries, T. The composition of Irish-type Zn-Pb ore fluids. 9th Biennial Meeting of the Society for Geology Applied to Mineral Deposits, 2007 Dublin. Irish Association of Economic Geologists, 279-282.

Wilkinson, J.J., Stoffell, B., Wilkinson, C.C., Jeffries, T.E. & Appold, M.S. 2009. Anomalously metal-rich fluids form hydrothermal ore deposits. *Science,* 323, 764-7.

Williams, E.A., Sergeev, S.A., Stossel, I. & Ford, M. 1997. An Eifelian U-Pb zircon date for the Enagh Tuff Bed from the Old Red Sandstone of the Munster Basin, SW Ireland. *Journal of the Geological Society,* 154, 189-193.

Williams, R.A. 1993. *The Berehaven Copper Mines, Allihies, Co. Cork S. W. Ireland,* Kenmare: A. B. O'Connor.

Williams-Jones, A.E. & Migdisov, A.A. 2014. Experimental Constraints on the Transport and Deposition of Metals in Ore-Forming Hydrothermal Systems. *Economic Geology,* Special Publication 18, 77-95.

Williams-Jones, A.E. & Samson, I. 1990. Theoretical estimation of halite solubility in the system NaCl-CaCl2-H2O: Applications to fluid inclusions. *Canadian Mineralogist,* 28, 299-304.

Woodhead, J. 2018. *Personal communication*.

Woodhead, J. 2013. The Neoproterozoic Roan Group in the Zambian Copperbelt: Sequence Stratigraphy, Alteration and Mineralization. PhD thesis, Colorado School of Mines.

Yardley, B.W.D. 2005. Metal Concentrations in Crustal Fluids and Their Relationship to Ore Formation. *Economic Geology,* 100, 613-632.

Zacharias, J. & Wilkinson, J.J. 2007. ExLAM 2000: Excel VBA application for processing of transient signals from laser ablation (LA-ICP-MS) of fluid inclusions and solid phases [abs]. Bern, Switzerland.

Zheng, Y.F. 1999. Oxygen isotope fractionation in carbonate and sulfate minerals. *Geochemical Journal of Japan,* 33, 109-126.

Zhong, R., Brugger, J., Chen, Y. & Li, W. 2015. Contrasting regimes of Cu, Zn and Pb transport in ore-forming hydrothermal fluids. *Chemical Geology,* 395, 154-164.

Zielinski, R.A., Bloch, S. & Walker, T.R. 1983. The Mobility and Distribution of Heavy Metals during the Formation of First Cycle Red Beds. *Economic Geology,* 78, 1574-1589.